Bearing Estimation Techniques for Improved Performance Spread Spectrum Receivers

John S. Thompson

A thesis submitted for the degree of Doctor of Philosophy.

The University of Edinburgh.

- November 1995 -

Abstract

The main topic of this thesis is the use of bearing estimation techniques combined with multiple antenna elements for spread spectrum receivers. The motivation behind this work is twofold: firstly, this type of receiver structure may offer the ability to locate the position of a mobile radio in an urban environment. Secondly, these algorithms permit the application of space division multiple access (SDMA) to cellular mobile radio, which can offer large system capacity increases. The structure of these receivers may naturally be divided into two parts: signal detection and spatial filtering blocks.

The signal detection problem involves locating the bearings of the multipath components which arise from the transmission of the desired user's signal. There are a number of approaches to this problem, but here the MUSIC algorithm will be adopted. This algorithm requires an initial estimate of the number of signals impinging on the receiver, a task which can be performed by model order determination techniques. A major deficiency of MUSIC is its inability to resolve the highly–correlated and coherent multipath signals which frequently occur in a spread spectrum system. One of the simplest ways to overcome this problem is to employ spatial smoothing techniques, which trade the size of the antenna array for the ability to resolve coherent signals. The minimum description length (MDL) is one method for determining the signal model order and it can easily be extended to calculating the required degree of spatial smoothing. In this thesis, an approach to analysing the probability of correct model order determination for the MDL with spatial smoothing is presented. The performance of MUSIC, combined with spatial smoothing, is also of great significance. Two smoothing algorithms, spatial smoothing and forward–backward spatial smoothing, are analysed to compare their performance.

If SDMA techniques are to be deployed in cellular systems, it is important to first estimate the performance improvements available from applying antenna array spatial filters. Initially, an additive white Gaussian noise channel is used for estimating the capacity of a perfect power–controlled code division multiple access system with SDMA techniques. Results suggest that the mean interference levels are almost halved as the antenna array size doubles, permitting large capacity increases. More realistic multipath models for urban cellular radio channels are also considered. If the transmitter gives rise to a number of point source multipath components, the bearing estimation receiver is able to capture the signal energy of each multipath. However, when a multipath component has significant angular spread, bearing estimation receivers need to combine separate directional components, at an increased cost in complexity, to obtain similar results to a matched filter.

Finally, a source location algorithm for urban environments is presented, based on bearing estimation of multipath components. This algorithm requires accurate knowledge of the positions of the major multipath reflectors present in the environment. With this knowledge it is possible to determine the position of a transmitting mobile unit. Simulation results suggest that the algorithm is very sensitive to angular separation of the multipath components used for the source location technique.

Declaration of originality

I hereby declare that this thesis and the work reported herein was composed and originated entirely by myself, in the Department of Electrical Engineering at the University of Edinburgh. The one exception was work reported in subsection 6.5.4, which was carried out jointly with Dr. Iain Scott, also from the Department of Electrical Engineering at the University of Edinburgh.

John Thompson

Acknowledgements

I would like to thank the following people for their invaluable assistance during the course of this PhD:

- Bernard Mulgrew and Peter Grant, my supervisors, for their continuous support and guidance. Also for reading and checking this thesis.
- Dr Ed Warner, currently at Roke Manor Reseach Ltd, for many fruitful discussions.
- Everyone in the Signals and Systems Group, including Gary, Iain, Mike, David Hughes, Dave Laurenson, Dave Cruickshank, Rajan, Herkole, Paul Bentley, Paul Strauch, Jon Dobson, Jon Altuna, Bill, Eng–Siong, Achilleas, Duncan, Ian, Richard and Justin.
- My parents for reading this thesis.
- My wife Nadine for putting up with me!
- The Ministry of Defence and the EPSRC for providing financial support.

Contents

List of Figures

List of Tables

Abbreviations

ACF	Auto–correlation function
AIC	Akaike information theoretic criterion
BER	Bit error ratio
BSD	Bearing standard deviation
CBF	Conventional beamformer
CCF	Cross–correlation function
CCI	Cross–correlation interference
CDF	Cumulative distribution function
CDMA	Code division multiple access
DPSK	Differential phase shift keying
DS–SS	Direct sequence spread spectrum
EVR	Eigenvalue ratio
FBS	Forward–backward smoothing
FBSS	Forward–backward spatial smoothing
GPS	Global positioning system
GSM	Global system for mobile
LCMV	Linearly constrained minimum variance
LOS	Line of sight
MDL	Minimum description length
MRC	Maximal ratio combining
MUSIC	Multiple signal classification
MV	Minimum variance
PDF	Probability density function
PN	Pseudo–noise
SNR	Signal–to–noise ratio
SS	Spatial smoothing
ULA	Uniform linear array

List of principal symbols

a	Amplitude scaling factor.
a_1, a_2	Major and minor ellipse axes.
$\boldsymbol{a}(\theta)$	Steering vector for bearing θ.
$\boldsymbol{a}(\theta, t_d)$	Steering vector for bearing θ and time delay t_d.
A	quadratic equation coefficient.
A_i	Adjacent interfering cell.
$\boldsymbol{A}$	Matrix of incoming signal steering vectors.
$\boldsymbol{A}_T$	Matrix of incoming signal steering vectors $\boldsymbol{a}(\theta, t_d)$.
b_k	k^{th} diagonal entry of the matrix $\boldsymbol{B}(q, \Theta)$.
B	quadratic equation coefficient.
B_f	Transmission signal bandwidth.
B_s	Baseband data bandwidth.
B_C	Channel bandwidth.
$\boldsymbol{B}$	Output matrix for the beamspace transformation.
$\boldsymbol{B}(q, \Theta)$	The matrix $\boldsymbol{A}^H \boldsymbol{F}_q^T (\boldsymbol{A}_s^+)^H$
c	The speed of light.
c_C	Cross–correlation value.
c_i	i^{th} eigenvalue of $\boldsymbol{R}_{F/B}$.
$c(t)$	Spread spectrum code, repeating with symbol period t_s.
C	quadratic equation coefficient.
C_C	Channel capacity.
CDF()	cumulative distribution function.
d	Scattering radius of multipath circle.
$d(t)$	Stream of data symbols.
$d_\theta(\theta)$	Brandwood derivative noise subspace projection.
$\boldsymbol{d}(\theta)$	Brandwood derivative of the steering vector $\boldsymbol{a}(\theta)$.
$D(n)$	the decision variable for the n^{th} symbol.

e_i	i^{th} largest eigenvalue of the estimated covariance matrix $\hat{\boldsymbol{R}}$.
f	RF carrier frequency.
$f(k)$	Model order criterion under the hypothesis that the model order is k.
$\boldsymbol{F}_p$	The p^{th} subarray selection matrix.
$\boldsymbol{g}_k$	length W Gold code vector.
$G(\boldsymbol{u}, \boldsymbol{v})$	Gold code set constructed from preferred m–sequences $\boldsymbol{u}$ and $\boldsymbol{v}$.
G	Nunber of exponentials used to generate a fading signal.
$h(i,t)$	Post–correlation, the i^{th} channel coefficient at time t.
H	Number of subarrays for spatial smoothing.
$H(\tau)$	Channel Impulse Response power at delay τ.
I	Value of an integral equation.
$\boldsymbol{I}$	Identity matrix.
J	Number of RAKE filter taps.
$\boldsymbol{J}$	Inversion matrix for forward–backward smoothing.
J_o	Bessel function of the first kind.
k	estimated model order.
k_0	Scaling factor for bearing standard deviation values.
k_1	Synchronous CDMA power suppression factor.
k_2	Asynchronous CDMA power suppression factor.
K	True model order.
$l(k)$	Log–likelihood function under the hypothesis that the model order is k.
L	Spatially smoothed covariance matrix size.
m	Nakagami m–parameter.
M	Uniform linear array size (in elements).
$n(t)$	Additive white Gaussian noise of power σ^2.
$\boldsymbol{n}(t)$	$M \times 1$ Additive white Gaussian noise vector of power σ^2.
N	Number of snapshots.
$\boldsymbol{N}(p,q)$	Cross–correlation noise matrix for the p^{th} and q^{th} subarrays.
$O()$	Order.
$p()$	Probability value.
P	Number of users in a CDMA system.
PDF()	probability density function.
$\overline{P}$	Mean power level for cross–correlation interference.
$\overline{P}_s(M,\theta)$	Mean power suppression factor for an M–element array spatial filter set to bearing θ.

q	Normalising constant.
Q	Number of multipath components resolved by a spread spectrum receiver.
r	The magnitude of a complex signal amplitude.
$\overline{r}$	The mean magnitude level.
$R(t)$	Auto–correlation function.
$r(t)$	Pre–correlation noise–corrupted baseband signal.
$\boldsymbol{r}(t)$	$M \times 1$ Pre–correlation noise–corrupted baseband signal vector.
R	Base–station to Mobile distance.
$\boldsymbol{R}$	Covariance matrix of the data vector $\boldsymbol{y}(t)$.
$\boldsymbol{R}_{W/B}$	Covariance matrix of the data vector $\boldsymbol{y}_T(t)$.
$\hat{\boldsymbol{R}}$	Estimated covariance matrix.
$\boldsymbol{R}_{F/B}$	Forward–backward smoothed covariance matrix.
s	signal power.
s_i	Interference power from one user.
$\boldsymbol{s}(t)$	Vector of incoming signals to an array.
$\boldsymbol{S}$	Covariance matrix of $\boldsymbol{s}(t)$.
S^k	Phase inversion operator on code–sequence vectors.
$S_p(\tau, \nu)$	Bello Function of the received signal as a function of excess time delay τ and Doppler frequency ν.
$S(\nu)$	Doppler power spectrum.
S/I	Signal to interference ratio.
t	time.
t_c	Chip period.
t_d	Time delay.
t_o	Initial channel tap time of arrival.
t_s	symbol period.
T^k	Cyclic left–shift operator on code–sequence vectors.
$\boldsymbol{u}$	eigenvector.
$\boldsymbol{U}$	matrix of eigenvectors.
v	vehicle velocity.
$\boldsymbol{v}_1, \boldsymbol{v}_2$	Two length W preferred pair m–sequences.
$w(k)$	penalty function under the hypothesis that the model order is k.
W	Spread spectrum processing gain.
$\boldsymbol{W}$	Beamspace transformation filter bank.
x	x–coordinate of mobile position.

$x(t)$	Post–correlation underlying baseband signal.
$\boldsymbol{x}(t)$	$M \times 1$ Post–correlation underlying baseband signal vector .
$\boldsymbol{X}$	The signal covariance matrix.
y	y–coordinate of mobile position.
$y(t)$	Post–correlation noise–corrupted baseband signal.
$\boldsymbol{y}(t)$	$M \times 1$ Post–correlation noise–corrupted baseband vector.
$y_T(t)$	$WM \times 1$ Post–correlation noise–corrupted baseband vector for W time slots.
$Y(\theta)$	beamformer pattern of a 2–element array with look direction 90^o.
z_i	The i^{th} eigenvalue of the estimated spatially smoothed matrix $\hat{\boldsymbol{\Psi}}$.
$z(j,n)$	The signal at the input of the j^{th} RAKE filter tap for the n^{th} symbol.
$\boldsymbol{Z}$	The noise subspace matrix.
$\alpha(N)$	weighting term for the penalty function $w(k)$.
$\boldsymbol{\alpha}, \boldsymbol{\beta}$	Vectors for the calculation of the variance of the MUSIC algorithm with spatial smoothing.
β	Normalised interference from one user in a nearby cell.
Γ	Number of Beamspace filters.
$\delta_c(t)$	Desired code auto–correlation function.
$\Delta\theta$	Error in source bearing measurement.
2Δ	The angular spread of a multipath component.
ζ_i	The i^{th} eigenvalue of the spatially smoothed covariance matrix $\boldsymbol{\Psi}$.
η_i	The i^{th} eigenvalue of the signal covariance matrix $\boldsymbol{X}$.
$\eta(t)$	Pre–correlation additive noise.
$\boldsymbol{\eta}(t)$	$M \times 1$ Pre–correlation additive noise vector.
θ	Source bearing.
λ	Eigenvalue of the covariance matrix $\boldsymbol{R}$.
λ_C	Carrier wavelength.
$\boldsymbol{\Lambda}$	Diagonal matrix of eigenvalues.
μ	weighting factor for the least mean squares algorithm.
ν	Doppler frequency.
ν_m	Maximum Doppler frequency.
ξ	Excess path length of second multipath.
$\vartheta(i,t)$	Pre–correlation channel coefficient.
ρ	Signal–to–noise ratio.
σ^2	Complex, single–channel additive white Gaussian noise power.
$\sigma(A_i)$	Area of an adjacent cell.

τ	Time delay.
υ	Base–station to reflector distance.
υ_1	Distance between consecutive bearing measurements.
ϕ	Demodulated carrier phase.
$\boldsymbol{\Psi}$	Spatially smoothed covariance matrix.
$\boldsymbol{\Psi}_{F/B}$	Forward–backward spatially smoothed covariance matrix.
$\partial X/\partial \upsilon$	The partial derivative of X with respect to υ.
a^*	Complex conjugate operation.
$\boldsymbol{R}_{pq}$	The p^{th} row and q^{th} column entry of $\boldsymbol{R}$.
$\boldsymbol{R}(p,q)$	The matrix $\boldsymbol{F}_p \boldsymbol{R} \boldsymbol{F}_q^T$.
$\boldsymbol{R}^T$	Matrix transpose operation.
$\boldsymbol{R}^H$	Matrix Hermitian transpose operation.
$\boldsymbol{R}^{-1}$	Matrix inverse operation.
$\boldsymbol{R}^+$	Pseudo–inverse operation.
tr$\boldsymbol{R}$	Matrix trace operation.
$\det \boldsymbol{R}$	Matrix determinant operation.
$\Re$	real part.
int	the integer part of a real number.
$\mathbb{Z}$	Integer space.
$\mathbb{R}$	Real space.
$\mathbb{C}$	Complex space.
$E()$	Statistical expectation operator.

Chapter 1
Introduction

In recent years, there has been an explosion of interest in wireless communication services. The potential of wireless is to allow anyone to communicate by voice or digital data, without being limited by the fixed telephone network. In practice, there is a diverse range of communications products for a wide variety of applications, from cellular telephones to high speed wireless data networks. There are many issues involved in the design of these systems, but generally the prime motivations are to provide an acceptable product to minimise costs and maximise profit. In the case of cellular communications, the availability of VLSI technology which is fast, powerful and inexpensive has driven designers to produce mobile telephones which employ complex signal processing techniques. This is a reply to the perceived demand for flexible, high–capacity cellular networks.

This thesis will consider the application of two military–derived techniques to mobile cellular radio systems, namely spread spectrum modulation and antenna arrays. The necessary algorithms to apply antenna arrays to spread spectrum signals will be described in this thesis. Some studies of the improvement in the capacity of cellular networks using these techniques are also described. Urban conurbations provide a very hostile environment for cellular radio systems, so the performance of antenna arrays under these conditions is analysed. The urban radio channel can provide a means for locating the position of a given mobile radio, and an algorithm is presented for this purpose. This chapter will commence by summarising the current state of wireless technology. It will focus on cellular radio systems, looking at the techniques that are currently employed, to see why spread spectrum and adaptive array techniques may be of use. Following this, a brief summary of the main areas of research documented in this thesis will be presented. To conclude, the structure of the thesis itself will be described.

1.1 Wireless Personal Communications

The recent development of wireless communications for personal and business use across the world has led to a major proliferation of systems and standards. For a full description and discussion of these systems, the reader is referred to the IEEE Communications Magazine special issues of December 1992 and January 1995 as well as the Proceedings of the IEEE special issue September 1994. The recent paper of Cox [1] is also recommended. Here the main categories will be briefly mentioned, before going on to look at cellular systems in more detail.

Currently, wireless communications systems may be broadly subdivided into 6 or 7 categories. These include:

(i). **Wireless Local Area Networks (WLANs):** These systems are designed for low mobility data communications in indoor environments such as offices and factories [2]. Spread spectrum techniques are widely used in these systems, because some of the early frequency allocations released in the United States (US) for unlicensed WLAN operation (amongst other applications) were the industrial, scientific and medical (ISM) bands. These permit transmissions of up to 1 watt, provided that spread spectrum modulation is used. However, the trend towards high speed data links means that WLAN products are likely to move away from spread spectrum techniques.

(ii). **Wide Area Wireless Data Systems:** These products provide low data rate digital communications to mobile users. The two best known networks [1] are Motorola's ARDIS network, which operates at 4.8 kb/s and Ericsson's RAM network which provides a data rate of 8 kb/s.

(iii). **Paging/Messaging Systems:** These are one way systems permitting short messages to be transmitted to a given user. High power base stations are used to reach mobile units, which can provide long usage time from low power batteries.

(iv). **Cordless Telephones:** Cordless technology was first developed in the 1970s to permit a telephone user to move around a room or building whilst making a call. A number of standards have since been developed, such as the European digital CT2 and DECT protocols [3], to alleviate the problem of illegal handsets; applications have also extended to data transmission and telepoint networks. In Singapore and Hong Kong, cordless telepoint networks have been a commercial success, providing a low power alternative to cellular systems.

(v). **Satellite Systems:** A few satellite communications networks currently exist, including Qualcomm's OMNItracs messaging system, which employs spread spectrum techniques. A number of proposals for satellite personal communication systems are currently being pursued. Most of these technologies also employ spread spectrum techniques, with the exception of Motorola's IRIDIUM network [4]. These systems are intended to provide cellular coverage in areas of low population density: however problems of low system capacity along with severe propagation losses due to shadowing from buildings, mountains, etc. may challenge the economic viability of these systems.

(vi). **Cellular Radio Systems:** Historically, cellular radio was the first means by which mobile telephony could be provided. These systems may be characterised by high power and high complexity base stations and mobile radios: these points are a necessity when providing adequate high mobility coverage in a variety of environments. The signal processing requirements of modern digital cellular systems are such that most of the handset hardware is devoted to these tasks.

The next section will look in more detail at cellular systems and standards, in particular at the methods used to permit a large number of users to communicate simultaneously.

1.2 Cellular Telephony

In order for a number of radio handsets to communicate simultaneously with a base station, their signals must be separated in some way. There are four well known methods to do this:

(i). **Frequency Division Multiple Access (FDMA):** This method permits a number of users to operate simultaneously by allocating each transmitter a separate radio frequency (RF) carrier or channel. The carriers are spaced sufficiently apart to prevent mutual interference occurring.

(ii). **Time Division Multiple Access (TDMA):** In this case all users transmit using the same RF carrier(s), but are allocated a unique time slot during which they alone may transmit.

(iii). **Code Division Multiple Access (CDMA):** All users transmit over the same RF carrier(s) and may transmit at the same time. Each user is identified by a unique code which is used to increase the bandwidth of the data transmission.

(iv). **Space Division Multiple Access (SDMA):** All users may transmit using one or more of the above protocols. Users operating simultaneously at the same RF frequency may be separated at the receiver according to their spatial location. Antenna array receivers are the most common method to exploit SDMA in practical analogue and digital networks.

The first cellular networks, such as the American advanced mobile phone service (AMPS) and the European total access communications system (TACS) employed analogue FDMA. Each user was allocated a different radio frequency (RF) channel for transmission, so that the number of channels specified system capacity. However, the efficiency of these systems, in terms of the traffic carried per unit of area and bandwidth, was low. In order to improve the situation, a second generation of cellular systems employing digital voice coding were developed, such as the European GSM system and the US IS–54 standard. These systems employ a combination of FDMA and TDMA access protocols to accommodate more users than analogue systems.

There are a number of cellular networks currently in use around the world, based on conflicting standards. To give an impression of the current situation, the networks in use in Europe and America will be discussed below:

(i). **Europe:** Two types of analogue network are currently used in Europe: TACS (in the UK, ETACS) operates in the 800–900 MHz RF band and the nordic mobile telephone (NMT) networks which operate at the 450 and 900 MHz bands. Digital networks have been introduced recently and the GSM system is successfully operated in the 900 MHz band across Europe. Each user generates a coded voice data sequence of 22.8kbps; training sequences and guard bands are then added. Eight users are time–multiplexed to give a total data rate of 270.833kbps, which can be susceptible to severe multipath propagation and inter–symbol interference: the training sequences are therefore needed for equalisation purposes. A modified version of GSM has been specified for the 1800 MHz band under the name DCS–1800. Two DCS-1800 networks have been successfully launched in the UK and it is also deployed in Germany.

(ii). **America:** The analogue AMPS network, operating in the 800–900 MHz band, is pre–eminent across America. In the United States, IS–54 compatible digital networks have recently been introduced in the AMPS bands. This system is upwardly compatible with AMPS and employs

the same channel data rate of 30 kHz. In 1993, the Telecommunications Industry Association (TIA) released the IS–95 standard, which specifies a CDMA scheme based on spread spectrum technologies: however, this system has yet to be deployed in the US. Licences to operate 1800 MHz band networks in areas across the US have recently been auctioned by the federal communications commission (FCC). The accompanying equipment standards are currently being processed by a joint technical committee of the TIA – there are seven systems being assessed, which are based on IS–54, IS–95 and cordless technologies [5].

Faced with this somewhat chaotic situation, the International Telecommunications Union (ITU) is attempting to define the nature of communications services in years to come, through the future public land mobile telecommunications systems (FPLMTS) programme. In Europe, research into this field is being co–ordinated under the title universal mobile telecommunications systems (UMTS) [6, 7]. The UMTS programme envisages an unified standard for cellular, cordless, paging, private mobile radio and low rate WLANs. The data rate may vary from 1 kb/s up to 2 Mb/s; the link quality will inevitably vary according to the prevailing propagation conditions, but must meet the requirements of the particular application.

In Europe, research into spread spectrum and CDMA techniques for the UMTS air interface is focussed around the code division testbed (CODIT) [8]. A number of data rates up to 128 kb/s are being implemented: initial results comparing CODIT with a rival TDMA testbed (ATDMA) suggest that CDMA may have a slight advantage for cellular applications [9]. Spread spectrum techniques in general are the subject of considerable research – see, for example, the proceedings of the IEEE 3rd international symposium on spread spectrum techniques and applications (ISSSTA) '94, held in Oulu, Finland. Two recent issues of the IEEE Journal on Special Areas in Communications, May–June 1994, were also devoted to the subject. Further discussion of this topic will be deferred to Chapter 2.

SDMA techniques as such are not new: dual antenna space diversity techniques are commonly used in cellular systems. However, the use of larger antenna arrays to properly exploit SDMA have only been considered more recently [10, 11]. A paper proposing passive source location techniques for cellular systems [12] appears to have been the pre–cursor to renewed interest in SDMA for cellular systems. Researchers have considered SDMA techniques for TDMA systems such as IS–54 [13] and for CDMA systems [14, 15]. A US company, called Arraycomm, has been formed specifically to design SDMA networks for cellular systems. Qualcomm, the company which developed the IS–95 standard, is also funding research into SDMA techniques for their CDMA system [16]. In Europe, as part of the UMTS programme, research is being conducted into SDMA techniques under the name TSUNAMI [17].

1.3 Summary of Main Research Areas

The main topic of this thesis is the operation of an antenna array receiver for spread spectrum signals. There are a number of ways to operate such a system, but for this work a bearing estimation architecture has been adopted. The signal processing task breaks down into two main areas: firstly, determining the bearings of the incoming signals and secondly, picking out the desired signal components whilst

suppressing interference. The purpose of this exposition is to look at the algorithms involved and to determine the performance improvements that might be obtained from this approach. A specific application of this receiver to locating the position of a spread spectrum transmitter in an urban environment is also considered.

There are a very large number of algorithms documented in the literature which perform the task of passive bearing estimation. From the available techniques, the MUSIC algorithm was selected as it provides good resolution without excessive computational complexity. However, this algorithm is known to perform poorly in the presence of coherent multipath signals. A simple solution exists to overcome this problem, spatial smoothing, but at the expense of reducing the effective size of the antenna array. The performance of such techniques is of considerable interest and will be studied in this thesis. Algorithms to estimate the number of signals present, in conjunction with the necessary degree of spatial smoothing, are also considered. This is because the performance of MUSIC is often poor, unless the correct underlying model order is known.

The bearing estimation techniques described in this thesis may be used to provide SDMA capability in a cellular radio system. The improvement in capacity offered by such an approach is of interest and has been the subject of considerable research recently. The capacity improvement available for simple channel models will be considered, because closed form solutions are obtainable. The results obtained by such methods provide only a simple approximation and more realistic channel models must also be considered. The performance of antenna arrays under such conditions will provide a more useful guide to how they can be successfully operated in cellular systems.

High frequency (HF) multipath channels have been exploited for many years to provide a source location ability. If the angles of arrival of multipath components from a desired microwave source in an urban area can be determined, analogous techniques may be developed for finding the transmitter's position. The feasibility of such an approach will be considered in this thesis.

1.4 Thesis Structure

After this brief introduction, Chapter 2 will describe spread spectrum and antenna array techniques in more detail. The operation and behaviour of spread spectrum systems are described – more details of CDMA schemes, such as IS–95, are also presented. The second half of this chapter is devoted to antenna array systems. An introduction to the wide variety of algorithms available for operating such receivers is provided. Techniques devised specifically for spread spectrum systems will also be considered.

Chapters 3 and 4 will move on to look at the operation of the MUSIC algorithm for performing bearing estimation. Chapter 3 concentrates on the subject of model order techniques for estimating the number of signals impinging on an antenna array. These algorithms are required in order to ensure that the proper operation of the MUSIC algorithm. Spatial smoothing techniques are needed for situations where coherent multipath components are present. It is possible to adapt model order algorithms to estimate the model order and the best degree of smoothing simultaneously: asymptotic results are presented for

the analysis of such an approach.

The topic of chapter 4 is bearing estimation algorithms. A number of techniques are introduced, including the MUSIC algorithm. The performance of MUSIC is discussed in more detail and the subject of spatial smoothing techniques is considered. The operation of MUSIC with spatial smoothing in multipath environments is an important practical concern. Complex equations are available for the performance of MUSIC with spatial smoothing: these are discussed with reference to the structure of the data covariance matrix. Simulation results are also presented to back up the analysis.

Chapter 5 will focus on the performance of bearing estimation receivers placed in the base stations of cellular systems. A simple line–of–sight channel is considered, along with the assumption of perfect power control. Results for the performance of CDMA systems are presented and modified for the case of antenna array receivers. Theoretical and simulation results are presented for the case of single cell antenna array receivers. There is also some discussion of antenna array systems operating in multi–cell CDMA systems.

Chapter 6 will look at the performance of cellular radio systems in more complex multipath environments. Realistic channel models for antenna array systems are described, extending previous research in this area. Two different types of channel model are then discussed in more detail. Initially, a point source multipath channel is considered, with results obtained for the bit error ratio performance. Initial simulation work for the case of multiple CDMA transmitters is also described. Secondly, the effect of multipath components with a finite angular spread is considered, with a view to the effectiveness of bearing estimation receivers in such situations.

In chapter 7, an algorithm to perform source location in a multipath environment is described. The performance of this technique is of great importance and has been analysed through a first order Taylor series expansion. Theoretical and simulation results are then presented to show the strengths and weaknesses of the algorithm. A modification of the MUSIC algorithm for locating multipath components in bearing and in time delay is described, in order to improve the accuracy of time delay estimates. A method for locating a source without information about the local environment is also presented.

Finally, Chapter 8 will draw conclusions from the work that has been described in this thesis. There is discussion of the achievements and limitations of the results obtained. Suggestions for relevant further work are also presented.

Chapter 2

Spread Spectrum and Adaptive Array Techniques

Spread spectrum communications and adaptive array techniques are two disparate examples of technologies that were originally developed with military applications in mind. Spread spectrum techniques provide a low power method of communication that is difficult to intercept or to jam. Adaptive arrays provide a means of nulling out undesired interference while still receiving a desired radar or communications signal. However, the end of the cold war and the resulting peace dividend has driven researchers in both fields to look for applications in the civilian sector. The increasing demand for universal mobile communications and the availability of fast, powerful VLSI technology means that spread spectrum and adaptive array techniques are now at the forefront of current research. This chapter will divide into two main parts, dealing separately with spread spectrum and adaptive array techniques respectively. The section on adaptive arrays will focus on mobile communications where possible, particularly where spread spectrum techniques are also applied.

2.1 Spread Spectrum Communications

The first spread spectrum systems to be devised appear to have been driven by a desire for improved accuracy in ranging systems. Radar techniques became the subject of serious research in the late 1930s leading to a forward–looking patent obtained in 1938 by Gustav Guanella of Brown, Boveri and Co, Switzerland [18]. This specified the idea of performing ranging by a wide–bandwidth signal, with the receiver using advanced synchronisation techniques to pick out signal returns. During the war, a patent was also taken out for a frequency–hopping system to guide torpedoes [19].

The foundation of modern statistical communication theory was laid down in the work of Claude Shannon [19], exemplified in the Hartley–Shannon theorem. This specified the channel capacity C_C, in terms of system bandwidth B_C Hz and signal to noise ratio SNR as follows:

$$C_C = B_C \log_2(1 + \text{SNR}) \tag{2.1}$$

The channel capacity may be thought of as the maximum possible data rate of any theoretical system. Shannon's work employed random signalling and he noted that maximum capacity would be obtained by a noise–like waveform with uniform power spectral density across the bandwidth B_C. Within a few

years, many of the familiar spread spectrum techniques had been developed, mostly in secret for the US Department of Defence. In 1949, John Pierce suggested the idea of asynchronous code division multiple access (CDMA) [19]. In the early 1950s, direct–sequence spread spectrum techniques were first developed under the the title of noise modulation and correlation (NOMAC). A hardware prototype of this technique was called the F9C and in 1956, Price and Green developed the concept of the now ubiquitous RAKE filter [20] to improve communication over multipath high frequency (HF) channels. For a more detailed survey of the early history of spread spectrum technology, which was mainly of a military nature, the reader is referred to [18, 21, 22] and the recent update [19].

In more recent times, spread spectrum has been used in the tracking and data relay satellites system (TDRSS), which was utilised for communications between the space shuttle and ground control, via two geostationary satellites [23, 24]. CDMA techniques are used in the US military's global positioning system (GPS) [23, Chapter 13] [25, Chapter 8], which is now accessible to civilian users. There are 18 GPS satellites in orbit, placed such that anyone on earth may always access at least 4 satellites. The satellites transmit Gold codes which may be used to calculate the relative delays to each satellite and hence determine the position of the GPS radio [23]. The US military has also developed the joint tactical information distribution system (JTIDS) [23] and the single channel ground and airborne radio system (SINCGARS) [26], both of which employ spread spectrum techniques.

Before proceeding to discussions on spread spectrum systems, the term itself must be defined. The method of [27] will be followed here, because of its simplicity. Define the Shannon bandwidth of a signal, B_s, as the bandwidth of the minimum signal–space representation of the baseband data stream. The Fourier bandwidth B_f may defined as the bandwidth of the transmitted signal representing the data stream. Any modulation scheme for which B_f is much greater than B_s may be considered to be "spread spectrum". Strictly speaking, this definition includes time division multiple access systems, but they will not be considered here: for more information see [28]. Other systems which comply with this definition will now be discussed.

2.2 Spread Spectrum Techniques

There are a number of methods by which the baseband data stream $d(t)$, of bandwidth B_s, may be converted to a transmission signal with a much larger bandwidth B_f. Four such techniques will now be considered:

(i). **Direct Sequence Spread Spectrum(DS–SS):** This technique operates by modulating the data sequence $d(t)$ by a pseudo-random code $c(t)$, whose period is equal to that of the data sequence t_s. In its simplest form, the code $c(t)$ is a long string of $+1$ and -1 *chips*, with chip period t_c. The resulting baseband signal, $t_x(t)$ is transmitted at the appropriate radio frequency (RF). At the receiver, the RF signal is downconverted to baseband to produce the signal $r(t)$. This is multiplied by the code $c(t)$ to produce the post–correlation signal $y(t)$, from which the original data sequence may be estimated. This process is illustrated in figure 2.1. The *processing gain* W of a DS–SS system may be defined as the length of the PN code, i.e. the ratio of the symbol period to the chip

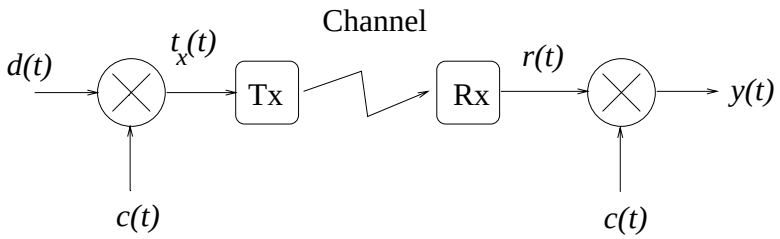

Figure 2.1: *A typical direct–sequence spread spectrum system.*

period, i.e. t_s/t_c.

(ii). **Frequency Hopping Spread Spectrum(FH–SS):** This technique employs a number of separate RF carriers for transmitting the data sequence $d(t)$ [29, Part 2,Chapter 2]. The signal is transmitted on different carriers at different times, under the control of a PN code which must be known to both transmitter and receiver. A simple example of a frequency hopping signal is shown in figure 2.2. The data itself is superimposed on to this signal by frequency or phase shift keying modulation.

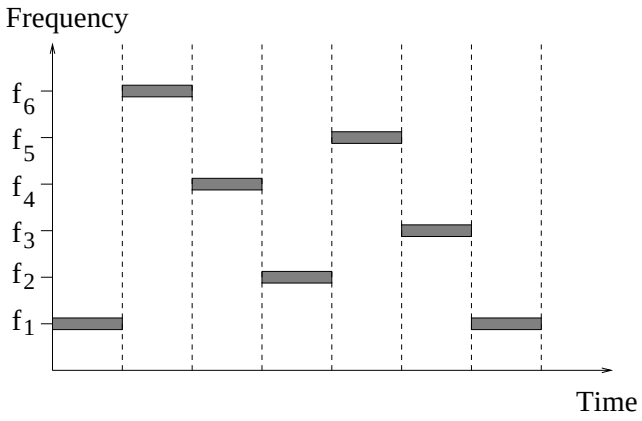

Figure 2.2: *A pattern of frequency hops for a DS-FH system.*

(iii). **Multi Carrier Spread Spectrum (MC–SS):** In contrast to frequency hopping, here the data is simultaneously transmitted on a number of narrowband carriers [30]. Using this concept to transmit over multipath channels is an old one, but there has recently been interest in using orthogonal carrier waveforms to permit multiple–access communication. In order to allow a number of users to transmit on the carrier frequencies, each user employs a different PN code which is transmitted in parallel across the carriers [31].

(iv). **Time Hopping Spread Spectrum (TH–SS):** The approach is similar to FH–SS systems, except that the transmission time is divided into blocks of time slots. In each block, the transmitter is active in only one time slot, chosen according to a pseudo–random code. This type of system is much less common than the other three.

For a more thorough review of spread spectrum techniques, see [25, 29, 32, 33]. In this thesis, DS–SS systems will be considered, so the rest of this section will focus on the advantages and operational characteristics of such systems.

2.2.1 Advantages of Direct Sequence Spread Spectrum

If a communications system employs DS–SS modulation, there will inevitably be an increase in hardware and general complexity. However, such systems have a number of benefits to compensate for this [25, 29]:

(i). **Lower Transmit Power:** The Hartley–Shannon theorem indicates the same capacity is achieved by DS–SS systems with a lower transmit power density (measured in Watts per Hertz) compared to narrowband systems. The processing gain quantifies the reduction of power that can be tolerated. If a system employs a PN code of length 100, it has a processing gain of 20 dB. This means that if the receiver requires 10 dB SNR for acceptable performance, the PN code may be received at a level of -10 dB.

(ii). **Military Applications:** Spread spectrum systems were originally developed with military applications in mind. Transmitting long PN codes ensures that communications links are harder to eavesdrop. In addition, DS–SS has some immunity, specified by the processing gain, to narrowband jammers present in the same RF bandwidth. For more detailed discussions of the performance of jammed DS–SS systems, see [29].

(iii). **Accurate Time Resolution:** Most spread spectrum receivers employ correlation detection of the desired code $c(t)$. The auto–correlation function (ACF) of most PN codes is similar to that of white noise, and a typical code auto–correlation function is shown in figure 2.3. The ACF

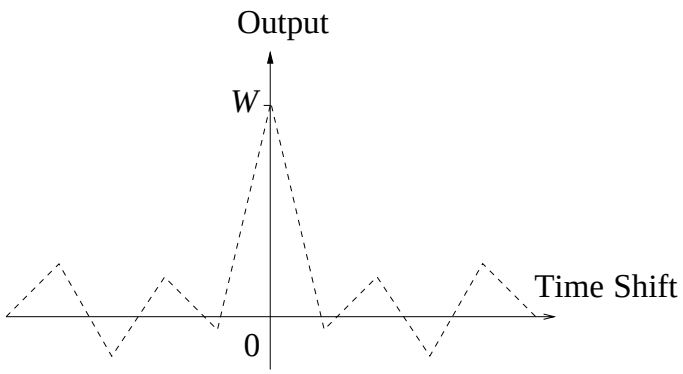

Figure 2.3: *A typical PN code auto–correlation function.*

shown in figure 2.3 takes non–negligible values only within one chip of the arrival of the code. This property means that spread spectrum techniques have been widely adopted for navigation purposes, including GPS.

(iv). **Multipath Capability:** The ability of DS–SS receivers to locate the arrival of the desired code in time makes them ideal for operation in severe multipath environments. A simple example of an urban channel and the associated channel impulse response is shown in figure 2.4. The form of the

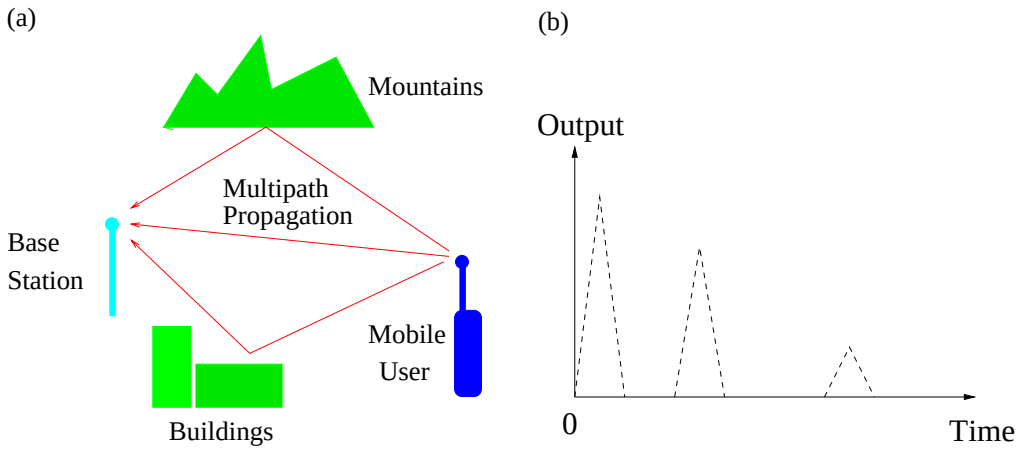

Figure 2.4: *(a) A typical urban multipath environment (b) The channel impulse response to a transmitted DS-SS code, measured at the output of the PN code correlator receiver.*

code ACF means that multipath components with time delays of greater than one chip period t_c may be separately resolved. Channel sounding devices employing PN codes with very small chip periods have been frequently used for measuring the multipath characteristics of communication channels [34–36].

(v). **Code Division Multiple Access (CDMA):** The current generation of European digital mobile telephones, based on the GSM and DCS–1800 standards, employ time and frequency division multiple access techniques. However, future mobile networks may achieve increased capacity by employing DS–SS techniques [37, 38]. In the United States IS–95 standard, a number of users may transmit on the same RF bandwidth by employing different PN codes to separate out their transmissions [39]. In this system interference from other users appears as benign background noise; as the number of active transmitters increases, the quality of each communication link degrades gracefully. The precise nature of such a multiple–access system is currently the focus of considerable research.

The format of DS–SS CDMA schemes will now be considered.

2.2.2 Code Division Multiple Access

In this multiple access scheme for mobile communications, all active mobiles in the system transmit at the same frequency. Each user can be identified by a unique PN code which is used only to modulate their data, prior to transmission. Similarly, all users receive information from the communications network at the same frequency, again with unique codes assigned to each user. There are a number of families of

codes which can be used to identify each transmission. The properties of such codes are discussed fully in [29, 40], however three of the most well known code sets are:

(i). m**–sequences:** These codes are generated using linear feedback shift register generators (LFSRG) [41]. If a length l generator is used to determine the code, the code itself will be of length $W = 2^l - 1$. One example of such a generator is shown in figure 2.5. The periodic ACF – defined

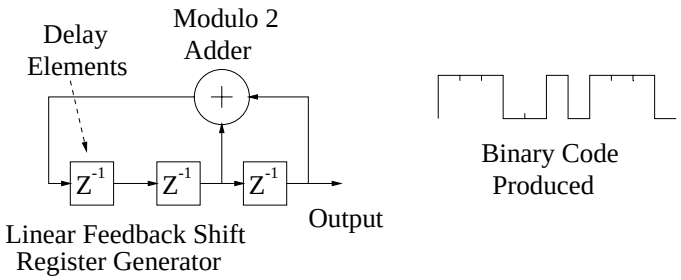

Figure 2.5: *A linear feedback shift register generator for binary m–sequences.*

as the correlation of the code with a periodically repeating copy of itself – of any m–sequence is two valued for integer chip shifts of the code. If the code shift is zero, the ACF takes the value W, otherwise it is -1. Unfortunately, if the code is modulated by data, the odd ACF occurs when the code undergoes a change in phase (e.g. from $+1$ to -1) during the correlation operation. In this case, the odd ACF can take larger magnitude values, causing self–noise interference to the receiver. The major difficulty with using m–sequences for CDMA is that there are relatively small numbers of them for a given length W: for example there are only 60 m–sequences of length 1023.

(ii). **Gold codes:** Gold code sets [42] are commonly used because so many more codes are available than for m–sequences. A total set of $W + 2$ codes is generated by the modulo–2 addition of a preferred pair of m–sequences of length W, using different integer shifts between the codes [42]. For example, if the two m–sequences are denoted as length W vectors $\boldsymbol{v}_1$ and $\boldsymbol{v}_2$, the complete Gold code set $G(\boldsymbol{v}_1, \boldsymbol{v}_2)$, containing $W + 2$ codes, is formed as follows:

$$G(\boldsymbol{v}_1, \boldsymbol{v}_2) = \{\boldsymbol{v}_1, \boldsymbol{v}_2, \boldsymbol{v}_1 \oplus \boldsymbol{v}_2, \boldsymbol{v}_1 \oplus T\boldsymbol{v}_2, \boldsymbol{v}_1 \oplus T^2\boldsymbol{v}_2, \ldots, \boldsymbol{v}_1 \oplus T^{L-1}\boldsymbol{v}_2\} \tag{2.2}$$

where $\oplus$ denotes modulo–2 addition and $T^k\,\boldsymbol{v}_2$ denotes the cyclic left–shift of $\boldsymbol{v}_2$ by k places. The periodic auto– and cross–correlation functions of the codes take on only three levels, with the maximum cross–correlation levels lower than the maximum possible for a pair of m–sequences of the same size. However, odd auto– and cross–correlations involve a larger number of possible values and may take on amplitudes much greater than for periodic correlations.

(iii). **Walsh codes:** Walsh or Hamadard codes of length 2^n represent the 2^n orthogonal basis functions over the finite alphabet ± 1 [43]. These codes may be used to provide orthogonal synchronous multiple channels. However, the asynchronous auto– and cross–correlation functions can take very high amplitudes.

The general operation of a CDMA cellular system will now be considered in more detail. System considerations break down into two main parts: (1) the reverse link from the mobile to the network base station and (2) the forward link from the base station to the mobile. This section will begin with the reverse link.

2.2.3 The Reverse Link

A simple block diagram of the reverse link, from the mobile to the base station, is shown in figure 2.6. Each mobile transmits to the base station over the same RF bandwidth, but using a different PN code

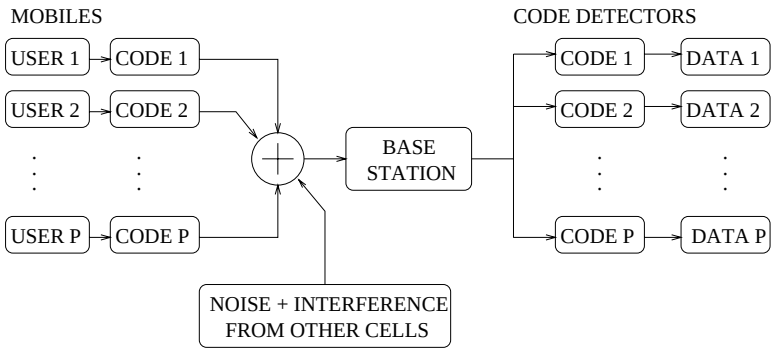

Figure 2.6: *A block diagram of the reverse link of a DS–SS CDMA System.*

(numbers 1,2,...,P) to distinguish its transmissions. One of the main difficulties with the reverse link is that it usually operates in an asynchronous fashion, which means that the levels of periodic and odd cross-correlation interference are unpredictable. A related problem is the near–far effect: if a mobile close to the base station transmits with the same power as one far away from the base, the signal from the former will swamp that of the latter.

In order to minimise the near–far problem, CDMA systems must employ power–control of the received signal. Such a system operates to ensure that the total received power from each mobile is the same. The system overhead involved in power control schemes is very large, so there has been considerable research into devising receivers which are more robust to power control errors. One method is to employ multi–user receivers which simultaneously decode all users transmissions: a tutorial on these techniques is given in [44]. Alternatively, the receiver may attempt directly to cancel CDMA interference, based on the received signal for each user [45, 46]. However, the performance improvement of such receivers in cellular CDMA systems may be limited when complete frequency re–use in all cells is applied. In this case, there are high levels of un–cancellable interference from other cells [39] – for a uniform distribution of users throughout an urban cellular system, interference from other cells has been calculated at 33% of the total CDMA cross–correlation interference.

One mechanism to reduce interference from other users is for each mobile to transmit only when the user is speaking, which has been shown to be about 40% of a total telephone conversation time. The

distribution of each user's transmissions means that this permits an increase in system capacity of only a factor of two [47]. An additional capacity increase may be obtained by reducing the size of each cell in the system, albeit at the cost of increased base station hardware. A common technique is to divide a circular or hexagonal cell into 3 sectors [48], each providing 120^o coverage of the original cell. This provides an increase in total capacity of about 3 times.

2.2.4 The Forward Link

The general layout of the forward link, from the base station to the mobiles, is shown in figure 2.7. Frequency division duplex (FDD) is often specified for CDMA systems, so that the forward link is

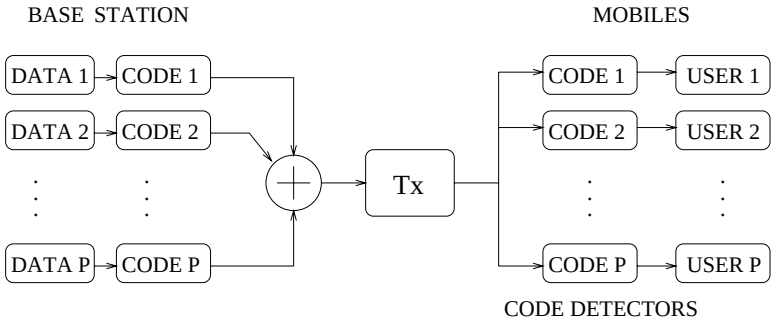

Figure 2.7: *A block diagram of the forward link of a DS–SS CDMA System.*

transmitted over a different RF band to the reverse link. The transmission of data to the mobiles is similar to system operation on the reverse link, except that each user's code is transmitted synchronously with the same power. This means that interference effects may be controlled more easily and there is no near–far problem in this case. The main difficulties occur at the border of cells, where there is strong interference from nearby cells. This may be overcome by increasing the transmit power to any mobile affected in this way, at the expense of mobiles closer to the base station.

2.2.5 The IS–95 Standard

In 1993, the US company Qualcomm, in association with a number of national service providers and international equipment suppliers, presented the draft IS–95 standard for mobile cellular CDMA systems. For a more detailed analysis of IS–95, see [37–39, 49, 50]. The essential points of the system described therein follow closely the discussion of the forward and reverse link system operation above. However, there are additional points which will not be strictly followed in this thesis, but which are worth mentioning.

(i). **Reverse Link Modulation:** A voice coder generates binary data at a rate of 9600 bits/s, which is encoded using a rate 1/3 convolutional code to protect against random errors. The output

data stream of 28.8 kbits/s is interleaved to protect against burst errors due to multipath effects. The output signal is grouped into blocks of 6 bits, which are encoded using 64–ary modulation. The output signal of 307 kbits/s is multiplied by a user–specific long PN code to give a signal bandwidth of 1.2288 Mbits/s. This signal is transmitted using filtered–offset QPSK, with the I and Q channels modulated by system specific codes of length 2^{15}. A dual–diversity receiver is used at the mobile for receiving on the reverse link.

(ii). **Forward Link Modulation:** The operation of the forward link is similar to the reverse link, except that a rate 1/2 convolutional code is used to give a coded data stream of 19.2 kbits/s. This signal is interleaved and modulated by the user–specific PN code without increasing the signal data rate. The output data rate is upconverted to 1.2288 Mbits/s by using a user–specific Walsh code. The resulting signal is transmitted using filtered QPSK, with the same I and Q codes used as for the reverse link. The users' transmissions are accompanied by a pilot signal which typically uses 10–20% of the total transmission power, in order to permit coherent demodulation at the mobile.

(iii). **Power Control:** In order to achieve strict power control on the reverse link, the mobile estimates the received power from the base station as a first estimate of the path–loss over the communications channel. The base station also transmits power up/down instructions to the mobile at a rate of 800 Hz. This arrangement is therefore a major control overhead for such a CDMA system.

(iv). **Soft Handover:** Where a mobile is on the border of two cells, both base stations may transmit to it with the same code as the receiver employs a RAKE filter to combine multipath energy coherently. This permits performance improvements for such mobiles. On the reverse link, the network selects the base station which receives the largest signal power level from the mobile.

(v). **System Capacity:** In theory, any multiple access scheme which employs a total bandwidth of W Hz should be as good as any other. However, the advantages of spread spectrum systems, such as lower power consumption, multipath capability, etc. make up for the disadvantages such as the necessity for power control. Complete frequency re–use and the asynchronous nature of CDMA techniques provide some capacity advantage over existing TDMA systems.

2.3 Antenna Array Architectures

Having introduced the subject of spread spectrum and CDMA techniques, the second half of this chapter will move on to discuss antenna arrays. There are a number of reasons for employing multiple antenna receivers, three of which are as follows:

(i). **Directional Capability:** If radio wave signals are received by an array of two or more suitably spaced antennas[1], it is usually possible to infer the bearings of the transmitters. This technique is frequently exploited in passive listening and sonar applications.

[1] Strictly speaking, the plural of antenna is antennae. However, the word antennas will be used in line with its frequent occurrence in the work of American researchers.

(ii). **Interference Suppression:** If a desired signal is corrupted by an interferer arriving from a different direction, antenna arrays may be used to filter out the interference. This principle has been used widely in military radar and communications applications. Recently, there has been considerable interest in antenna array techniques for mobile radio, as they can increase the capacity of such systems. The idea of suppressing interference from interfering transmitters in this way is often called space division multiple access (SDMA).

(iii). **Space Diversity Techniques:** A standard technique for combatting severe multipath effects on communications channels is to employ multiple receivers. Provided the antennas are sufficiently spaced, the probability of error is considerably reduced.

The techniques by which these points may be exploited using antenna arrays will now be discussed in much more detail. To begin with, mathematical models for describing the behaviour of antenna arrays will be introduced.

2.3.1 The Narrowband Channel Model

In this thesis, the narrowband antenna array model [51] will be used. The following assumptions are commonly made in its development:

(i). There are one or more transmitters operating at or near a specified radio frequency, denoted as f.

(ii). The received signal at each antenna element is corrupted by spatially and temporally white Gaussian noise of zero mean and variance σ^2.

(iii). All the transmissions are narrowband, in the sense that the Fourier bandwidth B_f of the signal is much smaller than the carrier frequency f.

The narrowband assumption is justifiable even in the case of IS–95 type spread spectrum systems, because the Fourier bandwidth is roughly 1.25 MHz while the carrier frequency is roughly 900MHz.

In order to progress further, the geometry of the antenna array must be specified. There are many ways of arranging the antenna elements, but probably the most widely known configuration is the uniform linear array (ULA). In order to avoid grating lobes, which are analogous to spatial aliasing effects, the antennas are spaced along a line at distances of $\lambda_C/2$ - half the carrier wavelength. A diagram of a typical ULA is shown in figure 2.8. The *steering vector* of an M–element ULA, $\boldsymbol{a}(\theta) \in \mathbb{C}^{M\times 1}$, is the impulse response of the array to a source at bearing θ and is given by:

$$\boldsymbol{a}(\theta) = [1, \exp\{j\pi\cos(\theta)\}, \ldots, \exp\{j(M-1)\pi\cos(\theta)\}]^T \tag{2.3}$$

where $\boldsymbol{a}^T$ denotes the vector transpose operation. The advantage of this configuration is its simplicity. However, linear arrays cannot separately resolve signals coming from opposite sides of the array:

moreover, they suffer from *endfire effects* because of the cosine terms present in equation (2.3). The Brandwood derivative vector $\boldsymbol{d}(\theta)$ [52] of the steering vector is calculated by taking the derivative of each entry with respect to θ. For $\theta = 0^o, 180^o$, the derivative vector takes large values, indicating that measurements of source transmissions at or near these bearings are very sensitive to noise. The array designer will usually ensure that signals arrive only from one side of the array, and that the endfire regions are blocked. The array configuration shown in figure 2.8 will be used throughout this thesis.

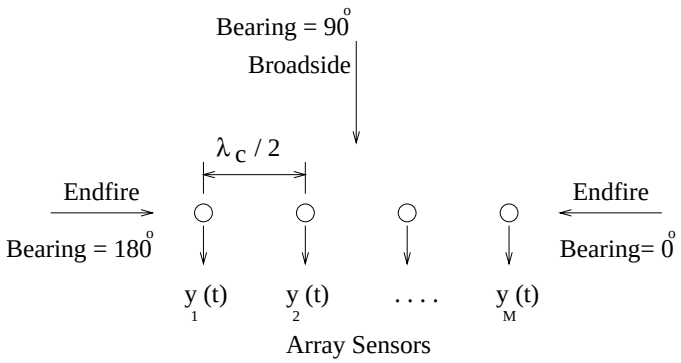

Figure 2.8: *The uniform linear array (ULA) configuration.*

Assuming that the received RF signal at each antenna is downconverted to baseband, it is possible to write the received signal vector $\boldsymbol{y}(t) \in \mathbb{C}^{M \times 1}$ as the following linear form:

$$\boldsymbol{y}(t) = [y_1(t), y_2(t), \ldots, y_M(t)]^T = \boldsymbol{A}\,\boldsymbol{s}(t) + \boldsymbol{n}(t) \tag{2.4}$$

There are K signals impinging on the array, whose amplitudes $\{s_k(t)\}$ are specified by the $K \times 1$ vector $\boldsymbol{s}(t)$. The matrix $\boldsymbol{A} \in \mathbb{C}^{M \times K}$ contains the column steering vectors for the K signals and $\boldsymbol{n}(t) \in \mathbb{C}^{M \times 1}$ contains the additive white Gaussian noise present at each antenna. A large number of array processing techniques are based on the covariance matrix $\boldsymbol{R}$ of $\boldsymbol{y}(t)$, which is defined as follows:

$$\boldsymbol{R} = E[\boldsymbol{y}(t)\boldsymbol{y}^H(t)] = \boldsymbol{A}\boldsymbol{S}\boldsymbol{A}^H + \sigma^2\boldsymbol{I} \tag{2.5}$$

The matrix $\boldsymbol{S}$ is the covariance matrix of the signal vector $\boldsymbol{s}(t)$ and $\boldsymbol{I}$ denotes the identity matrix. The notation $\boldsymbol{A}^H$ denotes the Hermitian transpose of the matrix $\boldsymbol{A}$. The matrix $\boldsymbol{X} = \boldsymbol{A}\boldsymbol{S}\boldsymbol{A}^H$ is often termed *positive semi-definite*, because it has K positive eigenvalues and $M - K$ zero eigenvalues. Performing the eigenvalue decomposition of $\boldsymbol{R}$, the following is obtained:

$$\boldsymbol{R} = \boldsymbol{U}_s(\Lambda_s + \sigma^2 I)\,\boldsymbol{U}_s^H + \sigma^2\boldsymbol{E}_n\boldsymbol{E}_n^H \tag{2.6}$$

The matrix $\boldsymbol{U}_s \in \mathbb{C}^{M \times K}$ denotes the K eigenvectors corresponding to the non–zero eigenvalues of $\boldsymbol{X}$. The matrix $\Lambda_s \in \mathbb{C}^{K \times K}$ is diagonal and contains the positive eigenvalues of $\boldsymbol{X}$, ordered according to

the eigenvector matrix $\boldsymbol{U}_s$. Collectively, the eigenvectors $\boldsymbol{U}_s$ are often called the signal subspace. The matrix $\boldsymbol{E}_n \in \mathbb{C}^{M \times M-K}$ contains the $M-K$ eigenvectors corresponding to the zero eigenvalues of $\boldsymbol{X}$. These eigenvectors are collectively called the noise subspace; as the eigenvalues are all equal to σ^2, the eigenvectors are not uniquely defined.

An extremely important property of the covariance matrix is that the columns of the noise subspace matrix $\boldsymbol{E}_n$ are all orthogonal to the columns of the steering vector matrix $\boldsymbol{A}$. This fact is often exploited by array processing algorithms, such as the MUSIC bearing estimation algorithm [53]. In practice, only a finite number of data samples $\{\boldsymbol{y}(t)\}$ are available, so that the covariance matrix can only be estimated approximately. If the receiver still wishes to exploit the orthogonality property of $\boldsymbol{A}$ and $\boldsymbol{E}_n$, correctly estimating the rank of $\boldsymbol{X}$ becomes of paramount importance. If K is underestimated, the orthogonality property no longer holds, so that the performance of subsequent algorithms will be poor. Fortunately, techniques such as Akaike information theoretic criterion and the minimum description length [51] exist to perform the rank estimation task – further discussion of these techniques is presented in chapter 3.

There are a large number of techniques for processing the signal vector $y(t)$. Some of the more important techniques are reviewed in this chapter, grouped under three main categories: (1) bearing estimation and adaptive beamforming techniques, (2) Wiener filtering and (3) blind channel estimation approaches. The first category of algorithms is explicitly based on the structure of the steering vector $\boldsymbol{a}(\theta)$.

2.3.2 Bearing Estimation and Adaptive Beamforming

This approach makes the assumption that the number of impinging signals K is less than the array size M. In this case, it is often possible to identify the signal bearings $\{\theta_k\}$ using a bearing estimation technique; further discussion of these algorithms will be deferred until chapter 4. The most common scenario is that the receiver has correctly identified a desired signal $s_1(t)$ arriving from bearing θ_1, and is subject to interference by multipath or other transmissions which arrive from other directions.

To estimate the form of the desired transmission, it is possible to apply a *data–independent* beamformer to the received signal [54]. The estimate of the desired signal $s_1(t)$ is given by the vector inner–product $\boldsymbol{a}^H(\theta_1)\boldsymbol{y}(t)$, where $\boldsymbol{a}^H$ denotes the Hermitian transpose. This technique is simple to compute and provides the optimal solution in the presence of additive spatially white noise. However, this technique may degrade in the presence of strong directional interference, as shown in part (a) of figure 2.9.

If the bearings of interfering signals are known, it is possible to design a filter $\boldsymbol{w}$ to place nulls in these directions, as shown in part (b) of figure 2.9 . There are a number of methods to perform this task, but one of the simplest is to minimise the quantity $|\boldsymbol{C}^H\boldsymbol{w} - \boldsymbol{f}|^2$ where $|\boldsymbol{f}|$ denotes the magnitude of the vector $\boldsymbol{f}$. The matrix $\boldsymbol{C}$ contains the column steering vectors for which the designer wishes to specify the beamformer response and the entries of $\boldsymbol{f}$ specify that response. The solution to this problem is simply given by:

$$\boldsymbol{w} = (\boldsymbol{C}\boldsymbol{C}^H)^{-1}\boldsymbol{C}\boldsymbol{f} \tag{2.7}$$

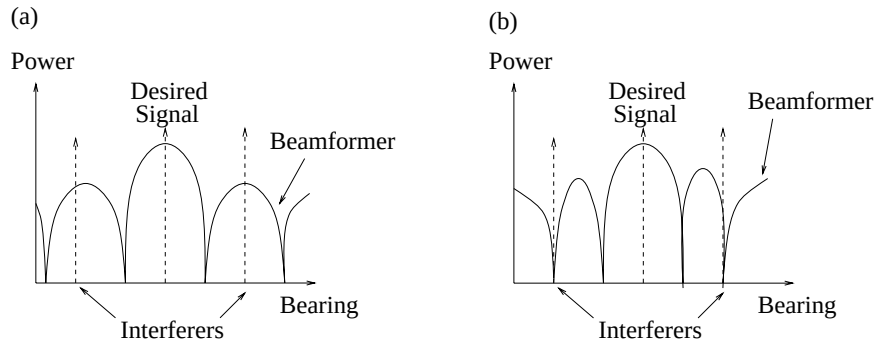

Figure 2.9: *Comparison of (a) the steering vector beamformer and (b) the adaptive beamformer.*

where $\boldsymbol{C}^{-1}$ denotes the matrix inverse of $\boldsymbol{C}$. The design of the beamformer must be performed carefully: placing nulls close to the desired signal leads to an ill-conditioned problem. This may result in a beamformer which is very sensitive to noise or interference from other directions. It is also possible to widen the main lobe of the beamformer by setting the derivative constraint $\boldsymbol{d}(\theta_1) = 0$. This is a useful condition for situations where the bearing of the desired signal is known only imprecisely.

This technique does not take account of the structure of the interference present in the data. In order to take advantage of the form of the received signal, it is possible to employ data–dependent, statistically optimum beamforming techniques. There are a large number of these [54–56], but one of the best known is the linearly constrained minimum variance (LCMV) technique due to Frost [57]. This technique minimises the output power of the beamformer, subject to the constraints $\boldsymbol{C}^H w = \boldsymbol{f}$. This problem can be solved by the method of Lagrange multipliers to obtain:

$$w = \boldsymbol{R}^{-1}\boldsymbol{C}[\boldsymbol{C}^H\boldsymbol{R}^{-1}\boldsymbol{C}]^{-1}\boldsymbol{f} \tag{2.8}$$

where $\boldsymbol{R}$ is the mean covariance matrix of $y(t)$, as defined in equation (2.5).

Statistically optimum techniques require accurate estimation of the desired signal parameters: otherwise, cancellation of the desired signal may occur. A second difficulty occurs when the interference is highly correlated with the desired signal, which can be due to so–called "smart jamming" or multipath propagation. Again, this may lead to cancellation of the desired signal: cures for this problem include moving arrays [58] or the spatial smoothing technique [59].

In order to apply statistically optimum techniques to actual data, where the underlying signal may be changing over time, it is common to employ adaptive algorithms. There are three well known techniques which may be employed:

(i). **Least Squares (LS) Estimation:** This algorithm operates by solving the weight equation, such as equation (2.8), directly. If N snapshots of the data vector $y(t)$ are available, the covariance

matrix $\boldsymbol{R}$ is estimated using:

$$\hat{\boldsymbol{R}} = \frac{1}{N}\sum_{i=1}^{N} \boldsymbol{y}(t_i)\boldsymbol{y}^H(t_i) \tag{2.9}$$

where t_i denotes the time at which the i^{th} snapshot was sampled. The matrix $\hat{\boldsymbol{R}}$ may also be used in a bearing estimation algorithm to determine the form of the constraint equation $\boldsymbol{C}^H \boldsymbol{w} = \boldsymbol{f}$. In the context of radar applications, least squares is sometimes called sample matrix inversion (SMI). The convergence performance of this algorithm, in terms of the number of snapshots N, is independent of the eigenvalues of the covariance matrix $\boldsymbol{R}$.

(ii). **Recursive Least Squares (RLS) Algorithm:** It is possible to derive an adaptive form of the least squares approach, which employs an exponential forgetting factor to de-emphasise past data.

(iii). **Least Mean Squares (LMS) Algorithm:** This algorithm has a much simpler form than the RLS algorithm, providing considerably reduced complexity. This algorithm estimates the maximum gradient towards the least squares solution at each step, and employs a weighting factor μ to control the change in the weight vector w. Unfortunately, the value of μ is bounded by the eigenvalues of R, so that convergence to the true weights can be much slower than for the RLS approach.

For a much more comprehensive discussion of adaptive algorithms and their performance, see [55,56,60].

The application of beamforming techniques to mobile communications appears to be quite recent. One of the first papers to consider antenna arrays for mobile communications was [12]. Bearing estimation techniques were proposed in order to determine the spatial locations of users within a given cell. Optimal beam patterns could then be defined to provide coverage across the cell, for both reverse and forward links. A later conference paper presented some results from a hardware trial [61], which demonstrated that bearing estimation techniques could locate a mobiles' position with reasonable accuracy, even in urban areas.

A simple scheme, using data independent spatial filters for both reverse and forward links, is discussed in [62]. The reverse link of an adaptive beamforming scheme was described in more detail in [63] and [64], where a bearing estimation algorithm was used to locate the bearings of each user. An adaptive beamformer was applied to the received signal to cancel interference from other users. Reference [63] also combined coherent multipath components from each mobile to improve performance. However, simulation results from [63] demonstrate that spatial filter techniques degrade compared to Wiener filter techniques under conditions of severe multipath propagation, where signal components arrive from a wide spread in direction. One approach to applying spatial filters in multipath channels may be to apply a derivative constraint in the look direction, to widen the main lobe of the beamformer [65]. Adaptive beamforming algorithms have also been discussed for the forward link of narrowband cellular systems [66, 67], with nulls placed in the directions of other mobiles operating at the same carrier frequency. However, the potential capacity of this approach appears to degrade for severe multipath channels [67] – the only way to improve capacity appears to be to move to larger transmit array sizes. Further discussion of antenna arrays in multipath scenarios will be presented in Chapter 6.

2.3.3 Wiener Filtering

The adaptive beamforming approach provides an intuitive approach to the problem of operating an antenna array, based on geometric reasoning. However, beamforming techniques perform poorly in the presence of the coherent signals which often occur in multipath–rich environments. Moreover, modelling each signal as arriving from a single direction may be inadequate for urban mobile communications. In order to improve the situation, it is possible to formulate the problem in a more abstract fashion using Wiener filtering techniques.

The Wiener filter solution for the filter coefficients w are given by:

$$w = \boldsymbol{R}^{-1} r \tag{2.10}$$

where the $M \times 1$ vector r represents the mean cross-correlation between the received signal vector $y(t)$ and the desired scalar signal $s_1(t)$. The advantage of this technique is that the bearing(s) of the desired signal do not need to be known. However, in order to use equation (2.10), a reference signal is required to estimate the vector r.

The general operation of a Wiener filter structure for an antenna array communications system is shown in figure 2.10. The receiver operates by estimating the covariance matrix $\hat{\boldsymbol{R}}$ from the data. In order to

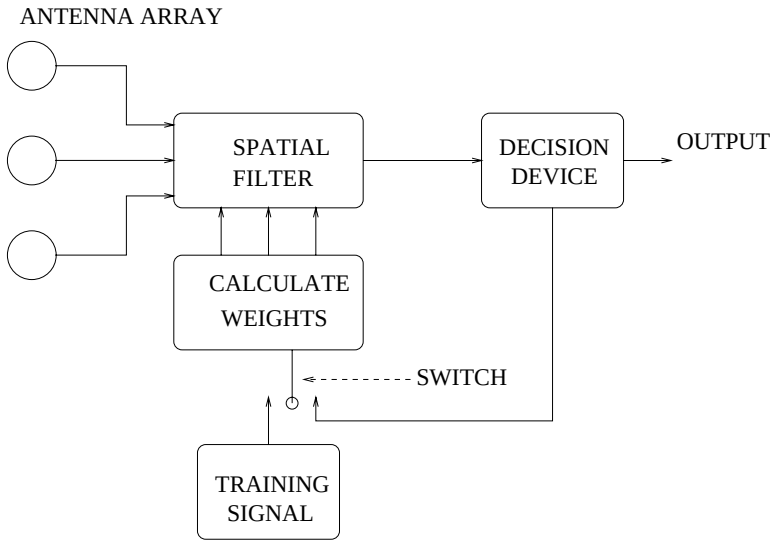

Figure 2.10: *The structure of a Wiener filter for an antenna array receiver.*

calculate the cross–correlation vector r, the receiver may use a training sequence or simply feedback the output data sequence. As with adaptive beamforming techniques, it is possible to employ LS, RLS or LMS algorithms to update the weight vector w.

One of the first papers to consider an adaptive array for a communications system was by Compton [68]. This system employed spread spectrum modulation and used the LMS algorithm to update the

weights of the spatial filter. The motivation for using antenna arrays in this case was the increased ability of the receiver to suppress interference from other sources, presumably in a military context. No training sequences were used, so the system used the post–correlation signal vector $y(t)$ for the reference signal. A similar system employing four phase modulation is described in [69] for military communications. In this case, a spread spectrum code of length $\approx$ 1000 chips is transmitted in the I–channel for synchronisation purposes: a much longer code of length $\approx 10^9$ is transmitted in quadrature for communicating the necessary data.

Spatial diversity is a standard approach for improving the quality of a communications link which suffers from fading effects due to multipath propagation. Two proposals for improving the performance of analogue cellular systems using space diversity are presented in [10, 70]. Wiener filter techniques are of interest in the design of antenna array receivers because they offer the ability to suppress interference from other transmitters as well as reducing fading effects. This point has been the subject of thorough research in several papers, beginning in [11]. This paper pointed out the diversity improvement that an antenna array may provide, particularly if the array spacing is large enough to obtain low signal correlation between antennas. There appears to be a trade-off between cancelling interference and diversity improvement: if the array cancels a large number of interferers, its ability to combat multipath fading is reduced [71]. The adaptive beamforming techniques described above are unable to cancel interference close to the desired signal, but with multipath fading, non–cancellable interference becomes a statistical phenomena.

A number of papers [11, 72–74] have employed a receiver structure similar to that of Compton, using decision feedback to provide the signal reference: the acquisition time of this array structure can be very long unless the desired signal SNR is large. A technique which employs knowledge of the desired signal bearing to reduce the convergence time [75] has been described. However, a more recent approach has been to take advantage of the new digital mobile communications specifications, such as the European GSM and American IS–54 systems. Both of these standards specify that data is transmitted in blocks, each with an accompanying training sequence. This sequence may be used to train the antenna array Wiener filter [13, 71], assuming that interference from other cells is asynchronous and uncorrelated with the training data. Once trained, the weights may be fixed or updated by decision feedback, according to the rate of change in the channel. Simulation results for an IS–54 system demonstrate that the LS technique is able to track fast channel variations much more effectively than the LMS algorithm [13]. In the case of the GSM system, results have shown the effectiveness of adaptive arrays in cancelling interference from a small number of users in other cells [76]. For slowly changing channels, the performance of the LMS algorithm appears to be better, although it may still be slightly inferior to the RLS or LS algorithms [77]. As a result, low complexity antenna array receivers, employing the LMS algorithm, have been proposed for indoor systems [78, 79].

In the UK, an 8–element antenna array system, using the European DECT cordless protocol, was constructed for a test program called SCARP. Some results from this work have been reported in [80] for a multipath environment, which demonstrates the ability of an adaptive array to improve the quality of a communications link. Following on from this, ERA Technology is co–ordinating a research program

called TSUNAMI which looks into adaptive array techniques for the European UMTS programme. The system to be tested is an 8–element array, again using the DECT standard, although this has been modified to include a training sequence for adaptive algorithms [17]. Three array configurations, linear, planar and circular, have been chosen for system testing in a number of indoor and outdoor environments. Early results suggest that adaptive arrays may permit considerable reductions in the time spread of multipath components in indoor environments, permitting increased data rates [81].

Adaptive array techniques based on Wiener filtering have been proposed recently for spread spectrum communications systems. However, as there are often a large number of co–channel users, usually exceeding the the number of elements in realisable adaptive arrays, interference cancellation techniques may not be so effective in this case [71]. An antenna array system for FH modulation has been proposed [82]: it looks ahead to the next carrier frequency, cancelling interference before the appearance of the desired signal. However, DS–SS systems have been discussed more frequently in connection with antenna arrays. One paper employs the receiver structure of Compton with a spread spectrum interference cancellation scheme to cope with signals arriving from the same direction [72]. A modification of the cancellation scheme to permit parallel cancellation of spread spectrum interference has been proposed [74]. The ability of spread spectrum techniques to resolve multipath components with different time delays means that spread spectrum antenna arrays may combine multipath energy in both time and space. A modified version of Compton's array, operating in such a manner has been proposed in [83]. More recently, adaptive antenna techniques have been proposed for umbrella cells in third generation CDMA cellular systems, to provide adequate coverage for areas in–between cells [84]. A colloquium paper by the same authors presents some results on the convergence time and beam patterns for a normalised form of the LMS algorithm [85]. A modified adaptive array receiver has also been proposed, which splits the baseband signal into two sub–bands, each of which is controlled by a separate adaptive algorithm [86].

2.3.4 Blind Techniques

The basic deficiency of Wiener filtering techniques is the requirement for a training signal to permit the receiver to obtain the correct spatial filter coefficients. Training sequences can become a significant overhead in any communications system, reducing its overall efficiency. Therefore, there has been considerable interest in using blind techniques which can identify the channel transmissions for a desired user without a training sequence. There are a number of approaches to this problem in the context of antenna arrays operating on the reverse link of a cellular system. Several of these techniques will now be discussed.

(i). **The Constant Modulus Algorithm (CMA):** This technique is a blind version of Wiener filtering techniques, which attempts to maintain a constant amplitude output for the received signal. This is a special case of the blind equaliser structures proposed by Godard [87]: it has been the subject of some debate, concerning whether it always achieves convergence – see [60, Chapter 21]. In any case, it appears to be one of the most widely used blind equalisers. A hardware CMA array

for use in a mobile has been implemented using the LMS algorithm [88]. Subsequent tests in an urban area demonstrated the ability of the array to pick out the strongest multipath and improve system performance in a fading multipath environment [89]. A system for successively cancelling a multi–user signal with a CMA array has been described in [90] – the form of the cancelled signal allowed its bearing to be determined.

(ii). **Oversampling Techniques:** The problem of correctly identifying and equalising minimum and non–minimum phase channels corrupted by inter–symbol interference is very difficult. In order to avoid problems with blind equalisers, recent approaches have focussed on correctly identifying the channel. Higher–order statistics have been used for channel identification because of their ability to recognise non-minimum phase channels. However, these techniques require long data sets to achieve satisfactory performance. Recently, 2nd order channel identification techniques based on oversampling the received signal have been discovered [91]. The oversampling may be achieved temporally or by using an antenna array. The original method relied on two cyclic covariance matrices, however a recent paper has shown how the technique may be implemented using one covariance matrix [92].

(iii). **Blind Source Separation:** A number of algorithms have been developed to distinguish statistically independent signals observed at antenna arrays [93–95]. These methods are based on the structure of 4^{th} order cumulants, which are normalised using the 2^{nd} order covariance matrix. An eigen–matrix decomposition may then be performed in order to determine the separate components present. As these algorithms normally employ higher–order statistics, large data lengths are required in order to obtain reliable results.

(iv). **Cyclostationary Approaches:** A cyclostationary signal exhibits the property of being correlated with a frequency shifted version of itself. Communications transmissions form an important set of cyclostationary signals and have been the subject of a number of techniques, most notably the SCORE algorithm [96, 97]. The cyclostationary property may be used to filter out undesired interference from other transmitters at different frequencies. This led to a proposal for an overlapping narrowband FDMA scheme, using the principal eigenvectors of cyclic covariance matrices to identify users operating at each frequency. A similar scheme has recently been proposed for IS–54 [98], which relies on phase differences between sources to obtain the K received signal waveforms for K sources.

(v). **Eigenfilters:** The use of eigenfilters to identify the received signal is particularly appropriate to the case of CDMA systems. This is because there is a desired signal with a reasonable SNR, which is corrupted by background interference from other users. The largest eigenvector of the post–correlation matrix $\boldsymbol{R}$ has been used to identify the form of a desired CDMA signal at a base station antenna array [99]. In order to suppress interference from other users, the covariance matrix of the pre–correlation signal is subtracted from $\boldsymbol{R}$: however, the effectiveness of this approach will depend on the cross–correlation values of the other codes present. This method has also been extended to the case of a multipath channel, where several multipath signals are resolved in time. In this case, the receiver operates in by applying J spatial filters – calculated from the

principal eigenvector method – to pick out J multipath components. These are then combined using a conventional RAKE filter, as shown in figure 2.11. A similar structure has been described

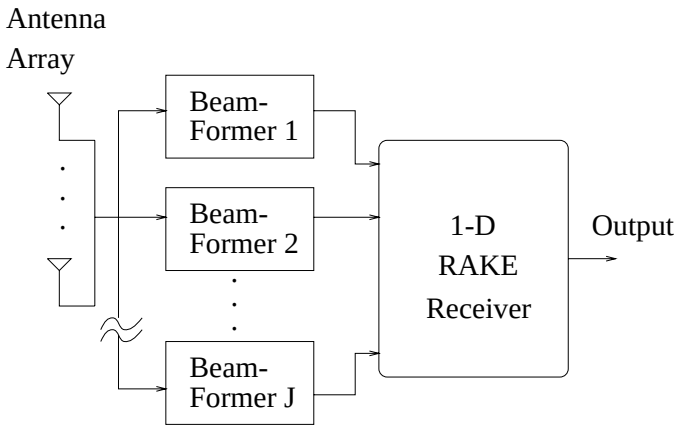

Figure 2.11: *The 2-D RAKE filter combiner (after [100]).*

for applying antenna array techniques to an IS–95 system [16]. However, the receiver requires additional hardware to employ the 64–ary decoders which are used on the reverse link.

The drawback of any blind identification technique is that the receiver has no direct means of ensuring that it has picked out the desired signal rather than undesired interference. This will be a particular problem where these techniques are operated in multi–user environments. The best solution to this problem, in the case of spread spectrum systems, is to ensure that all mobiles are subject to accurate power control so that multiple–access interference is minimised.

2.4 Conclusion

In this chapter, the topics of spread spectrum communications and adaptive arrays have both been introduced. These techniques were first developed for military radar and communications applications. However, there has recently been a trend to apply both techniques to mobile communications systems in order to provide increased capacity. In this thesis, direct–sequence spread spectrum techniques in combination with antenna array techniques will be analysed in more detail. In particular, bearing estimation techniques combined with fixed spatial filters will be of interest. To provide some comparison, eigenfilter techniques will also be studied for multipath channels.

Chapter 3

Signal Detection Techniques

This chapter describes how signal detection techniques may be used in an antenna array receiver. If it is intended to apply bearing estimation techniques such as MUSIC to measured data, the number of signals present must be known. Two information theoretic criteria for estimating the model order are introduced, along with a method for analysing their performance. These techniques fail in the presence of coherent signals, so a modified approach employing spatial smoothing is described. The results required to estimate the performance of such a scheme are then derived. Finally, there is a discussion on how these techniques may be extended to spread spectrum receivers.

3.1 Model Order Determination Techniques

High resolution bearing estimation techniques, such as the MUSIC algorithm [53] and maximum likelihood approaches [101] require an estimate of the number of signals impinging upon the antenna array. The first methods for estimating the number of received signals were based on subjective threshold testing, see for example the references in [102]. However, the performance of this approach is critically dependent on the selection of the threshold level used for determining the model order. This defect led researchers to the Akaike information theoretic criterion (AIC) and the minimum description length (MDL) approach of Schwartz and Rissanen [102]. These techniques produce a single objective result, so that no judgements on behalf of the system operator are needed.

Other techniques have been developed more recently, to improve upon the performance of the AIC/MDL. The original derivation contained a large number of superfluous parameters, so alternative criteria have been developed using only the covariance matrix eigenvalues [103], or by assuming the signals to be deterministic [104]. Methods have also been developed to improve performance for signals corrupted by coloured noise using two arrays [105] and for coherent signals [106] by performing a maximum–likelihood search over all possible signal bearings. However, in this chapter, attention will be restricted to the AIC and MDL criteria.

3.1.1 Signal Model

The signal model used here is simply that for a conventional narrowband system: discussion of the signal detection problem in the case of CDMA receivers will be deferred to the end of this chapter. The received signal is assumed to conform to the linear model of equation (2.4):

$$y(t) = \boldsymbol{A}\, s(t) + n(t) \tag{3.1}$$

where $y(t) \in \mathbb{C}^{M\times 1}$ corresponds to the received signal at an M–element array. The vector $s(t) \in \mathbb{C}^{K\times 1}$ denotes the K underlying signals received by the array, which are assumed to be zero–mean Gaussian white processes which are mutually independent and uncorrelated between samples. The vector $\boldsymbol{n}(t) \in \mathbb{C}^{M\times 1}$ represents the complex white Gaussian noise of zero mean and variance σ^2 corrupting the data. The matrix $\boldsymbol{A} \in \mathbb{C}^{M\times K}$ contains the K steering vectors $\boldsymbol{a}(\theta_k) \in \mathbb{C}^{M\times 1}$ that represent the impulse response of the array to the signal directions $\{\theta_k\}$. Note that it will be assumed that $K < M$.

The covariance matrix $\boldsymbol{R}$ of the vector $y(t)$ is given by equation (2.5):

$$\boldsymbol{R} = E[\boldsymbol{y}(t)\boldsymbol{y}(t)^H] = \boldsymbol{A}\boldsymbol{S}\boldsymbol{A}^H + \sigma^2\boldsymbol{I} \tag{3.2}$$

where $\boldsymbol{I} \in \mathbb{C}^{M\times M}$ denotes the identity matrix and $\boldsymbol{S} \in \mathbb{C}^{K\times K}$ denotes the covariance matrix of the vector $s(t)$. The notation $y(t)^H$ denotes the Hermitian transpose of $y(t)$. The matrix $\boldsymbol{X} = \boldsymbol{A}\boldsymbol{S}\boldsymbol{A}^H$ represents the signal covariance matrix and is of rank K: the term $\sigma^2\boldsymbol{I}$ is the covariance matrix of the spatially white noise. As the signal covariance matrix is semipositive, performing the eigenvalue decomposition of $\boldsymbol{R}$ produces two classes of eigenvalue/eigenvector pairs. The K largest eigenvalues and their eigenvectors are called the signal subspace, because the eigenvectors span the column space of the matrix $\boldsymbol{A}$. The other $M - K$ eigenvalues are of magnitude σ^2 and the eigenvectors are collectively termed the noise subspace. The i^{th} largest eigenvalue of $\boldsymbol{R}$ will be denoted λ_i.

In a practical situation, the array receiver has access to only a finite number of snapshots, N, of the received signal. It can therefore only estimate the covariance matrix $\boldsymbol{R}$, using the maximum–likelihood unstructured estimator $\hat{\boldsymbol{R}}$:

$$\hat{\boldsymbol{R}} = \frac{1}{N}\sum_{n=1}^{N} \boldsymbol{y}(t_n)\boldsymbol{y}^H(t_n) \tag{3.3}$$

The notation $\{t_n\}$ denotes the time at which the n^{th} snapshot of the received signal vector $y(t)$ was taken.

3.1.2 Information Theoretic Criteria

The AIC and MDL were first proposed as viable detection algorithms for the purpose of estimating K for the case of array processing in [102]. These techniques were developed in the general setting of determining the best fit from a number of possible parameterised probability distributions to a given finite length data sequence. In this case, the proposed distributions are simply semipositive matrices of rank k (representing the signal covariance matrix) added to scaled identity matrices (i.e. the noise

covariance matrix). An introduction to the resulting criteria is given in [102], but both criteria have the same general form:

$$f(k) = l(k) + w(k) \tag{3.4}$$

where $f(k)$ is the criterion, $w(k)$ is a penalty function and $l(k)$ is the following log-likelihood function:

$$l(k) = N \ln\{(\frac{1}{M-k} \sum_{i=k+1}^{M} e_i)^{M-k} / \prod_{i=k+1}^{M} e_i\} \tag{3.5}$$

where N denotes the number of snapshots used to form the estimated covariance matrix $\hat{\boldsymbol{R}}$, whose i^{th} largest eigenvalue is denoted as e_i. The penalty function has the form:

$$w(k) = \alpha(N)[k(2M-k)] \tag{3.6}$$

where $\alpha(N) = 1$ for the AIC and $\alpha(N) = \frac{1}{2}\ln(N)$ for the MDL criterion. The model order K is determined as the value of k for which $f(k)$ is minimised.

As an example of how the AIC and MDL criteria operate, a covariance matrix was generated for the case of a single source arriving from a bearing of 90^o with a signal–to–noise ratio at one antenna of 10 dB. There were 100 snapshots taken of the signal to form the covariance matrix, whose eigenvalues were: 80.211, 1.352, 1.212, 1.139, 0.974, 0.807, 0.668 and 0.569. The calculated values for the AIC and MDL are shown in table 3.1. It may be seen from the table that the minimum value for both the AIC and the

k	0	1	2	3	4	5	6	7
AIC	3057.103	89.896	99.838	109.025	112.333	116.167	121.290	126.000
MDL	1528.552	64.487	86.392	105.313	118.690	129.726	138.800	145.063

Table 3.1: *The values of the AIC and MDL criteria.*

MDL correctly occurs at a model order of 1.

3.2 The Performance of the AIC and MDL

The properties of these techniques have been thoroughly analysed for Wishart–distributed [107] covariance matrices, using two probability measures [108] :

(i). $p(A_1)$**, the probability of underestimating the model order by 1:** [1] This probability measure holds asymptotically for a Wishart–distributed covariance matrix composed from N independent snapshots. As a consequence it is assumed that the K^{th} eigenvalue e_K is asymptotically Gaussian distributed with mean λ_K and variance λ_K^2/N. The average noise subspace eigenvalue $\hat{\sigma}_n^2$ is independent of λ_K, with mean value $\sigma_n^2 = \sigma^2$ and asymptotic variance $\sigma^4/N(M-K)$. The probability $p(A_1)$ is simply given by:

$$p(A_1) = \int_{-\infty}^{\gamma} \exp\{-\omega^2/2\} d\omega \tag{3.7}$$

Details of the evaluation of γ are given in appendix B.

(ii). $p(A_2)$**, the probability of overestimating the model order by 1:** This parameter is significant mainly for the AIC criteria, which is known to have a finite probability of overestimating the model order, even for large values of N. The reader is directed to [108] for details of the calculation of this probability function.

As an example of the distributions obtained from calculating the probability $p(A_1)$, results have been obtained for two uncorrelated Gaussian distributed signals arriving at an 8–element uniform linear array (ULA) with bearings 90^o and 80^o. Both signals have the same SNR, which is defined to be that measured at one antenna. The distributions are shown in figure 3.1, along with a horizontal line representing $p(A_1) = 0.5$. Part (a) is calculated with N =100 and the SNR of both signals varied according to the horizontal axis. In part (b), the signals both have an SNR of -7 dB, and the value of N is varied from 10 to 500. Clearly, the performance of the MDL criterion in both cases is dependent on the threshold where $p(A_1) = 0.5$: where the signals' SNR or the value of N is below the threshold performance is very poor; above the threshold performance is good.

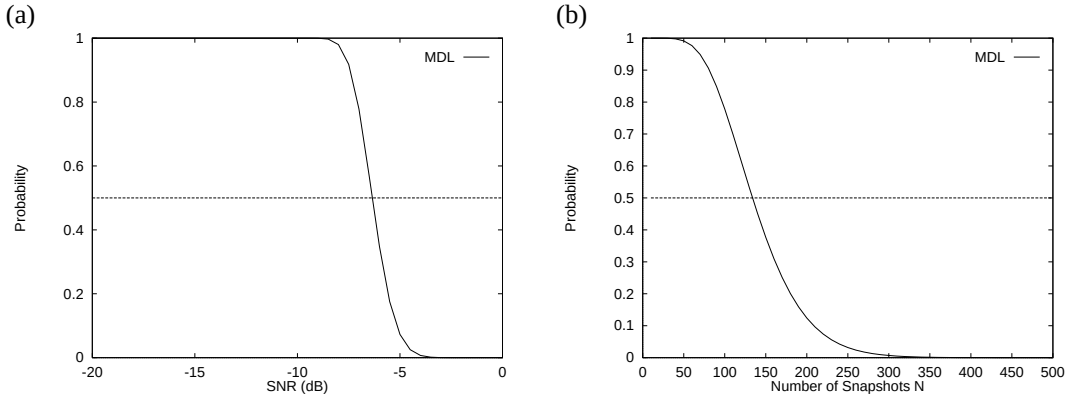

Figure 3.1: *The probability $p(A_1)$ plotted against (a) SNR of the two received signals (b) the number of snapshots N.*

In this chapter, consideration will be given to the MDL technique because it is a strongly consistent estimator [108]. However, it is also known to be over–penalised, so that the threshold $p(A_1) = 0.5$

[1] Strictly speaking, the probability measure $p(A_1)$ also includes the case where the value of the AIC or the MDL at $K-1$ and K are identical. This occurrence is also included in the definition of $p(A_2)$ for model orders K and $K+1$.

occurs at a higher SNR than for the AIC. Both the AIC and MDL perform satisfactorily when the incident signals seen at the array are approximately uncorrelated over the sample time used to form the covariance matrix $\hat{\boldsymbol{R}}$. However, if the signals are highly correlated, an alternative approach is required.

3.3 Coherent Signal Scenarios

3.3.1 Spatial Smoothing Techniques

If there is complete correlation between the K signals during the sampling period, the rank of the signal subspace reduces to 1. Under these conditions, the MDL or AIC criteria will underestimate the model order, which can seriously affect the performance of subsequent algorithms. In particular, the MUSIC algorithm requires correct model order estimates so that it can exploit the orthogonality of the noise subspace to the columns of the matrix $\boldsymbol{A}$. In order to solve this problem a procedure called spatial smoothing (SS) [59] was devised, by which a smaller covariance matrix $\boldsymbol{\Psi}$ of size $L \times L$ is formed from partitions of the covariance matrix $\boldsymbol{R}$. There are $H = M - L + 1$ partitions and $\boldsymbol{\Psi}$ is given by:

$$\boldsymbol{\Psi} = \frac{1}{H} \sum_{h=1}^{H} \boldsymbol{F}_h \boldsymbol{R} \boldsymbol{F}_h^T \tag{3.8}$$

where $\boldsymbol{F}_h^T$ denotes the transpose of $\boldsymbol{F}_h$. The matrix $\boldsymbol{F}_h$ is of size $L \times M$ and its i^{th} row and j^{th} column entry is defined by:

$$\boldsymbol{F}_h(i,j) = \begin{cases} 1 & \text{if } j = i + h - 1 \text{ and } 1 \leq i \leq L \\ 0 & \text{otherwise} \end{cases} \tag{3.9}$$

More recently, a modified smoothing technique called forward-backward spatial smoothing (FBSS) has been described and analysed [109, 110]. Given the covariance matrix $\boldsymbol{R}$, the forward backward covariance matrix $\boldsymbol{R}_{F/B}$ is formed as follows:

$$\boldsymbol{R}_{F/B} = \frac{1}{2}(\boldsymbol{R} + \boldsymbol{J}\boldsymbol{R}^*\boldsymbol{J}) \tag{3.10}$$

where $\boldsymbol{R}^*$ denotes the complex conjugate of $\boldsymbol{R}$. The matrix $\boldsymbol{J}$ is defined so that its p^{th} row and q^{th} column entry is zero unless $p = M + 1 - q$, whereupon it equals 1. The matrix $\boldsymbol{R}_{F/B}$ is then substituted into the spatial smoothing algorithm, in place of the matrix $\boldsymbol{R}$. This procedure can reduce the number of sub–arrays P, compared to spatial smoothing alone, so the performance of the MUSIC algorithm may improve.

The purpose of this algorithm is to incorporate spatial correlations into the covariance matrix and restore the full rank of the signal matrix $\boldsymbol{X}$. It is necessary to decide how many subarrays are to be used and

what the resulting model order will be. This may be achieved simply by applying the MDL criterion to every possible smoothed covariance matrix in turn [111]. The matrix or matrices with the highest model order may then be used in the MUSIC algorithm.

The MDL criterion is preferable to the AIC at high SNR values, because it is unlikely to over–estimate the model order of a given covariance matrix, so that the receiver is more likely to correctly find the covariance matrix or matrices with the largest model order. Thus, the algorithm presented in [111] extends the usefulness of the MDL technique to provide a general approach to estimating the model order of a given set of received data. It is flexible enough to cope with coherent signals and its only drawback is the additional computational burden. This algorithm requires all possible spatially smoothed covariance matrices to be calculated; in order to apply the MDL to each matrix, the eigenvalue decomposition of that matrix must be performed.

It is useful to be able to measure the performance of this approach with finite data, which can be estimated from the analysis of [108]. However, the statistics of the covariance matrix eigenvalues must be altered in line with the effect of spatial smoothing. The derivation of the appropriate equations will now be presented.

3.3.2 Asymptotic Eigenvalue Variances

The purpose of this subsection is to determine the first and second order statistics of the smoothed matrix eigenvalues. With this information, the results given in appendix B may be extended to determine the asymptotic behaviour of the MDL criterion under spatial smoothing. The effect of spatial smoothing on the eigenvalues of the covariance matrix $\hat{\boldsymbol{R}}$ is substantial. Denote the eigenvalues of $\hat{\boldsymbol{\Psi}}$ as z_i, $1 \leq i \leq L$ and the eigenvalues of $\boldsymbol{\Psi} = E[\hat{\boldsymbol{\Psi}}]$ as ζ_i. As before, the mean of an estimated eigenvalue is given by $E[z_i] \approx \zeta_i$. The variance of the eigenvalues is considerably more involved, however.

Provided that the rank of signal subspace for a smoothed covariance matrix is at least i, the asymptotic variance of the i^{th} eigenvalue may be calculated. It has been obtained by Pillai and Kwon in equations (A.18) and (A.33) of [109]:

$$E[(z_i - \zeta_i)^2] = E[\Delta\zeta^2] \approx \frac{1}{H^2 N} \sum_{x,y=1}^{H} \boldsymbol{u}_i^H \boldsymbol{F}_x \boldsymbol{R} \boldsymbol{F}_y^T \boldsymbol{u}_i \boldsymbol{u}_i^H \boldsymbol{F}_y \boldsymbol{R} \boldsymbol{F}_x^T \boldsymbol{u}_i \tag{3.11}$$

where $\Delta\zeta^2$ denotes the squared error in the estimate z_i and $\boldsymbol{u}_i$ denotes the i^{th} eigenvector of $\boldsymbol{\Psi}$. This expression is accurate to order $O(1/N)$, as are the other asymptotic mean and variance expressions given in this chapter.

The other requirement is to calculate the variance of the noise subspace eigenvalue estimate $\hat{\sigma}_n^2$. Unfortunately, the effect of spatial smoothing makes this much harder to calculate. The eigenvectors spanning the noise subspace of $\boldsymbol{\Psi}$ are not uniquely defined (unless $K = L - 1$) because the eigenvalues are all

equal to σ^2. However, the noise subspace projection matrix $\boldsymbol{Z}$ is always uniquely defined and is given by the equation:

$$\boldsymbol{Z} = \sum_{i=K+1}^{L} \boldsymbol{u}_i \boldsymbol{u}_i^H = \boldsymbol{I} - \sum_{i=1}^{K} \boldsymbol{u}_i \boldsymbol{u}_i^H \tag{3.12}$$

The expectation of $\hat{\sigma}_n^2$ may be therefore be obtained from the projection of $\boldsymbol{\Psi}$ onto $\boldsymbol{Z}$:

$$E[\hat{\sigma}_n^2] \approx \frac{1}{L-K} E[\text{tr}\{\boldsymbol{Z}\hat{\boldsymbol{\Psi}}\}] = \frac{1}{H(L-K)} \text{tr}\{\sum_{a=1}^{H} \boldsymbol{Z}\boldsymbol{F}_a \boldsymbol{R} \boldsymbol{F}_a^T\} \tag{3.13}$$

where tr$\{\}$ denotes the trace operation. This equation may be used to determine the variance of σ_n^2. Following [112], one may write that the error in σ_n^2, $\Delta\sigma_n^2$, is given by:

$$\Delta\sigma_n^2 = \hat{\sigma}_n^2 - \sigma_n^2 \approx \sum_{p,q=1}^{L} \frac{d\sigma_n^2}{d\boldsymbol{\Psi}_{pq}} \Delta\boldsymbol{\Psi}_{pq} \tag{3.14}$$

where the notation $\boldsymbol{\Psi}_{pq}$ denotes the p^{th} row and q^{th} column entry of the matrix $\boldsymbol{\Psi}$ and $\Delta\boldsymbol{\Psi}_{pq}$ the estimation error in that entry. By expanding equation (3.13) into a summation of products and taking the derivative with respect to $\boldsymbol{\Psi}_{pq}$, it is found that:

$$\frac{d\sigma_n^2}{d\boldsymbol{\Psi}_{pq}} = \frac{\boldsymbol{Z}_{qp}}{L-K} \tag{3.15}$$

It is well known that for an estimated covariance matrix $\hat{\boldsymbol{R}}$, the error terms $\Delta\boldsymbol{R}_{mn} = \hat{\boldsymbol{R}}_{mn} - \boldsymbol{R}_{mn}$ may be related by the according to the equation:

$$E[\Delta\boldsymbol{R}_{mn}\Delta\boldsymbol{R}_{pq}] = (1/N)\boldsymbol{R}_{mq}\boldsymbol{R}_{pn} \tag{3.16}$$

The corresponding error term present in the estimated spatially smoothed covariance matrix entry $\hat{\boldsymbol{\Psi}}_{pq}$, $\Delta\boldsymbol{\Psi}_{pq}$, may be expanded into terms involving $\Delta\boldsymbol{R}$:

$$\Delta\boldsymbol{\Psi}_{pq} = \frac{1}{H} \sum_{x=0}^{H-1} \Delta\boldsymbol{R}_{p+x,q+x} \tag{3.17}$$

Applying these results to equation (3.14), the asymptotic variance of $\hat{\sigma}_n^2$ is given by:

$$\begin{aligned} E[(\Delta\sigma_n^2)^2] &= E[\frac{1}{(L-K)}(\sum_{m,n=1}^{L} \boldsymbol{Z}_{nm}\Delta\boldsymbol{\Psi}_{mn})\frac{1}{(L-K)}(\sum_{p,q=1}^{L} \boldsymbol{Z}_{qp}\Delta\boldsymbol{\Psi}_{pq})] \\ &= \frac{1}{(H(L-K))^2} \sum_{a,b=0}^{H-1} \sum_{m,n=1}^{L} \sum_{p,q=1}^{L} E[\boldsymbol{Z}_{nm}\Delta\boldsymbol{R}_{m+a,n+a}\boldsymbol{Z}_{qp}\Delta\boldsymbol{R}_{p+b,q+b}] \end{aligned}$$

$$\approx \frac{1}{N(H(L-K))^2}\sum_{a,b=0}^{H-1}\sum_{m,n=1}^{L}\sum_{p,q=1}^{L}\boldsymbol{Z}_{nm}\boldsymbol{R}_{m+a,q+b}\boldsymbol{Z}_{qp}\boldsymbol{R}_{p+b,n+a}$$

$$= \frac{1}{NH^2(L-K)^2}\mathrm{tr}\{\sum_{a,b=1}^{H}\boldsymbol{Z}\boldsymbol{F}_a\boldsymbol{R}\boldsymbol{F}_b^T\boldsymbol{Z}\boldsymbol{F}_b\boldsymbol{R}\boldsymbol{F}_a^T\} \tag{3.18}$$

This result applies for any spatially smoothed matrix $\boldsymbol{\Psi}$. Where spatial smoothing has restored the full rank of $\boldsymbol{X}$, the noise subspace eigenvectors are always orthogonal to the steering vectors $\boldsymbol{a}(\theta_k)$ and it is possible to replace $\boldsymbol{R}$ by the matrix $\sigma^2\boldsymbol{I}$. These results provide the necessary statistics for the eigenvalue z_K and the value $\hat{\sigma}_n^2$ for the spatial smoothing case.

3.3.3 Modifications for Forward–backward Spatial Smoothing

The forward–backward matrix $\boldsymbol{R}_{F/B}$, defined in equation (3.10) has the property that $\boldsymbol{R}_{F/B} = \boldsymbol{J}\boldsymbol{R}_{F/B}^*\boldsymbol{J}$. This means that the eigenvalues of $\boldsymbol{R}_{F/B}$, c_i, may be expressed in terms of $\boldsymbol{R}_{F/B}$ and its eigenvectors $\boldsymbol{\psi}_i$ (ordered by decreasing eigenvalue):

$$c_i = \boldsymbol{\psi}_i^T\boldsymbol{R}_{F/B}^*\boldsymbol{\psi}_i^* = (\boldsymbol{\psi}_i^H\boldsymbol{R}_{F/B}\boldsymbol{\psi}_i)^T = \boldsymbol{\psi}_i^H\boldsymbol{J}\boldsymbol{R}_{F/B}^*\boldsymbol{J}\boldsymbol{\psi}_i \tag{3.19}$$

Equating terms in the above equation gives $\boldsymbol{\psi}_i^T = \boldsymbol{\psi}_i^H\boldsymbol{J}$ and $\boldsymbol{\psi}_i^* = \boldsymbol{J}\boldsymbol{\psi}_i$. This means that equation (3.19) may be expanded using equation (3.10) to give:

$$c_i = \frac{1}{2}\boldsymbol{\psi}_i^H(\boldsymbol{R} + \boldsymbol{J}\boldsymbol{R}^*\boldsymbol{J})\boldsymbol{\psi}_i = \frac{1}{2}(\boldsymbol{\psi}_i^H\boldsymbol{R}\boldsymbol{\psi}_i + \boldsymbol{\psi}_i^T\boldsymbol{R}^*\boldsymbol{\psi}_i^*) = \boldsymbol{\psi}_i^H\boldsymbol{R}\boldsymbol{\psi}_i \tag{3.20}$$

Equation (3.20) can also be applied to any spatially smoothed matrix derived from the matrix $\boldsymbol{R}_{F/B}$. This expansion of c_i in terms of $\boldsymbol{R}$ means that equation (3.11) may be used directly to calculate eigenvalue variance for the FBSS case. The only modification required is to insert the correct eigenvector $\boldsymbol{\psi}_i$ in place of $\boldsymbol{u}_i$. The same procedure applies for correctly evaluating equation (3.18).

The results provided in the last two subsections allow one estimate the performance of the MDL criterion with SS or FBSS applied. The modified equations from [108] may be evaluated for all values of H to determine which value of H will give the best ensemble mean performance for a given model order K. In practice, the most interesting cases are where the degree of spatial smoothing H has led to the full rank of the signal matrix $\boldsymbol{X}$ being restored. The evaluation of the probability $p(A_1)$ may therefore be limited to such cases.

3.3.4 The Conditional Signal Model

The equations so far have been derived for the case of signals which are uncorrelated between samples in time. This approximation is not realistic for communications channels, where time variations in the channel must be much slower than the symbol rate to permit satisfactory bit error ratio performance. In order to estimate the performance of the array receiver in this case, it is possible to use the conditional signal model.

The conditional signal model makes the assumption that the underlying signal does not change between realisations of the sample covariance matrix $\hat{\boldsymbol{R}}$. In this case, the variance of the *signal* eigenvalues is reduced considerably because the underlying signal is identical in all its realisations; the only perturbation to the estimated covariance matrices is due to background noise. Denote as η_K the K^{th} largest eigenvalue of the signal covariance matrix $\boldsymbol{X} = \boldsymbol{A}\boldsymbol{S}\boldsymbol{A}^H$ (or its spatially smoothed equivalent). The variance of the K^{th} eigenvalue becomes:

$$var_{cond} = \frac{N(var_{wish}) - \eta_K^2}{N} \tag{3.21}$$

where var_{wish} denotes the result of equation (3.11) in the case of a spatially smoothed covariance matrix. Alternatively, for an unsmoothed covariance matrix, the term $N(var_{wish})$ simply reduces to λ_K^2. These results may be substituted in the equations given in appendix B to estimate the detection probabilities for the conditional model. This model is useful as it permits the variance equations to be used for an arbitrary set of N signal vectors $\{s(t)\}$.

3.4 Results

In this section, numerical results are shown to illustrate the effect of the theoretical equations. In the particular scenario chosen, an 8-element ULA is receiving two perfectly correlated narrowband signals, whose bearings are 23^o and 45^o. Note that a bearing of 90^o indicates a signal arriving perpendicular to the array and that all the simulations have been performed using the conditional model. Both signals are complex exponentials which have the same signal-to-noise ratio (SNR), which is defined to be that measured at one sensor only. The reference sensor was chosen to be the end sensor at one side of the array and there was 0^o phase shift between the signals at that sensor. 100 snapshots of the received data were used to form the unsmoothed covariance matrix. Four partitions of the matrix were then used to form a spatially smoothed covariance matrix of size $L = 5$.

The smoothed signal subspace is of size 2, so the smaller signal eigenvalue determines the performance of the model-order selection algorithm [108]. The mean of this eigenvalue and the estimated noise eigenvalue $\hat{\sigma}^2$ are shown in figure 3.2. The theoretical values calculated from the matrix $\boldsymbol{R}$ are shown as lines and simulation results are shown as points. For each simulation point, 1000 Monte Carlo runs were undertaken.

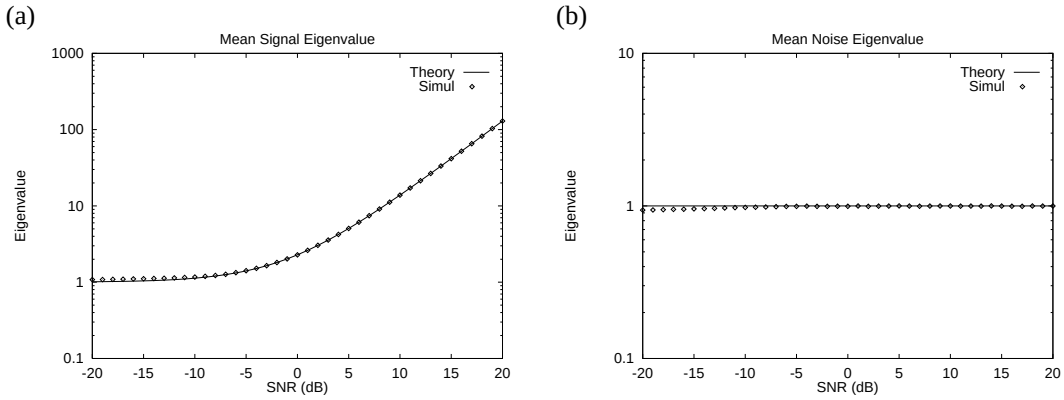

Figure 3.2: *The mean of (a) the second largest signal eigenvalue and (b) the parameter $\hat{\sigma}^2$ plotted against SNR.*

At reasonable SNR values, there is a good match between theory and simulation. However, at very low SNR the signal eigenvalue is larger than expected and the value of $\hat{\sigma}^2$ reduces. This is because the standard deviation of all the eigenvalues is comparable to the difference between the signal and noise eigenvalues. As a consequence, the signal and noise eigenvalues are subject to considerable correlation leading to the bias in the simulation results.

Figure 3.3 show the variance of the signal eigenvalue and of $\hat{\sigma}_n^2$. Again, there is good comparison between the results at reasonable SNR, but the results diverge at low signal power levels.

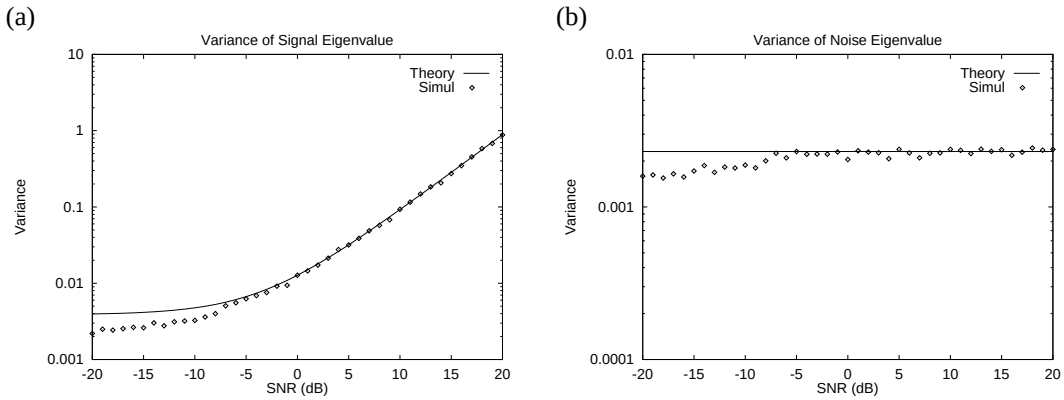

Figure 3.3: *Plots for the variance of (a) the second largest signal eigenvalue and (b) the parameter $\hat{\sigma}^2$ plotted against SNR.*

These results have been used to predict one measure of the performance of the MDL criterion, as shown in figure 3.4. The signal and noise eigenvalue variances have been used to calculate the probability of underestimating the model order, $p(A_1)$, using the equations from [108].

Figure 3.4 demonstrates that the variance equations have been successfully modified to predict the probability measure $p(A_1)$ for a spatially smoothed covariance matrix. In this case, the theoretical estimate of $p(A_1)$ is seen to be slightly pessimistic compared to the simulated results. This deviation occurs due to a slight bias in the eigenvalues at low SNR and low numbers of snapshots N. Correlations between the eigenvalues under these conditions can seem to improve the performance of the MDL

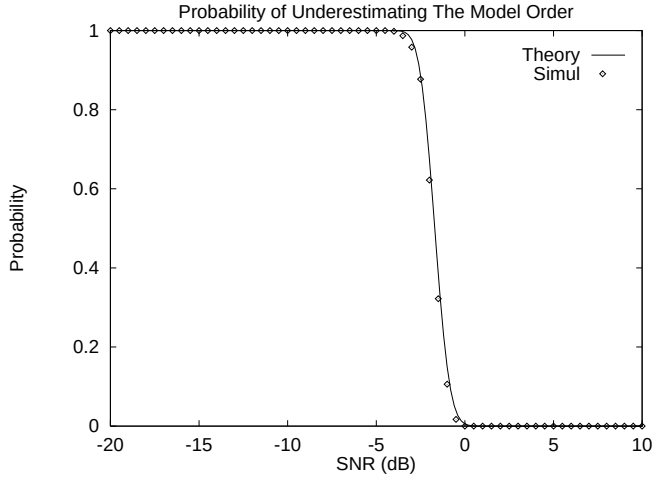

Figure 3.4: *The probability $p(A_1)$ of underestimating the model order for the MDL, vs SNR.*

criterion, but these effects are artificial. The theoretical results provide a more realistic measure of the SNR required to obtain adequate performance.

Next, some results are presented to confirm that the modifications derived for the forward-backward smoothing case are correct. The linear array used in this case had 10 elements, and forward–backward spatial smoothing was applied so that the smoothed matrix size was L =6. The number of snapshots was still 100 and the two correlated sources remained exactly the same as for figures 3.2 – 3.4. Figure 3.5 shows the mean and variance plots of the smaller signal eigenvalue for this scenario against SNR. From the results, there is a good match between the theoretical values and the simulation points at reasonable SNR values.

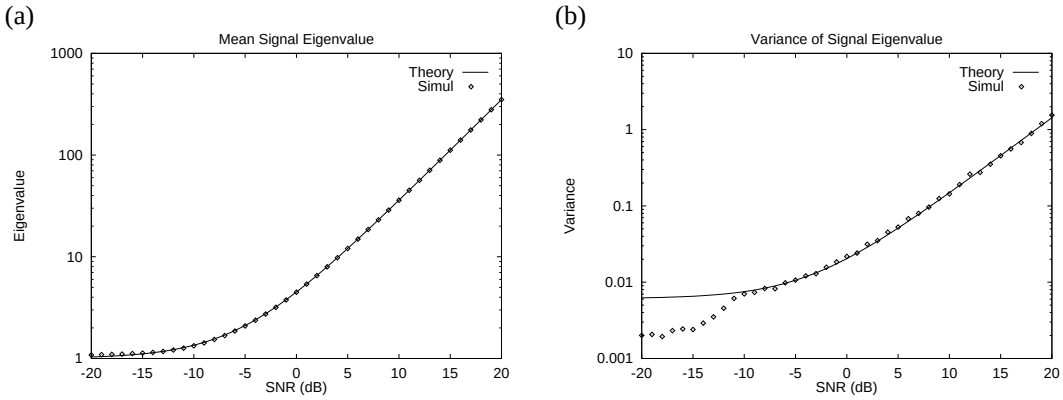

Figure 3.5: *Plots for (a) mean and (b) variance of the smaller signal eigenvalue vs SNR, using forward-backward smoothing.*

Finally, it is possible to evaluate the probability $p(A_1)$ for all possible smoothed covariance matrix sizes, L. This has been done for the case of two sources at bearings of 95^o and 120^o, with a phase shift of 120^o at the edge of the array. The antenna array size is 8, N =100 and the FBSS algorithm was used. The signals were assumed to be of the same SNR, coherent and to be generated by the conditional model. The results are shown in figure 3.6, plotting the signals' SNR against the smoothed matrix size H and the

probability $p(A_1)$. Comparing the results, it is possible to determine which value of L will produce the best performance at a given SNR: in this case, the curves suggest similar performance for all covariance matrix sizes $L > 4$.

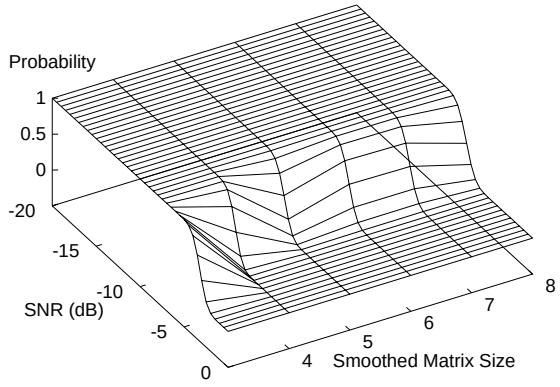

Figure 3.6: *The probability $p(A_1)$ for two coherent signals plotted against the signals' SNR and the smoothed matrix size L.*

All of these results have been calculated for signals with a fixed SNR. If the signals are known to follow a given probability distribution, it is possible to average the results over all signal phases and the relevant SNR values to obtain a measure of the overall system performance.

3.5 The Spread Spectrum Signal Acquisition Problem

The techniques described above may be applied to conventional narrowband communications systems, where the received signal is sampled in the I and Q channels once per symbol. However, in CDMA systems, the received signal has to be sampled W times over one symbol period for a length W spread spectrum code. The general form of a spread spectrum bearing estimation receiver is shown in figure 3.7. The received signal at each antenna is demodulated to baseband and passed through a matched filter for the desired PN–code. Before the receiver can begin to process the received data, it must apply signal detection techniques to the output of the matched filter for each of the W time slots of the PN–code.

The scheme by which the time slots are searched through depends on the bandwidth of the spread spectrum signal as compared to the detection processing rate of the receiver [113–115]. In early receivers, each slot was checked in turn (serial acquisition) in order to minimise the detection processing requirement. The penalty paid is the potentially large time delay to find a spread spectrum signal. In order to overcome this, one may employ parallel searches through a number of time slots simultaneously. For wide bandwidth spread spectrum signals, the computational complexity may be prohibitive, so that a hybrid scheme of searching serially through blocks of time slots is more attractive.

In order to check whether a signal is present in a given time slot, the received power may compared to a threshold power level. The level is set to maximise the probability of detecting a signal, whilst

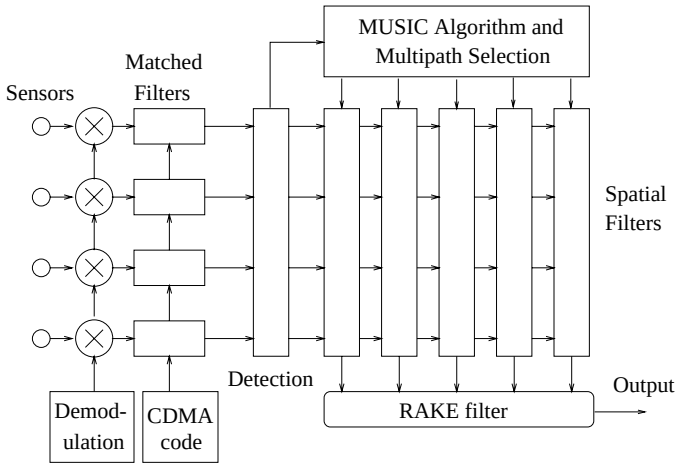

Figure 3.7: *The general form of a spread spectrum bearing estimation receiver.*

minimising false alarm probabilities [25][Chapter 6] [116]. In order to apply this technique to the received signal from an antenna array, one may average the power levels measured at each antenna element. If the receiver detects the presence of one or more signals in a given time slot, it is possible to proceed with signal acquisition procedures. In the case of the bearing estimation receiver array, this is the MDL algorithm applied to all possible smoothed matrices using SS or FBSS, so that coherent multipath signals may be separately resolved.

Once the model order algorithms have been applied to all the chosen time slots, the MUSIC algorithm may be applied to the data in time slots where multipath signals have been detected. This provides the receiver with the bearings of all the separately resolved multipaths which have been received. In order to determine which multipaths are to be used by the receiver for making a data decision, the bearings may be used to determine spatial filters for each multipath. The filter output measures the signal and noise power present at the given delay and bearing. This may be used directly as a rough SNR measurement, or it is possible to apply a threshold detector similar to those used in single antenna spread spectrum receivers [115, 116]. The receiver may therefore select only the multipath components with the largest SNR for decision making. One consequence is that over–estimating the number of significant multipath components, because of the occurrence of spurious peaks in the MUSIC algorithm's power density spectrum, is not a major problem. Discussion of how the multipath components are combined using a RAKE filter will be deferred to chapter 6.

The signal detection scheme may therefore be summarised as follows:

(i). Search through the W time slots.

(ii). Apply a power threshold to each slot to detect the presence of multipath signal energy.

(iii). Where a signal is detected, the following method is applied:

(a) Apply the MDL technique to all possible spatially smoothed covariance matrices. Select the

matrix with the largest number of signals.

(b) Apply the MUSIC algorithm to the chosen matrix, using the model order estimate, to find the multipath bearings.

(c) Estimate the signal power actually present at each multipath bearing.

(d) Select the signals with the largest SNR to be used in a RAKE filter for data symbol estimation.

An alternative method for CDMA signal synchronisation has been described in the literature. It makes no assumption concerning the form of the received signal, but instead it assumes that a CDMA signal is present in one of the time slots. The correct slot is chosen by looking for the minimum mean–squared–error Wiener filter across the time slots [117], or by using a maximum likelihood detector [118]. However, this type of approach is not particularly suited to the bearing estimation receivers described in this thesis.

3.6 Conclusion

This chapter has obtained theoretical results for the effect of spatial smoothing techniques upon the eigenvalues of the covariance matrix. These results are useful in analysing the performance of model-order selection criteria such as the AIC or MDL under spatial smoothing. Simulation results have shown a good match to the derived equations, except under conditions of low SNR and small numbers of snapshots. In these situations, the asymptotic estimates of the eigenvalues provide a better measure of the likely performance of the system. The application of these techniques to a CDMA receiver have also been discussed and a method described to detect the significant multipath components present in the received signal.

Chapter 4

Bearing Estimation Algorithms and Coherent Sources

This chapter will introduce the subject of narrowband bearing estimation algorithms and will discuss several of the most popular techniques. The MUSIC algorithm [53] has been chosen for further analysis, because 1) it provides a good compromise between complexity and resolution, 2) its operation is well understood. However, one of the main deficiencies of the MUSIC algorithm is its inability to correctly locate highly correlated or coherent sources.

One simple method for overcoming this problem is to employ spatial smoothing techniques [59, 110], which trade the size of the array for the ability to resolve coherent sources. In this chapter, two spatial smoothing techniques – spatial smoothing (SS) and forward–backward spatial smoothing (FBSS) – are evaluated to assess their relative performance. This is achieved by analysing the structure of the covariance matrix and by using equations for the asymptotic statistics of the bearing estimates. The results show that the performance of SS depends on the source bearings and angular separations[1] The FBSS technique can offer improved performance, depending on the relative phases of the source signals. Finally, other spatial smoothing techniques are briefly discussed.

4.1 Principles of Direction of Arrival Estimation

The purpose of direction of arrival (DOA) algorithms is to locate the bearings of a number of signals impinging on a multi–element antenna array. In this chapter, attention will again be focussed on the narrowband model described in section 3.1.1. All symbols are assumed to have the same meaning as in chapter 3, unless otherwise stated. The measured baseband signal vector at the receiver, $y(t)$, is given by equation (2.4):

$$y(t) = \boldsymbol{A}\, s(t) + n(t) \tag{4.1}$$

All the terms in this equation have the same meanings as in section 2.3.1. For the purposes of this chapter, the receiver is interested only in estimating the columns of the matrix $\boldsymbol{A}$, or equivalently the

[1] Both of these characteristics are important – endfire effects mean that sources arriving in that region require a larger angular spacing to be resolved than for sources in the broadside region (cf figure 2.8).

source bearings $\{\theta_k\}$. As the receiver contains an M–element uniform linear array (ULA), as shown in figure 2.8, the steering vector $\boldsymbol{a}(\theta)$ is given by:

$$\boldsymbol{a}(\theta) = [1, \exp\{j\pi\cos(\theta)\}, \ldots, \exp\{j(M-1)\pi\cos(\theta)\}]^T \tag{4.2}$$

There is a large number of bearing estimation algorithms documented in the literature, including: conventional beamforming [119], the minimum variance algorithm [120], the minimum norm technique [121], ESPRIT [122], MUSIC [53], weighted subspace fitting [123], as well as techniques based on higher–order statistics [124, 125] and on maximum–likelihood approaches [51, 101]. Most of the techniques based on second–order statistics employ the data covariance matrix $\boldsymbol{R}$, defined in equation (2.5):

$$\boldsymbol{R} = E[\boldsymbol{y}(t)\boldsymbol{y}(t)^H] = \boldsymbol{A}\boldsymbol{S}\boldsymbol{A}^H + \sigma^2\boldsymbol{I} \tag{4.3}$$

Bearing estimation algorithms directly exploit the structure of $\boldsymbol{R}$ to estimate the matrix $\boldsymbol{A}$, following similar procedures to those for spectral analysis. A subset of these techniques will now be discussed, highlighting issues of resolution and complexity.

(i). **Conventional Beamforming (CBF)**

This technique [119] operates in a similar manner to the discrete Fourier transform (DFT) with the output power density spectrum for bearing θ, $P_{CBF}(\theta)$, produced by the equation:

$$P_{CBF}(\theta) = \boldsymbol{a}^H(\theta)\boldsymbol{R}\boldsymbol{a}(\theta) \tag{4.4}$$

This technique provides an unbiased estimate of the observed power density at a given bearing: however, leakage effects due to finite array sizes mean that closely spaced sources cannot be separately resolved. To improve this, the same techniques can be applied to conventional beamforming as to the DFT, such as windowing the data, zero padding, etc. However, as with the DFT, the CBF algorithm provides a poor trade-off between the number of sensors and resolution [126], so that a number of better techniques have been devised.

(ii). **Minimum Variance Technique (MV)**

The problem with CBF techniques arises from beam pattern constraints: there is a trade-off between the sidelobe level and the width of the main beam. In this technique [120], the best possible beam pattern is chosen mathematically. It turns out that the minimum variance beam pattern involves calculation of the inverse of the covariance matrix. The resulting power density spectrum, $P_{MV}(\theta)$, is given by the equation:

$$P_{MV}(\theta) = \frac{1}{\boldsymbol{a}^H(\theta)\boldsymbol{R}^{-1}\boldsymbol{a}(\theta)} \tag{4.5}$$

where $\boldsymbol{R}^{-1}$ denotes the matrix inverse of $\boldsymbol{R}$.

Calculating the inverse of the covariance data matrix makes this technique more computationally intensive than the CBF technique. However, by reducing the sidelobes of the spatial filters, the MV estimate of the spatial power spectrum can provide better resolution.

(iii). **Maximum Likelihood Techniques**

Maximum likelihood statistical methods [51, 101] can be used to estimate the source bearings. This is achieved by maximising a K dimensional log–likelihood function for K source bearings. However, the function to be maximised is often highly non–linear with local minima, which presents a formidable problem in practical computation. Brute force searches of the log–likelihood function are computationally expensive, whilst simpler searching procedures, such as genetic algorithms and alternating projection [127], cannot be guaranteed to find the global maximum. This technique will not be considered further in this thesis.

(iv). **The MUSIC Algorithm**

The MUSIC algorithm operates by calculating the eigenvalue decomposition of the covariance matrix $\boldsymbol{R}$. The result of this operation is that the eigenvalue/eigenvector pairs may be separated into two classes: 1) K signal eigenvectors which span the space of the signal matrix $\boldsymbol{X} = \boldsymbol{A}\boldsymbol{S}\boldsymbol{A}^H$ 2) noise eigenvectors which are orthogonal to the matrix $\boldsymbol{X}$. Provided the column matrix of noise eigenvectors $\boldsymbol{E}_n \in \mathbb{C}^{M \times M-K}$ can be correctly determined, the source bearings can be identified as those which are orthogonal to each column of $\boldsymbol{E}_n$. This procedure is possible, because the columns of $\boldsymbol{E}_n$ are orthogonal to the columns of $\boldsymbol{X}$ and hence to those of $\boldsymbol{A}$. This requires only a one–dimensional search for source bearings and the power density spectrum for the MUSIC algorithm is given by:

$$P_{MUS}(\theta) = \frac{1}{\boldsymbol{a}^H(\theta)\boldsymbol{E}_n\boldsymbol{E}_n^H\boldsymbol{a}(\theta)} \tag{4.6}$$

The effect of using finite data is that the signal bearings are identified as those with the smallest projection on the estimated noise subspace. One difficulty with this algorithm is that the model order of $\boldsymbol{X}$ must be correctly identified, for the orthogonality property to hold. If the model order is underestimated, $\boldsymbol{E}_n$ will contain components of the signal subspace, so that the algorithm is likely to fail. Overestimating the model order is not such a serious problem, except that spurious peaks may occur in the density spectrum due to absence of some of the noise eigenvectors from $\boldsymbol{E}_n$. Model order estimates may be obtained in from the algorithms discussed in chapter 3.

In practical situations, the receiver only has access to a finite number of snapshots, N, of the signal vector $\boldsymbol{y}(t)$. The maximum likelihood unstructured estimate of $\boldsymbol{R}$ from the data, $\hat{\boldsymbol{R}}$, is then given by equation (3.3). In order to compare qualitatively the performance of the CBF, MV and MUSIC techniques, all three have been employed to resolve two uncorrelated sinusoidal signals. Both signals have a signal–to–noise ratio (SNR) of 20dB, with one at a bearing of 35^o and the other at 45^o. All three are using $N = 50$ data snapshots from a linear array with $M = 8$ sensors. The results are shown in figure 4.1, with the signal bearings shown as vertical lines. As can be seen, only the MUSIC algorithm

successfully resolves two sources, which are separated by only 10^o: the other two techniques interpret the two sources as a single source.

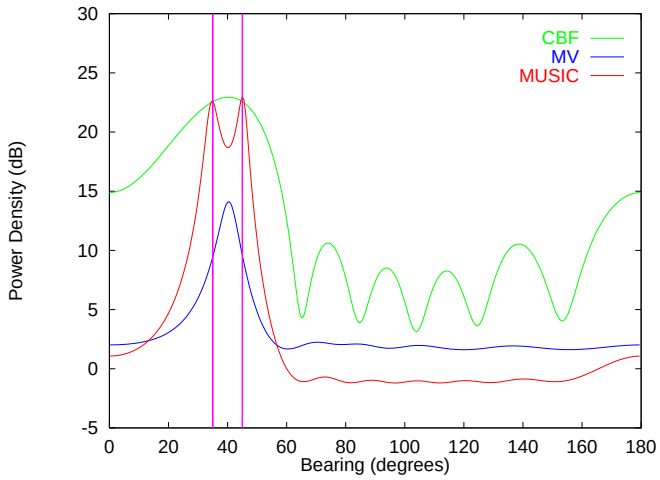

Figure 4.1: *A comparison of bearing estimation algorithms with two signal sources present.*

For the rest of this chapter, the MUSIC algorithm will be discussed in more detail. This technique is one of the most popular algorithms in the literature and has been subject to extensive analysis - see [101,128–132]. For the purposes of this thesis, the main deficiency of MUSIC is its poor performance in the presence of highly correlated or coherent signals: one solution to this problem is to employ spatial smoothing.

4.1.1 Spatial Smoothing Algorithms

One assumption made in the derivation of MUSIC is that the incoming signals are mutually uncorrelated over the time of observation. If all the signals present originate from different transmitters or are modulated with different data streams, they will be only partially correlated. However, if they result from multipath responses from the same transmitter, the signals are "coherent" and the assumption is invalid.

The signal subspace is always spanned by the vectors present in the matrix $\boldsymbol{A}$. However, if the signals are coherent, the matrix $\boldsymbol{S}$ becomes singular, so that some of its eigenvalues are zero. This means that part of the signal subspace is indistinguishable from the noise subspace. As a result, the observed noise subspace is no longer orthogonal to the steering vectors in the matrix $\boldsymbol{A}$ and the MUSIC algorithm fails. One solution is to resort to the maximum likelihood techniques mentioned above, although this loses all the computational advantages of the MUSIC algorithm.

A simple approach to permit the MUSIC algorithm to be used even in the case of coherent sources is to employ the spatial smoothing techniques described in section 3.3.1. Originally, these algorithms were intended only for linear array configurations. However, an interpolation technique has been described

recently, which permits the application of spatial smoothing to arrays of arbitrary geometry [112]. Two recent papers have also shown how to apply spatial smoothing algorithms to the special case of circular arrays [133, 134].

The original spatial smoothing (SS) technique modifies the data covariance matrix, $\boldsymbol{R}$, according to equation (3.8) to produce a smoothed matrix $\boldsymbol{\Psi}$:

$$\boldsymbol{\Psi} = \frac{1}{H} \sum_{h=1}^{H} \boldsymbol{F}_h \boldsymbol{R} \boldsymbol{F}_h^T \tag{4.7}$$

The covariance matrix $\boldsymbol{\Psi}$ may be used to generate a MUSIC power density spectrum in the normal manner. A geometrical interpretation of the technique is shown in figure 4.2: subarrays are formed by working in the forward direction only. It is easy to show [135] that to separately resolve K coherent sources, it is required to average over at least K different subarrays. This means that the antenna array must contain at least $2K$ elements.

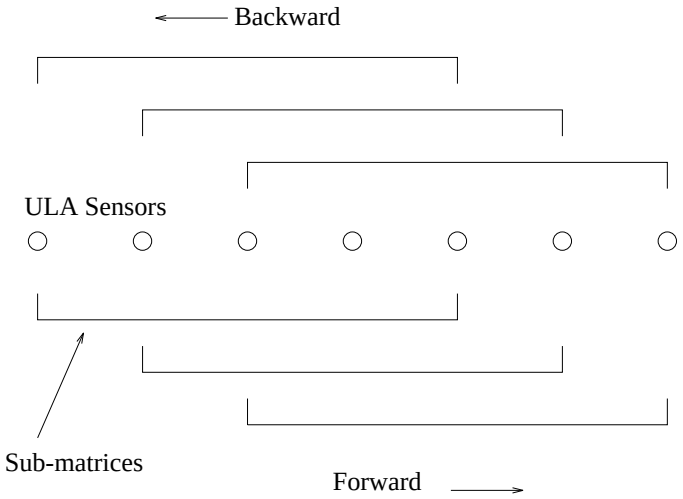

Figure 4.2: *Forward and backward spatial smoothing.*

Forward–backward spatial smoothing (FBSS) works by forming covariance matrices in both the forward and backward directions, as shown in figure 4.2. This is equivalent to averaging the original covariance matrix $\boldsymbol{R}$ according to equation (3.10):

$$\boldsymbol{R}_{F/B} = \frac{1}{2}(\boldsymbol{R} + \boldsymbol{J}\boldsymbol{R}^*\boldsymbol{J}) \tag{4.8}$$

This operation on its own is called forward–backward smoothing (FBS). The matrix $\boldsymbol{R}_{F/B}$ may also be substituted in equation (4.7) in place of $\boldsymbol{R}$ to obtain the FBSS covariance matrix. It has been shown [110, 136] that to resolve K coherent sources, as little as $3K/2$ array elements may be required. As will be seen below, there are some situations where FBSS behaves in the exactly the same manner as

the SS technique: in these cases $2K$ array elements are still required.

As an example of the operation of spatial smoothing techniques, two coherent sinusoids impinge on an 8–element ULA from bearings 130^o and 150^o. Both signals had an SNR of 20 dB and $N = 50$ data snapshots were available. The SS technique with $L = 7$ was applied to the data covariance matrix, as well as the FBS technique with $L = 8$. The power density spectrum of the unsmoothed MUSIC algorithm along with the spectra for the two smoothing techniques are shown in figure 4.3. This figure

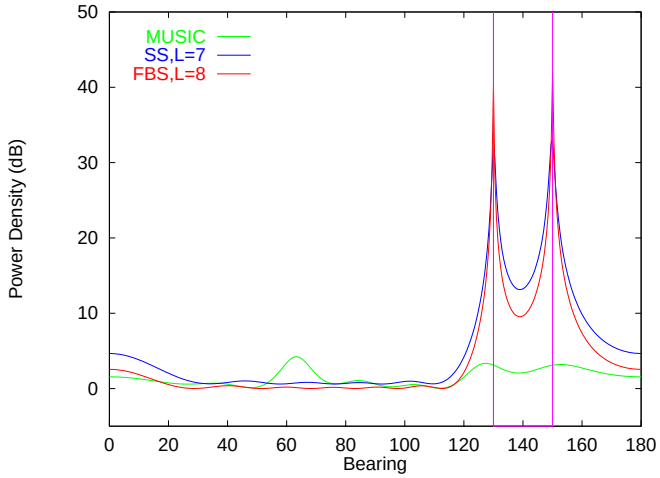

Figure 4.3: *The power density spectra of unsmoothed MUSIC, MUSIC with SS ($L = 7$) and MUSIC with FBS ($L = 8$) for two coherent sources.*

demonstrates that the conventional MUSIC algorithm has failed completely. However, applying either spatial smoothing algorithm restores the full rank of the signal subspace, permitting MUSIC to be successfully used.

4.1.2 Statistical Analysis of the MUSIC Algorithm

Determining the performance of the MUSIC algorithm with finite data, with or without spatial smoothing techniques applied, is of major importance. There are two main approaches to this subject in the literature. The first method is to determine the statistics of the power density spectrum itself: this permits the derivation of a resolvability criterion for the MUSIC algorithm [128] – that is to find the conditions under which two closely spaced sources will be resolved as two separate peaks, rather than combining to form one peak. Similar work has also been performed for MUSIC combined with spatial smoothing algorithms [109, 137]. However, this type of analysis is usually restricted to the case of two sources and will not be considered in this thesis.

A more general technique for analysing the MUSIC algorithm is to derive an equation for the variance of the signal peaks of the MUSIC spectrum [131, 132]. As before, these results have been extended to MUSIC with spatial smoothing techniques [112, 138]. One useful form of the variance equation for the unsmoothed MUSIC algorithm is given in [132]. Denoting the error in the estimate of the bearing of the

k^{th} signal as $\Delta\theta_k$, the asymptotic variance of that error is given by the equation:

$$E[\Delta\theta_k^2] \approx \frac{\sigma^2}{N d_\theta(\theta_k)}\{[\boldsymbol{S}^{-1}]_{kk} + \sigma^2[\boldsymbol{S}^{-1}(\boldsymbol{A}^H\boldsymbol{A})^{-1}\boldsymbol{S}^{-1}]_{kk}\} \tag{4.9}$$

The scalar value $d_\theta(\theta_k)$ is given by the matrix product $2\{\boldsymbol{d}^H(\theta_k)\boldsymbol{E}_n\boldsymbol{E}_n^H\boldsymbol{d}(\theta_k)\}$, where $\boldsymbol{d}(\theta_k)$ is the Brandwood vector derivative of $\boldsymbol{a}(\theta_k)$ [52]. Finally, the notation $\boldsymbol{S}_{ij}$ denotes the i^{th} row and j^{th} column entry of $\boldsymbol{S}$. The approximation in equation (4.9) is accurate to order $O(1/N)$ [138], which also holds true for all other variance expressions considered in this chapter. For large values of the SNR with mutually uncorrelated sources, the variance of each bearing estimate is inversely proportional to the SNR of the desired source. Remarkably, under these conditions, MUSIC is a large sample realisation of maximum likelihood methods [101]. However, as the correlation between the sources increases the matrix $\boldsymbol{S}^{-1}$ becomes ill-conditioned and the variance can become very large compared to maximum likelihood approaches.

The equivalent equation for the MUSIC algorithm combined with spatial smoothing techniques is more complex. The results have been obtained by Rao and Hari [138] and for spatial smoothing the equation is:

$$E[\Delta\theta_k^2] \approx \frac{2}{d_\theta(\theta_k)^2 N H^2}[\sum_{p,q=1}^{H}\boldsymbol{\beta}^H\boldsymbol{R}(p,q)\boldsymbol{\beta}\boldsymbol{\alpha}^H\boldsymbol{N}(q,p)\boldsymbol{\alpha} + \Re\{\sum_{p,q=1,p\neq q}^{H}\boldsymbol{\beta}^H\boldsymbol{N}(p,q)\boldsymbol{\alpha}\,\boldsymbol{\beta}^H\boldsymbol{N}(q,p)\boldsymbol{\alpha}\}] \tag{4.10}$$

where $\Re$ denotes the real part of a complex value. The matrix $\boldsymbol{R}(p,q)$ is given by $\boldsymbol{F}_p\boldsymbol{R}\boldsymbol{F}_q^T$; $\boldsymbol{\alpha}$ and $\boldsymbol{\beta}$ are defined as:

$$\boldsymbol{\alpha} = \boldsymbol{E}_n\boldsymbol{E}_n^H\boldsymbol{d}_S(\theta_k) \quad \text{and} \quad \boldsymbol{\beta} = \boldsymbol{U}_S\Lambda_S^{-1}\boldsymbol{U}_S^H\boldsymbol{a}_S(\theta_k) \tag{4.11}$$

The matrix $\boldsymbol{U}_S \in \mathbb{C}^{L\times K}$ contains the K signal eigenvectors of the smoothed covariance matrix, $\Lambda_S \in \mathbb{R}^{K\times K}$ is a diagonal matrix containing the K smoothed signal eigenvalues. The matrix $\boldsymbol{N}(p,q)$ is defined in a similar way to $\boldsymbol{R}(p,q)$ with $\boldsymbol{N}(p,q) = \sigma^2\boldsymbol{F}_p\boldsymbol{F}_q^T$. The vector $\boldsymbol{a}_S$ is the steering vector for the smoothed array and $\boldsymbol{d}_S$ is its brandwood derivative. It has been noted [138], that the second part of equation (4.10) becomes very small compared to the first part at high SNR values. The vector $\boldsymbol{\beta}$ may be expressed as:

$$\boldsymbol{\beta} = (\boldsymbol{A}_S^+)^H\boldsymbol{S}_S^{-1}\imath_k \tag{4.12}$$

where S_S is the smoothed signal matrix and $\boldsymbol{A}_S$ is the matrix of smoothed steering vectors. The vector $\imath_k \in \mathbb{C}^{1\times K}$ is the k^{th} column of the $K \times K$ identity matrix $\boldsymbol{I}$ and the notation $\boldsymbol{A}^+$ denotes the

pseudo-inverse of $\boldsymbol{A}$. Expanding the matrix $\boldsymbol{R}(p,q)$ as $\boldsymbol{F}_p \boldsymbol{A}\boldsymbol{S}\boldsymbol{A}^H \boldsymbol{F}_q^T + \boldsymbol{N}(p,q)$, equation (4.10) may be written as:

$$\begin{aligned} E[\Delta\theta_k^2] &\approx \frac{\sigma^2}{NHd_\theta(\theta_k)}\{[\boldsymbol{S}_S^{-1}]_{kk} + \sigma^2[\boldsymbol{S}_S^{-1}(\boldsymbol{A}_S^H\boldsymbol{A}_S)^{-1}\boldsymbol{S}_S^{-1}]_{kk}\} \\ &+ \frac{2}{d_\theta(\theta_k)^2 NH^2}\sum_{p,q=1,p\neq q}^{H}\{[\boldsymbol{S}_S^{-1}\boldsymbol{B}(p,\Theta)^H\boldsymbol{S}\boldsymbol{B}(q,\Theta)\boldsymbol{S}_S^{-1}]_{kk}\}\boldsymbol{\alpha}^H\boldsymbol{N}(q,p)\boldsymbol{\alpha} \\ &+ \frac{2}{d_\theta(\theta_k)^2 NH^2}\sum_{p,q=1,p\neq q}^{H}(\boldsymbol{\beta}^H\boldsymbol{N}(p,q)\boldsymbol{\beta}\,\boldsymbol{\alpha}^H\boldsymbol{N}(q,p)\boldsymbol{\alpha} + \Re\{\boldsymbol{\beta}^H\boldsymbol{N}(p,q)\boldsymbol{\alpha}\,\boldsymbol{\beta}^H\boldsymbol{N}(q,p)\boldsymbol{\alpha}\}) \end{aligned} \tag{4.13}$$

where $\boldsymbol{B}(q,\Theta) \in \mathbb{C}^{K\times K}$ is a diagonal matrix, given by:

$$\boldsymbol{B}(q,\Theta) = \boldsymbol{A}^H\boldsymbol{F}_q^T(\boldsymbol{A}_S^+)^H = \begin{bmatrix} b_1 & 0 & \dots & 0 \\ 0 & b_2 & \dots & 0 \\ \vdots & \vdots & \ddots & \vdots \\ 0 & \dots & 0 & b_K \end{bmatrix} \tag{4.14}$$

The k^{th} diagonal entry of $\boldsymbol{B}$, b_k, depends on the phase shift between the steering vectors $\boldsymbol{a}^H(\theta_k)\boldsymbol{F}_q^T$ and $\boldsymbol{a}_S^H(\theta_k)$. For the FBSS case, the matrix $\boldsymbol{S}_S$ would be replaced by the equivalent FBSS signal matrix $\boldsymbol{S}_{F/B}$ in the equations above. The first term of equation (4.13) is equivalent to equation (4.9) and the other terms are cross terms to compensate for the formation of $\boldsymbol{\Psi}$ from partitions of $\boldsymbol{R}$.

4.1.3 Analysis of the Covariance Matrix

Equations (4.9) and (4.13) explicitly show that the performance of the MUSIC algorithm with or without smoothing techniques is proportional to entries of the inverse matrices of $\boldsymbol{S}$, $\boldsymbol{S}_S$ or $\boldsymbol{S}_{F/B}$. Therefore, if one looks at what the smoothing techniques do to the eigenvalues of these matrices, it should be possible to explain the major effects observed in the behaviour of the MUSIC algorithm. In the analysis of the matrix eigenvalues, a useful criterion is the condition or eigenvalue ratio (EVR), which is defined to be:

$$\text{EVR} = \frac{\lambda_{max}}{\lambda_{min}} \tag{4.15}$$

where λ_{min} and λ_{max} represent the smallest and the largest eigenvalues, respectively, of the given matrix. To make legitimate comparisons, the received signal power levels should be kept constant: other parameters such as signal bearings and phase may then be varied to see the effect on the EVR. If the EVR is small, the columns of $\boldsymbol{S}$ and hence the underlying signals are approximately uncorrelated, which suggests MUSIC will perform well. If the EVR is large, the matrix is close to being singular and

MUSIC will perform poorly. In terms of the variance equations, the scalar value $(1/\lambda_{min})$ is the largest eigenvalue of $\boldsymbol{S}^{-1}$: the more ill-conditioned the $\boldsymbol{S}$ matrix is, the larger the variance of the MUSIC bearing estimates.

Similarly, the variance equations involve the inverse of the matrix $\boldsymbol{A}^H\boldsymbol{A}$ (or $\boldsymbol{A}_S^H\boldsymbol{A}_S$), which is altered as the source bearings change. When the sources are sufficiently spaced, the off-diagonal terms of this matrix are small, so that the eigenvalues are all approximately unity. However, when the sources are closely spaced, the off-diagonal terms become large and the EVR of $\boldsymbol{A}^H\boldsymbol{A}$ becomes very large.

In the general case of K coherent sources, the matrix $\boldsymbol{S}$ is of the form:

$$\boldsymbol{S} = \begin{bmatrix} s_1^2 & s_1 s_2 \exp\{j\phi(1,2)\} & \dots & s_1 s_K \exp\{j\phi(1,K)\} \\ s_1 s_2 \exp\{-j\phi(1,2)\} & s_2^2 & \dots & s_2 s_K \exp\{j\phi(2,K)\} \\ \vdots & \vdots & \ddots & \vdots \\ s_1 s_K \exp\{-j\phi(1,K)\} & s_2 s_K \exp\{-j\phi(2,K)\} & \dots & s_K^2 \end{bmatrix} \tag{4.16}$$

The amplitude of the k^{th} source is denoted as s_k and scalar $\phi(i,j)$ indicates the phase at the reference sensor between sources i and j. For the rest of this chapter, the reference for the phases $\phi(i,j)$ will be placed at the centre of the ULA.

4.1.3.1 Spatial Smoothing

For spatial smoothing, H sub-matrices are formed from L element subarrays and are averaged to form a smoothed covariance matrix $\boldsymbol{\Psi}$. The reference for the smoothed steering vector $\boldsymbol{a}_S(\theta)$ will be defined to be at the centre of the array, so that:

$$\boldsymbol{a}_S(\theta) = [\exp\{-j(\frac{L-1}{2})\pi\cos(\theta)\}, \exp\{-j(\frac{L-3}{2})\pi\cos(\theta)\}, \dots, \exp\{j(\frac{L-1}{2})\pi\cos(\theta)\}]^T \tag{4.17}$$

This definition may be used in combination with results from [139] to show that the i^{th} row and j^{th} column entry of the smoothed signal matrix $\boldsymbol{S}_S$ is given by:

$$[\boldsymbol{S}_S]_{ij} = s_i s_j \exp\{j\phi(i,j)\}\frac{1}{H}\sum_{p=0}^{H-1}\exp\{-j(((H-1)/2)+p)\pi(cos(\theta_i)-cos(\theta_j))\} \tag{4.18}$$

The summation term is real for both even and odd L: it will be denoted as c_C below. The behaviour of this cross-correlation value has been analysed extensively in [139]. The magnitude of $(\boldsymbol{S}_S)_{ij}$ generally decreases as H increases, so that the EVR of $\boldsymbol{S}_S$ will also improve. The rate of the decrease in c_C with H depends on the source bearings and their separation. For the simple case of two sources, the matrix

$\boldsymbol{S}_S$ is given by:

$$\boldsymbol{S}_S = \begin{bmatrix} s_1^2 & s_1 s_2 c_C \exp\{j\phi(1,2)\} \\ s_1 s_2 c_C \exp\{-j\phi(1,2)\} & s_2^2 \end{bmatrix} \tag{4.19}$$

The eigenvalues of the smoothed signal matrix $\boldsymbol{S}_S$ are given by:

$$\det(\boldsymbol{S}_S - \lambda \boldsymbol{I}_2) = 0 \tag{4.20}$$

where $\det$ denotes the matrix determinant. This equation leads to a quadratic equation in λ: applying the formula for the roots of a quadratic equation gives:

$$\lambda = \frac{(s_1^2 + s_2^2)}{2} \pm \frac{1}{2}\sqrt{(s_1^4 + s_2^4 + 2s_1^2 s_2^2(2c_C^2 - 1)} \tag{4.21}$$

The eigenvalues of $\boldsymbol{S}_S$ depend on the value c_C. If c_C is close to one, λ has roots near 0 and $(s_1^2 + s_2^2)$: if c_C is small, the eigenvalues are close to s_1^2 and s_2^2. It is useful to note that the eigenvalues do not depend on the phase term $\phi(1,2)$, which suggests that varying the signal phases has no significant effect on the variance of the SS algorithm.

4.1.3.2 Forward-backward Spatial Smoothing

To simplify the analysis of forward-backward spatial smoothing, spatial smoothing is applied as before. The forward-backward smoothing may be applied to the resulting forward and backward matrices to form the final covariance matrix, $\boldsymbol{\Psi}_{F/B}$. Thus:

$$\begin{aligned} \boldsymbol{\Psi}_{F/B} &= \frac{1}{2}(\boldsymbol{\Psi} + \boldsymbol{J}\boldsymbol{\Psi}^*\boldsymbol{J}) \\ &= \frac{1}{2}(\boldsymbol{A}_S \boldsymbol{S}_S \boldsymbol{A}_S^H + \boldsymbol{J}\boldsymbol{A}_S^* \boldsymbol{S}_S^* \boldsymbol{A}_S^T \boldsymbol{J}) + \sigma^2 \boldsymbol{I} \\ &= \frac{1}{2}(\boldsymbol{A}_S [\boldsymbol{S}_S + \boldsymbol{S}_S^*] \boldsymbol{A}_S^H) + \sigma^2 \boldsymbol{I} \\ &= \boldsymbol{A}_S \boldsymbol{S}_{F/B} \boldsymbol{A}_S^H + \sigma^2 \boldsymbol{I} \end{aligned} \tag{4.22}$$

The third line of the above formula follows because $\boldsymbol{J}\boldsymbol{A}_S^* = \boldsymbol{A}_S$, etc. Therefore, the value of $[\boldsymbol{S}_{F/B}]_{ij}$ is given by:

$$[\boldsymbol{S}_{F/B}]_{ij} = [\boldsymbol{S}_S]_{ij} + [\boldsymbol{S}_S^*]_{ij} = s_i s_j c_C \cos\phi(i,j) \tag{4.23}$$

The magnitude of the cross-correlation term can lie between $s_i s_j c_C$ and zero, depending on the relative signal phase $\phi(i,j)$. In the case of two sources, $\boldsymbol{S}_{F/B}$ is given by:

$$\boldsymbol{S}_{F/B} = \begin{bmatrix} s_1^2 & s_1 s_2 c_C \cos\phi(1,2) \\ s_1 s_2 c_C \cos\phi(1,2) & s_2^2 \end{bmatrix} \tag{4.24}$$

Solving for the eigenvalues, as in equation (4.20), gives the values of λ:

$$\lambda = \frac{(s_1^2 + s_2^2)}{2} \pm \frac{1}{2}\sqrt{(s_1^4 + s_2^4 + 2s_1^2 s_2^2[2c_C^2 \cos^2(\phi(1,2)) - 1])} \tag{4.25}$$

For two coherent signals, the variance of the FBSS method clearly depends on the relative signal phase $\phi(1,2)$. If $\phi(1,2) = 0, \pi$ radians, the matrix $\boldsymbol{S} = \boldsymbol{S}^*$, so the off-diagonal terms of $\boldsymbol{S}_{F/B}$ are not cancelled, leaving the EVR identical to the spatial smoothing case. This means the error variance will be the same as for spatial smoothing. Alternatively, if $\phi(1,2) = \frac{\pi}{2}, \frac{3\pi}{2}$ radians, the off-diagonal terms of $\boldsymbol{S}_{F/B}$ cancel completely, so that the EVR reaches a minimum. The improvement that may be offered by FBSS depends on how well SS alone has reduced the magnitude of the correlation c_C. Similarly, for the FBS algorithm alone, the performance of the MUSIC algorithm can be improved, except in the case where $\phi(1,2) = 0, \pi$ [137].

In the general case of K sources, the EVR of a forward–backward smoothed covariance matrix is less than or equal to that of the original smoothed or unsmoothed covariance matrix [138]. Depending on the signal phases, the FBSS algorithm can offer significant improvements in scenarios where spatial smoothing has failed to reduce signal correlation, particularly when signals are closely spaced.

The phase dependence of the FBSS algorithm means that in some cases, using $(K/2)$ subarrays with FBSS is insufficient to restore the full rank of the signal matrix $\boldsymbol{S}_{F/B}$ [110]. Indeed, if all the relative phase terms $\phi(i,j)$ are 0 or π, the algorithm performs in the same manner as SS with the same subarray size L. However, this is an extreme case: applying FBS to a spatially smoothed covariance matrix usually improves the performance of the MUSIC algorithm and in some cases, FBSS may be able to resolve the same number of sources using a larger subarray size than SS. Where the number of sources is larger than half the number of antenna elements, it provides the only opportunity to resolve all the sources.

4.2 Other Spatial Smoothing Techniques

Two other spatial smoothing techniques described in the literature are based on squaring the data covariance matrix. The first method is due to Kirlin and Du [140], and the spatially smoothed covariance matrix is defined as follows:

$$\boldsymbol{\Psi}_{K/D} = \frac{1}{H^2}\sum_{i,j=1}^{H} \boldsymbol{F}_i \boldsymbol{R} \boldsymbol{F}_j^T \boldsymbol{F}_j \boldsymbol{R} \boldsymbol{F}_i^T = \frac{1}{H^2}\sum_{i,j=1}^{H} \boldsymbol{R}(i,j)\boldsymbol{R}(j,i) \tag{4.26}$$

It is suggested that $H \geq K$ to resolve K sources as for spatial smoothing. The matrix $\boldsymbol{\Psi}_{K/D}$ may also

be subject to forward–backward smoothing to obtain a variant of the FBSS algorithm. The rationale for using this technique [140] is that the matrix $\boldsymbol{\Psi}_{K/D}$ includes some parts of the original covariance matrix which are not explicitly present in the definition of the spatially smoothed covariance matrix. However, the matrices $\boldsymbol{R}(i,j)$ and $\boldsymbol{R}(j,i)$ specified in (4.26) do appear in equation (4.10): as a result, they do affect the asymptotic variance of MUSIC with spatial smoothing.

The second technique is described in [141] and is termed quadratic spatial smoothing (QSS). In this case, the covariance matrix is subject to a squaring operation as follows:

$$\boldsymbol{R}_Q = \boldsymbol{R}\boldsymbol{R}^H \tag{4.27}$$

The matrix $\boldsymbol{R}_Q$ may then be subject to SS or FBSS in place of the original covariance matrix $\boldsymbol{R}$. This technique is very similar, but not absolutely identical, to the Kirlin and Du approach.

An algorithm to completely de–correlate the multipath sources has been described in [142]. However, it requires an initial estimate of the number of sources and their bearings: these are used in an iterative procedure to obtain the correct signal locations. Another spatial smoothing technique called the steered pattern averaging technique (SPAT) [143] employs sub–arrays which are steered in different directions to produce a number of independent covariance matrices for averaging. Both these techniques require as many sub–arrays as the original spatial smoothing algorithm and neither has been considered further in this thesis.

It is also possible to employ the Toeplitz approximation method (TAM) to reduce signal correlation. In this case, the receiver averages the top–left to bottom–right diagonals of the covariance matrix in order to give it a Toeplitz structure. Unfortunately, this approach makes incorrect assumptions about the underlying signals, so that the bearing estimates obtained from this technique are not consistent [141]. This observation was backed up by numerical experience during the work of this PhD and this approach has also not been pursued in this work.

Finally, a modification of the FBS technique was proposed in [144] as a general technique to overcome coherent sources: instead of adding the forward and backward covariance matrices, they were subtracted from one another. It was claimed that this method was sufficient to resolve an arbitrary number of coherent sources. However, the author was able to provide a simple counterexample [135] to demonstrate that this claim was untrue and that the technique was flawed.

4.3 Results and Discussion

In this section, the equations quoted for the MUSIC algorithm and for the spatial smoothing techniques will be applied to particular scenarios to illustrate the points made in the analysis of spatially smoothed covariance matrices. It should be pointed out, however, that equation (4.10) is very complex and the above analysis is only intended to explain the major effects observed in the behaviour of SS/FBSS. In

all the simulations the number of elements M in the uniform linear array was eight and each signal's SNR was set to be 17dB. All signals were generated using complex exponentials of constant amplitude and one hundred snapshots were used to form covariance matrices in each case.

Figures 4.4 and 4.5 show the effect of signal correlation on the variance and the $\boldsymbol{S}$ matrix EVR for various algorithms. There are two sources, the first at a bearing of 90^o (which is defined to be the array broadside) and the second at 60^o. The correlation between the two sources is varied from zero to one and the variance plots are all for the first source, though the variance of the other source behaves in a similar manner. It is noticeable that behaviour of the EVR curves in figure 4.5 is similar to that of the variance curves in figure 4.4. However, it should be pointed out that it is only meaningful to compare EVR graphs whose subarray size, L, is the same.

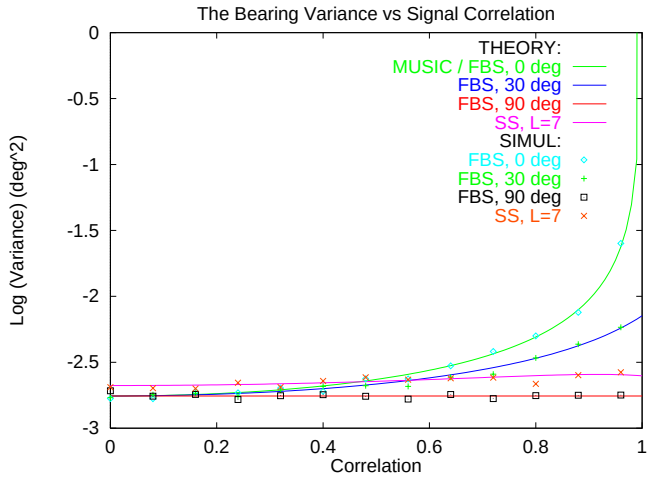

Figure 4.4: *Comparison of variance of MUSIC, SS and FBS techniques vs signal correlation.*

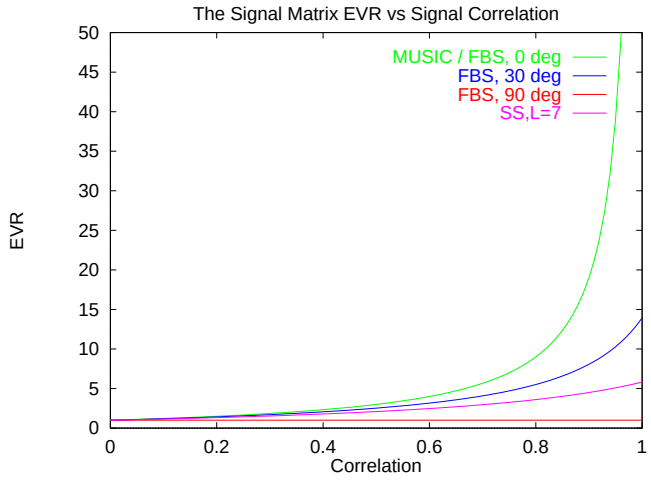

Figure 4.5: *Comparison of the signal matrix EVR of MUSIC, SS and FBS techniques vs signal correlation.*

The spatial smoothing algorithm, formed from two sub-matrices (H=2) so that the subarray size L =7, is reasonably robust to signal correlation, although in this case the FBS algorithm with L =8 out-performs

it at low signal correlation. The performance of the FBS algorithm is less clear-cut for high correlations. The best possible outcome occurs when the relative signal phase is $\frac{\pi}{2}$ (90^o) as shown on the graph. The variance for a relative signal phase of $\frac{\pi}{6}$ (30^o) is also shown: it is inferior to the previous curve, but better than that for a phase shift of 0, where FBS cannot reduce the signal correlation so it gives the same performance as for MUSIC without FBS. The fact that the variance depends considerably on the relative signal phases means that the variance for a given phase can lie anywhere in the region spanned by the three curves.

The next two figures, 4.6 and 4.7, shows the effect of angular separation on SS, FBS, FBSS with two coherent sources and MUSIC with two uncorrelated sources. The first source is at a bearing of 90^o and the bearing of the second source is chosen to give the correct angular separation. The variance of the 90^o source is plotted only for angular separations up to 80^o: as the bearing of the second source approaches 0^o or 180^o, "endfire" effects mean that the variance of the bearing estimate increases without bound.

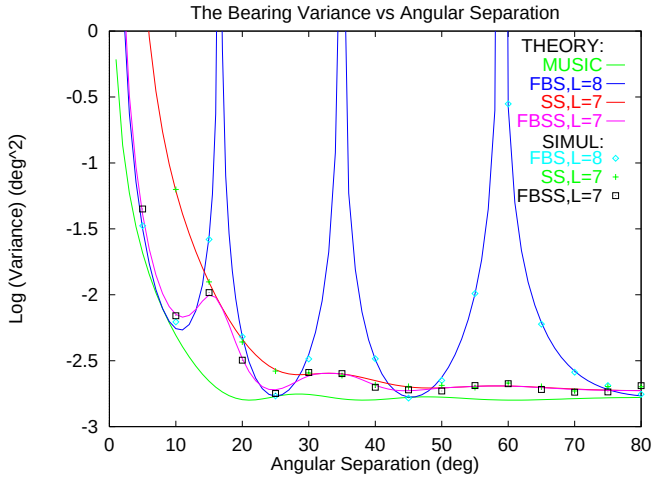

Figure 4.6: *Comparison of variance of MUSIC, SS, FBS and FBSS techniques vs angular separation.*

The EVR of the matrix $\boldsymbol{A}^H\boldsymbol{A}$ has been plotted for L=8 in figure 4.7 (denoted AhA) to show its effect on the MUSIC algorithm. The EVR of $\boldsymbol{A}^H\boldsymbol{A}$ and thus the variance of the MUSIC algorithm is large for closely spaced sources, as one would expect, but reduces to an approximately constant level for an angular separation of greater than 10^o or so. The reference sensor was set at one end of the ULA, so that the relative phase of the two signals at the middle of the array changes. This emphasises the relative phase dependence of the FBS algorithm. As expected from the analysis, the performance of FBS is oscillating between that of MUSIC with no signal correlation and MUSIC with a correlation factor of 1 - i.e. infinite EVR and variance.

The SS algorithm with L =7 improves more slowly than the MUSIC algorithm with no correlation, as the signal separation is increased. This is because the EVR of both the matrix $\boldsymbol{S}$ and the matrix $\boldsymbol{A}$ depend on signal separation. The FBSS technique with L =7 generally performs better than SS and for closely spaced sources the variance can be improved considerably according to the relative signal phase.

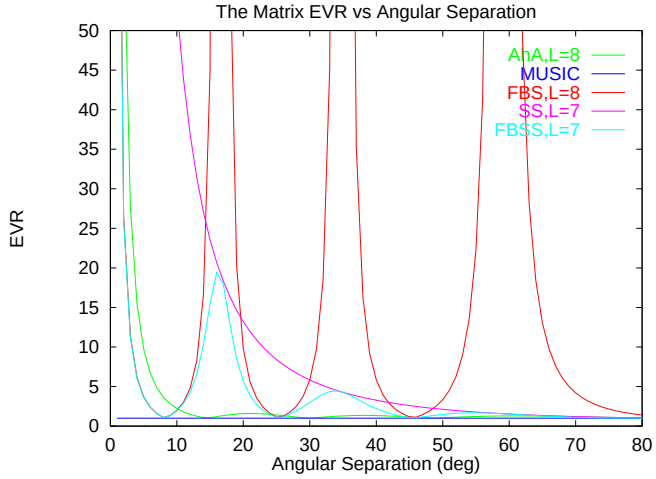

Figure 4.7: *Comparison of the signal matrix EVR of MUSIC, SS, FBS and FBSS techniques and the EVR of the matrix* $\boldsymbol{A}^H \boldsymbol{A}$ *with* $L = 8$ *vs angular separation.*

Figures 4.8 and 4.9 show the effect of signal phase on the performance of SS, FBS, FBSS algorithms and MUSIC (with zero correlation). The two sources are at 96^o and 78^o and their relative phase at the centre of the ULA varies from 0–360^o. The variance is plotted for the source at 96^o and the performance of the SS algorithm with L =7 is approximately constant with the signal phase. The FBS technique is again shown to provide improved performance for some signal phases – the sinusoidal variation in the eigenvalues show up in the EVR of the $\boldsymbol{S}$ matrix and in the variance curve. This type of behaviour is also shown in the results of Chang and Yeh [137]. In a similar manner, the FBSS algorithm with L =7 is seen to perform as well as or better than SS, with the variance also sinusoidally changing with signal phase.

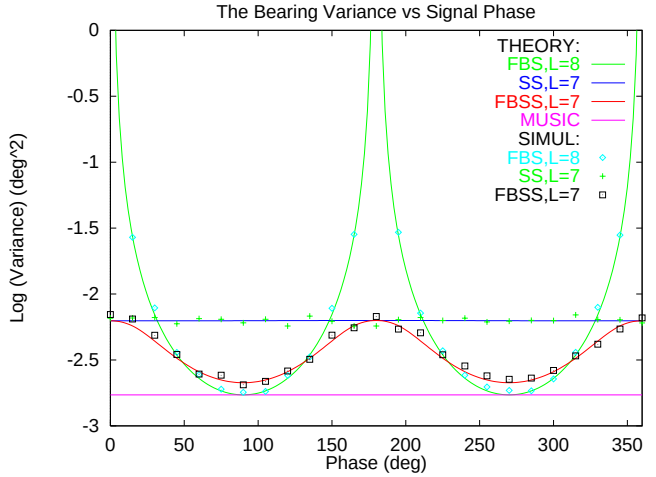

Figure 4.8: *Comparison of variance of MUSIC, SS, FBS and FBSS techniques vs signal phase.*

The analysis of FBSS in the previous section showed that its performance will normally be as good as or better than SS with the same amount of spatial smoothing and this is demonstrated in these results.

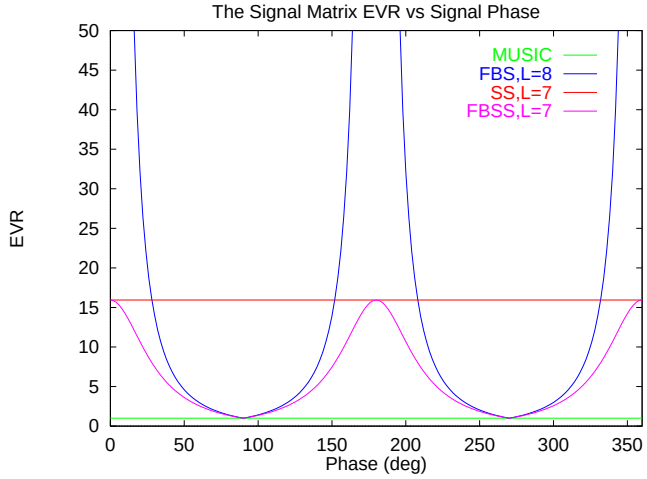

Figure 4.9: *Comparison of the signal matrix EVR of MUSIC, SS, FBS and FBSS techniques vs signal phase.*

Similarly, FBSS with less than K subarrays for K coherent sources (in the case of figures 4.8 and 4.9, simply the FBS technique with L =8) still has some chance of resolving the sources, unlike the SS algorithm.

It seems likely that the variations in phase will affect the performance of the FBSS technique for larger numbers of signals, and this effect is shown in figures 4.10 and 4.11. In the figure 4.10, the FBSS algorithm with L =7 is attempting to resolve three sources at 60^o, 120^o and 90^o. The phases of the first two sources at the centre of the ULA are varied with respect to that of the third source, which is fixed at 0^o.The theoretical variance is shown for the source at 120^o. When the relative phases of the three signals are 0^o or 180^o, the algorithm cannot restore the full rank of the signal matrix and the variance is seen to rise towards infinity.

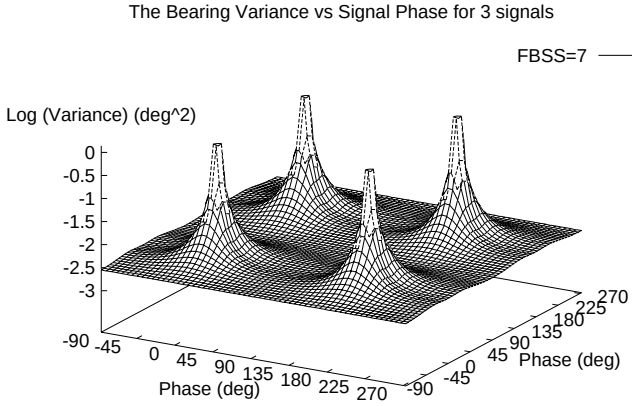

Figure 4.10: *The Variance of FBSS with L =7 for a source at bearing 120^o vs signal phase for 3 sources.*

A similar effect is shown in the figure 4.11. In this case, four signals are impinging on the array from

bearings 60^o, 120^o, 80^o and 100^o. The phases of the first two sources are varied with respect to those of the second two sources, which are both fixed at 0. The theoretical variance shown is for the source at 80^o. Here the situation is more complex: if the relative phases of three of more sources coincide at 0 or π (180^o), the variance of those sources will again rise to infinity. In both cases, there is a reasonable statistical chance of resolving all sources, but where FBSS with L =7 fails, the amount of smoothing required for FBSS must be increased towards that required by SS.

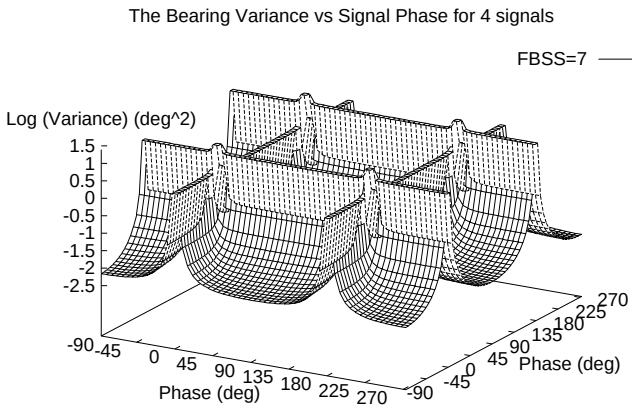

Figure 4.11: *The Variance of FBSS with $L = 7$ for a source at bearing 80^o vs signal phase for 4 sources.*

The number of subarrays required in SS/FBSS algorithms to minimise the variance of the MUSIC algorithm is an interesting problem. Figure 4.12 shows the variance of spatial smoothing for different numbers of subarrays vs signal separation. As in figure 4.6, the first source is at 90^o and the bearing of the other source is varied to obtain the correct angular separation. In this case, there is little difference in performance for the different subarray sizes in general. For closely spaced sources, it seems that the improvement in the condition of $\boldsymbol{S}$ obtained by increasing K is cancelled out by the smaller effective array size. No single array size performs significantly better than all the others under all conditions, so it seems simplest to pick one subarray size that performs reasonably well, such as $L = 7$.

Finally, the performance of the quadratic spatial smoothing algorithms described in section 4.2 has been checked by Monte Carlo simulation. The signal scenario was identical to that for figures 4.6 and 4.7. The SS algorithm using L=7 was compared to the Kirlin and Du technique using L=7 (without forward–backward smoothing) and the Quadratic technique, with the squared covariance matrix again used with SS with matrix size L=7. The bearing estimate variance for the source at 90^o has been plotted against source separation and the results are shown in figure 4.13. In the graph, the Kirlin and Du technique is denoted as "K/D" and the quadratic technique as "QUAD". The theoretical variance curve for SS with L =7 is shown as a line, labelled "Theory".

The results show in this case that there is little difference in performance between the three techniques. This appears to be a typical result, which was confirmed in several other simulations. In some cases, the quadratic and Kirlin/Du methods performed slightly better than SS (or FBSS). However, the performance

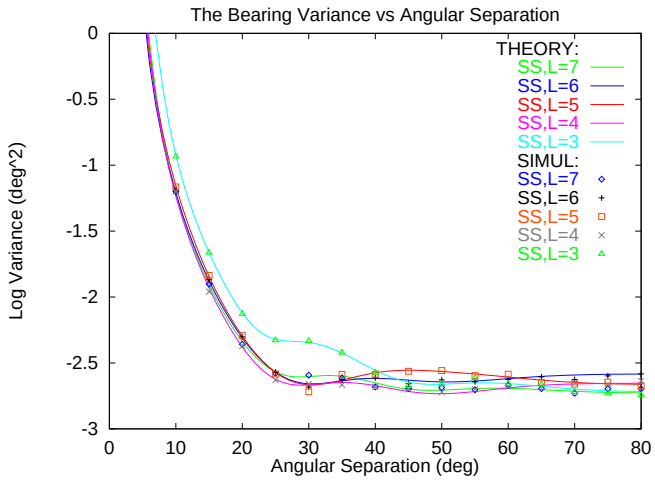

Figure 4.12: *Comparison of variance of Spatial Smoothing vs angular separation.*

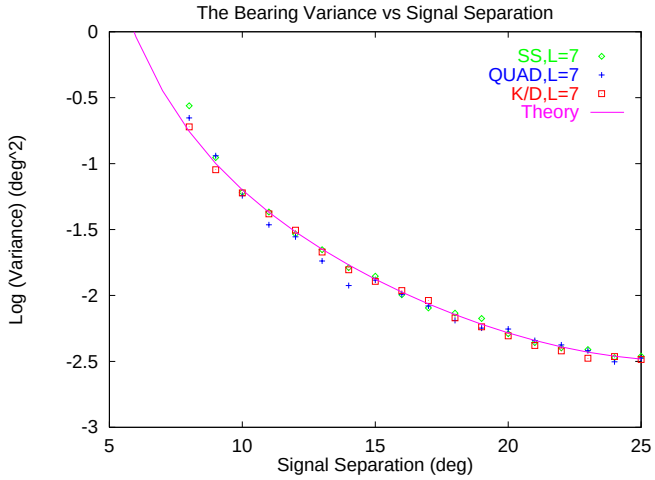

Figure 4.13: *Comparison of the performance of SS, Quadratic and Kirlin/Du methods, plotting signal separation against bearing variance.*

improvement was generally small and could be attributed to the statistical nature of Monte Carlo simulation. It would appear from these results that employing a squaring operation as part of the spatial smoothing process does not provide a significant and consistent improvement in the statistical performance of the MUSIC algorithm.

To summarise, it is clear that to resolve K sources with K subarrays, the FBSS algorithm is usually preferable to the SS technique. In addition, FBSS may resolve K sources using less than K subarrays, unlike the SS technique. The quadratic and Kirlin/Du methods do not seem to provide much improvement over the basic SS and FBSS techniques.

4.4 Conclusion

The MUSIC algorithm performs robustly in the presence of uncorrelated signals and signals with small correlation factors. When the correlation factor tends towards one, the signal scenario resembles that of coherent multipath returns, or smart signal jamming. In the case of coherent signals, the MUSIC algorithm is unable to resolve the different bearings, even at high SNR values. In this case, an alternative approach, such as spatial smoothing, must be used.

In this chapter, the performance of spatial smoothing techniques has been qualitatively linked to the eigenvalue ratio of the signal matrix $\boldsymbol{S}$. The performance of spatial smoothing depends on the bearings and separation of the sources. The FBSS algorithm with the same smoothing as SS has the potential to provide better estimates of the source bearings, depending on the relative signal phases. In some cases, the FBSS approach can resolve K sources with less than K subarrays, unlike the SS technique. Theoretical and simulation results have been presented to confirm these points. Simulation results have also been obtained for quadratic smoothing techniques: however, these techniques do not appear to offer consistent improvements in performance over the SS and FBSS algorithms.

Chapter 5

Spatial Filtering for CDMA Signals

Previous chapters in this thesis have addressed the topic of determining the angles of arrival of spread spectrum signals at an array of receivers. The hardware and computational requirements are much greater than for a single antenna receiver, so it is useful to be able to quantify the performance improvement that such an arrangement would offer to a cellular system. Two important performance measures of a communications system are the signal-to-interference (S/I) ratio of the desired signal and the mean bit error ratio (BER).

In this chapter, the reverse link (from the mobile to the base station) will be assumed to be an additive white Gaussian noise (AWGN) channel. Making the additional assumption that accurate bearing estimates are available, it is possible to estimate theoretically the performance of a single-cell code division multiple access (CDMA) system employing power control. Monte Carlo simulations have also been performed to confirm the results obtained. Similar results seem to be applicable to the forward link. Finally, the theory is extended to estimate the S/I ratios obtained for cellular operation over both the forward and reverse links.

5.1 Background and Channel Model

This chapter will apply analysis similar to that performed in [12, 14, 15]. A bearing estimation technique is assumed to correctly locate the bearing of a desired user. A spatial filter, whose look direction is set to the measured bearing, is used to pick out the energy of the desired signal whilst suppressing interference from other users. No interference cancellation or adaptive beamforming techniques will be used, in order to simplify the analysis.

The question of whether bearing estimation algorithms are appropriate for CDMA signals in particular has been the subject of debate. One 1993 conference paper [99] suggested that bearing estimation could not be applied to pre–matched filter data, because of the number of users and the number of multipaths. In addition, the low SIR of each signal would require prohibitively large amounts of data to obtain reliable estimates. However, post matched filter data suppresses the power of background noise and interference from other users and separates the multipath components in time. In [99], both the pre–matched filter and post matched filter array covariance matrices were used to estimate the response of the array to the desired signal. Assuming the incoming signals to be modelled as point sources, bearing estimation would also appear to be a legitimate estimation technique for the received signal. Further discussion of the problem of estimating the received signal will be deferred until Chapter 6.

The purpose of this chapter is to analyse the S/I and BER improvement of a base station adaptive array over a conventional omni–directional receiver. To this end, some simplistic assumptions will be made about the radio channel and the CDMA system:

- For each CDMA user, an additive white Gaussian noise channel [145] will be assumed for both the reverse and forward links. This means that there is a single line–of–sight propagation path between the mobile and the base station.
- Where multiple users are in operation, the reverse link channels of all users will be subject to perfect power control so that each CDMA code arrives at the base station with the same power.
- The angle of arrival each user on the reverse link is known exactly, which implies the deployment of an effective bearing estimation technique at the base station antenna array.
- The time of arrival of each CDMA user's code is known, so that the base station is correctly synchronised.
- The receiver demodulates the RF signal to baseband using I and Q channel receivers and employs DPSK data modulation and de-modulation.

Both the forward and reverse links are crucial to the performance of a CDMA cellular system. In order to assess the benefits of deploying an antenna array in the base station, the analysis will begin with the reverse link.

5.2 The Reverse Link

To begin with, consider a base station containing a single receiver element, which observes signals from P active CDMA users. The complex baseband signal obtained from the receiver, $r(t)$, may be defined as follows:

$$r(t) = a\,d_1(t-t_1)c_1(t-t_1)\exp\{j\phi_1\} + a\sum_{p=2}^{P} d_p(t-t_p)c_p(t-t_p)\exp\{j\phi_p\} + \eta(t) \qquad (5.1)$$

where the first term represents the desired CDMA signal, the second is the total co-channel interference and finally $\eta(t)$ is additive white Gaussian noise. The amplitude of each signal a is a constant, because perfect power control is employed. The notation $d_p(t)$ and $c_p(t)$ indicates the random data sequence and the infinitely repeating CDMA code sequence of the p^{th} user, respectively. The scalar t_p is the time at which the p^{th} user began transmission and ϕ_p is the demodulated carrier phase term. The variables ϕ_p and t_p are random variables with the former distributed uniformly over $[0, 2\pi]$. The variable t_p has a uniform distribution over $[0, t_s]$, where t_s denotes the symbol period.

The base station receiver structure will contain one set of matched filters for each active CDMA code present on the reverse link. The desired user's filter attempts to maximise the signal-to-noise ratio (SNR) of the post–correlation signal $y_1(t)$, which is given by:

$$
\begin{aligned}
y_1(t) &= \int_{t-t_s}^{t} r(\omega) c_1(\omega - [t-t_s]) d\omega \\
&= \int_{t-t_s}^{t} a d_1(\omega - t_1) c_1(\omega - t_1) \exp\{j\phi_1\} c_1(\omega - [t-t_s]) d\omega \\
&\quad + \int_{t-t_s}^{t} a \sum_{p=2}^{P} d_p(\omega - t_p) c_p(\omega - t_p) \exp\{j\phi_p\} c_1(\omega - [t-t_s]) d\omega + n(t) \qquad (5.2)
\end{aligned}
$$

where $n(t)$ denotes the post–correlation noise. At the time instant t_0, when the desired signal is sampled for making a data decision, the signal $d_1(t)$ is subject to cross–correlation interference from other users and noise effects – the second and third terms respectively of the bottom line of equation (5.1). The current data symbol is reconstructed from the DPSK decision variable $2\Re\{y_1(t)y_1^*(t-t_s)\}$, where y^* denotes the complex–conjugate operation and $\Re$ denotes the real part of a complex number. If too many users attempt to transmit at the same time, the estimated data sequence for each user will contain a large number of errors, causing a catastrophic collapse of the system. This chapter will show how this problem can be alleviated by employing adaptive arrays at the base station.

5.2.1 Spatial Filtering for Antenna Arrays

Consider the received signal on the reverse link for a CDMA base station containing an M–element uniform linear array. The p^{th} signal arrives with bearing θ_p, so that the pre–correlation signal vector $\boldsymbol{r}(t) \in \mathbb{C}^{M\times 1}$ is given by:

$$
\boldsymbol{r}(t) = a d_1(t-t_1) c_1(t-t_1) \exp\{j\phi_1\} \boldsymbol{a}(\theta_1) + a \sum_{p=2}^{P} d_p(t-t_p) c_p(t-t_p) \exp\{j\phi_p\} \boldsymbol{a}(\theta_p) + \boldsymbol{\eta}(t) \quad (5.3)
$$

where $\boldsymbol{a}(\theta)$ is the array steering vector defined in equation (2.3) and $\boldsymbol{\eta}(t) \in \mathbb{C}^{M\times 1}$ represents additive white Gaussian noise. This equation holds provided that the spread spectrum signal bandwidth B_f is much smaller than the carrier frequency f, as explained in section 2.3.1. The post–correlation vector for the desired user $\boldsymbol{y}_1(t) \in \mathbb{C}^{M\times 1}$ is obtained by correlating the elements of $\boldsymbol{r}(t)$ with the code $c_1(t)$ according to equation (5.2).

There are a number of methods to recover the desired signal $d_1(t)$ whilst filtering out undesired interference, as explained in chapter 2. It is possible to design filters to place nulls in the directions of other CDMA users, with data independent or statistically optimum beamformers. However, as P may be much larger than M, only a few interferers may be completely cancelled. For simplicity, the vector product $\boldsymbol{a}^H(\theta_1)\boldsymbol{y}_1(t)$ will be used to pick out the desired signal, where $\boldsymbol{a}^H$ denotes the Hermitian transpose. If there are a large number of users with a uniform spread in angle, this beamformer will in any case be

close to the optimum filter for suppressing noise and interference [14].

5.2.2 Antenna Array Receiver Simulation

In order to analyse the effect of using an antenna array receiver in a CDMA system, simulation work was undertaken, with the following additional assumptions and conditions:

- One set of length $W = 31$ Gold codes were used to model multiple-access interference.
- The receiver was a uniform linear array (ULA), which can only detect signals unambiguously from one side of the array. As a result, each transmitter's bearing was uniformly distributed over [30^o,150^o] in order to mitigate the endfire effects associated with ULA geometries. Results for a broadside beamformer (i.e. bearing 90^o) in the presence of interference from all directions have previously been presented in [146].
- Rectangular pulse shaping was assumed, so that the receiver PN–code correlation operation is a linear process.

The main intention of this section is to derive an equation for the average S/I ratio generated when a set number of users, P, are present. Gilhousen et. al. [38] state that the average interference generated for the reverse link, as measured at a single antenna base station, is given by the equation:

$$S/I = \frac{W}{(P-1) + (\sigma^2/s)} \tag{5.4}$$

where s is the signal power of each CDMA user and W is the processing gain of each CDMA code. Note that this equation defines S/I to include the in-phase and quadrature noise components (of total power σ^2), with respect to the desired signal, so that the correlator receiver suppresses the power of all other users by a factor of $(1/W)$. This value is based on an equivalent noise bandwidth calculation, but in the examples given below for both synchronous and asynchronous correlations it was found that the average power suppression was better than this[1].

5.2.3 Analysis of Gold Code Cross-correlation Interference

5.2.3.1 Calculation of Synchronous Gold Code Cross-correlation Levels

The term *synchronous* in the context of CDMA system operation implies that the time of arrival for all active CDMA codes is the same [2]. This assumption is true for the forward link [38], but will not hold

[1] The values and graphs in the next sections have been calculated using a slightly different calculation method compared to [146], so that the results will not be exactly the same.

[2] This assumes that the multipath channel dispersion is negligible.

for the reverse link because of the different locations of the mobiles. However, the synchronous case provides the basis for analysing asynchronous CDMA interference which occurs on the reverse link.

Gold codes may be defined as follows: denote two length W m–sequences as length W binary vectors $\boldsymbol{v}_1$ and $\boldsymbol{v}_2$, following the notation of [40]. Provided the two codes are a preferred pair, the set of $W+2$ Gold codes $G(\boldsymbol{v}_1, \boldsymbol{v}_2)$ may be obtained from equation (2.2):

$$G(\boldsymbol{v}_1, \boldsymbol{v}_2) = \{\boldsymbol{v}_1, \boldsymbol{v}_2, \boldsymbol{v}_1 \oplus \boldsymbol{v}_2, \boldsymbol{v}_1 \oplus T\boldsymbol{v}_2, \boldsymbol{v}_1 \oplus T^2\boldsymbol{v}_2, \ldots, \boldsymbol{v}_1 \oplus T^{W-1}\boldsymbol{v}_2\} \tag{5.5}$$

where the operator T^k denotes the cyclic left–shift of the adjacent vector by k places and $\oplus$ denotes modulo-two addition. Binary codes are often specified using the levels 0 and 1: here, the usual transformation $[0, 1] \rightarrow [1, -1]$ is applied. Gold codes are block codes [145], because $(W+2)$ codes in total are produced by the modulo–2 addition of two preferentially selected PN-codes of length W. Therefore, in the context of CDMA communications the *periodic* cross–correlation may be defined as the correlation of an infinitely–repeating interfering code with a desired code. This may be written as:

$$wt(\boldsymbol{g}_b \oplus T^k\boldsymbol{g}_c) = wt(T^l\boldsymbol{g}_d) = wt(\boldsymbol{g}_d) \tag{5.6}$$

where $wt()$ denotes the weight or sum operator and $\boldsymbol{g}_b$ denotes the b^{th} Gold code from the set $G(\boldsymbol{v}_1, \boldsymbol{v}_2)$. Equation (5.6) represents the interference seen at a matched filter for code $\boldsymbol{g}_b$ because of the presence of code $\boldsymbol{g}_c$. The presumption of synchronous interference requires that the code shift $k = 0$. This equation will reduce to one or two equations involving the shift–and–add properties of the m-sequences $\boldsymbol{v}_1$ and $\boldsymbol{v}_2$. For example, the shift–and-add property of $\boldsymbol{v}_1$ may be expressed as:

$$\boldsymbol{v}_1 \oplus \boldsymbol{v}_1 = 0 \quad \boldsymbol{v}_1 \oplus T^k\boldsymbol{v}_1 = T^l\boldsymbol{v}_1 \text{ where } k \neq l, k \neq 0, l \neq 0 \tag{5.7}$$

This property has the same form for code $\boldsymbol{v}_2$, which means that code $\boldsymbol{g}_d$ may be obtained as a sum of $\boldsymbol{v}_1$ and $\boldsymbol{v}_2$, without explicit knowledge of $\boldsymbol{g}_b$ or $\boldsymbol{g}_c$. However, the prerequisite is that the shift–and-add properties of $\boldsymbol{v}_1$ and $\boldsymbol{v}_2$ must be known.

For the simulation work reported in this chapter, the m–sequences octal 51 and 73 were used to generate 33 length 31 Gold codes. The desired user was allocated code $\boldsymbol{g}_1 \equiv \boldsymbol{v}_1$. Evaluating equation (5.6) for all other codes led to a mean power level of 2.5, which when normalised to the auto-correlation peak level of $W^2 = 31^2 = 961$ gives a mean interference level $\overline{P}_{syn} = 0.002601 \equiv -25.8$ dB. The scalar $W\overline{P}_{syn}$ will be denoted as k_1.

5.2.3.2 Asynchronous Gold Code Interference

One method to obtain the power suppression factor for asynchronous Gold codes is to obtain the relevant probability density function (PDF). Specifically, the required PDF here is that for the ensemble average cross-correlation interference seen at the output of the matched filter for a desired code, due to the presence of a single interferer. The term *asynchronous* will be taken here to describe CDMA interference observed on the reverse link, consistent with the definition of the time delays $\{t_p\}$ in section 5.2 as real numbers in the range $[0, t_s]$.

In order to determine the nature of the asynchronous CDMA interference, equation (5.6) will now be evaluated for all integer values of k and d, for a desired code $\boldsymbol{g}_b$, to generate a cross–correlation interference (CCI) table of the resulting values d and l. If the weights of each code are known, it is possible to determine the *a priori* probability of a given interference level w occurring, $p(w)$, for a random integer time delay. The length 31 Gold codes have six different weights ± 1, ± 7 and ± 9. For the desired code $\boldsymbol{g}_1$, the probability of these pairs of weights occurring are $\frac{16}{32}$, $\frac{10}{32}$ and $\frac{6}{32}$ respectively.

In an asynchronous system, the time shift k will not generally be an integer value, but is instead chosen from a uniform distribution. If the time of arrival t_p is not an integer, the interference level w will lie on a linear transition between two values w_1 and w_2 which occur for the first integer time delay below t_p and the first integer delay above t_p respectively [3]. It is thus possible to define the *a posteriori* probability of w lying on the transition between the two values w_1 and w_2, $p(w_2|w_1)$, which is conditional on the probability $p(w_1)$. As an example, both sets of probabilities have been calculated for the first code $\boldsymbol{g}_1$ from the Gold code set (i.e. simply the preferred m-sequence $\boldsymbol{v}_1$). The probabilities $p(w_2|w_1)$ can be calculated in practice from the "CCI" table mentioned above. The process of generating periodic Gold code CCI may be modelled as a finite state machine as shown in figure 5.1.

The boxes show the *a priori* probabilities of the interference being at a given amplitude for a single interferer. The lines then show the conditional probabilities for the amplitude changing from one state to another. For example, the total probability of the interference being in the transition from ± 9 to ± 7 is:

$$p(\pm 9 \rightarrow \pm 7) = p(\pm 9)p(\pm 7|\pm 9) = \frac{6}{32} \times \frac{10}{31} = 0.06048 \tag{5.8}$$

with the numerical result expressed to four significant figures. This table may be used to determine the PDF for the Gold code interference due to a single user, which is shown in figure 5.2. A similar method for the construction of CCI PDFs for general code sets is described in [147].

To calculate the average interference power $\overline{P}_1$ due to one interfering source, the following integration is performed:

$$\overline{P}_1 = \int_{-9}^{9} \omega^2 \text{PDF}(\omega) d\omega = 20.33 \tag{5.9}$$

[3] This is a roundabout way of expressing the fact that the cross–correlation function of two codes with rectangular pulse shaping is a linear function of the time shift.

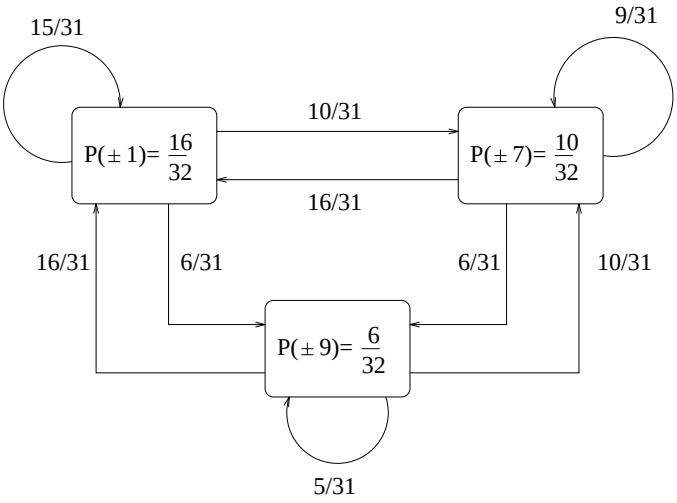

Figure 5.1: *The Finite State Machine Interpretation of Gold Code Interference, for Gold code* g_1.

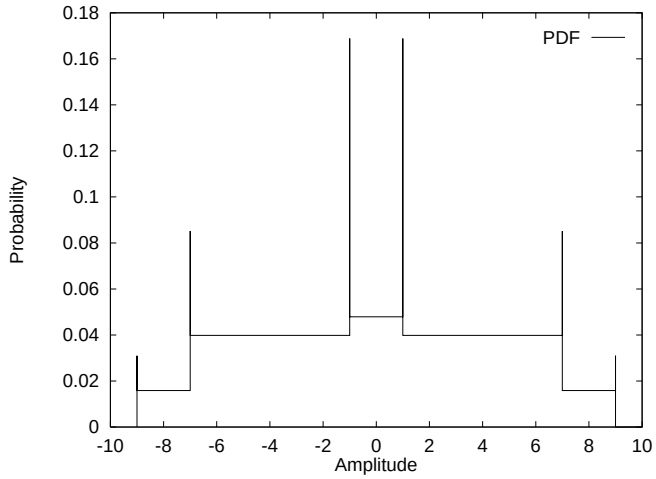

Figure 5.2: *The PDF of periodic Gold Code Cross-correlation Interference.*

where PDF(ω) denotes the periodic CCI PDF. Clearly this does not cover the situation where a data transition occurs on an interferer's signal during the correlation process – this is called the *odd* correlation function. To include this eventuality, a new function S^k will be defined, which multiplies the last k chips of the interfering code by -1. The general form of the odd cross–correlation function may therefore be expressed as:

$$wt(g_b + S^k[T^k g_c]) = wt(S^k[T^l g_d]) \tag{5.10}$$

There are many more integer interference levels possible, because the three-level cross-correlation property no longer holds and the resulting PDF has non-zero values in the range [-17,17]. However, equation (5.10) may be evaluated in the same way as equation (5.6) for all values of d and k to produce the finite state machine construction of odd cross–correlation interference. The PDF for odd CCI has been calculated from the finite state machine for code $\boldsymbol{g}_1$ and is shown in figure 5.3.

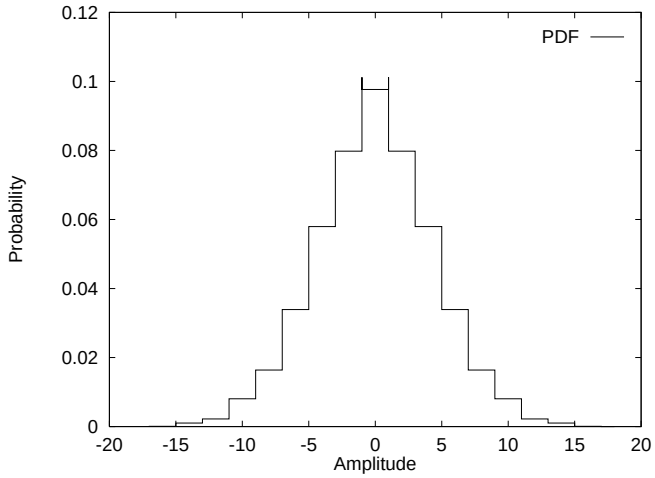

Figure 5.3: *The PDF of odd Gold Code Cross-correlation Interference.*

The mean power $\overline{P}_2$ in this case becomes 19.80. Assuming that data transitions occur with probability 0.5, the PDFs for periodic and odd cross–correlations may be averaged to obtain an overall PDF for Gold Code CCI. The form of this PDF is likely to resemble a triangular distribution: a triangular approximation to the true PDF has therefore been suggested [147, 148]. The two mean power values for periodic and odd CCI may be averaged and normalised with respect to the auto-correlation peak, which is W^2 = 961, to give the mean asynchronous CCI power value $\overline{P}_{asy}$ = 0.02088 ≡ -16.80 dB. This can be incorporated into the equation for the simulated S/I, giving:

$$S/I = \frac{W}{k_2(P-1) + (\sigma^2/s)} \tag{5.11}$$

where $k_2 = W\overline{P}_{asy}$.

The next issue to be discussed is the power suppression of other CDMA users by a linear array. It has already been pointed out that an M antenna diversity system suppresses white Gaussian noise by a factor M. Is the same true of other CDMA users?

5.2.4 The Effect of Spatial Filtering

5.2.4.1 The Suppression of Power From Other Directions

The effect of one unwanted CDMA user on the desired signal may be specified by the vector $c\,\boldsymbol{a}(\theta)$, where θ is the user's bearing (in radians) and c is the complex cross-correlation output from the reference sensor. In order to check the mean power suppression, $\overline{P}_s(M,\theta)$, the following integral must be performed [4] :

$$\overline{P}_s(M,\theta) = 3M^2/\{2\pi \int_{\pi/6}^{5\pi/6} |\boldsymbol{a}^H(\theta)\,\boldsymbol{a}(\omega)|^2 d\omega\} \tag{5.12}$$

This integral is related to Bessel functions of the first kind. As it stands there appears to be no simple analytic method to determine the result in closed form. Therefore, numerical methods are necessary to solve the problem. The well known limitation of endfire effects with ULAs are symptomatic of an additional problem, which is that $\overline{P}_s$ varies with the bearing θ [15]. This means that for a certain distribution of users throughout the cell, the S/I observed for some users will be better than that for other users, even if perfect power control is operating.

The assumption of 120^o sectorisation means that the antenna spacing may be increased to $\lambda_C/\sqrt{3}$ [67], where λ_C denotes the carrier wavelength, without obtaining grating lobes (which are analogous to aliasing effects in signal sampling). Equation (5.12) has been evaluated for two antenna spacings $\lambda_C/2$ and $\lambda_C/\sqrt{3}$, for a number of bearings and antenna sizes, in figures 5.4 and 5.5.

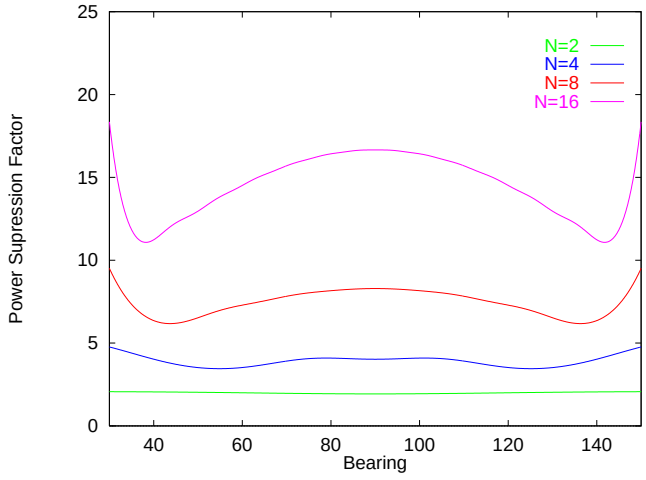

Figure 5.4: *The mean power suppression of a ULA with a spacing of* $\lambda_C/2$.

Comparison of the two figures shows broadly similar results for the two antenna spacings, when the antenna size is the same. The curves in figure 5.5 are smoother and subject to less variation than those in figure 5.4. However, antenna spacing of $\lambda_C/2$ may be preferable, according to how the boundary

[4] The M^2 factor arises because that is the value of $|\boldsymbol{a}^H(\theta)\,\boldsymbol{a}(\theta)|^2$, using equation (2.3).

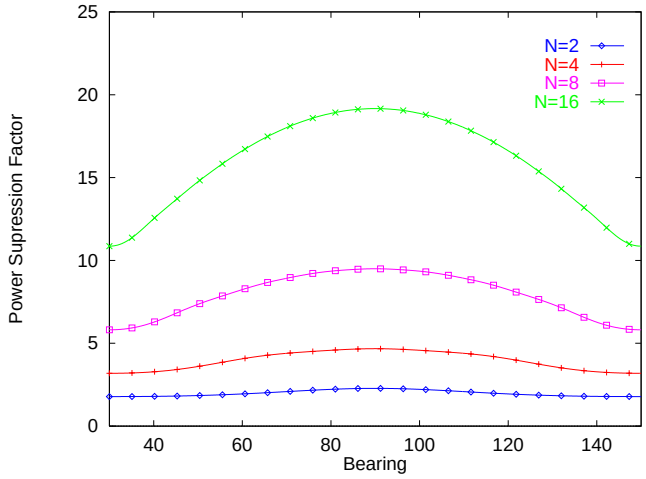

Figure 5.5: *The mean power suppression of a ULA with a spacing of* $\lambda_C/\sqrt{3}$.

between two 120^o sectorised antenna arrays is handled. The $\lambda_C/\sqrt{3}$ spaced array suffers from the problem that a beamformer with an intended direction near to 30^o has significant gain in the region of bearings near 150^o and vice versa, unlike the $\lambda_C/2$ spaced array.

In the case of these array configurations, it is more useful to estimate the worst case performance of the array as shown in figures 5.4 and 5.5, rather than the mean performance. Therefore, in the simulation work the desired source has been placed at the bearing with the worst power suppression factor for each array size. The $\lambda_C/2$ array configuration has been used as the worst case suppression factors are slightly better than those for the $\lambda_C/\sqrt{3}$, although the mean power suppression factor is better for the latter array. A table of the mean and worst case power suppression factors, along with the bearings at which the latter occur is shown in table 5.1.

	$\lambda_C/2$ **spacing**			$\lambda_C/\sqrt{3}$ **spacing**		
	$\overline{P}_s(M,\theta)$			$\overline{P}_s(M,\theta)$		
No of Antennas	**Mean**	**Worst**	**Bearing**	**Mean**	**Worst**	**Bearing**
2	1.998	1.933	90^o	1.986	1.782	30^o / 150^o
4	3.903	3.455	54.9^o / 125.1^o	3.973	3.188	30^o / 150^o
8	7.432	6.175	43.7^o / 136.3^o	7.963	5.813	30^o / 150^o
16	14.43	11.08	38.2^o / 141.8^o	15.95	10.86	30^o / 150^o

Table 5.1: *The mean and worst power suppression factors, with bearings for the latter, for* $\lambda_C/2$ *and* $\lambda_C/\sqrt{3}$ *spacing ULAs.*

5.2.4.2 The Statistics of the Filter Output

The effect of a spatial filter on interference that arrives with a uniform distribution in angle is very non-linear. This means that simple statistical assumptions about the interference at the output may not be good enough to provide accurate estimates of the system performance. To illustrate this point,

consider the equation for the magnitude response of a 2-element array with look direction $90^o(\frac{\pi}{2})$ to an interferer at bearing θ:

$$Y(\theta) = \sqrt{\frac{1}{2} + \frac{1}{2}\cos(\pi\cos(\theta))} \tag{5.13}$$

If the values of θ are restricted to $[0,\frac{\pi}{2}]$, $Y(\theta)$ is strictly increasing and is one-to-one and onto the range $[0,1]$. Under these conditions the function Y is invertible, with inverse Y^{-1}.

The cumulative distribution function (CDF) of the variable r , defined as $\{r : r = Y(\theta), 0 \leq \theta \leq \frac{\pi}{2}\}$, is given by:

$$\text{CDF}(r_0) = p(r \leq r_0) = \frac{2}{\pi}Y^{-1}(r_0) = \frac{2}{\pi}\cos^{-1}[\frac{1}{\pi}\cos^{-1}(2r_0^2 - 1)] \tag{5.14}$$

Differentiating the CDF function gives the probability density function PDF(r_0), which is defined as $\lim_{\Delta r \to 0} p(r_0 \leq r \leq r_0 + \Delta r)$. For the function Y, it is given by:

$$\begin{aligned} \text{PDF}(r_0) \quad = \quad & \frac{8r_0}{\pi^2}[1 - (2r_0^2 - 1)^2]^{-\frac{1}{2}} \times \\ & [1 - (\frac{1}{\pi}\cos^{-1}(2r_0^2 - 1))^2]^{-\frac{1}{2}} \\ & (0 \leq r_0 \leq 1) \end{aligned} \tag{5.15}$$

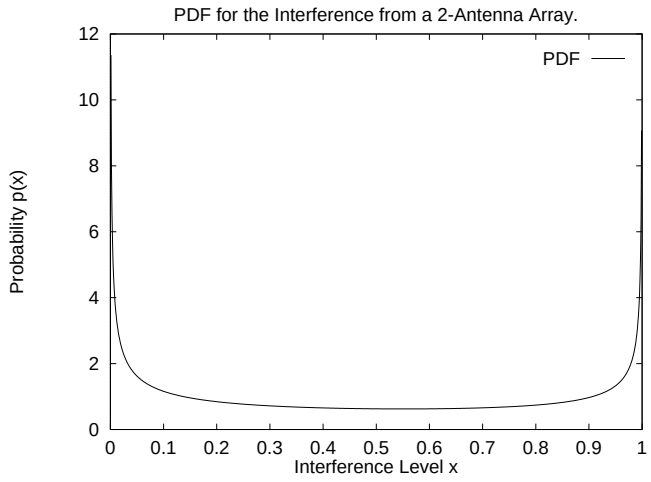

Figure 5.6: *The PDF of interference from a 2–element antenna array.*

The PDF function is shown in figure 5.6. When M >2, the magnitude function Y contains more than one sinusoidal function of θ and becomes difficult to invert analytically. Each time the gradient of $Y(\theta)$ is zero, then there is an infinite spike in the PDF. As the value of M increases, the PDF will contain more infinite spikes. In the case of M=2, the spikes in the curve indicate a high probability that the interference will be close to 1 or to 0.

In order to estimate the effect of interference of this type, a Bernoulli distribution has been proposed as a good model [12, 14]. The spatial filter is replaced by a step function which has a gain of 1 with probability $1/P_s(M,\theta)$ and a gain of zero otherwise. This effectively models the filter as a brick-wall, whose spatial width is the equivalent interference width. A pictorial representation of the approximation for an 8 element ULA with look direction 90^o is shown in figure 5.7. This figure also shows what has

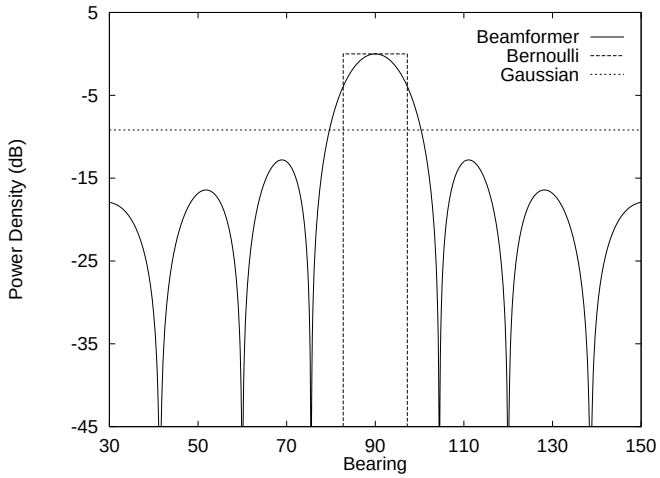

Figure 5.7: *The Bernoulli and Gaussian filter approximations.*

been termed a Gaussian approximation to the filter. This assumes that filter suppresses interference from all directions by a uniform amount, so that the output interference has a Gaussian distribution. It seems likely that the Bernoulli approximation will produce better estimates of system performance, as it provides a better approximation to the filter's behaviour.

5.2.5 Estimation of the System Performance

For both the Gaussian and Bernoulli approximations, the power suppression for an M–element array with look direction θ is simply $\overline{P}_s(M,\theta)$. Therefore, equation (5.11) may now be modified for an M–antenna receiver with a desired user at bearing θ, as follows:

$$S/I = \frac{W\overline{P}_s(M,\theta)}{k_2(P-1) + (\overline{P}_s(M,\theta)\sigma^2/[Ms])} \tag{5.16}$$

This equation may be used directly to predict the BER performance, assuming the interference to be Gaussian. Specifically, the BER of a signal received from an AWGN channel with DPSK demodulation is given by [145]:

$$\text{BER} = \frac{1}{2}\exp(-S/I) \tag{5.17}$$

Note: Gold code interference does not strictly follow a Gaussian distribution unless the number of interferers tends to infinity, according the central limit theorem. A closed form expression for the approximate BER using the Bernoulli distribution, which was discussed in section 5.2.4.2, is given by:

$$\text{BER} = \sum_{m=0}^{P-1} \left(\begin{array}{c} P-1 \\ m \end{array} \right) p(B)^m (1-p(B))^{P-1-m} (\frac{1}{2} \exp[-S/I(m)]) \tag{5.18}$$

where $p(B)$ denotes the probability of one user being in the main beam (i.e. having unity gain). The notation $S/I(m)$ denotes the signal-to-interference ratio for m users.

The Bernoulli approximation also provides the ability to estimate the probability $p(\text{BER} > \text{BER}_0)$ of a scenario occurring where the desired user's mean BER is worse than a set threshold BER_0. This may be done by calculating the number of users m_0 for which the BER threshold was first exceeded. The probability is then simply given by the equation:

$$p(\text{BER} > \text{BER}_0) = \sum_{m=m_0}^{P-1} \left(\begin{array}{c} P-1 \\ m \end{array} \right) p(B)^m (1-p(B))^{P-1-m} \tag{5.19}$$

5.3 Simulation Results

For the simulation, the noise power σ^2 was set to be $\frac{1}{31}$ times that of the desired signal. The bearing of the desired signal was set to be 90^o. Theoretical and simulation results are shown in figure 5.8: the former are plotted as lines, whereas the latter are shown as points. The horizontal axis measures the number of active CDMA interferers in terms of the number of Gold codes available: 100% indicates the presence of 32 interferers as all 33 codes are being used. This does not prevent other sets of codes being used to accommodate more users in the same sectored cell.

Figure 5.8 shows that equation (5.16) provides a good fit to the simulated data. Each time the number of antennas is doubled, the worst-case S/I values shown in the graph increase by 2–3 dB, according to the values in table 5.1. This type of improvement should offer considerable improvements in BER or capacity, depending on system requirements.

The curves in figures 5.9 and 5.10 show comparisons between simulated BER results and those calculated from the Gaussian and Bernoulli assumptions respectively. Again, the predicted results are plotted as lines, while the simulation results are shown as points. As expected, for a given number of users the worst-case BER performance improves considerably as the number of antenna elements increases. However, the improvement shown in the simulation results is not as good as that predicted by the Gaussian model. The more pessimistic results obtained from the Bernoulli approximation provide a much better fit to the results that are observed in this case. It is clear that as the number of users increases, the BER results converge towards the curves for the Gaussian model. This result follows because the Bernoulli distribution tends towards a Gaussian distribution as the number of components (in this case

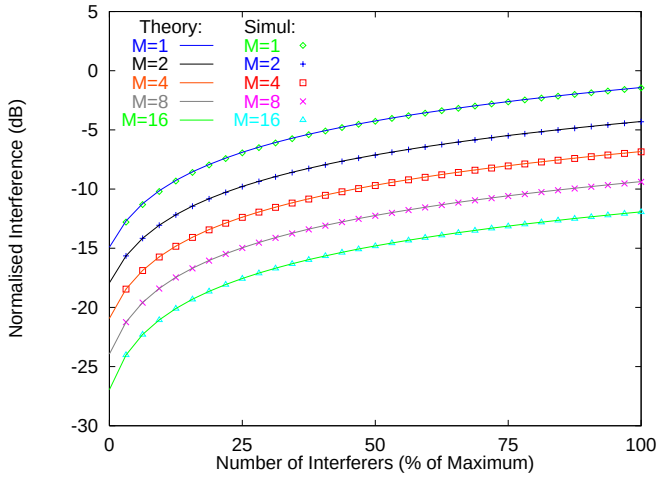

Figure 5.8: *Theoretical and simulated results for Interferer Power Suppression in an M –sensor element receiver.*

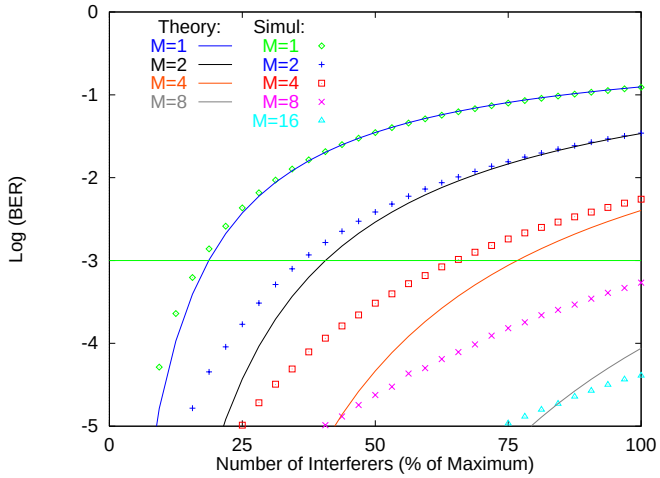

Figure 5.9: *Comparison of theoretical BER values using the Gaussian approximation and simulation results for an M –sensor element receiver.*

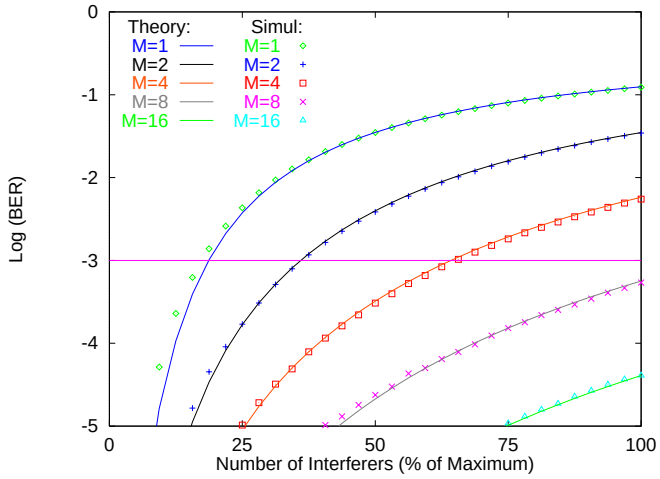

Figure 5.10: *Comparison of theoretical BER values using the Bernoulli approximation and simulation results for an M–sensor element receiver.*

interfering CDMA users) becomes large.

A common threshold for acceptable speech quality using a vocoder for human speech is that the mean BER should be 10^{-3} or less [38]. This is shown as a horizontal line in figures 5.9 and 5.10: this may be used as a crude measure of system capacity. For a single cell system containing 3 sectors, the mean capacity of 1 sector is likely to be 33% for full loading. On average this criterion is obtained even with only 2 antennas. However, increasing the number of antennas allows a sector to cope with heavy loading: 8 antennas permits 100% capacity whilst maintaining an average BER of 10^{-3}. Extending these results to longer code lengths, the BER curves will be closer to the Gaussian approximation for a given percentage of interferers, because more users can be accommodated on the same bandwidth.

These BER results have been averaged over a large number of different scenarios, each with different locations for the interfering mobiles. It is of interest to estimate the probability of a scenario occurring where the distribution of the mobiles is such that a given BER threshold is not attained for the desired mobile. One obvious scenario occurs when the mobiles are closely spaced, so that the spatial filter for the desired user cannot suppress the CDMA interference. The probability of the BER exceeding 10^{-3} has been calculated using equation (5.19) and the results are shown in figure 5.11. For a given number of users and antenna array elements, there is clearly a finite probability of unacceptable BER performance. This can be reduced by increasing the number of antenna elements, as might be expected.

5.4 Extension to The Forward Link

The forward path, from the main transmitter to each mobile receiver, may be subjected to a similar analysis. The same set of weights may be applied to the transmitter as to the receiver, so as to transmit most of the power in the line-of-sight path to the desired receiver.

It is also assumed that each CDMA signal is transmitted with equal power, so that forward path conditions

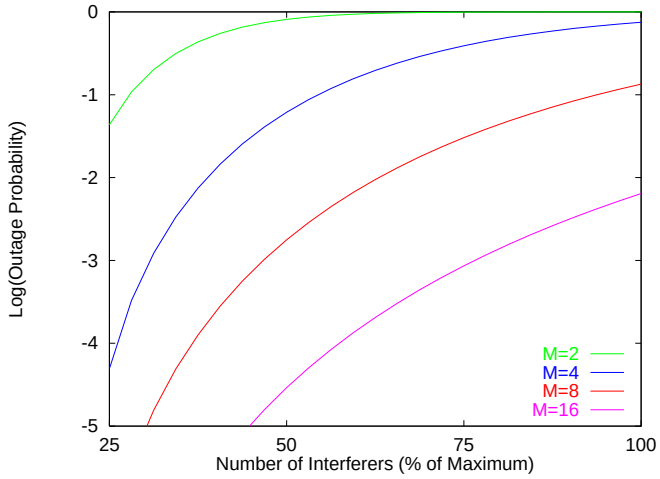

Figure 5.11: *The probability of a mobile distribution giving a mean BER*$> 10^{-3}$ *for an* M*–sensor element receiver.*

are similar to those of the reverse path. The equation for the S/I ratio is therefore identical to equation (5.17), except that the signal power, s, will vary with the distance, R, from the main transmitter. Assuming synchronous transmission of codes, the mean cross-correlation levels will tend to be much lower than that for asynchronous correlations. For the example of Gold code g_1 the mean synchronous interference level from one interfering user is 9 dB below that for asynchronous interference which is observed on the reverse link. Alternatively, orthogonal Walsh codes may be employed for synchronous transmission on the forward link [49], which would mean that the performance of each user is totally unaffected by multiple–access interference. In both cases, the reverse link is the limiting factor for CDMA capacity.

5.5 Cellular System Considerations

The analysis so far has only considered system performance for a single cell. In any practical mobile telephone system, the coverage area must be subdivided into cells in order to provide reasonable radio coverage and user capacity. In this section, a uniform layout of identically sized hexagonal cells will be assumed [38]. As before, each cell is sectorised into three sub-cells, each with 120^o coverage. It is assumed that complete frequency re-use is in operation, so that for the reverse link all mobiles in all cells transmit with the same frequency. This assumption implies that base station and mobile receivers will both be subject to interference from outside the cell as well as within the cell.

The effect of interference from neighbouring cells will now be analysed for both communications links, beginning with the reverse link.

5.5.1 Reverse Link Analysis

The hexagonal cell layout is shown in figure 5.12. Each cell is sectorised by a factor of three as shown, so

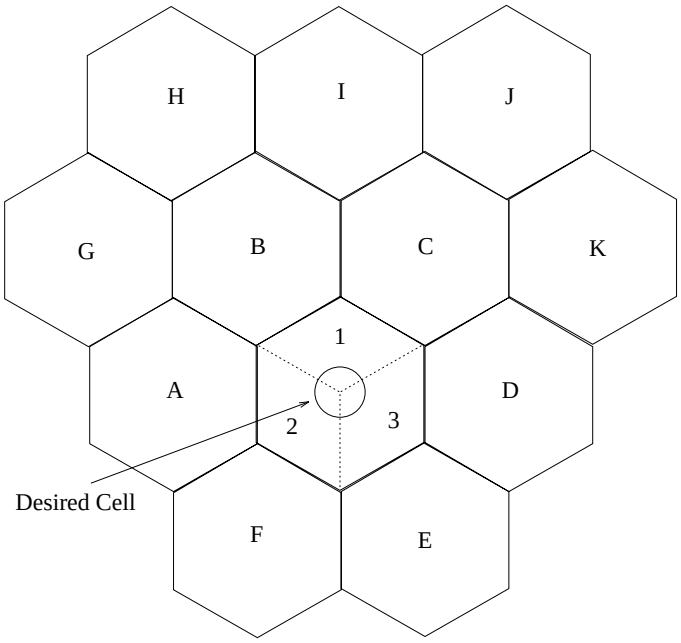

Figure 5.12: *The ideal hexagonal cell layout.*

that each base station receiver provides 120^o coverage. If one considers the sectorised cell labelled "1", it observes interference from two cells in the first layer of surrounding cells, namely B and C. Similarly, for the second layer, cells G-K are additional sources of CDMA interference. In order to provide an initial estimate of the interference caused, the following assumptions will be made:

- A uniform distribution of users is assumed throughout the cellular system. If one sectorised cell contains P users, each cell will contain a total of $3P$ active mobiles.
- Each mobile in an interfering cell is subject to perfect power control by its home base station.
- The propagation between an interfering mobile and the desired base station will be assumed to follow a path loss law with exponent 4 [38]. No fading effects will be considered here, as in [15].
- The interference will be assumed to be omni–directional, with uniform power observed at the base station from all directions.

These assumptions simplify the analysis considerably, compared to the likely conditions that will be observed in practice. However, they do provide a basis for estimating the likely effect of introducing adaptive arrays into existing cellular systems.

Compared to the analysis performed earlier in this chapter, the major alteration is that the background noise level is now due to inter-cell interference, which will change with the number of users present. In order to determine the effect of this, the average interference power s_i observed at the desired base station due to one user in an interfering cell must be estimated. The mobile under consideration transmits so that the received power s at its home base station is equal to that from every other user in the same sector.

Assuming that s is set to be the same for all base stations in the cellular system, s_i may be normalised by s. The interference power seen at the desired base station then depends only on the distances between the mobile and its home and the desired base stations. Denoting the former as R_1 and the latter as R_2, the ratio of s_i to s is given by [15]:

$$\frac{s_i}{s} = (\frac{R_1}{R_2})^4 \tag{5.20}$$

In order to estimate the effect of inter-cell interference, equation (5.20) must be evaluated for all possible positions of the mobile in the adjacent cell. This is equivalent to evaluating the following integral:

$$I = \frac{1}{\sigma(A_i)} \int_{A_i} \frac{s_i}{s} dA_i \tag{5.21}$$

where A_i denotes one interfering hexagonal cell and $\sigma(A_i)$ denotes the area of that cell. Equation (5.21) has been evaluated by Monte Carlo integration for the first two layers of interfering cells with the following results. For the first layer the result of the integral, denoted as β_1, was 0.0636. For the second layer the value obtained, β_2, was 0.00294. Given that there are on average $6P$ interfering users in the first layer and $12P$ users in the second layer, this means that level of inter-cell interference is 0.428 times the in-cell interference. Alternatively, approximately 30% of the total interference is due to inter-cell interference.

Equation (5.16) may thus be modified for a cellular system to give:

$$S/I = \frac{WP_s(M,\theta)}{k_2[(P-1) + \beta_1(6P) + \beta_2(12P)]} \tag{5.22}$$

The first term in the denominator is the interference from users in the same cell as the desired user, the second arises from the $6P$ users in the two interfering cells in the first layer (B and C in figure 5.12) and the third comes from the $12P$ users present in the five interfering cells in the second layer (cells G-K). Background noise due to thermal effects etc. has been neglected for this equation. Equation (5.22) may be evaluated for the worst case signal bearings as before to obtain a comparison between sectorised base station receivers with different numbers of antenna elements. The results are shown in figure 5.13. For large numbers of interferers, the normalised interference levels are roughly 1.5 dB greater than for the single cell case, shown in figure 5.8. However, the S/I value for a given capacity again shows a 2–3 dB improvement each time the antenna array size is doubled.

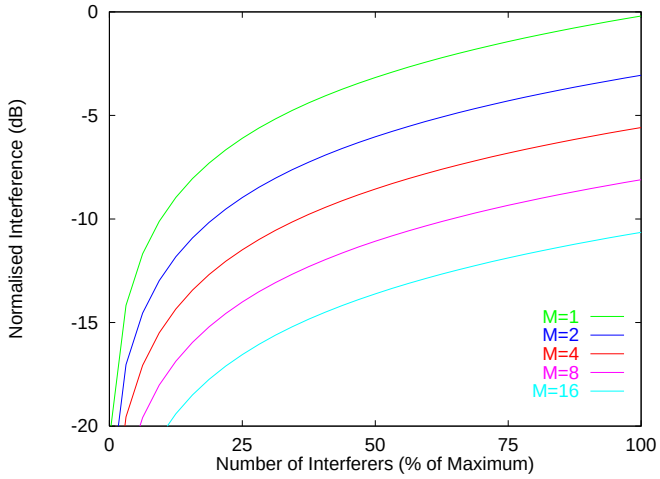

Figure 5.13: *The normalised interference for the reverse link.*

5.5.2 Forward Link Analysis

In this subsection, a worst-case situation will be considered to provide some measure of the improvement offered by antenna array transmission on the forward link. The case for a mobile placed near to the boundary of three cells is generally accepted as the limiting case for the performance of a cellular CDMA system [37], as shown in figure 5.14. The mobile is assumed to be at distance R_0 from base stations

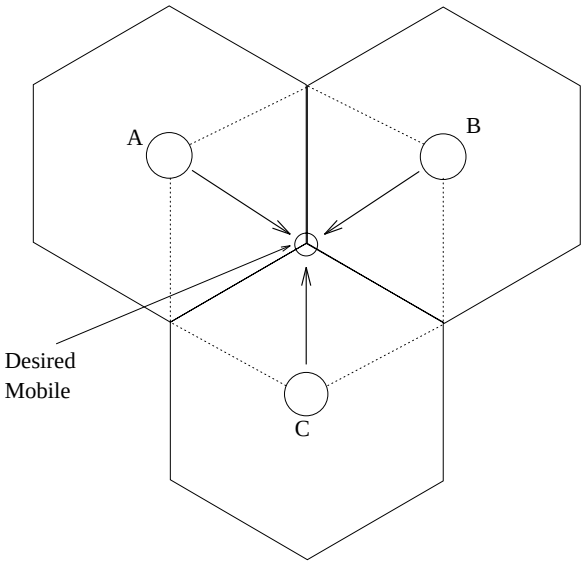

Figure 5.14: *The worst-case location for a mobile on the forward link.*

A, B and C: it will be assumed to be in communication with base station A. As before, each cell sector contains P users and each base station transmits synchronously to all the mobiles in its sector with the same power. The parameters of all the cells relevant to the interference observed at the mobile are given in table 5.2.

Base Stn Group	Number of Sectors	Mobile Radius	Mobile Bearing	$\overline{P}_s(2,\theta)$	$\overline{P}_s(4,\theta)$	$\overline{P}_s(8,\theta)$	$\overline{P}_s(16,\theta)$
1	1	R_0	90^o	1.933	4.025	8.291	16.655
2	2	R_0	90^o	1.933	4.025	8.291	16.655
3	6	$2R_0$	$30^o/150^o$	2.065	4.765	9.513	18.352
4	6	$2.646R_0$	$70.9^o/109.1^o$	1.965	3.947	7.870	15.790

Table 5.2: *Table of desired and interfering base station sector parameters for forward link, including the power suppression levels for antenna sizes M = 2,4,8 and 16.*

To summarise, the mobile sees synchronous interference from $P-1$ other mobiles present in the same sector of cell A (group 1). It also sees asynchronous interference from $2P$ users present in the nearest sectors of cells B and C (group 2). In addition [37], there are 6 base stations sectors at a distance of $2R_0$ from the mobile (group 3) and 6 at a distance $2.646R_0$ (group 4). The S/I level seen by the mobile for base stations employing omni–directional antennas is given by:

$$S/I = \frac{W}{k_1(P-1) + k_2[(2P) + (2^{-4})(6P) + (2.646^{-4})(6P)]} \tag{5.23}$$

If the base stations now contain M–element transmit antennas, and each base station transmits each user's information in the direction of that mobile, the mean interference power will be reduced. The S/I obtained for the antenna array case is:

$$S/I = \frac{W}{[k_1(P-1)/\overline{P}_1] + k_2[(2P/\overline{P}_2) + (6P)(2^{-4}/\overline{P}_3) + (6P)(2.646^{-4}/\overline{P}_4)]} \tag{5.24}$$

where the notation $\overline{P}_k$ is shorthand for $\overline{P}_s(M,\theta_k)$, the power suppression factor for the k^{th} group of base stations as specified in table 5.2. Otherwise, system parameters are unchanged from those used in section 5.3. Equations (5.23) and (5.24) have been evaluated for varying numbers of users and antenna elements and the results are shown in figure 5.15.

As with previous results in this chapter, employing adaptive antenna transmission considerably improves system performance. The interference levels shown here are generally worse for the same capacity and antenna size than those shown in figure 5.13. However, the analysis described here is somewhat pessimistic: soft handoff techniques combined with a forward link power control scheme, such as those described in [37], would considerably improve the S/I for a mobile placed at a cell boundary.

5.6 Discussion and Comparison of Results

Results for both single cell and cellular system operation show that base station antenna arrays operating over simple AWGN channels provide significant S/I and BER improvements for CDMA systems. This means that for the same capacity as a single receiver configuration, the quality of the communications link may be considerably improved. Alternatively, the capacity of the cell may be increased with an

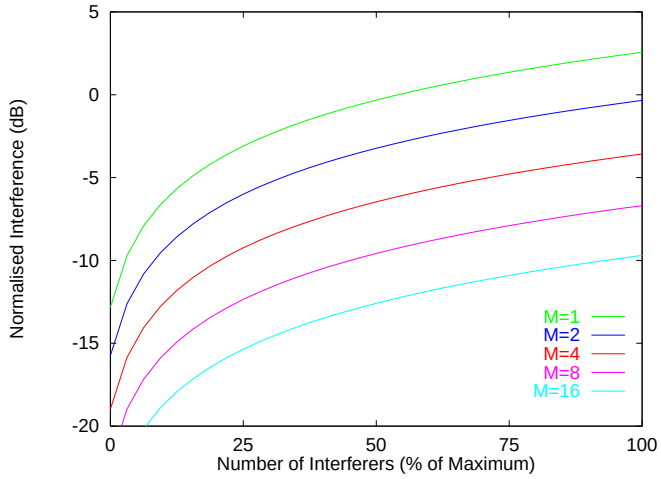

Figure 5.15: *The normalised interference for the forward link.*

adaptive array, whilst maintaining the same link quality as for single receiver base stations. These results are not surprising, as an antenna array has the capability to exploit the spatial diversity of a sectorised cell to reduce unwanted interference while a single antenna receiver has no spatial discrimination at all.

It is interesting to compare the results presented here, with those already documented in the literature. Swales et. al. [12] present analysis of a (narrowband) non–sectorised cellular system, which is capable of forming M Bernoulli–type beams of angular width $\frac{360^o}{M}$. This means that for a uniform distribution of mobiles, the base station can offer M times as many channels for a given mobile to communicate over in the same frequency. Hence, for any modulation scheme, the antenna array will considerably reduce the outage probability for a given S/I threshold at a given capacity. This would suggest a considerable capacity increase, as the S/I level increases in proportion to M: in the analysis reported here, this is not quite true because of the variable width of ULA beams with angle of arrival.

Two more recent journal papers focus specifically on the capacity improvements offered by sectorisation and adaptive antenna schemes. The first paper [15] considers a number of sectorisation and adaptive antenna schemes which could be implemented at the base station of a cellular system. The channel model used is similar to that presented in section 5.5 and theoretical results were derived for coherent PSK modulation. Not surprisingly, the best BER performance by far was obtained for a system employing 120^o sectorisation and 3-element adaptive arrays in each sector. This paper also discusses adaptive antennas at the mobile for directional transmission to the base station, which would reduce interference to neighbouring cells. However, such a concept may be difficult to implement in practice, unless the forward link is very directional. In many cases, particularly in urban environments, the mobile may observe incoming signals from a wide spread of angles [149], making directional transmission difficult on the reverse link.

The second paper [14] provides an extension of the theoretical analysis of [38] to a base station configuration containing a circular receive and transmit array, with no sectorisation. Perfect power

control is assumed for in–cell interference and the modulation scheme is again PSK. A much more rigourous analysis of inter-cell interference is included, considering the effects of fast Rayleigh and slower log-normal fading. As mentioned earlier, the Bernoulli approximation is used to model the effect of a spatial filter on directional interference. Results are presented for the outage probability of both the forward and reverse links, with an SNR of 7 dB chosen as the acceptable quality threshold. Again, results show a considerable performance improvement, even for small antenna sizes (5–7 elements).

Several points should be made concerning the limitations of the analysis presented in this chapter.

- The analysis presented did not include voice activity detection schemes, which allow transmissions to occur only when a caller is speaking (35–40% of the total call duration is often quoted). Modelling this effect by a Bernoulli random variable [38] shows that an additional two-fold capacity increase may be obtained through employing such a system.
- Perfect power control has been assumed. Recent results suggest that a more realistic model for the power of each user is a log-normal random variable, with a standard deviation of 1.5 dB for stationary or slowly moving mobiles. A standard deviation of 2.5 dB has been measured for faster vehicles [49]. Clearly, such effects will be detrimental to system capacity, whatever antenna configuration is present in the base station [150].
- It has been assumed that each transmitter had a single line-of-sight path to the receiver. In practice, there may be several multipaths received from each source. This increases the complexity of the signal processing required and may reduce the system gain.

5.7 Conclusion

This chapter has addressed the capacity of a CDMA system employing adaptive antennas. Using a simple channel model, significant capacity increases have been demonstrated for small antenna arrays operating in both single cell sectors and general cellular systems. Adaptive arrays are thus an important receiver architecture for taking advantage of the different locations of cellular users to reduce CDMA interference levels. However, two points of note are that the antenna array's ability to suppress interference depends on the source bearing and that steering vector filters are best modelled using the Bernoulli distribution. A method has also been presented for determining the probability density function of CDMA interference, which can be useful in determining the performance of CDMA networks. It is important to determine the performance of CDMA systems when operating in more realistic channels, which include multipath fading effects. This subject will be discussed in much more detail in the next chapter.

Chapter 6

Array Processing and Fading Channels

This chapter will discuss the performance of array processing techniques for more realistic channel models. In many environments, most notably urban areas, modelling the radio channel by a single line of sight path is inadequate. There are usually many obstacles between the transmitter and receiver, which means the base station will observe a number of copies of the signal – this is called multipath propagation. Often the transmitter and/or the receiver are in motion, giving rise to a received signal that varies with time.

This chapter will look briefly at the basic models for narrow-band channels, before moving on to look at frequency selective channel modelling. This type of analysis is more appropriate for spread spectrum systems, as the transmission bandwidth is often much wider than the coherence bandwidth of the channel. This work will be applied to antenna arrays in order to determine how the behaviour of communications systems are modified under such conditions. Two channel types will be considered, beginning with point source models for the separately resolvable multipath components. The effect of finite fading frequencies and self–noise interference are considered and some results are also presented for multiple CDMA users. Secondly, channels which involve a finite spread in angle of arrival for a received signal will be analysed to see how system performance on the reverse and forward links changes.

6.1 The Urban Mobile Radio Channel

This section will seek to define the characteristics of a typical mobile radio channel observed in areas of large population concentrations. Specifically, environments containing a number of obstacles, such as buildings, walls and traffic, will be considered. In this situation, a number of possible mechanisms exist to facilitate the propagation of radio waves from the transmitter to the receiver. In order to expedite the introduction, parameters for the radio system to be used throughout this chapter are defined in table 6.1. The typical characteristics of a narrowband signal[1] received in the 900 MHz band will be initially considered. This may be extended to include the effect of transmitting a wide bandwidth signal.

[1] In this chapter, the term narrowband will be taken to mean that the coherence bandwidth of the channel is much wider than that of the received signal, so that the channel is flat–fading.

Parameter	Value
Data Rate	10 kb/s
CDMA Code Length	127 Chips
CDMA Chip Rate	1.27 MChips/s
Carrier Frequency	900 MHz
Modulation	DPSK
Vehicle Speed	30 mph
Fading Frequency	50 Hz

Table 6.1: *The spread spectrum system parameters for chapter 6.*

6.2 Narrowband Channel Modelling

Effective communication in urban areas is an extremely complex subject; indeed, it has been described as involving "problems so difficult they challenge the imagination" [30, p11]. Consider a base station, placed on top of a high building, attempting to communicate with a mobile receiver placed at street level. In an urban area, there are a large number of buildings present, which can block or assist the transmitted electromagnetic (EM) signal. Indeed, there are several mechanisms by which the signal may propagate through an environment [151]. These are described below and illustrated pictorially in figure 6.1:

(i). **Line–of–sight (LOS) propagation:** Not surprisingly, this mode of EM wave motion occurs when the mobile is clearly in view of the base station, so that the first Fresnel zone of the signal is not being blocked [152]. For many locations of the mobile in an urban cellular environment this is not true, so other methods of propagation must account for the transmitted signal reaching the mobile.

(ii). **Reflection:** This occurs when the EM energy from the mobile is deflected off a building in order to reach the base station. In an urban area, reflection is a significant factor in allowing acceptable radio communications.

(iii). **Diffraction:** Where an obstacle such as a building blocks the LOS path, EM signals may diffract over roofs or round the sides of buildings to reach the base station. This involves only low power outer Fresnel zones reaching the base station unobstructed, so that the received signal power tends to be much lower than that for LOS communication.

(iv). **Scattering:** When an EM wave reaches an obstacle or group of obstacles, energy can sometimes be reflected randomly in a large number of directions. This occurrence is the most difficult to predict analytically.

Typically, two or three of these mechanisms account for the propagation of an EM wave in an urban environment. As a result, there are a large number of paths by which energy from the base station may reach the mobile. In order to explain the characteristics of the signal received by the mobile, it is common to appeal to three separate effects.

The most significant mechanism, in terms of receiver performance is *fast fading* [30, Chapter 1] [152, 153] [154, Chapter 1]. In an urban area, the received signal at the mobile is the summation of a large number of

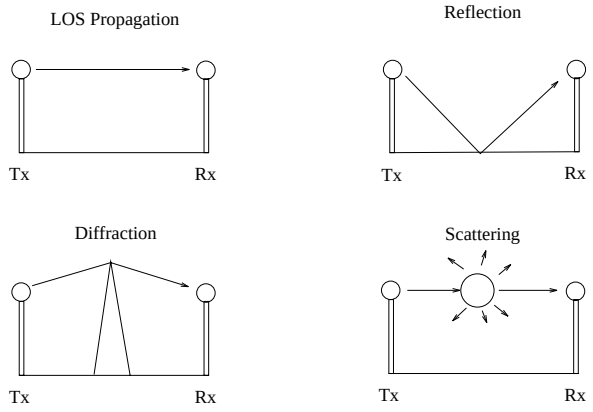

Figure 6.1: *Modes of electromagnetic propagation.*

independent multipath components. The received signal may be subject to constructive or deconstructive interference, according to the phases of the multipaths. It is commonly assumed that the received signal is *wide–sense stationary* for the mobile moving short distances up to a few tens of carrier wavelengths or so [35]. In the context of mobile radio, this means that variations in the received signal envelope occur mainly due to phase-changes of the same multipath components. These fluctuations can be significant, because at 900 MHz multipath electrical length changes of only a few centimetres can alter the given component's phase by 90–180^o. This means that constructive interference patterns may rapidly change into deconstructive interference or *deep fades* with a small alteration in position. Quantitatively, this corresponds to frequent changes of signal power in the range 20–30 dB [152, Chapter 5].

Movement of the mobile over longer distances changes the paths by which the signal is received by the mobile. This leads to a slower variation in the average received signal power, often called *shadowing* [155] . The accepted model for the variation in the average power is a log–normal distribution, whose standard deviation is in the range 4–12 dB [12] [152, Chapter 3] [154, Chapter 2]. The average signal power also depends on the mobile's distance from the base station, according to a path loss law [152–154]. Normally the power will be proportional to R^{-n} where R is the distance and n is usually termed the path–loss exponent. The value of n has been measured in a large number of environments and numbers in the range of 2–5.5 have been quoted [38]. However, the most common choice of n for modelling cellular radio systems is 4, which corresponds to plane–earth propagation [152, Chapter 2].

It is possible to employ a power control system to mitigate the effects of fading on its transmitted signal, so that shadowing and path–loss mechanisms can be compensated for. However, if the mobile is moving quickly, fast fading effects may be too rapid and unpredictable to cope with. Therefore, the distribution of the fast fading signal is vital in predicting the performance of any mobile radio system. Many measurements of microwave narrowband mobile radio channels have been carried out for both indoor and outdoor environments. Where a LOS path exists between the transmitter (Tx) and receiver (Rx), the probability density function (PDF) of the received signal usually follows a Rician distribution [156]. However, in this chapter, the worst case situation will be considered, where there is no LOS path propagation. When this occurs, the most common statistical characterisation for the

fast–fading received signal envelope is the Rayleigh distribution.

6.2.1 The Rayleigh Distribution

The Rayleigh distribution arises as the distribution of the root-sum-square of two independent Gaussian distributed variables. This model is important because it describes the envelope of the received signal where it is made up of a large number of independent, equal amplitude multipath components. In practice, these occur because there are many independent scatterers present between the transmitter and receiver. All the components may be assumed to be drawn from the same distribution, so that the central limit theorem may be applied. Hence, as the number of scatterers tends to infinity, the I and Q components of the signal become uncorrelated and each will tend towards Gaussian distribution.

The probability density function of the Rayleigh distribution is given by:

$$\text{PDF}(r) = \frac{r}{\overline{r}^2} \exp(\frac{-r^2}{2\overline{r}^2}) \tag{6.1}$$

The variable r denotes the root-sum-square of the I and Q channel components and $2\overline{r}^2$ denotes the mean power of the received signal. It has been noted that the sum of 6 or more independent sine waves [30, p68] [152, Chapter 5] can give rise to a distribution that is very close to the Rayleigh distribution , except at the extreme peaks. As the received signal comprises two identical, independently distributed (iid) Gaussian random variables, the phase will be uniformly distributed over the range $[0, 2\pi]$.

The Rayleigh distribution provides a description of the ensemble of all possible received signal envelopes. However, it does not indicate how the received signal alters with time. The time variation is mainly dependent on the velocity of the mobile, which gives rise to a *Doppler shift* in carrier frequency of the received signal.

6.2.2 The Doppler effect

The Doppler effect [152, Chapter 5] occurs due to relative motion between the transmitter and receiver. The most common instance in everyday life occurs when the frequency of a siren on an ambulance or police car is observed to change as it approaches and passes a stationary observer. The observed frequency of the signal increases when the relative motion brings the transmitter closer to the receiver. Alternatively, when the transmitter moves away from the receiver, the observed frequency is reduced. The precise frequency variation is given by the following equation:

$$\Delta\nu = v/\lambda_C \tag{6.2}$$

where $\Delta\nu$ denotes the observed change in frequency, v denotes the velocity of the transmitter and receiver towards each other and λ_C denotes the carrier wavelength of the propagating signal.

If there is non-zero relative motion between the transmitter and receiver, the effect on the received multipath signal is that it changes with time. However, it should be emphasised that the time dependency of the signal is caused by the receiver moving through an EM field with varying multipath channel characteristics. The faster the relative motion, the more quickly the received signal changes. This will lead to difficulties in tracking the received signal effectively.

6.3 Frequency Selective Channel Modelling

Having considered how narrowband channels may be modelled, it is now possible to extend these results to frequency selective channels, which are often observed in spread spectrum systems. In this case, the bandwidth of the transmitted signal is often wider than the coherence bandwidth of the channel, so that different frequency components of the signal are subject to independent fading effects – frequency selective fading [43, Chapter 7]. In the time domain, the result of this effect is that the impulse response of the channel consists of a number of impulses of varying amplitude, each with an associated time delay. In addition, the multipath components change in time because of the Doppler effect, which means that the multipaths are subject to time selective fading [154, Chapter 2].

In order to assess these effects simultaneously, consider sounding the channel with an infinite bandwidth signal, e.g. an impulse. The received signal represents the impulse response of the channel and it may be characterised by two-dimensional Bello functions [157]. There are a large number of these, all related by Fourier transform relationships. However, the most useful function for visualising the channel impulse response is probably $S_p(\tau,\nu)$, the function of the complex received signal against time delay τ and Doppler frequency ν. It is defined as the summation of all components with the correct time delay and Doppler frequency [154, Chapter 2]:

$$S_p(\tau,\nu) = \sum_i a_i(t)\exp\{-j\phi_i(t)\} \quad \text{where} \quad \tau_i(t)=\tau, \quad \nu_i(t)=\nu \tag{6.3}$$

where $a_i(t)$ denotes the amplitude of the i^{th} path with delay $\tau_i(t)=\tau$ and Doppler frequency $\nu_i(t)=\nu$; the notation $\phi_i(t)$ denotes its phase. This equation indicates the fact that a finite number of propagation paths exist between the base station and mobile. However, as this number is indeterminate and possibly quite large, $S_p(\tau,\nu)$ is usually taken to be a continuous function of τ and ν [154, Chapter 2].

This function allows the received signal to be characterised in terms of both time dispersion and associated frequency fading effects. In practice, however, one only has access to finite bandwidth signal transmissions. Consider the transmission of a data–modulated spread spectrum code $c(t)$, which has a chip period of t_c, code period t_s and processing gain $W = t_c/t_s$. The baseband received signal is passed through I and Q filters matched to the code $c(t)$ to give the post–correlation signal $x(t)$:

$$x(t) = \int_{t-t_s}^{t} d\omega \int_{0}^{\infty} d\tau \int_{-\infty}^{\infty} S(\tau,\nu) d(\omega-\tau) c(\omega-\tau) c(\omega-t-t_s) \exp(j2\pi\nu\tau) d\nu \qquad (6.4)$$

where $d(t)$ denotes the transmitted symbol stream, which has minimum period t_s. For large values of W, the periodic and odd code auto–correlation functions, denoted as $\delta_c(t)$, take on non–negligible values within one chip of the time of arrival of the code. This is usually taken to mean that multipath components separated in time delay by at least t_c may be separately resolved. An approximation to $S(\tau,\nu)$ may therefore be calculated using $c(t)$ with time resolution t_c. Two typical time delay vs Doppler frequency *power spectra* calculated in this manner are shown in figure 6.2 (taken from [35] and [30] respectively).

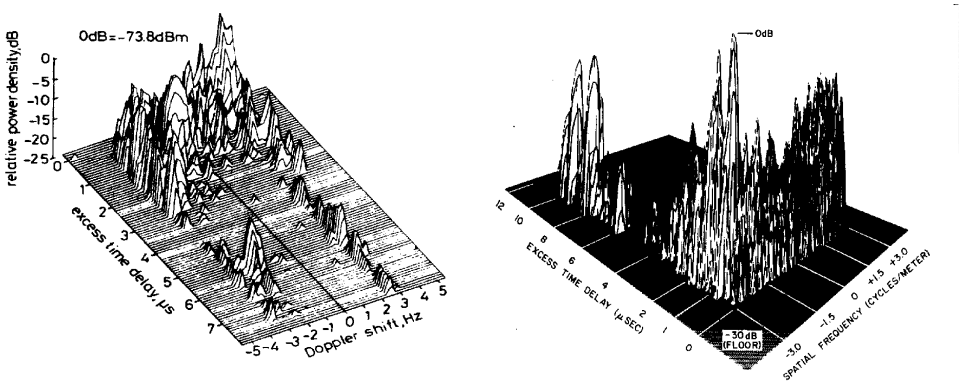

Figure 6.2: *Two typical time delay vs Doppler frequency profiles taken from [35] and [30] respectively.*

The time resolution of $y(t)$ means that if the channel impulse response contains significant multipath components over a time t_m, the spread spectrum receiver will observe int$\{1 + \frac{t_m}{t_c}\}$ components – the time bandwidth product of the channel and the transmitted signal [43]. This leads to a discrete-time channel approximation of $y(t)$, which is due to Turin [158]. This model is much simpler to use in practical simulation work than equation (6.4). Assuming the CDMA receiver can separately resolve Q components, the model consists of Q fading components as follows:

$$x(t) = \sum_{q=1}^{Q} h(q,t) \delta_c(t - (t_o + (q-1)t_c)) \qquad (6.5)$$

where t_o denotes the initial time of arrival of the start of the first PN code chip for the first channel tap. The value of $\delta_c(t)$ is given by:

$$\delta_c(t) = \int_{t-t_s}^{t} d(\omega) c(\omega) c(\omega - t + t_s) d\omega \qquad (6.6)$$

Each channel tap can in theory be obtained by integrating equation (6.4) only over the range of excess time delays represented by one channel tap. In practice, the overall results will not be seriously

altered if each tap coefficient $h(q,t)$ is modelled as a narrowband fading signal. The receiver only has access to the noise corrupted estimate of $x(t)$, denoted as $y(t)$. Sampling $y(t)$ at time instants $t_o + nt_s$,$t_o + nt_s + t_c$,$t_o + nt_s + 2t_c$, ..., $t_o + nt_s + (Q-1)t_c$ provides the Q taps of the received multipath signal for the n^{th} symbol.

6.3.1 Frequency Fading Distributions

It is commonly assumed that the coefficients $\{h(q,t)\}$ are independent random variables, which are wide–sense–stationary. This means that a different group of scatterers is responsible for each coefficient $h(q,t)$ and that over the time of interest, that group of scatterers remains the same. Close study of profiles like those in figure 6.2 shows two independent modes of scattering: near–in and far–out scattering [37]. These two mechanisms may be used to generate the channel taps $\{h(q,t)\}$ in simulation work.

Near–in scattering [37] refers to the first set of multipaths that arrive at the mobile from the base station. These are usually due to scatterers close to the mobile, such as buildings on nearby streets. A transition then occurs as the time–delay increases, so that most of the multipaths are due to isolated reflections from distant buildings or hilly terrain. The Doppler frequency characteristics of these two modes of multipath propagation will now be discussed in turn.

6.3.1.1 Near–in Scattering

The most commonly used model for close in scattering effects consists of a circle of point scatterers placed around the location of the mobile [153]. In physical terms, these scatters would be buildings close by the mobile's location. This type of scattering has been extensively analysed by several authors [152,159,160]. In this section the simplest model, due to Clarke [159], will be quickly sketched. It is assumed that the mobile receives from or transmits to a large number of scatterers, with a uniform distribution of angle round a circle of a specified radius. This leads to the Doppler frequency of the received signal having a cosine relationship with angle. A two-dimensional slice of the power spectrum $S(\nu)$ for a small value of $\tau = \tau_0$ has the following form:

$$S(\nu) = |S_p(\tau_0, \nu)|^2 = \frac{a}{1 - (\frac{\nu}{\nu_m})^2} \qquad |\nu| \leq \nu_m \tag{6.7}$$

where a denotes a scaling factor and ν_m denotes the maximum Doppler frequency, which corresponds to the vehicle velocity. The value of $S(\nu)$ is zero when $|\nu| > \nu_m$. This equation gives rise to singularities at $\nu = \pm\nu_m$: however, the general form of the spectrum fits closely to observed power spectra [152, Chapter 5]. The Wiener–Khinchine theorem [156] may now be applied to equation (6.7) to obtain the auto-correlation function (ACF) of the channel impulse response at delay τ_0. It turns out to be simply a scaled Bessel function of the first kind (denoted as J_o):

$$R(\tau_0, t) = \frac{1}{2\pi} \int_{-\infty}^{\infty} S(\nu) \exp\{j\nu t\} d\nu = a J_o(2\pi\nu_m t) \tag{6.8}$$

This type of scattering model is widely used throughout the literature of channel modelling and simulation and is often termed the classical Doppler model. The probability density function of the received signal will clearly be approximated by a Rayleigh distribution; the parameter $h(q,t)$ may then be calculated in one of two ways. The first method involves modelling the received signal as filtered white noise. It is possible to design infinite-impulse response filters [161, 162] to approximate the frequency distribution of equation (6.7).

The method used in this chapter is to combine G exponentials [30, p70] [163], according to equation (6.9):

$$h(q,t) = \sum_{g=1}^{G} a_g \exp(j\{2\pi\nu_g t + \phi_g\}) \tag{6.9}$$

where a_g is the amplitude of the g^{th} path and ϕ_g is a random phase uniformly distributed over $[0, 2\pi]$. The Doppler frequencies ν_g are chosen from a probability distribution in order for $h(q,t)$ to have a correct power spectrum. To simulate near–in scattering, the amplitudes a_g were chosen to be equal, so that the ACF of the variables ν_g is approximately equal to equation (6.8), with the scalar a chosen appropriately. The auto-correlation function of the variable $h(q,t)$ must be monitored carefully[2]. If the model is run over a long enough time, periodicities occur and the auto-correlation function diverges from equation (6.8). Thus it is normal to re-initialise the sine wave phases and frequencies after a suitable time delay.

The COST-207 models utilise the classical Doppler model to simulate multipaths arriving for excess time delays of less than 500 ns. A diagram of the scattering model and the power spectrum is shown in figure 6.3. In figure 6.2, the crescent shape of the Doppler profile is clearly visible at low time-delay values.

6.3.1.2 Far–out Scattering

As the excess time–delay increases, the classical Doppler model provides a poorer approximation to measured time delay/Doppler power spectra. In physical terms, this is because longer time delays mean that the multipaths observed must be due to reflections from distant objects such as large buildings or hills [37]. The range of Doppler frequencies associated with this form of scattering becomes much narrower and so sharp peaks tend to be observed in time delay/Doppler power spectra [35]: see particularly the contrast in figure 8 of [34]. Narrow sharp peaks in the Bello function may be observed

[2] The author acknowledges Dr P.Hulbert of Roke Manor for pointing this out.

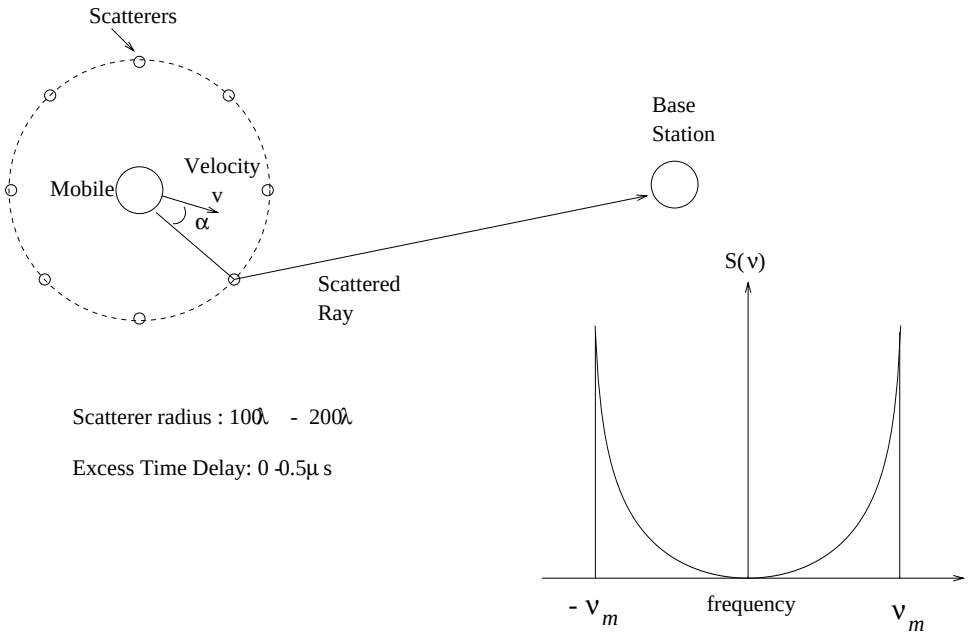

Figure 6.3: *The classical Doppler fading model*

in the profiles of figure 6.2 at longer time–delays.

A more appropriate model for this type of scattering is again described in the COST-207 models [163], which approximates each peak as a Gaussian distribution with mean Doppler frequency ν_1 and standard deviation ν_2 which specifies the sharpness of the peak. So for larger values of τ_0, the 2–D slice of the delay–Doppler power spectrum becomes:

$$S(\nu) = [S_p(\tau_0, \nu)]^2 = a \exp(-\frac{(\nu - \nu_1)^2}{\nu_2^2}) \tag{6.10}$$

The corresponding auto-correlation function is:

$$R(\tau_o, t) = a \exp(j\nu_1 t - \frac{1}{2}\nu_2^2 t^2) \tag{6.11}$$

Geometrically speaking, the location of the reflector can be assumed to lie on an ellipse, with the mobile and base station located at its foci. The major axis of the ellipse is then equal to the path length of the multipath component.

This type of scattering is much more difficult to simulate using filtered white noise, as the Doppler power spectrum is not symmetrical about the y–axis. Here, this model has again been implemented for the work in this chapter using equation 6.9. This time, however, the Doppler frequencies have been chosen from an appropriate Gaussian distribution. The COST-207 models describe two types of Gaussian model, each of which is the summation of two Gaussian profiles. However, the second profile is always at least

10 dB below the first so only the more important multipath component will be described here. The type

Model Type	Mean Fading Frequency	Standard Deviation
1	-0.8ν_m	0.05ν_m
2	0.7ν_m	0.1ν_m

Table 6.2: *The mean and standard deviation Doppler frequencies for the main peak of the two Gaussian COST–207 models.*

1 model is deemed appropriate for excess time delays of 500ns-2μs, while type 2 is to be used for excess time delays greater than 2μs. A diagram of the scattering model and the power spectrum that arises in this case is shown in figure 6.4.

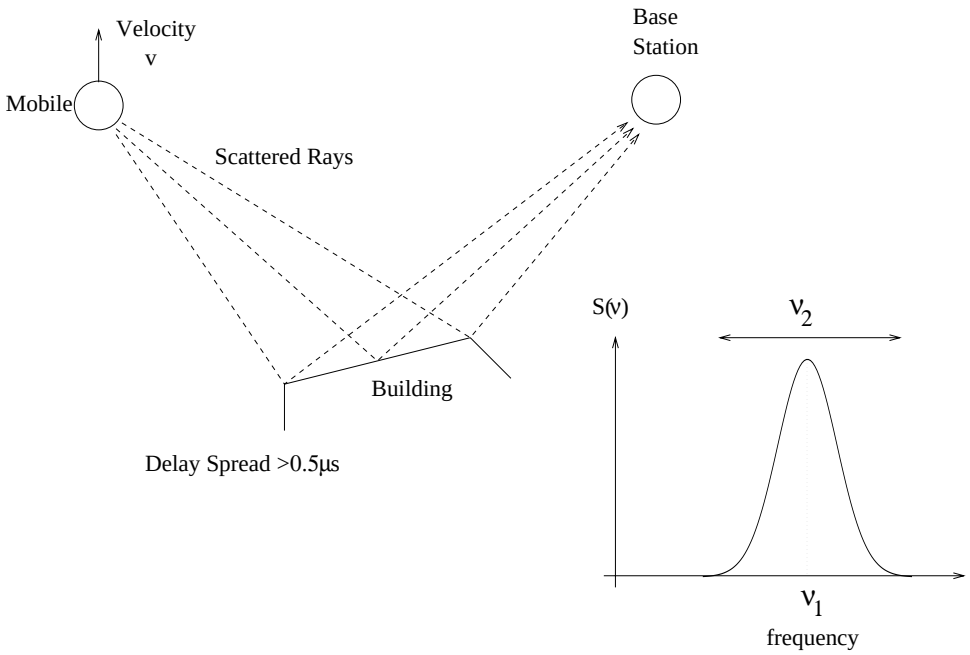

Figure 6.4: *The Gaussian fading model*

6.4 Channel Modelling and Array Processing

Given that models exist to adequately describe the urban mobile radio channel, it is useful to be able to extend these models to the array processing case. In particular, it is important to be able to model the reverse link signal seen by the base station array. So as to achieve this, some assumptions about the mobile to base station link are required. As in previous chapters, it will be assumed that the antenna array is a uniform linear array (ULA).

Firstly, it will be assumed that the distance between the mobile and base–station is sufficient to place the mobile in the far–field, with respect to the receiver. Secondly, there are no local scatterers close to the base station, so that all antenna elements have an unobstructed view of the multipath components coming from the mobile. Finally, the reverse and forward links are carried out over separate carrier frequencies, but with the same bandwidth so that the shadowing characteristics of the channel are

reciprocal [30, Chapter 6] [164]. This means that the time delay/Doppler power spectra are the same for both links. It is also assumed that the forward link frequencies are outside of the coherence bandwidth of the reverse link channel. Hence, if the mobile were to transmit at both frequencies simultaneously, the fast fading seen for each resolvable tap on both links would be iid random variables.

Equation (6.9) may easily be extended to the problem of simulating the received signal from a mobile at a base station antenna array containing M elements. In general, it shall be assumed that a frequency–selective channel with Q resolvable paths at each antenna may be modelled by Q discrete vectors. Define the vector $\boldsymbol{h}(q,t)$ which represents the q^{th} resolvable path at time t. It may be expressed as:

$$\boldsymbol{h}(q,t) = \sum_{g=1}^{G} a_g \exp(j\{2\pi\nu_g t + \phi_g\})\,\boldsymbol{a}(\theta_g) \tag{6.12}$$

The parameters have exactly the same meaning as for equation (6.9), except that $\boldsymbol{a}(\theta_g)$ denotes the steering vector of the g^{th} multipath as it impinges on the base station ULA. This formulation is similar to [165], except that in that paper the variable a_g was modified to include a log–normal term to simulate shadowing effects.

For the rest of this chapter, the amplitudes a_g will again be made equal for all g. This means that for large G, the statistics of each entry of $\boldsymbol{h}(q,t)$ will be approximated by a Rayleigh distribution. In this chapter, G will be set to 100. The temporal auto–correlation function of each entry will still follow the close–in or far–out scattering models according to the distribution of ν_g. The spatial covariance matrix of $\boldsymbol{h}(q,t)$, $\boldsymbol{R}(q)$, may be defined as follows:

$$\boldsymbol{R}(q) = E[\boldsymbol{h}(q,t)\boldsymbol{h}^H(q,t)] = \sum_{g=1}^{G} a_g a_g^* \boldsymbol{a}(\theta_g)\boldsymbol{a}^H(\theta_g) \tag{6.13}$$

This matrix will specify the correlation between the entries of $\boldsymbol{h}(q,t)$: the larger the spread in angles $\{\theta_g\}$, the lower the cross–correlation values in general.

The rest of this chapter will consider two different types of channel model, using equation (6.12):

(i). **A point source frequency selective channel:** This is a very crude model for the reverse link channel occurring in a typical urban (TU) macro-cell. The mobile is far enough away for each component $\boldsymbol{h}(q,t)$ to consist of a single multipath arriving from a single direction.

(ii). **A wide angle non–frequency selective channel:** This model takes into account that fact that in a multipath environment, the received signal will arrive from a spread of angles. It is studied for comparison with the point source model to see what changes occur. For simplicity, the channel is non–frequency selective, so that Q=1. This situation might actually occur in urban micro–cells or small suburban cells.

6.5 The Point Source Frequency–selective Channel

6.5.1 The Channel Model

This subsection describes the point channel model that has been used. The COST–207 report [163] describes a number of different channel models appropriate to different scenarios. In this case, the model for a typical urban (TU) environment has been adapted for spread spectrum simulation. The equation describing the impulse response power profile $H(\tau)$ of the TU channel is:

$$H(\tau) = \exp(-k\tau) \qquad 0 < t < 7\mu s, k = 10^6 \tag{6.14}$$

For a chip rate of 1.27 MHz, the value of t_c is approximately 800ns. Using this value, one may obtain the following five tap channel:

Tap	Delay (μs)	Power (dB)	Fading Power Spectrum	Bearing
1	0	0	Classical Doppler	90^o
2	0.8	-3	Gaussian Type 1	87.5^o
3	1.6	-6	Gaussian Type 1	94.0^o
4	2.4	-9	Gaussian Type 2	78.6^o
5	3.2	-12	Gaussian Type 2	100.0^o

Table 6.3: *The 5 tap typical urban channel.*

Each tap contains one significant multipath which is modelled as coming from a single direction. It should be noted that the exponentially decaying profile described in table 6.3 represents the average of a large number of measured channels. At a given time, the actual channel observed in an urban area is likely to vary significantly from the one described here.

The noise–corrupted, post–correlation signal vector received at the antenna array $\boldsymbol{y}(t)$ is therefore:

$$\boldsymbol{y}(t) = \sum_{q=1}^{5} \boldsymbol{h}(q,t)\delta_c(t - [t_o + (q-1)t_c]) + \boldsymbol{n}(t) \tag{6.15}$$

where $\boldsymbol{n}(t)$ denotes additive spatially and temporally white noise of power σ^2. The function $\delta_c(t)$ is defined in equation (6.6). The vector $\boldsymbol{h}(q,t)$ is of course proportional to the steering vector $\boldsymbol{a}(\theta_q)$, where θ_q is specified in table 6.3.

6.5.2 The Bearing Estimation Receiver Structure

The bearing estimation receiver structure operates as described in section 3.5 and is shown in figure 6.5. The received spread spectrum signal is demodulated to baseband and correlated with the desired CDMA

code. For a frequency–selective channel, Q multipath vectors are obtained. Model order and bearing estimation algorithms are used to locate the number of signals and their bearings for each of the Q vectors. The J multipath components with the largest power outputs are passed to a set of spatial filters to pick out those components. The outputs of the spatial filters are then combined using a conventional RAKE filter [20].

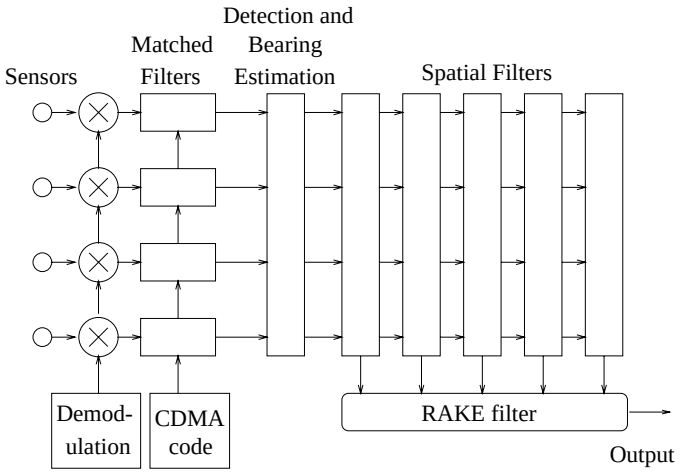

Figure 6.5: *The spatial filter CDMA receiver structure.*

There are a number of methods to operate a RAKE filter. For this section, a very simple method, DPSK RAKE filter combining, has been used because its properties are well known [43]: its structure is shown in figure 6.6. Denoting the n^{th} symbol sample for the j^{th} multipath component as $z(j,n)$, the decision

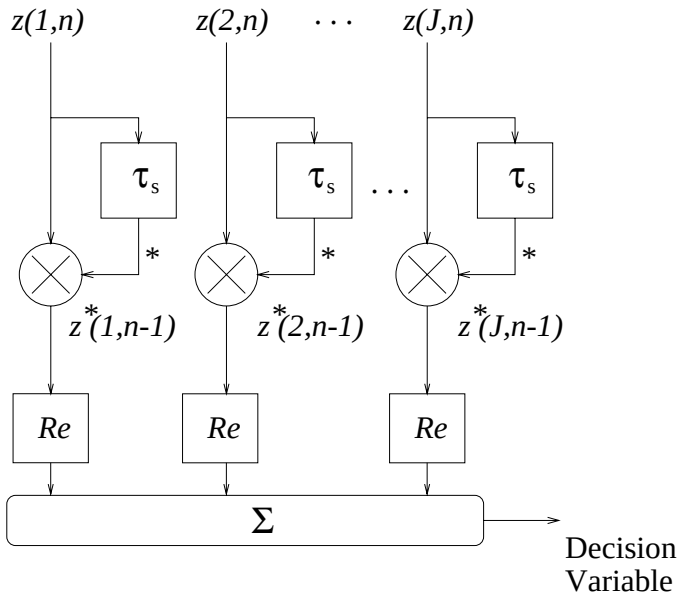

Figure 6.6: *The DPSK RAKE filter receiver.*

variable, $D(n)$, for a DPSK RAKE filter is given by the equation [43, Chapter 7]:

$$D(n) = \sum_{j=1}^{J} \Re\{z(j,n)z^*(j,n-1)\} \tag{6.16}$$

where $z^*(j,n-1)$ denotes the complex conjugate of $z(j,n-1)$, which has been delayed by one symbol period t_s for DPSK detection. If the first channel tap for the n^{th} symbol arrives at time t_0, the j^{th} multipath has excess time delay τ_j and bearing θ_j. For an antenna array receiver, the value $z(j,n)$ is given by:

$$z(j,n) = \boldsymbol{a}^H(\theta_j)\boldsymbol{y}(t_0+\tau_j) \tag{6.17}$$

When J taps with unequal SNR values ρ_j are combined by this method, the bit error ratio (BER) for a slowly–fading channel [3] is given by [43, Chapter 4]:

$$\text{BER} = \frac{1}{2^{2J-1}} \sum_{m=0}^{J-1} \sum_{n=0}^{J-1-m} \left(\begin{array}{c} 2J-1 \\ n \end{array} \right) \sum_{j=1}^{J} \frac{\Pi_j}{\rho_j} \left(\frac{\rho_j}{1+\rho_j}\right)^{m+1} \tag{6.18}$$

where ρ_j denotes the SNR of the j^{th} tap (not in dB) and Π_j is given by:

$$\Pi_j = \prod_{i=1, i\neq j}^{J} \frac{\rho_j}{\rho_j - \rho_i} \tag{6.19}$$

In the special case of a frequency non–selective channel, the BER reduces to the term $1/2(1+\rho_1)$. Comparing this result with that for an additive white Gaussian noise (AWGN) channel, the BER performance is much poorer as it is now only inversely related to the SNR. In order to achieve a BER of 10^{-3}, a SNR of 27 dB is required as opposed to 8 dB for a AWGN channel.

6.5.3 Practical CDMA System Performance

For all the results given in this chapter, the parameters of table 6.1 are assumed to apply, unless otherwise stated. Also, two different measures of SNR have been used for the results in this chapter. *Input SNR* denotes the SNR measured at the output of the code correlators for the first tap of the multipath channel at one antenna receiver. *Output SNR* is measured at the output of the spatial filter for the first tap of the multipath channel.

In order to demonstrate that coherently combining multipath energy is worthwhile, consider a receiver

[3] The term "slowly–fading" implies in the case of DPSK signalling that the underlying signal (without data modulation) does not change in amplitude or phase over two consecutive symbols.

with a single antenna. The BER performance has been simulated for the channel described in section 6.5.1, for a Doppler frequency of 50 Hz. Theoretical results have also been calculated using the approximation derived in appendix C. The results are shown in figure 6.7, with theoretical results shown as lines and simulation results as points.

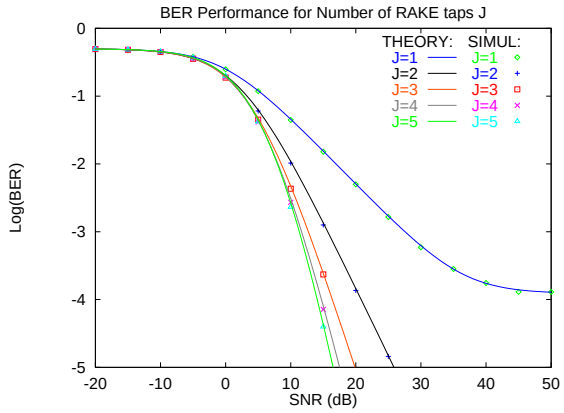

Figure 6.7: *The BER performance for number of RAKE taps J*

Clearly, the addition of one or two RAKE taps makes a considerable difference in the BER performance, allowing acceptable communication at much lower SNR values. However, there is a diminishing return in performance by increasing the number of taps to four or five, because of the reduced signal power present on these taps.

The performance of a single antenna receiver has been contrasted with that of antenna array receiver, both using 1 or 3–tap RAKE filters. The bearing estimation algorithm MUSIC, using N = 50 snapshots, was used by the antenna array to locate the bearings of each multipath signal. The multipaths were then constructively combined using the correct steering vectors and then a RAKE filter as described above was incorporated. Simulation results are plotted for BER vs input SNR in figure 6.8 for array sizes M = 1 and 8.

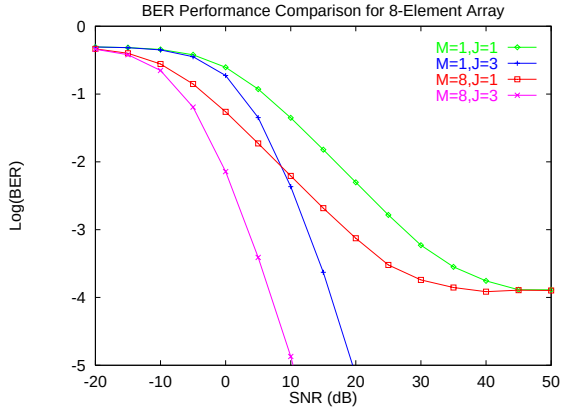

Figure 6.8: *Comparison of BER performance for M = 1 and 8 element arrays*

Because each multipath arrives from a single bearing, the received signals across the array for that multipath have a correlation factor of 1. Under these conditions, the base station array will increase the SNR of each multipath according to the number of array elements. However, no extra diversity will be introduced into the RAKE filter. This means that *in this case* array processing does not provide an extra means of overcoming the limitations due to Rayleigh fading and tracking errors. Comparing the curves for $M = 1$ and $M = 8$ antenna elements with 1 or 3 RAKE filter taps, this observation is seen to be true.

So far, the effects of self-noise, due to non-ideal spread spectrum code auto-correlation functions have been ignored. In practice there will be small contributions in each tap of the RAKE filter, which are due to correlations from the other multipath components. These will again limit the high SNR performance of the system. In the case of array processing receivers, these effects can be reduced, provided that the multipaths arrive from different directions. This effect has been measured by determining the auto–correlation function of a randomly chosen length 127 Gold code, which was then be used to simulate self–noise effects.

Figure 6.9 shows the effect on base station receivers with different array sizes M and RAKE filter taps J. Note that the horizontal axis this time represents the mean *output* SNR of the beamformer for the first multipath component. For $J = 1$, increasing the antenna array size reduces self–noise effects considerably, because the array is able to exploit the spatial diversity of multipath energy. However, as the number of RAKE taps J increases, the irreducible BER associated with self–noise reduces and for a single receiver with $J = 3$, the effect is negligible for at a BER of 10^{-5}.

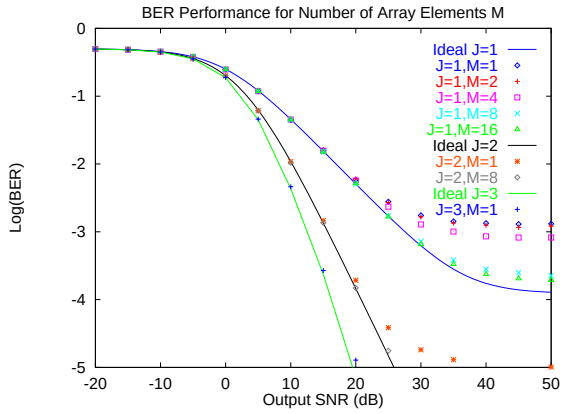

Figure 6.9: *The BER performance of an M – element array with J RAKE taps and self–noise effects*

6.5.4 Array Processing: Multiple Users

In this subsection[4], simulation work to determine the performance of the reverse link of a single–cell, fading channel, multiple user CDMA system is discussed. To begin with, some assumptions were made

[4] The work reported in this subsection only was carried out jointly with Dr Iain Scott of the Electrical Engineering Dept at Edinburgh University.

concerning the system under consideration:

- Each user was randomly allocated a length–127 Gold Code and employed DPSK modulation.
- Each users transmission was subject to a different realisation of the 5–tap typical urban channel described in section 6.5.1. Each multipath component was allocated a random bearing in the range $[30^o, 150^o]$.
- The bearings of the desired user's multipath components were assumed to be correctly estimated.
- Relative to the desired user, each interfering transmission was allocated a random time delay, which was fixed for the duration of all simulations.
- Power control was employed, so that shadowing effects could be neglected and the mean power of each incoming user's signal was the same.
- The maximum fading frequency for all users was 50 Hz.

For the purposes of the simulation, 15 users were assumed to be in operation. The spread of directions of arrival of the multipath components received from the 14 interfering users are shown in 6.10. The first multipath of the desired user arrived from broadside (90^o) – the appropriate beamformer for an 8–element array is also shown. The number of antenna elements in the base station was varied and the

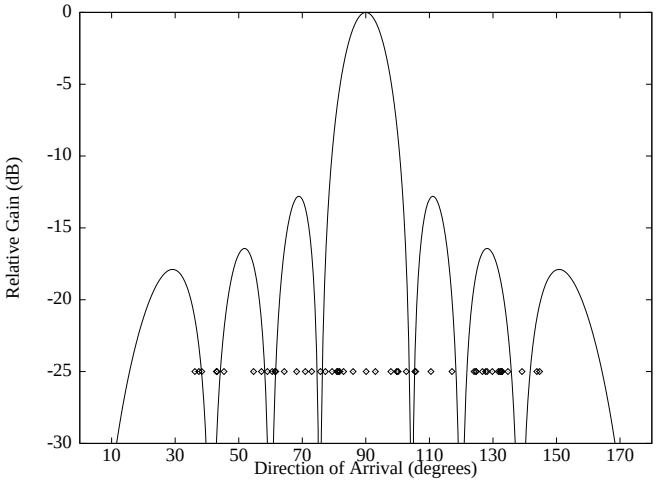

Figure 6.10: *The directions of arrival of the multipath components from 14 interfering users.*

corresponding BER for the desired user measured at different SNR levels. The results are plotted for output SNR against BER in figure 6.11.

Clearly, the wide angular spread of multipath components in this case meant that the antenna array receiver was able to exploit the spatial diversity of interference. Once the antenna array contains 4 elements, the irreducible BER falls to approximately 10^{-3}. This gives rise to a tolerable level of system performance. As in chapter 5, the performance improvement offered by an antenna array depends

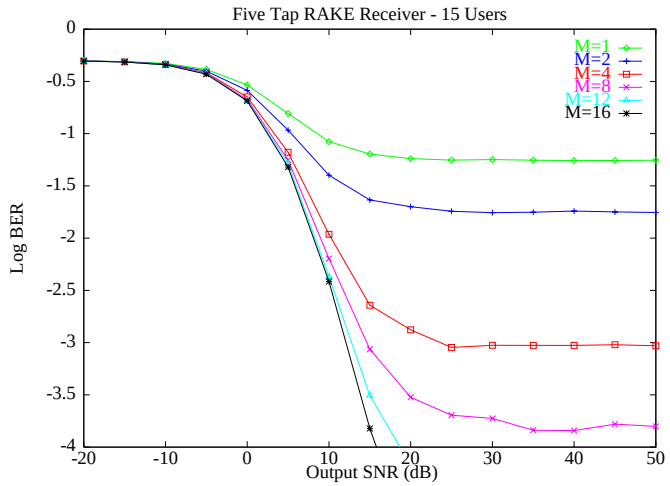

Figure 6.11: *The BER performance for a desired user, using a base station antenna array with a 5 tap RAKE receiver.*

critically on the distribution of CDMA users in the cell. These results show what might happen in a typical case. However, as discussed in section 5.2.4, the BER of a given user is usually dictated by how many interfering multipaths arrive within one array beamwidth of the desired multipath components.

6.5.5 Array Processing:Re–Transmission on the Forward Link

In order to permit an antenna array transmitter to operate on the forward link, directional information obtained on the reverse link may be used. Energy may be radiated in the directions of the major multipath components received on the reverse link to communicate with the desired mobile, whilst limiting co-channel CDMA interference. Two major cases to consider are shown in figure 6.12.

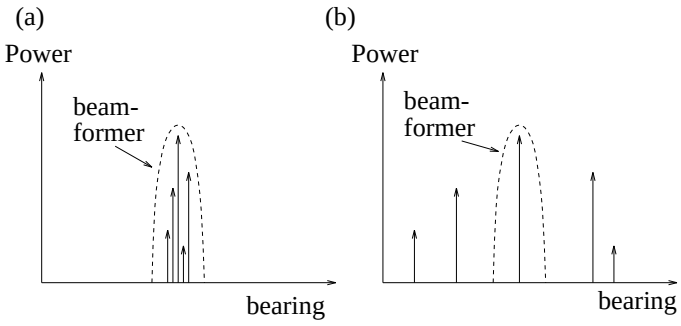

Figure 6.12: *a) Multipath engergy arrives from a narrow spread in angle b) Multipath energy is widely distributed in angle.*

If the major multipath bearings $\{\theta_p\}$ are very close, so that correlation between all the steering vectors is close to 1 (case a), re-transmission is simple to perform. The transmission array need only transmit the desired mobile's CDMA signal once using the steering vector for the largest power multipath on the reverse link. Energy from this transmission will propagate in the directions of all the major multipath

components, as shown in figure 6.12 (a), so that the mobile receives a similar multipath channel to that measured by the base station. The mobile may employ a RAKE filter to combine the multipath energy coherently and exploit the multipath diversity.

Alternatively, the major multipath bearings $\{\theta_p\}$ may be spread in azimuth so that the cross-correlation between all the steering vectors is close to 0 (case b). If the antenna transmits in only one direction, the mobile may receive only one significant Rayleigh–fading multipath component giving it poor BER performance. In order to improve the situation, a modified version of a technique called transmission diversity may be used. This has been suggested for both TDMA [166] and CDMA protocols [167]; it has also been used in a trial CDMA system [168]. The mobile's signal is transmitted by two or more widely spaced antennas, with a time delay between the them to allow the multipath energy to be received in different code time slots at the mobile. Assuming the signals are independent, the mobile can obtain diversity by combining the signals in a RAKE filter. The idea is illustrated in figure 6.13. This concept

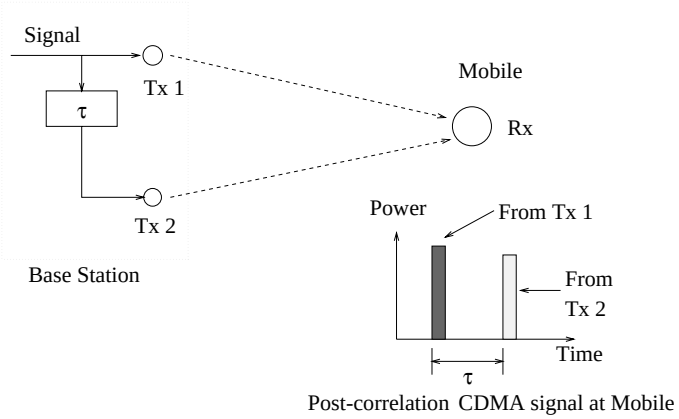

Figure 6.13: *The diversity transmission technique*

may be modified to the adaptive array case by transmitting the complete CDMA code in the directions of the 2 or 3 largest power multipaths. These multipaths have unknown amplitude coefficients on the forward link, so that for a fixed power transmission budget a loss in received power may result at the mobile. As a consequence, the receiver must try to ensure that the diversity obtained outweighs any loss in the received SNR. Depending on the times of arrival of the multipath components, energy may have to be transmitted in the chosen directions at different times in order that each multipath should arrive in a different time slot at the mobile receiver. An alternative approach is to transmit different parts of the CDMA code in different directions [169]: however, this scheme increases the receiver complexity and appears most suited to indoor flat–fading channels. Finally, it should be noted that diversity transmission and multiple direction transmission techniques are most effective when the receiver has a RAKE filter which is able to track and combine a sufficient number of channel taps.

6.6 The Finite Angular Spread Multipath Channel

Until now, each significant multipath component on the reverse link has been modelled as arriving from a single direction. This assumption allows BER performance to be estimated easily and provides an obvious scheme for transmitting energy back towards the mobile user. This means that adaptive arrays may be used to obtain significant capacity gains in both directions. However, this assumption may not be true for practical channels, particularly where the mobile is close to the base station. In this case, scatterers round the mobile may give rise to multipath signals at the base station which have a wide spread in angle.

6.6.1 Modelling Finite Angular Width on The Reverse Link

The multipath channel will now be modelled as flat–fading, so that it consists of a single vector $\boldsymbol{h}(1,t)$. This has been done in order to observe the effect of a multipath having a finite angular width, so that the point source model may be altered accordingly. The bearings of the constituent multipath components will be allowed to vary according to a specified distribution: initially the form of this distribution, as described in the literature, will be discussed.

Most of the existing models are intended for describing near–in scattering round the mobile, as described in section 6.3.1.1. This is due to the fact that this type of propagation accounts for a large proportion of the received power on both the forward and reverse links, particularly in the case of narrowband systems operating over a flat–fading channel. The first model to be used in the literature is probably due to Lee [170]. It was used to analyse the correlation between the fading signals seen at two base station antennas, separated by a known distance. The transmitted signal was narrowband in nature, and the received signal was assumed to be generated predominately by near–in scattering close to the mobile. Lee proposed a probability density function (PDF) for the angle of arrival of a scattered component, which is given by:

$$\mathrm{PDF}(\theta) = \frac{q}{\pi}\cos^n(\theta - \theta_0) \tag{6.20}$$

where θ_0 is the angle of arrival the mobile itself, q is a normalising constant to make the function a PDF and the power n controls the beamwidth of the scattering.

Other methods have been used since for modelling the angular spread of near-in scattering. In [63], the authors place a number of scatterers on a circle, each giving rise to a signal with a Rayleigh distribution. Alternatively, a Gaussian distribution for the angle of arrival has been used in [67, 171], with the mean value indicating the mobile angle of arrival and the standard deviation modelling the multipath spread in angle. However, perhaps the most convenient model has been suggested by Salz and Winters [172], which is a simplification of Lee's model. It is shown in figure 6.14. The mobile is placed at radius R from the mobile, and is surrounded by a circle of scatterers with radius d. They assume that the multipath

scattering seen at the base station is uniformly distributed over the range of bearings $[\theta_0 - \Delta, \theta_0 + \Delta]$, where 2Δ is the scattering angle. This model allows simple analytical results to be obtained for the correlation between antennas for a near-field scattering signal and will be the model used for proceeding work.

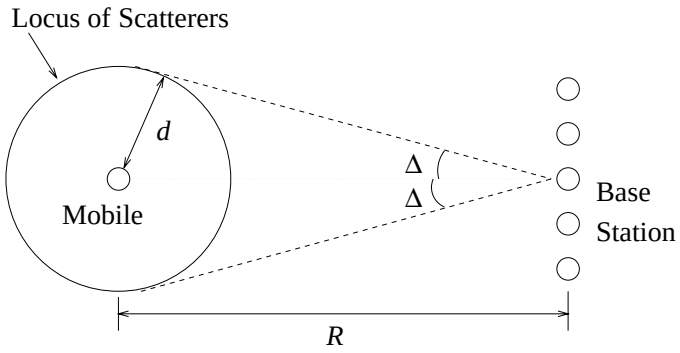

Figure 6.14: *The multipath channel model due to Salz and Winters (after [172]).*

Far–out scattering mechanisms have received considerably less attention, because they are of secondary significance to narrow–band systems. However, the Salz/Winters model may be adapted to far–out scattering in the case where EM energy is reflected from an obstacle of cross–section $2d$ at a distance R from the receiver. The angular width 2Δ for this type of scattering will again depend on the width of the major reflector and its distance from the base station.

6.6.1.1 Experimental Channel Measurements

Assuming that the channel vector $\boldsymbol{h}(1,t)$ is generated by near–in scattering, what values of the scattering angle 2Δ are realistic in practice?

The value of Δ may be calculated if R and d are known. The value of the d has been estimated from the spatial correlation function of the received signal at a base station antenna array. It would appear that the value of $2d$ should be at least the distance between buildings on the opposite sides of the street where the mobile is located [30, p65]. A typical value of 100 feet (30 metres) has been suggested for $2d$, [30, p65]; Lee has suggested 200-400 λ_C (for 900 MHz, this would be 60-120 metres) [37].

The scattering width of multipath signals using *narrowband* channel sounding techniques has been documented in several papers. However, as urban and suburban channels vary widely, they provide only a guide to the range of values of Δ that might occur in practice. In addition, the correlation values for near–in scattering using narrowband measurements may tend to be lower than the actual value, as they will also include far–out scattering effects. One of the first measurements was performed by Lee [170] for a narrowband 836 MHz transmitter located 3 miles away from the base station. From the cross-correlation values between two antennas, a scattering width of 0.4^o was estimated. More recently, measurements were made in the Liverpool area with a carrier frequency of 900 MHz and a Tx–Rx

spacing of 1.3 km [171]. The Gaussian scattering model was used and results were measured for radial and circumferential routes. The former giving rise to angular standard deviations of 1–3^o (approximately equivalent to scattering widths 2Δ of 3.5–10.4^o [5]), while the latter gave deviations of 3–6^o (approx. 10.4–20.8^o scattering width). A standard deviation of approximately 3^o (approx 10.4^o scattering width) was estimated for an 8–element antenna array operating at a carrier frequency of 870 MHz, with a Tx–Rx distance of 1 km in three separate locations in Sweden [173]. Using Lee's suggestion of d = 200λ_C, a somewhat lower scattering width of 2Δ = 7^o is obtained for R = 1 km.

6.6.1.2 Reverse Channel Description

The multipath channel, as seen at the array, consists of the superposition of a number of equal amplitude multipath components, whose bearings are selected from a uniform distribution. The mobile's bearing is θ_1 and the maximum deviation in bearing is $\pm\Delta$. Assuming that the number of constituent multipaths G tends to infinity, the mean covariance matrix of the channel coefficient vector $\boldsymbol{h}(1,t)$ is given by:

$$\boldsymbol{R}(1) = E[\boldsymbol{h}(1,t)\boldsymbol{h}(1,t)^H] = \boldsymbol{U}\boldsymbol{\Lambda}\boldsymbol{U}^H = \frac{a}{2\Delta}\int_{\theta_1-\Delta}^{\theta_1+\Delta} \boldsymbol{a}(\omega)\boldsymbol{a}^H(\omega)d\omega \tag{6.21}$$

where the term $\boldsymbol{U}\boldsymbol{\Lambda}\boldsymbol{U}^H$ represents the eigenvalue decomposition of the signal space and a represents a scaling factor. Analytical formulae for calculating the entries of $\boldsymbol{R}(1)$ are given in [172]. Assuming the fading signal at each array antenna follows a Rayleigh distribution, the received signal from the channel may be characterised as a multinormal random variable with mean vector 0 and covariance matrix $\boldsymbol{R}(1)$. If the multipath originates from one direction only, the matrix will be singular with rank one. However, as the multipath spread becomes wider, the correlation between antenna elements will reduce. In this case the eigenvalues and vectors of $\boldsymbol{R}(1)$ specify the Rayleigh–distributed random processes that make up the channel vector $\boldsymbol{h}(1,t)$. This means that correctly tracking the received signal will exploit spatial diversity present at the receiver.

The flat–fading model used here is assumed to be generated by near–in scattering, as with the models used in the previous subsection. Hence, the temporal auto–correlation function of the channel seen at the m^{th} antenna, $h_m(1,t)$, is simply given by equation (6.8) with the amplitude a scaled appropriately and the delay $\tau_o = 0$. The square root envelopes of the entries of the estimated covariance matrix $\hat{\boldsymbol{R}}(1)$, calculated from N snapshots of $\boldsymbol{h}(1,t)$, have a Nakagami distribution [174]. The important parameter of the Nakagami distribution is the m–parameter, which is inversely related to the normalised variance of the entries of $\hat{\boldsymbol{R}}(1)$. In this case, the m–parameter of the entries of $\hat{\boldsymbol{R}}(1)$ is given by:

$$m = [(1/N) + (1/N^2)\sum_{i,j,i\neq j}^{N} R(0,(i-j)t_s)R(0,(j-i)t_s)]^{-1} \tag{6.22}$$

[5] This comparison is based on equivalent standard deviations. The Salz/Winters model with angular width 2Δ has a standard deviation of $\Delta/\sqrt{3}$.

where $R(0,t)$ is defined in equation (6.8) with a=1 and t_s is the symbol period. The derivation of this equation is given in appendix C. In order to successfully track the multipath fading vector $\boldsymbol{h}(1,t)$, the value of N should be small to minimise the m–parameter. However, in practice one has access only to the post–correlation data vector $\boldsymbol{y}(t)$, which is defined in this case as follows:

$$\boldsymbol{y}(t) = \boldsymbol{h}(1,t)\delta_c(t) + \boldsymbol{n}(t) \tag{6.23}$$

where $\delta_c(t)$ is defined in equation (6.6) and $\boldsymbol{n}(t)$ represents spatially and temporally white Gaussian noise of power σ^2. Calculating the reverse channel covariance matrix $\boldsymbol{R}_r$ from $\boldsymbol{y}(t)$ involves noise terms whose variances are proportional to $(1/N)$. This means that the choice of N to minimise equation (6.22) must be large enough for the entries of $\boldsymbol{R}_r$ not to be excessively noise–corrupted. For the conditions in this chapter (i.e. a data rate of 10 kHz and fading frequency 50 Hz), the m–parameter values for some example values of N are shown in table 6.4. For the rest of this chapter, covariance matrices have been

N	5	50	500	5000
m	1.002	1.207	5.595	39.998

Table 6.4: *Values of the m–parameter for different numbers of snapshots N.*

formed from N=50 snapshots, which maintains a reasonably low m–parameter value.

6.6.1.3 Assessing the Effect of Angular Spread

For both near–in and far–out scattering, the exact form of the angular distribution of multipath energy is probably of secondary significance. On the reverse link, what matters is the mean covariance matrix of the received signal: this specifies the signal cross-correlations between antenna elements and hence the inherent diversity of the received signal. Two useful theoretical measures of antenna array receiver performance are:

(i). **Maximal Ratio Combining (MRC):** In the presence of white noise, MRC is the optimal method to combine a number of signals [175]. This method involves scaling each antenna output according to the signal power present. Here, the MRC output SNR has been calculated for the mean channel covariance matrix $\boldsymbol{R}(1)$ by evaluating its trace. The result is scaled suitably for comparison with other results.

(ii). **Source Bearing Beamformer:** In this case, a spatial filter whose bearing is that of the mobile's location is consistently applied to the the received data. The method is of additional interest later on, as the output signal will follow a Rayleigh distribution [107].

There are several techniques for tracking such a signal, including optimum combining algorithms which employ periodic training sequences [13]. Here, techniques which do not require a training sequence will

be considered, as the bearing estimation techniques described in this thesis employ covariance matrices which are not sensitive to data modulation. In order to reliably pick out the desired signal, its mean SNR should be much greater than 1, which necessitates accurate power control.

(i). **Beamspace Transformation:** A simple approach to processing the received signal is to pass the signal vector through a bank of spatial filters, denoted as $M \times 1$ vectors $\boldsymbol{w}_i$, which transform the signal into beamspace [56]. The signal outputs may be treated in a number of ways, but in this chapter *selection diversity* will be used to choose the largest output only. The manner in which the selection is made will now be described briefly. If Γ spatial filters are used, the filter bank may be denoted as the $\Gamma \times M$ matrix $\boldsymbol{W} = [\boldsymbol{w}_1 \ldots \boldsymbol{w}_\Gamma]$. The measured covariance matrix $\hat{\boldsymbol{R}}_r$ is transformed to the beamspace matrix $\hat{\boldsymbol{B}}$, according to:

$$\hat{\boldsymbol{B}} = \boldsymbol{W}^H \hat{\boldsymbol{R}}_r \boldsymbol{W} \tag{6.24}$$

The spatial filter $\boldsymbol{w}_i$, corresponding to the largest diagonal entry of $\hat{\boldsymbol{B}}$, may then be applied to the N snapshots of array data to recover the mobile's data sequence. The output SNR for this technique is given by $(\boldsymbol{w}_i^H \hat{\boldsymbol{R}}(1) \boldsymbol{w}_i)/(\boldsymbol{w}_i^H \boldsymbol{w}_i)$, assuming the noise power σ^2 is normalised to 1. For the simulations in this thesis, $\Gamma = M$ orthogonal steering vectors were used. The bearing of the first filter θ_0 was chosen as required; the other $M-1$ steering vector bearings are specified by:

$$\theta = cos^{-1}[(\pi \cos(\theta_0) + (2n\pi/M))/\pi] \qquad n = 1, 2, \ldots, M-1 \tag{6.25}$$

The circular phase term present in the argument of the $\cos^{-1}$ term should be made to lie in the region $[-\pi, \pi]$ to obtain the filter bearings.

(ii). **Spatial Filter Techniques:** It is of interest to determine how a single spatial filter performs, when attempting to track a multipath signal. The conventional beamformer power spectrum has been calculated for the covariance matrix $\hat{\boldsymbol{R}}_r$ in each case to select the bearing θ with the largest power output. As with the beamspace transformation, the appropriate steering vector spatial filter is applied to the array data to recover the desired user's signal: hence, the output SNR is calculated in the same manner. This method is quite similar to jitter diversity [176], where the receiver estimates the source bearing from a large number of snapshots and tracks the movement of the nearest signal peak snapshot by snapshot.

(iii). **Eigenfilters:** In this case, the receiver performs an eigenvalue decomposition of the covariance matrix $\hat{\boldsymbol{R}}_r$. The eigenvector or "eigenfilter" corresponding to the largest eigenvalue, $\boldsymbol{u}_1$, is chosen and applied to the array data to produce a scalar output. The output SNR is simply given by the largest eigenvalue of $\hat{\boldsymbol{R}}(1)$, so that in the presence of white noise, the eigenfilter method will achieve the maximum output SNR among all single filter techniques [60].

(iv). **Spatial Smoothing Approach:** The spatial filter approach described above employs only one filter for the received signal. It is also possible to apply spatial smoothing to the matrix $\hat{\boldsymbol{R}}_r$

to resolve multipath components at bearings $\{\theta_j\}$. The power of each may be calculated from $\boldsymbol{a}^H(\theta_j)\hat{\boldsymbol{R}}(1)\boldsymbol{a}(\theta_j)/\boldsymbol{a}^H(\theta_j)\boldsymbol{a}(\theta_j)$. The largest components (here, those within 10 dB of the largest multipath) may be combined in a RAKE filter. Assuming J components are combined by ideal maximal ratio combining, the output SNR for this case only is explained in Appendix C and given by:

$$\text{SNR} = \frac{[\sum_{j=1}^{J} \boldsymbol{a}^H(\theta_j)\hat{\boldsymbol{R}}(1)\boldsymbol{a}(\theta_j)]^2}{\sum_{j=1}^{J}[\boldsymbol{a}^H(\theta_j)\hat{\boldsymbol{R}}(1)\boldsymbol{a}(\theta_j)\boldsymbol{a}^H(\theta_j)\boldsymbol{a}(\theta_j) + 2\sum_{k=1}^{j-1}\Re\{\boldsymbol{a}^H(\theta_j)\boldsymbol{a}(\theta_k)\boldsymbol{a}^H(\theta_k)\hat{\boldsymbol{R}}(1)\boldsymbol{a}(\theta_j)\}]} \tag{6.26}$$

6.6.1.4 Simulation Results

In order to provide an initial comparison of the four methods, each technique was applied to the noisy covariance matrix estimate of $\hat{\boldsymbol{R}}_r$. The input SNR, which was defined in section 6.5.3, was set to 20 dB for all simulations with the signal vector $\boldsymbol{h}(1,t)$ composed of $G = 100$ multipath components. The output SNR was measured for the different techniques ten thousand times in each case as part of a Monte Carlo simulation. The simulations have been performed for a source at a bearing of 90^o to the array. This bearing was chosen as previous results for the channel model show that cross–correlation between antennas falls most rapidly in this case [172]. For signals arriving from other directions with the same beamwidth, the cross–correlation between array antennas will be higher.

A comparison of the spatial filter and eigenfilter methods for the reverse link, in terms of the output SNR, is shown in figure 6.15. Results are shown for uniform linear arrays with half-wavelength spacing

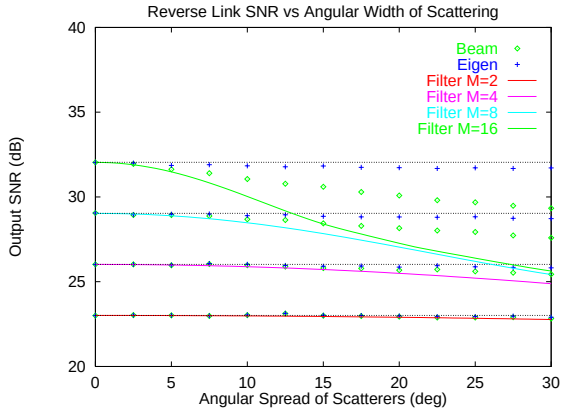

Figure 6.15: *The Mean output SNR for the reverse link vs scattering width for array sizes M = 2,4,8 and 16.*

and the specified number of antenna elements. The covariance matrices used were calculated from 50 snapshots of a signal with a maximum fading frequency of 50 Hz and a data rate of 10 kHz. The multipath signal was always generated using the near–in scattering model. The output SNR values for ideal maximal–ratio combining are shown as horizontal lines for 2,4,8 and 16 antenna elements in figure 6.15. The points marked “Beam” show the measured results for the spatial filter technique and “Eigen”

shows the SNR resulting from using the eigenfilter approach. Finally, the lines labelled "Filter" denote the SNR calculated for a beamformer placed at the source bearing. These curves tend towards a constant output SNR for large scattering widths [166] as the array size increases. This effect occurs because increasing the array size reduces the beamwidth and the receiver picks out less of the signal energy: this cancels out the noise gain of the larger antenna.

The output SNR values from the eigenfilter approach are better than those obtained from the spatial filter, for large scattering widths because the eigenfilter tracks the signal in all dimensions, while the spatial filter is constrained to a high–dimensional surface specified by the vector $\boldsymbol{a}(\theta)$. Figure 6.15 shows the eigenfilter suffers a small loss compared to the optimal SNR obtained by MRC, because the m–parameter of the covariance matrix $\hat{\boldsymbol{R}}(1)$ is greater than unity. It should also noted that the spatial filter method performs better than the "Filter" curves because the filter bearing can change to follow the variations of the received signal and partially exploit the spatial diversity present.

Results have also been obtained for the spatial smoothing method described above, denoted as method (C), and for the beamspace transformation method, denoted as (B). In order to avoid confusion in figure 6.15, the results are presented in table 6.5. The performance of the beamspace method depends on the bearing θ_0 of the first spatial filter. For $M = 8$, θ_0 has been varied in the range $[0^o, 42^o]$ and for $M = 16$, in the range $[0^o, 29^o]$ [6], to determine the best and worst performance for different values of scattering angle. For comparison the spatial filter method is denoted as (A) and the eigenfilter method as (D).

M = 8	Scattering Angle				M = 16	Scattering Angle			
Elements	0^o	10^o	20^o	30^o	**Elements**	0^o	10^o	20^o	30^o
A(dB)	29.07	28.81	28.17	27.67	**A(dB)**	32.11	31.03	30.07	29.37
Best B(dB)	29.07	28.57	27.37	27.00	**Best B(dB)**	32.06	30.34	29.45	28.71
θ_0	0^o	2^o	28^o	27^o	θ_0	0^o	24^o	5^o	20^o
Worst B(dB)	25.16	26.64	27.12	26.50	**Worst B(dB)**	28.41	30.12	29.17	28.47
θ_0	29^o	29^o	7^o	6^o	θ_0	20^o	7^o	18^o	11^o
C(dB)	29.07	28.62	28.70	28.43	**C(dB)**	32.11	31.61	31.46	31.40
D(dB)	29.08	29.01	28.83	28.80	**D(dB)**	32.11	31.78	31.73	31.75

Table 6.5: *Comparison of (A) spatial filter method (B) beamspace transformation (C) spatial smoothing method and (D) eigenfilter method.*

These results demonstrate that resolving separate multipath components with spatial smoothing to combine coherently the multipath energy improves the receiver performance. However, marginally superior performance is obtained by the eigenfilter method with considerably less computation, even though ideal MRC combining was assumed for method (C). The behaviour of the beamspace transformation scheme varies somewhat depending on the value of θ_0. However, the best SNR values are not significantly worse than those for method (A); the variation in SNR is also considerably less for large values of multipath scattering. This would appear to be due the incoming signal appearing in two or three adjacent spatial filters, providing diversity gain. The loss in performance compared to methods (C) and (D) may be offset against the much simpler implementation and computation costs of the beamspace transformation

[6] The upper bearing of these two ranges specifies roughly where one of the other beamformers reaches bearing 0^o.

approach.

To provide some comparison of the effectiveness of spatial filtering, a table is shown below of the 3 dB beamwidths of an antenna array of a given size with a look direction of 90^o. Comparing the values

Number of Antenna Elements	3 dB Beamwidth
2	60^o
4	26.3^o
8	12.8^o
16	6.4^o

Table 6.6: *The beamwidths of M–element antennas, with a 90^o look direction.*

of table 6.6 with the results of figure 6.15 and table 6.5, it is seen for each value of M that significant degradation in SNR for both the spatial filter and beamspace approaches occurs only as the angular spread of the signal increases above the beamwidth of the associated spatial filter. Finally, it should be noted that all the above methods will be subject to further degradations at low SNR, because the signal vector estimates will be subject to larger perturbations due to noise.

6.6.1.5 Diversity Considerations

Whilst the measured SNR provides an initial measure to compare receiver structures, it is insufficient to completely characterise system performance. In the simple case of a source transmission arriving from a single direction, the received signal may be completely described by a steering vector which is scaled by a single complex Gaussian random variable. However, as the angular width of the source's signal increases, the cross–correlation between the received signals across the antenna array reduces, so that the received signal vector follows a complex Gaussian multivariate distribution. The eigenvalue decomposition of the mean covariance matrix $\boldsymbol{R}(1)$ of the received signal provides information on the constituent random processes present in the signal and their amplitudes.

If perfect maximal ratio combining is applied to the received signal vector, the receiver is able to track the independently fading components which are present. This means that the receiver can exploit the spatial diversity of the antenna array [71], whose extent depends on the number of significant eigenvalues calculated from $\boldsymbol{R}(1)$. As a guide to the diversity present on the channels considered above, the principal eigenvalues from the covariance matrices calculated for different array sizes and signal scattering angles are shown in figure 6.16. Comparing the results with table 6.6, the second largest eigenvalue of $\boldsymbol{R}(1)$ is seen to become significant when the scattering width is comparable to the beamwidth of the array.

In order to estimate quantitatively the effect on the receiver, one may use the following procedure. Take the K significant eigenvalues from $\boldsymbol{R}$, λ_k, and scale them according to the background noise level and denote the resulting values as ρ_k (c.f. section 6.5.2). The PDF of the signal at the output of an ideal maximal ratio combiner is given by Proakis [43]:

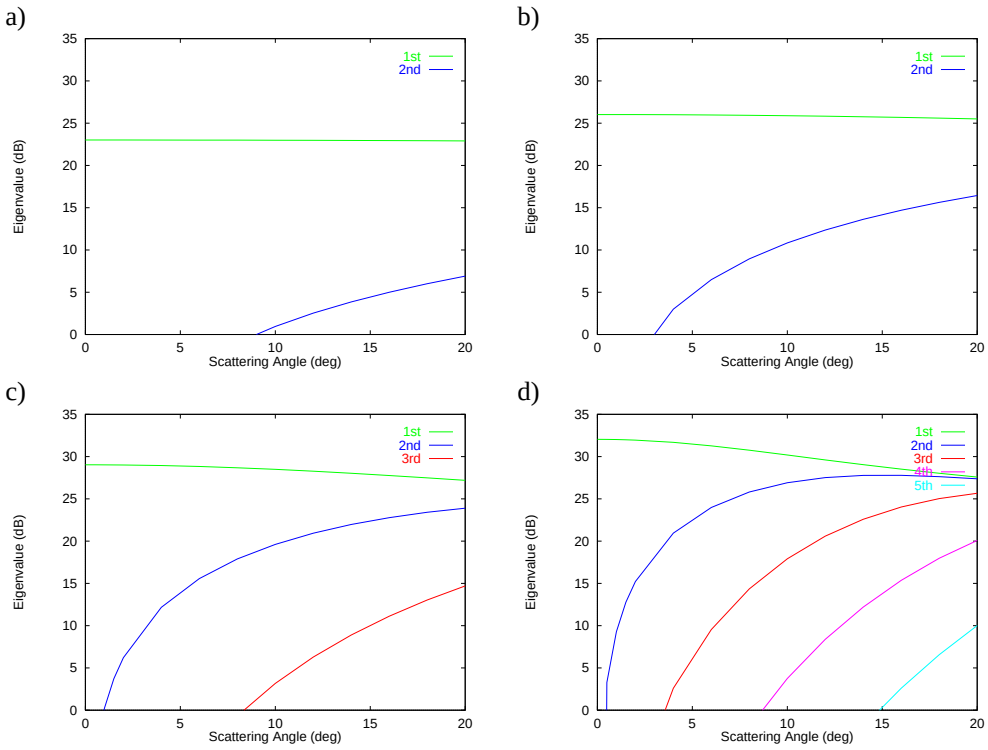

Figure 6.16: *The principal eigenvalues of the covariance matrices for different array sizes and signal scattering angles: a) M =2 b) M =4 c) M =8 d) M =16.*

$$\text{PDF}(x) = \sum_{k=1}^{K} \frac{\Pi_k}{\rho_k} \exp\{-x/\rho_k\} \tag{6.27}$$

where the value of Π_k is given by equation (6.19). The CDF of the distribution is then given by:

$$\text{CDF}(x) = \int_0^x \text{PDF}(\omega) d\omega = \sum_{k=1}^{K} \Pi_k (1 - \exp\{-x/\rho_k\}) \tag{6.28}$$

As an example, the theoretical CDFs for the MRC output from an incoming signal with bearing 90^o, scattering width 20^o and an input SNR of 20 dB have been calculated for M = 2,4,8 and 16. To check the results by simulation, the eigenfilter method has applied to 50 snapshots of the same slowly–fading channel(i.e. ν_m=0) to calculate the output SNR. This procedure was repeated 10000 times to determine the CDF. Both sets of results shown in figure 6.17 fit well, as the eigenfilter approach is approximately equivalent to the theoretical MRC curve in this case. As the number of antenna elements M increases, the exploitable diversity increases. At a probability of 0.001, the SNR improvement is of the order of 6 dB each time M is scaled by 2, double what would be expected for noise rejection alone.

It is of interest to compare the CDFs for the spatial filter, beamspace transformation and eigenfilter approaches, for M=16, under the same conditions as the previous figure. Results are shown in figure

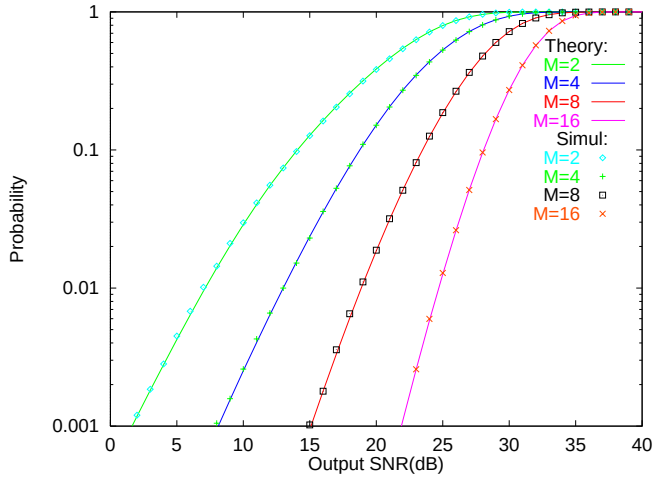

Figure 6.17: *The CDFs of the theoretical and simulated MRC outputs for a signal impinging on an M–element ULA with bearing 90^o ,input SNR of 20 dB and scattering width of 20^o .*

6.18 for all three approaches, labelled "Beam", "Beamspace"[7] and "Eigen" respectively. Interestingly, the spatial filter CDF follows that of the eigenfilter closely: the main difference appears to be due to the loss in SNR specified in table 6.5. In addition, the CDF of the beamspace technique shows only a slight loss in SNR and diversity compared to the spatial filter method. However, all three approaches seem to exploit most of the diversity present in the received signal, and will provide significant BER performance improvement at reasonable input SNR over the curve labelled "Filter". This represents the Rayleigh distributed output from a spatial filter placed at the source bearing.

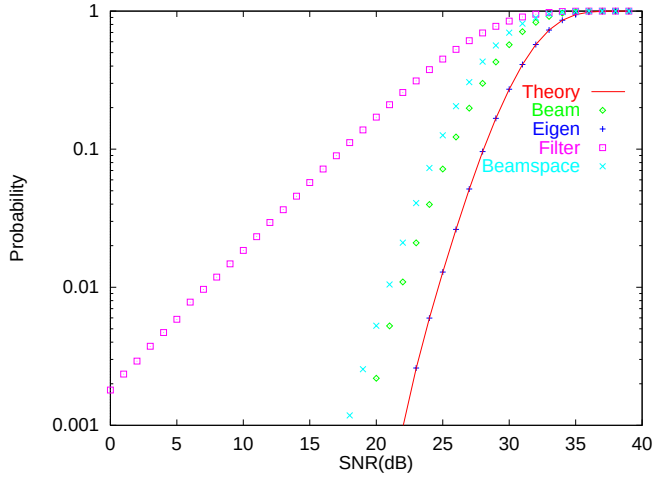

Figure 6.18: *The CDFs of the beamformer, eigenfilter, MRC, beamspace and source bearing steering vector filters for a signal impinging on a 16–element ULA with bearing 90^o , input SNR of 20 dB and scattering width of 20^o .*

From these results, it seems clear that the eigenfilter approach provides performance close to that offered by ideal maximal ratio combining for any scattering width. If the scattering width is narrow, spatial

[7] The results for the beamspace technique are shown for the "worst" set of filters, with output SNR = 29.17 dB and $\theta_0 = 18^o$.

filtering performs almost as well. However, as the scattering width increases above the beamwidth of the array, spatial filtering approaches degrade in terms of the SNR. The loss in SNR can be overcome by spatial smoothing techniques, but only at a cost of increased complexity. In any case, spatial filtering and eigenfilters already appear to exploit the diversity of the channel effectively. Bearing estimation techniques require accurate knowledge of the array manifold, which will involve periodic re–calibration of the signal phases. This can be avoided in receivers using eigenfilter methods, although it may prevent the antenna array from being used to re–transmit on the forward link.

The point source channel provides a good model for a multipath component, provided its angular width is somewhat smaller than the beamwidth of the array. However, as the angular width increases, spatial diversity can be exploited to increase the effective number of independent Rayleigh fading components which are coherently combined. The DPSK BER equation (6.18) may be simply adapted to handle the case where a J–tap DPSK RAKE filter combines J signals containing Y independent components, where $Y > J$. The BER becomes:

$$\text{BER} = \frac{1}{2^{2J-1}} \sum_{m=0}^{J-1} \sum_{n=0}^{J-1-m} \left(\begin{array}{c} 2J-1 \\ n \end{array} \right) \sum_{y=1}^{Y} \frac{\Pi_y}{\rho_y} \left(\frac{\rho_y}{1+\rho_y}\right)^{m+1} \tag{6.29}$$

where ρ_y is the SNR of the y^{th} component. The product term Π_y, defined in equation (6.19), is modified to include a product of order $Y-1$.

6.6.2 Array Processing on the Forward Link

Given that the multipath components received at an array antenna base station have some spread in angle, it is important to quantify the effect of this. Intuitively, one would expect that as the multipath angular width widens, a simple beamformer will tend to capture less of the available energy, reducing the received SNR for that multipath. Similarly, re-transmitting energy on the forward link using the same beamformer weights will not reach all the scattering components so that the forward link SNR for that multipath is also reduced.

6.6.2.1 Modelling the Forward Link Channel

In order to model the forward link channel, it shall be assumed that the frequency separation between the reverse and forward links is sufficient that one is outside the coherence bandwidth of the other. In the IS–95 standard, the channel separation is of the order of 40 MHz, so that this assumption would be appear to be justified in this case. To simplify the analysis, it will be assumed that the steering vector of the array is the same for both carrier frequencies. Therefore, if the mobile were to transmit at the forward link frequency, the channel vector $\boldsymbol{h}_f(1,t)$ would be identically distributed to the reverse link vector $\boldsymbol{h}(1,t)$, but independent of it.

If one were to apply an arbitrary filter $\boldsymbol{w}$ to N snapshots of $\boldsymbol{h}_f(1,t)$, the average output power would

be given by $[w^H \hat{\boldsymbol{R}}(1) w]/(w^H w)$, where $\hat{\boldsymbol{R}}(1)$ is formed from the N snapshots of $h_f(1,t)$. By the principle of reciprocity on the forward and reverse links [30, p60], this value also represents the power received at the mobile if the antenna array transmitted to it using the complex conjugate weight vector w^*. The total power transmitted by the antenna array is equal to that transmitted by the mobile. This method will be used to simulate the forward link from the base station to the mobile. The algorithms for determining what weights to use for transmission to the mobile will now be considered.

6.6.2.2 Forward Link Transmission Techniques

There are a number of techniques which permit the array to re-transmit to the mobile. These will now be considered in turn:

(i). **Weight Re-transmission:** If a single weight vector w is calculated for receiving the signal on the reverse link, it is possible to use the complex conjugate vector w^* for transmitting on the forward link. This principle has been suggested for the case of a single spatial filter $\boldsymbol{a}(\theta)$ [12, 62] and for an approach based on adaptive beamforming [67]. It may also be performed using an eigenfilter u_1 or the weight vector calculated from optimum combining [13]. Finally, it should be noted that this approach has even been suggested for beamspace transformation techniques [76].

(ii). **Transmission Feedback [177]:** This method for narrowband systems proposes that the base station periodically transmit training sequences to the mobile. Based on information transmitted back from the mobile, the base station may alter its transmission weights. This method has the advantage of being able to measure the forward link channel characteristics directly. However, it seems to be most suitable for slowly changing channels and has the disadvantage of requiring extra control overhead. It will not be considered further in this thesis.

(iii). **Time Division Duplex Transmission [178] [30, p498]:** An alternative method to obtain the transmission weights is to specify a time division duplex (TDD) air interface. This method will work better than FDD methods over slowly–fading channels, as in this case the slow and fast fading effects will be reciprocal. It is also possible to transmit several delayed versions of the CDMA signal in such a way as to permit the channel to perform a RAKE filtering operation on the signal [178]. However, this method requires guard bands between the transmissions in each direction to prevent cross-talk. In addition, the performance of the system degrades as the fading rate of the channel increases. As the IS–95 standard specifies FDD signalling, this method will also not be considered further.

The work which is presented next considers blind channel transmission techniques, which have no knowledge of the forward link channel parameters, except through measurements of the reverse link. The maximum SNR that can be obtained in this way is to use the eigenvector corresponding to the largest eigenvalue of $\boldsymbol{R}_r$ for the transmission weights[8] . The output SNR at the mobile is then the largest

[8] This assumes that the receiver can obtain a perfect estimate $\boldsymbol{R}_r$, which is unlikely to be possible in practice.

eigenvalue of $\boldsymbol{R}(1)$. The comparative performance of weight transmission systems using eigenfilter, spatial filter and beamspace transformation weights will now be discussed.

6.6.2.3 Simulation Results for The Forward Link

In the simulations described below, a covariance matrix was formed from reverse link data to determine the best receive vector w, using the spatial filter, eigenfilter or beamspace transformation. The array proceeded to transmit on the forward link to the mobile, using the complex conjugate vector w^*. Each realisation of the reverse and forward links was obtained using $G = 100$ multipath components, each with the same bearing and Doppler frequency. However, the initial phases of the multipath on the two links were iid random variables, uniformly distributed over $[0, 2\pi]$. This does not account for any alteration in the channel, due to shadowing, in the time between measuring the reverse link channel and re-transmitting on the forward link. Given that the simulation used a low fading rate, however, this appears to be a reasonable assumption.

Figure 6.19 shows the output SNR against beamwidth for array sizes M = 2,4,8 and 16. Weight vectors were obtained from N=50 snapshots of the reverse link, using the spatial filter and eigenfilter methods described in section 6.6.1.3. The total transmission power budget for all antenna array sizes was the same as that used by the mobile on the reverse link, such that a single antenna transmission would achieve a mean output SNR of 20 dB at the mobile. The results were calculated for 50 snapshots of the forward link: they are shown for the spatial filter (label "Beam") and the eigenfilter (label "Eigen"), as well the maximum SNR, which is the largest eigenvalue of $\boldsymbol{R}(1)$ (label "Theory"). Finally, horizontal lines are shown in figure 6.15 for the maximum output SNR achievable for each array size, assuming perfect knowledge of the forward link channel.

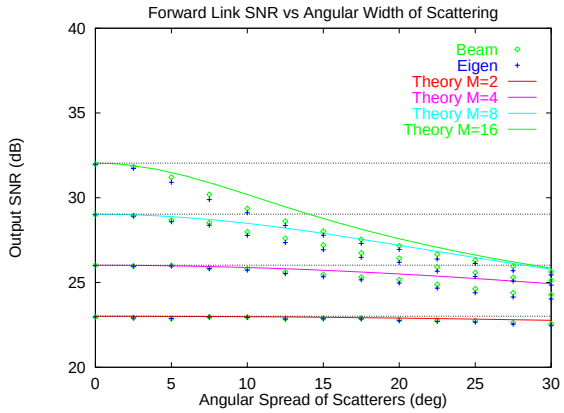

Figure 6.19: *The mean output SNR for the forward link vs scattering width for array sizes M = 2,4,8 and 16.*

The results show that the performance of the eigenfilter and beamformer techniques are quite similar in this case. However, both techniques' performance is slightly worse than for the maximum achievable, because the reverse link estimated matrix $\hat{\boldsymbol{R}}_r$ provides channel parameter estimates with a high variance.

Unfortunately, at large scattering angular widths, all three approaches perform considerably worse than the correct transmit weights which could be used if the forward link channel characteristics were known at all times.

A comparison is shown in table 6.7 between the spatial filter and beamspace transformation techniques – methods A and B, respectively. Again, the performance of the former is comparable to the best results for method B. Poor choice of θ_0 leads to some degradation in performance.

8 Elements	**Scattering Angle**				**16 Elements**	**Scattering Angle**			
	0^o	10^o	20^o	30^o		0^o	10^o	20^o	30^o
A(dB)	29.04	28.22	26.53	25.20	**A(dB)**	32.12	29.45	27.14	25.86
Best B(dB)	29.05	28.49	26.44	25.26	**Best B(dB)**	32.10	29.47	27.08	25.71
θ_0	4^o	4^o	7^o	27^o	θ_0	1^o	4^o	1^o	18^o
Worst B(dB)	25.10	25.46	25.67	24.44	**Worst B(dB)**	28.43	28.68	26.80	25.33
θ_0	29^o	28^o	28^o	0^o	θ_0	20^o	21^o	20^o	5^o

Table 6.7: *Comparison of (A) spatial filtering and (B) beamspace transformation techniques.*

6.6.2.4 Obtaining Diversity Reception at the Mobile

In order to permit performance improvements at the mobile, it is possible to directly employ the CDMA transmission technique [168], which was described in section 6.5.5. Each antenna of the array transmits the CDMA signal subject to a delay (relative to the first antenna) of $(m-1)t_c$, where m denotes the antenna number. If M antennas transmit over the channel modelled by $\boldsymbol{h}(1,t)$, the mobile receives M signals in different time slots. Assuming that the array transmit power is the same as for the mobile, the mean power received at the mobile is given by $(tr\{\boldsymbol{R}(1)\})/M$. Hence, diversity transmission would achieve an output SNR of 20 dB for all the antenna sizes described above.

Clearly, the problem with this approach is that if $\boldsymbol{h}(1,t)$ consists of a single steering vector $\boldsymbol{a}(\theta)$, then transmitting using the vector $\boldsymbol{a}^*(\theta)$ is much more efficient in terms of the output SNR. Indeed, the diversity transmission approach simply leads to an SNR loss of M dB compared to transmitting the steering vector and achieves no additional diversity gain. For a more general channel there will still be some loss in output SNR, compared to the weight transmission approaches described above, but this method can exploit any channel diversity present.

In scenarios where the channel matrix $\boldsymbol{R}(1)$ has a small number of significant eigenvalues, it is advantageous to keep the number of separate transmissions small. Two possible methods to achieve this are:

(i). **Sub–array Transmission:** One may divide the linear array into a number of contiguous transmission sub–arrays. Each sub-array transmits the CDMA code with a suitable delay, as for the diversity transmission algorithm, to allow multipaths to be combined coherently with a RAKE filter. The transmission weights for each sub–array may be decided using one of the re-transmission

techniques above, e.g. spatial filter, eigenfilter, etc. As the transmitted power is split equally between sub–arrays of size L, the total output SNR from a RAKE filter at the mobile cannot be greater than that for a single transmission from an array size L. However, this technique provides improved diversity at the mobile, assuming the channel has sufficient angular spread: there is also reduced RAKE filter complexity at the mobile, compared to the transmission diversity technique. In practice, the effectiveness of the technique will depend on the the signal cross–correlation terms present in the matrix $\boldsymbol{R}(1)$.

(ii). **Transmission using MUSIC/Spatial Smoothing:** A second approach is to apply spatial smoothing and MUSIC to the reverse link covariance matrix, in order to separate the received signal into a small number of directional components. The base station may transmit the CDMA code in each chosen direction, with suitable delays to allow each transmission to arrive in a different time slot.

In order to demonstrate the improvement that may be obtained from multiple transmission, the CDFs have been calculated for the overall SNR of the signal at the mobile for a number of transmission schemes. The reverse link beamformers and the forward link complex–conjugate re–transmission SNR values have been calculated in the same manner as for figure 6.18. The only difference is that ideal maximal ratio combining has been assumed at the mobile for the diversity transmission technique. The results are shown in figure 6.20.

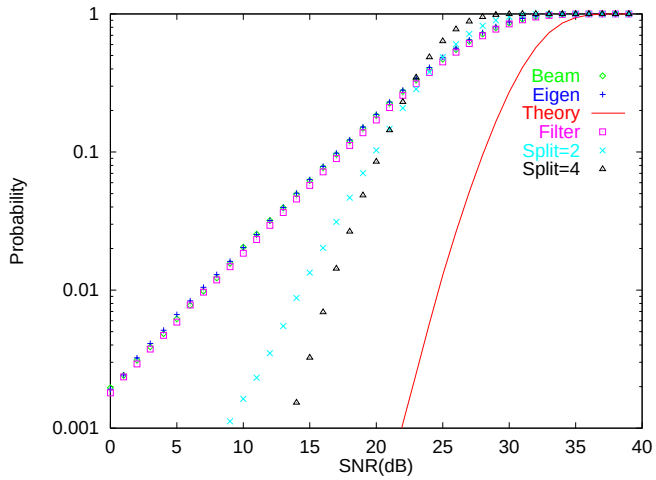

Figure 6.20: *The CDFs for the overall SNR received at the mobile for a number of transmission algorithms, with array size M=16, source bearing 90^o and scattering width 20^o.*

The received signals for transmission algorithms employing beamformer transmission (labelled "beam"), eigenfilter transmission (labelled "eigen") and for transmission with a beamformer at the source bearing are all seen to follow a Rayleigh distribution. These techniques are unable to provide any additional diversity at the mobile. Results are also shown for antenna transmission (with eigenfilters) using 2 (L=8) and 4(L=4) sub–arrays. The loss in mean SNR is evident for sub–array transmission. Transmitting a single eigenfilter achieved an average output SNR of 27.0 dB, two filters gave 26.2 dB and four gave

25.0 dB. However, the latter two methods provide significant diversity gain at the mobile because the separate components may be combined coherently with a RAKE filter. At low SNR values, there will be little to choose between any of the transmission techniques. However, as the SNR increases, the BER performance of each approach will depend on distribution of the tail of the CDF. In this case, sub–array transmission and the spatial smoothing technique can provide improved performance. Finally, it should be emphasised that all techniques provide a considerable loss in SNR compared to the best possible CDF (labelled "Theory"), which could be obtained only by direct measurement of the forward link channel parameters. On slowly fading channels, the performance can be improved considerably by using transmission feedback or time–division–duplex approaches.

6.6.2.5 Discussion

Transmission diversity schemes provide an effective means of providing extra multipath diversity at the mobile, for two antennas. However, increasing the number of transmitting antennas in this scheme may not improve the performance of the mobile's receiver. This is because the number of multipath components for the mobile to track become large; self–noise effects will also become a problem. Finally, for channels with small scattering widths, the antenna array size may have to be very large in order for each transmission to fade independently.

If the channel covariance matrix contains only a few principal eigenvectors, "blind" transmission techniques, such as sub–array transmission, provide diversity at the mobile whilst maintaining some spatial directivity in the direction of the mobile. As a result, sub–array transmission may reduce the level of CDMA interference from other users, compared to transmission diversity. The output SNR performance of sub–array transmission is also generally better than for transmission diversity, but may be considerably worse than the optimum output SNR which could be achieved with knowledge of the forward link channel.

The main difficulty in performing forward link transmission is to estimate the diversity order of the channel under consideration. This can only be achieved by averaging the reverse link channel covariance matrices over a reasonable amount of independent data. This provides an estimate of the number of principal components present. In any case, provided the overall SNR at the mobile is sufficiently large, two or three independently fading signals may provide sufficient diversity: increasing the order of diversity generally provides diminishing returns.

A more serious problem for implementation of antenna array transmission within the existing IS–95 standard, compared to transmission diversity, is the use of a coherent pilot tone on the forward link. This tone is transmitted on a separate CDMA code from other users, at a higher power to permit mobile receivers to perform coherent PSK detection of their coded signals. The simplest solution to the problem would be to transmit the pilot tone in all directions, using either an omni–directional transmitter or an antenna array transmitter. In either case, there exists the possibility that the received signal for the pilot will vary significantly from that received for a given mobile user. As a result, future CDMA

specifications may need to be altered to permit the use of antenna array transmission techniques.

6.7 Conclusion

In this chapter, the extension of channel modelling techniques to the case of antenna arrays has been discussed so that the effects of fading multipath channels can be measured. Two separate channel models have been considered: firstly a point source frequency selective channel, whose reverse–link performance for antenna–arrays does not differ significantly from single antenna receivers. In this case, a RAKE filter is required to coherently combine multipaths to overcome Rayleigh fading. The second model consists of a flat–fading channel, made up of a number of directional components. In this case, eigenfilters combine the received signal effectively to exploit the available spatial diversity. Spatial filter and beamspace methods can still partially exploit the available diversity, although the output SNR tends to reduce as the width of the multipath scattering widens. The bearing estimation receiver is less attractive than the eigenfilter structure in terms of obtaining the best performance over a communications channel. However, it is still useful in situations where mobile bearings are required, such as for the source location technique described in Chapter 7. On the forward link, the antenna array can provide directional transmissions to reduce interference to other users. However, the receiver must ensure that the mobile receives a frequency–selective channel to compensate for the effect of Rayleigh fading. Where a multipath component has a wide scattering angle, multiple sub–arrays may be used to maintain directional transmissions whilst exploiting spatial diversity.

Chapter 7

Source Location

One application for bearing estimation techniques in a multipath environment is to locate the position of a transmitting mobile. In this chapter an algorithm is presented to perform such a task. It is based on the adaptation of a 2–ray channel model frequently encountered in high frequency (HF) and underwater source location problems. The performance of the algorithm is estimated from a first order Taylor series expansion and confirmed by Monte–Carlo simulation.

Estimating the time delay between multipaths is conventionally limited by the chip rate of the received spread spectrum code. To improve the situation, a variant of the MUSIC algorithm is presented for simultaneously estimating a multipath's bearing and time delay. The transmitter location algorithm requires the position of a multipath reflector as one of the parameters, which would normally be estimated from terrain databases. An alternative approach for locating the reflector is also discussed, which uses a mobile antenna array receiver.

7.1 Direction Finding and Source Location

In order to locate the position of an active transmitter, one common approach is to employ a given set of parameter measurements made at a number of different receiver locations [179, 180]. Suitable measurement parameters for such a calculation are (relative) time delays involved in receiving the transmitted signal [181] or received power [182]. This principle may be used in reverse for navigation purposes, most notably the Global Positioning System (GPS) [25].

In order to avoid the need for multiple receiver sites, in certain situations it is possible to exploit multipath information to locate the source at a single receiver site. This method is often termed single site location (SSL) and is suitable for locating high-frequency (HF) transmissions or for underwater passive sonar applications. The simplest model for this technique has one direct (line of sight) path and one reflected ray. The reflected ray is presumed to occur due to the ionosphere reflection in HF propagation or due to the ocean surface/sea bed in underwater acoustic propagation. In both cases, the reflecting surface may be modelled as flat so that the geometry of the wave propagation is very simple. If the bearings of the two multipath components are known, the problem reduces to accurately estimating the time delay between the LOS and reflected paths. For more information on such approaches, see [183–185] and the references therein.

The approach taken in this chapter is based on SSL techniques, but the problem is made more difficult by

the nature of urban microwave propagation. This means that the propagation geometry and the resulting algorithm become correspondingly more complex.

7.2 Basic Model for Source Location

This section will present the background to the source location problem and will define the parameters necessary for the algorithm. Consider the frequency selective channel shown in figure 7.1.

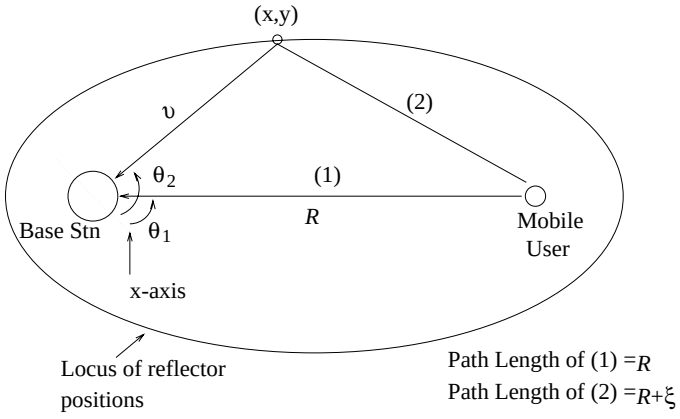

Figure 7.1: *The two-ray frequency selective model for source location.*

Both propagation paths shown in the figure are assumed to lie on a horizontal plane. The main path, denoted as (1), is assumed to follow a direct path between the mobile user and the base station. The second path (2) occurs due to a reflection from an obstacle in the environment. If the time of arrival of the second multipath is known, the location of the reflecting object may be located on an ellipse, whose foci are the locations of the transmitter and receiver [186]. The parameters shown in figure 7.1 are defined as follows:

- Bearing of multipath (1) $\equiv \theta_1$
- Bearing of multipath (2) $\equiv \theta_2$
- Base station–reflector distance $\equiv \upsilon$
- Reflector position $\equiv (x, y) = (\upsilon \cos(\theta_2 - \theta_1), \upsilon \sin(\theta_2 - \theta_1))$
- Base station to mobile distance $\equiv R$
- Time delay between the arrival of multipath (1) and (2) $\equiv t_d$
- Excess path length of (2) $\equiv \xi = t_d c$

where c denotes the speed of light. The co-ordinates of the mobile are measured relative to an arbitrary x–axis, with the origin at the antenna array (shown as a line in figure 7.1). The one exception is the position of the reflector (x, y), which is measured with the direct path as the x–axis.

7.3 Derivation of the Algorithm

In order to estimate the position of the mobile (i.e., the value of R), the following information is needed: i) the multipath bearings θ_1 and θ_2 ii) the value of υ (or equivalently the location of the reflector (x, y)) and iii) the associated excess path length ξ of multipath (2) associated with the excess time delay t_d. The major and minor axes of the reflector ellipse shown in figure 7.1 will be defined as a_1 and a_2 respectively. From the geometry of ellipses, it is now possible to write [187]:

$$\begin{aligned} a_1^2 - a_2^2 &= R^2 && (7.1)\\ R + \xi &= a_1 && (7.2)\\ \frac{4(x-(R/2))^2}{a_1^2} + \frac{4y^2}{a_2^2} &= 1 && (7.3) \end{aligned}$$

Equation (7.3) may be written as:

$$4a_2^2(x-(R/2))^2 + 4a_1^2y^2 = a_1^2a_2^2 \tag{7.4}$$

Substituting equation (7.1) into (7.4) gives:

$$4(a_1^2 - R^2)(x-(R/2))^2 + 4a_1^2y^2 = a_1^2(a_1^2 - R^2) \tag{7.5}$$

Secondly, equation (7.2) may be substituted into (7.5) to remove the variable a_1, such that:

$$4((R+\xi)^2 - R^2)(x-(R/2))^2 + 4(R+\xi)^2y^2 = (R+\xi)^2((R+\xi)^2 - R^2) \tag{7.6}$$

Equation (7.6) may be simplified to give a quadratic equation in R, whose coefficients A,B and C are:

$$\begin{aligned} A &= 4y^2 - 8x\xi - 4\xi^2\\ B &= 8\xi x^2 + 8\xi y^2 - 4\xi^2 x - 4\xi^3\\ C &= 4\xi^2x^2 + 4\xi^2y^2 - \xi^4 && (7.7) \end{aligned}$$

The value of R may be obtained from the quadratic formula:

$$R = \frac{1}{2A}[-B \pm \sqrt{B^2 - 4AC}] \tag{7.8}$$

The two solutions for R correspond to the two possible ellipses which meet at the reflector. One extends in the negative direction, giving a negative value for R. The other one, which extends in the positive direction, is the one required here, so the correct value of R is the positive root of the quadratic equation. The position of the mobile user relative to the origin x–axis line through the base station array is given by $(R\cos\theta_1, R\sin\theta_1)$.

7.4 Perturbation Analysis

In order to estimate the performance of the technique, one may expand equation (7.8) according to a Taylor series [187]. In this case, it has been assumed that the variables θ_1, θ_2, υ and ξ are the independent random variables. Hence, the Taylor series will be a function of the error terms of all these variables, denoted as $\Delta\theta_1$, $\Delta\theta_2$, $\Delta\upsilon$ and $\Delta\xi$ respectively. The mean error values of all four variables are assumed to be zero. So, limiting the expansion to a first–order approximation, the mean error values of X and Y, ΔX and ΔY, are also zero.

The first–order variance expressions involve partial derivatives of all the independent variables. These are given by:

$$\begin{aligned}
\Delta X^2 &= (\frac{\partial X}{\partial \upsilon})^2\Delta\upsilon^2 + (\frac{\partial X}{\partial \theta_1})^2\Delta\theta_1^2 + (\frac{\partial X}{\partial \theta_2})^2\Delta\theta_2^2 + (\frac{\partial X}{\partial \xi})^2\Delta\xi^2 \\
\Delta Y^2 &= (\frac{\partial Y}{\partial \upsilon})^2\Delta\upsilon^2 + (\frac{\partial Y}{\partial \theta_1})^2\Delta\theta_1^2 + (\frac{\partial Y}{\partial \theta_2})^2\Delta\theta_2^2 + (\frac{\partial Y}{\partial \xi})^2\Delta\xi^2
\end{aligned} \tag{7.9}$$

provided that θ_1, θ_2, υ and ξ are mutually independent Gaussian random variables. The necessary partial derivatives for solving the equations in (7.9) are presented in appendix D. As the equations involve only first–order derivative terms, the results asymptotically converge to the true values as the errors in θ_1, θ_2, υ and ξ become small. The expressions for the errors in X and Y are quite complex, so the equations have been evaluated for a number of different conditions to determine the performance of the technique. In the results, errors are presented in terms of the root mean squared error, which is simply the square root of the sum of the variances of the estimates of X and Y.

7.5 Results and Discussion

In order to confirm the theoretical results, a number of Monte–Carlo simulations have been performed. In all the simulations, the variables θ_1, θ_2, υ and ξ were drawn from independent Gaussian random distributions whose mean was the true value in each case. The mean and standard deviation of these variables could then be altered to assess their effect on the algorithm.

For the first set of simulations, the parameters used are specified in table 7.1. Using these parameters,

Parameter	Mean	Std Dev
θ_1	90^o	0.05-1^o
θ_2	95-150^o	0.05-1^o
ξ	200 m	2 m
υ	496 m	4.96 m
R	400 m	-

Table 7.1: *The parameters for the first simulation.*

the mean value of θ_2 was set to four different values, and Monte–Carlo simulations performed in each case. During each simulation, the standard deviations of both θ_1 and θ_2 were varied between 0.05^o and 1^o. This allowed the effect the angular spacings of the two multipaths (i.e. the variable $(\theta_2 - \theta_1)$) on the algorithm to be clearly seen. The simulation results are shown in figure 7.2 as points. Equation (7.9) has been used to calculate first order estimates of the standard deviations and these results are shown as lines.

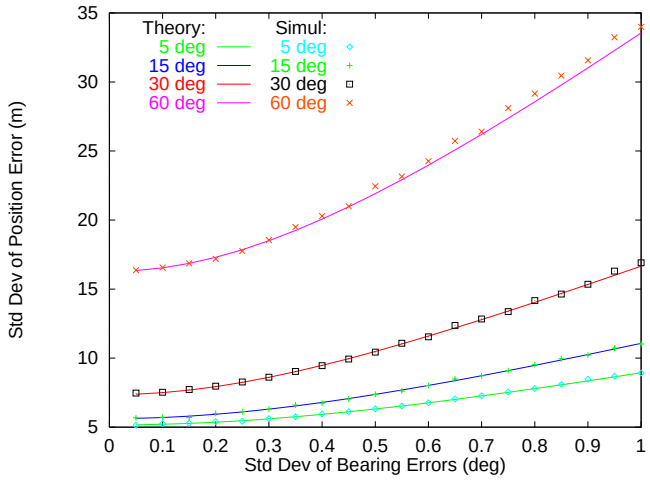

Figure 7.2: *The position error as a function of the bearing difference* $(\theta_2 - \theta_1)$.

It is seen that increasing the value of $(\theta_2 - \theta_1)$ has a drastic effect on the position error. Indeed if $(\theta_2 - \theta_1)$ = 180^o, the equations have no solution. This is because the only absolute distance information present in the algorithm is the reflector location measurement υ. This information is used to estimate the value of R - the closer θ_2 is to θ_1, the smaller the error in the estimation of R. Alternatively, as the value of $(\theta_2 - \theta_1)$ increases, the equations become more ill-conditioned. The same trend has been observed when the horizontal axis of figure 7.2 becomes the standard deviation of υ or ξ.

It is also worth noting that the first–order perturbation approximation breaks down for large values of the bearings standard deviation (BSD). This is because the higher–order terms are no longer negligible and begin to have an effect on the error in R. As a result, Monte–Carlo simulations should be used to check the algorithm's performance where large measurement errors are involved.

The next simulation considered the effect of scaling the standard deviation of θ_2 by a factor k_0, relative to that of θ_1. The bearing θ_2 was set to be 95^o; otherwise, the simulation conditions were identical to those in table 7.1. Specifically, the standard deviation of θ_2 was multiplied by a factor k_0 = 1, $\sqrt{2}$, 2, $\sqrt{8}$ and 4 times that for θ_1. This is equivalent to an increase in variance of θ_2 by 1–16 times the variance of θ_1: this would reflect the signal–to–noise ratio (SNR) of the second multipath being 0-12 dB below that of the first, assuming a linear relationship between SNR and bearing variance. The results are shown in figure 7.3, with the standard deviation scaling factor k_0 indicated for each case.

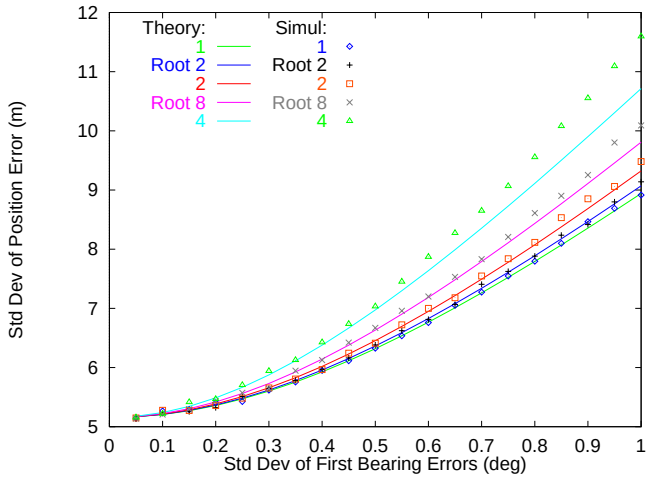

Figure 7.3: *The position error as a function of relative bearing standard deviations.*

Not surprisingly, the position error increases as the standard deviation of θ_2 increases over θ_1. However, even when k_0 changes from 1 to 4, the effect on the position error appears negligible at low values of the BSD. When the standard deviation of θ_1 is 1^o and the value k_0 changes from 1 to 4, the position error increases only by 30%. So, it appears that in this case, the equations are not over–sensitive to large bearing errors in θ_2 alone. Finally, it is noticeable that when the BSD values are large, particularly with $k_0 = \sqrt{8}$ or 4, the Monte–Carlo simulation results are larger than the predicted values. Again, this would appear to be attributable to the higher order terms of the Taylor expansion becoming significant in value.

The next parameter of interest was the excess path length ξ. The simulation parameters in this case are shown in table 7.2. Note that the question mark indicates that the mean value of υ will alter in accordance

Parameter	Mean	Std Dev
θ_1	90^o	0.05-1^o
θ_2	95^o	0.05-1^o
ξ	200-1600 m	1% of mean
υ	?	1% of mean
R	400 m	-

Table 7.2: *The parameters for the third simulation.*

with ξ. The results are shown in figure 7.4, with the value of ξ indicated for each curve. In this case,

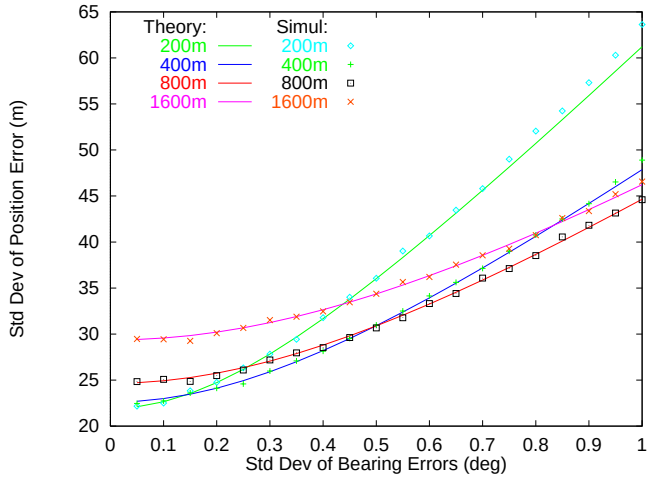

Figure 7.4: *The position error as a function of the excess path length* ξ.

the situation is not so clear cut. For small BSD values, the position error increases with increasing ξ. However, as the bearing error increases, the situation changes so that increasing ξ actually decreases the position error. For the parameters chosen, a value of ξ equal to 800 m provides the minimum position error for BSD values of 1^o.

The final parameter of interest is the mobile to base station distance R and its effect on the position error. Setting the excess path delay ξ to be 400 m (standard deviation 4 m), the range was varied between 500-4000 m. Otherwise, the scenario conditions are identical to to those in table 7.2. The results are shown in figure 7.5, with the value of R specified for each curve.

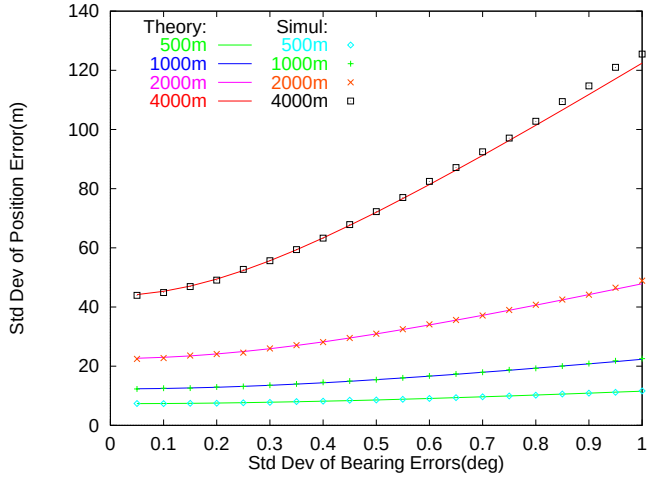

Figure 7.5: *The position error as a function of the distance* R.

Intuitively, one might expect that doubling the value of R would simply double the position error. For small values of the BSD, this appears to hold true. However, as the value of the BSD increases, this linear relationship no longer applies. When the bearings standard deviation is 1^o, increasing R from

2000 m to 4000 m increases the position error by a factor of about 2.5.

To summarise the results of the simulations in this section, the position error is very sensitive to the value of $(\theta_2 - \theta_1)$ which is a serious disadvantage. Increasing the standard deviation of θ_2 compared to θ_1 does not affect the position error significantly. Altering the parameter ξ has different effects on the position error, according to the accuracy of the bearing estimates. Finally, increasing the value of R increases the position error and for BSD values around 1^o the rate of increase becomes slightly larger.

7.6 Discussion

The previous section has looked at the effect of certain parameters on the source location algorithm. In practice, the location of the mobile and the channel between it and the base station will determine the performance of the algorithm. Perhaps the most serious deficiency of the algorithm is the fact that its performance is altered substantially according to the difference in angles between the two components used for source location. The performance of the technique may be improved by averaging results using more delayed multipaths, if available. However, the direction of the mobile is completely specified by the bearing θ_1, which will limit the accuracy achievable by this technique.

The sources of error affecting the practical measurement of the parameters θ_1, θ_2, υ and ξ will now be considered in turn.

(i). **Bearing Measurement:** The multipath bearings may be measured using a technique like the MUSIC algorithm. As discussed in chapter 4, the performance of the algorithm is a function of the number of snapshots, number of antennas and the SNR. However, in more realistic multipath channels, such as those discussed in chapter 6, the variance of the bearing estimates can also depend vitally on the multipath angular spread. In this case, the technique requires to average over a number of independent realisations of the channel – how frequently these occur depends on the fading rate of the channel and hence the mobile's speed. Of course, using too many channel realisations may lead to additional sources of error due to the mobile having moved a significant distance over the time of observation.

(ii). **Multipath Reflector Measurement:** The location of the reflector for the delayed multipath requires accurate mapping of the area under observation. Practical location of multipath reflectors can only ever be a matter of guess work, with the algorithm using the location of the most prominent building or landscape feature lying in the direction of the multipath's arrival. Errors in the measurement of υ will thus depend on two factors: 1) Errors in the database of landscape features 2) Errors due to choosing the wrong reflector for a given multipath. The former type of errors are easier to quantify and less likely to be catastrophic than the latter.

(iii). **Excess Path Length Measurement:** If the transmitter emits a code of a given chip rate t_c, the smallest excess time delay between multipaths that can be unambiguously resolved, using a conventional digital matched filter for the desired CDMA code, is simply t_c. This places a severe limit on the accuracy of practical excess path delay measurements (which may be estimated from

the time delay knowing the speed of light). However, the situation may be improved by extending high–resolution spectral estimators, such as MUSIC, into both the bearing and excess time delay domains. One possible approach to this problem will now be described.

7.7 High Resolution Estimation of Multipath Parameters

The original formulation of the MUSIC algorithm was intended only for the estimation of the source bearings of narrowband transmissions [53]. However, algorithms have since been developed for determining simultaneously the bearings and carrier frequencies of a number of narrowband sources [188] and for accurately estimating the relative time delays of a number of multipath signals received from a single spread spectrum transmitter [189, 190]. Combining the ideas behind these two approaches, an algorithm will now be described for estimating the relative time delays and bearings of a number of multipath components, received by an antenna array from a spread spectrum source. This technique may not be able to resolve multipaths closely spaced in time, but it does permit increased accuracy in time delay measurements.

Consider a single spread spectrum transmission, which is not subject to data modulation. The electromagnetic signal is subject to multipath propagation and reaches the spread spectrum receiver array by several paths. The baseband received signal vector at the $M-$ element array $\boldsymbol{r}(t)$ is given by:

$$\boldsymbol{r}(t) = \sum_{i=1}^{K} \vartheta(i,t) c(t - t_i)\, \boldsymbol{a}(\theta_i) + \boldsymbol{\eta}(t) \tag{7.10}$$

where K denotes the number of separately resolvable multipaths, $\vartheta(i,t)$ the complex amplitude of the i^{th} component and t_i its time delay, relative to the arrival of the first multipath component. The vector $\boldsymbol{\eta}(t)$ denotes additive white Gaussian noise which corrupts the received signal and $c(t)$ denotes the transmitted spread spectrum pseudo–noise (PN) code. The code is periodic with period t_s, and chip rate t_c, so that the processing gain W = t_s/t_c. It will be assumed that the maximum delay of any multipath component $\{t_i\}$ is smaller than the code period t_s.

It is possible to directly estimate the multipath components using $\boldsymbol{r}(t)$: however, the approach of [189, 190] will be followed here. The vector $\boldsymbol{r}(t)$ will subject to I and Q matched filters containing the desired code $c(t)$ to produce the post–correlation data vector $\boldsymbol{y}(t)$:

$$\boldsymbol{y}(t) = \sum_{i=1}^{K} h(i,t) \delta_c(t - t_i)\, \boldsymbol{a}(\theta_i) + \boldsymbol{n}(t) \tag{7.11}$$

where $\boldsymbol{n}(t)$ is the additive noise at the output of the code matched filter, $h(i,t)$ the post–correlation channel tap complex amplitude and $\delta_c(t)$ denotes the periodic correlation function of the code $c(t)$. The functions $h(i,t)$ and $\delta_c(t)$ may be defined as:

$$h(i,t) = \int_{t-t_s}^{t} \vartheta(i,\omega)\, d\omega \tag{7.12}$$

$$\delta_c(t) = \int_0^{t_s} c(\omega)c(t - t_s + \omega)d\omega \tag{7.13}$$

The signal vector $y(t)$ will now be sampled in the I and Q channels at the chip rate: assuming the baseband receiver bandwidth is at least $2W$, the additive noise will be spatially and temporally white. A vector $\boldsymbol{y}_T(t) \in \mathbb{C}^{MW\times 1}$ of all the data from all the antennas for one complete period of the code may then be constructed as follows:

$$\boldsymbol{y}_T(t) = [y_1(t), y_1(t+t_c), \ldots, y_1(t+(W-1)t_c), y_2(t), y_2(t+t_c), \ldots, y_M(t+(W-1)t_c)]^T \tag{7.14}$$

where $y_m(t)$ denotes the complex signal from the m^{th} antenna at time t. The signal component of $\boldsymbol{y}(t)$ may be assumed to be composed of K scaled "steering vectors" $\boldsymbol{a}_T(\theta, t_d)$ which reflect the bearing and excess time delay of each multipath component. The vector $\boldsymbol{a}_T(\theta, t_d) \in \mathbb{C}^{WM\times 1}$ is defined by the equation:

$$\boldsymbol{a}_T(\theta, t_d) = [\delta_c(t_d), \ldots, \delta_c(t_d + (W-1)t_c), e^{j\pi cos(\theta)}\delta_c(t_d), \ldots, e^{j(M-1)\pi cos(\theta)}\delta_c(t_d + (W-1)t_c)] \tag{7.15}$$

It will now be assumed that the arrival time of the first multipath component t_0 is known. A covariance matrix for N snapshots of the signal data can be constructed according to the formula:

$$\hat{\boldsymbol{R}}_{W/B} = \frac{1}{N}\sum_{i=0}^{N-1} \boldsymbol{y}_T(t_0 + (i \times t_s))\boldsymbol{y}_T^H(t_0 + (i \times t_s)) \tag{7.16}$$

For the matrix $\hat{\boldsymbol{R}}_{W/B} \in \mathbb{C}^{WM\times WM}$ to be of full rank, $N > WM$. Taking the expectation of $\hat{\boldsymbol{R}}_{W/B}$, the familiar covariance matrix structure is obtained:

$$\boldsymbol{R}_{W/B} = \boldsymbol{A}_T \boldsymbol{S}\boldsymbol{A}_T^H + \sigma^2 \boldsymbol{I} \tag{7.17}$$

The matrix $\boldsymbol{A}_T \in \mathbb{C}^{WM\times K}$ contains the K column vectors $\boldsymbol{a}_T(\theta_k, t_K)$ and $\boldsymbol{S} \in \mathbb{C}^{K\times K}$ is the covariance matrix of the multipath component amplitudes $h(k, t)$. The rank of the signal subspace $\boldsymbol{A}_T \boldsymbol{S}\boldsymbol{A}_T^H$ depends on the number of independent multipath components present - for now the rank will assumed to be K. It is possible to calculate the eigenvalue decomposition of $\boldsymbol{R}_{W/B}$, determine the size of the noise subspace and calculate the matrix $\boldsymbol{E}_n \in \mathbb{C}^{WM\times WM-K}$ which contains all the column noise eigenvectors. The power density spectrum using the MUSIC algorithm may then be calculated as:

$$P_{MUS}(\theta, t) = \frac{1}{\boldsymbol{a}^H(\theta, t)\boldsymbol{E}_n\boldsymbol{E}_n^H\boldsymbol{a}(\theta, t)} \tag{7.18}$$

In order for K multipath components to be resolvable, the following must hold:

(i). The cross–correlation between the K multipaths must be less than unity, so that the rank of $\boldsymbol{S}$ is K.

(ii). Not more than $M-1$ multipath components can have the same delay.

(iii). Not more than $W-1$ multipath components can occur at different time delays but the same

bearing.

Concerning the first point, the cross–correlation between any two spatially separated multipaths with the same time delay may be reduced through the use of spatial smoothing techniques. This involves forming covariance matrices according to equation (7.16) and averaging them using SS or FBSS as described in chapter 4. The effect of spatial smoothing on coherent multipaths with different time delays is more difficult to quantify and is a matter for further research. In the case of a single receiver, spatial smoothing in time can only be used where the PN code has a Vandermonde form [189]. The other cure is to employ sufficient data samples to de–correlate the multipaths through fading effects. Following [188], the other two points specify the conditions on the vectors $\{\boldsymbol{a}(\theta_k, t_k)\}$ under which the columns of $\boldsymbol{A}_T$ are linearly independent.

Finally, it should be noted that for a typical PN code such as an m–sequence the correlation function $\delta_c(t)$ only takes non–negligible values within one chip ($\pm t_c$) of the time of arrival of the code. Hence, if the multipaths are known to arrive within a certain range of time delays $[0, t_{max}]$, only the time samples in that range need to be used in $\boldsymbol{R}_{W/B}$ – data samples at larger delays may be removed without significant degradation in the algorithm's performance. Thus, the decision to employ post–correlation data in the algorithm permits a large decrease in the computation necessary to locate multipaths.

As a simple example of the technique, a sample signal has been generated for a channel consisting of four multipath components. The PN–code used was 15 chips long [1] and N = 300 snapshots were taken of the noise–corrupted data. The array contained M=8 elements and the SNR of the multipaths at the output of one set of I and Q–channel code matched filters was 10 dB. The parameters of the multipath components are given in table 7.3. The quoted Doppler frequency is normalised to the sampling frequency of the

Multipath Number	Bearing	Time Delay (chips)	Doppler Frequency (Hz)
1	35^o	2.0	0.5
2	75^o	4.3	0.25
3	150^o	10.25	0.673
4	120^o	13.75	0.125

Table 7.3: *The multipath component parameters.*

receiver. The resulting power density spectrum generated using the modified MUSIC algorithm is shown in figure 7.6. In this case, the four multipath components are correctly identified using this technique.

7.8 Locating the Multipath Reflector

Until now, it has been assumed that the location of the reflector which gives rise to the delayed multipath signal is known. However, it is theoretically possible to locate the reflector using two or more bearing

[1] Rectangular pulse shaping was assumed and the function $\delta_c(t)$ was that of an m–sequence, i.e. the peak amplitude was 15 and for all other integer delays, the amplitude was -1.

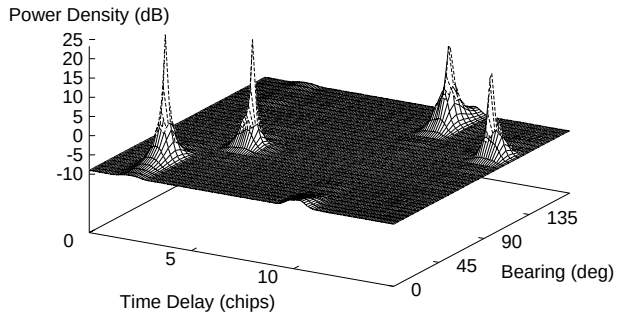

Figure 7.6: *The power density spectrum of the received signal using the MUSIC algorithm in time delay and bearing.*

measurements made from a mobile antenna array. The scenario considered in this section is shown in figure 7.7.

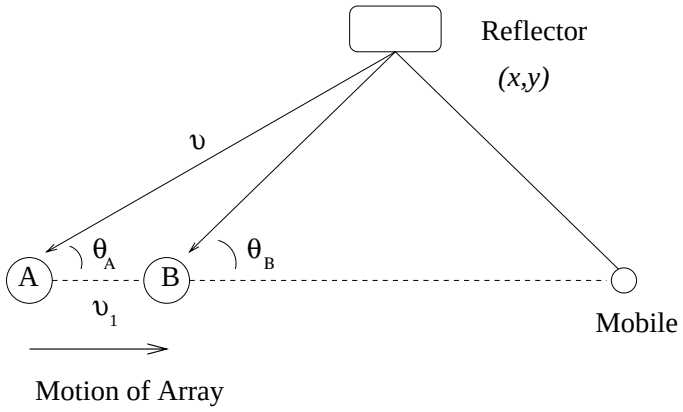

Figure 7.7: *The scenario for locating the multipath reflector.*

In this case the moving array makes two bearing measurements at locations A and B, denoted as θ_A and θ_B. For convenience, it has been assumed that the motion of the array is in the direction of the mobile user. If the distance between locations A and B, υ_1, is known the reflector location relative to the origin A may be estimated from two linear equations:

$$x(\tan\theta_A) - y = 0 \text{ and } x(\tan\theta_B) - y = \upsilon_1(\tan\theta_B) \tag{7.19}$$

Solving for x and y gives:

$$x = \frac{\upsilon_1 \tan\theta_B}{\tan\theta_B - \tan\theta_A} \text{ and } y = \frac{\upsilon_1 \tan\theta_A \tan\theta_B}{\tan\theta_B - \tan\theta_A} \tag{7.20}$$

As is normal in the case of two linear equations, the solution becomes very ill–conditioned if the gradients of the two lines, namely $\tan\theta_A$ and $\tan\theta_B$, become close. As a consequence, the change in measured bearing from location A to B must be significant for good results. For example, consider a scenario where υ_1 = 100 m (with an unbiased standard deviation of 1 m, due to measurement error). The change in bearing $\theta_B - \theta_A$ is varied from 5-40^o to observe the effect on the error in position location. The standard deviation of bearing errors is 1^o and again all independent variables are modelled as Gaussian. The standard deviation of the position error has been estimated from 10000 Monte Carlo simulations in each case. The results are given in table 7.4.

$(\theta_B - \theta_A)$	5^o	10^o	20^o	40^o
Mean υ (m)	879.0	472.7	265.0	155.0
Std dev of position error (m)	754.4	69.7	16.7	5.1
Std dev Error as % of mean	85.8 %	14.7 %	6.3 %	3.3 %

Table 7.4: *The standard deviation of position error against the source bearings difference.*

The results demonstrate a drastic reduction in the percentage positioning errors as the value of $(\theta_B - \theta_A)$ increases. However, this may mean that the values of $(\theta_A - \theta_1)$ and $(\theta_B - \theta_1)$ will also be large, which implies that the performance of the source location algorithm will be poor. A more fundamental problem is deciding whether the same reflector is responsible for both reflected multipath signals. If the shadowing changes significantly while the array moves over the distance υ_1, the technique will not work.

7.9 Conclusions

In this chapter, an algorithm has been developed to estimate the location of a transmitting mobile based on a 2–ray multipath model. A first order Taylor series expansion has been used to estimate the performance of the technique, with Monte–Carlo simulations used to check the results. The main difficulty with the algorithm is the fact that its performance depends on the separation between the two multipath bearings. If this is made to increase, the performance of the algorithm degrades considerably.

A technique to provide accurate estimates of the relative time delay between multipaths has also been presented. It is based on an extension of the MUSIC algorithm into two dimensions, one of space and one of time delay. One requirement of the original algorithm is that the location of the multipath reflector must be known. In order to avoid the use of terrain databases, a technique to locate the position of the second multipath reflector has also been described. However, this technique only works well for large bearing separations between the two bearing measurements, which may compromise the performance of the source location technique.

Chapter 8
Conclusions

This thesis has been concerned with the design and operation of antenna array bearing estimation receivers for spread spectrum signals. Algorithms for performing the necessary signal processing tasks have been analysed and a technique for locating a transmitter in an urban area presented. Results for simple cellular radio models demonstrate that antenna array receivers and transmitters have considerable potential for improving system capacity. Analysis of the operation of bearing estimation receivers in multipath fading channels has also been presented. This chapter will draw together the main conclusions of the work and briefly discuss its limitations. Some suggestions for further research in this area are also presented.

8.1 Summary of the Work

This thesis has discussed in some detail the concept of a bearing estimation antenna array processor for direct–sequence spread spectrum modulation. This type of communication signal permits the receiver to separate multipath components whose relative delays are larger than the chip rate of the transmitted pseudo–noise code. This work made the assumption that the carrier frequency was much larger than the Fourier bandwidth so that any multipath channel may be modelled at an array receiver as a finite series of vectors, one for each multipath component received. Each vector is composed of K significant versions of the transmitted signal, arriving from different directions. Assuming that K is less than the array size M, it is possible to resolve the individual bearings using the MUSIC algorithm. As the received signal is made up of potentially coherent multipath components, a spatial smoothing technique may be used to ensure the successful application of MUSIC.

The MUSIC algorithm requires an initial estimate of the number of impinging signals, a task which may be performed by a model order estimation technique such as the minimum description length (MDL) algorithm. This approach employs the eigenstructure of the data covariance matrix, to estimate the number of signals present. Unfortunately, this method provides erroneous model order estimates when the signal subspace is rank deficient, as in the case of coherent multipaths. It is possible to use spatial smoothing techniques to restore the full rank of the signal subspace, so it is important to be able to estimate the algorithm performance in this case. In chapter 3, results have been presented to extend the performance analysis of Zhang et al [108] for the MDL to spatially smoothed covariance matrices, so that the operating conditions of the algorithm may be determined.

The spatial smoothing (SS) and forward–backward spatial smoothing (FBSS) algorithms are two possible methods to allow MUSIC to resolve coherent multipath signals. Some theoretical analysis and simulation

results have been presented to demonstrate the differences between these two algorithms. The SS technique has been shown to be sensitive to signal bearings and separations. Employing FBSS with the same degree of smoothing has some chance of improving the performance of MUSIC, particularly for closely spaced sources. However, the performance improvement that may be attained depends on the relative phases of the signals. Simulation results were also presented for two quadratic smoothing techniques: however, both techniques appear to make little difference to the performance of MUSIC.

The thrust of the work of chapter 5 was to analyse the performance improvement attainable by employing antenna arrays in a simple additive white Gaussian noise (AWGN) channel model. Results for both single cell and cellular systems demonstrate that antenna arrays can improve the error ratio performance for a given number of active mobiles: alternatively, the system capacity can be increased for a given quality threshold. However, space division multiple access can only be exploited if the mobiles are spread throughout the cell. Antenna arrays cannot separate two signals arriving from the same direction, so there is a finite probability that an antenna array could not improve the quality of the communication links. For AWGN point source channels, this probability may be reduced by increasing the array size.

Before antenna arrays may be deployed in practical cellular systems, realistic channel models are required to provide a sterner test of their capabilities. Chapter 6 has extended the COST–207 models, which are often used in mobile radio simulation work, to the case of antenna array receivers. If the received signal on the reverse link consists of a number of point source multipath signals, the antenna array cannot provide increased diversity at the receiver. However, it is a simple matter to provide effective performance at the mobile on the forward link by re–transmitting energy in the directions of the 2 or 3 largest received multipath components. Alternatively, if one of the received multipaths has a wide spread in angle, the receiver may exploit the spatial diversity present. Bearing estimation approaches were shown to degrade when the angular width of the received signal is wider than the main lobe of the array spatial filters. Spatial smoothing techniques may be used to estimate the bearings of the multipaths present, so that they may be coherently combined. However, this approach is much more computationally expensive than for eigenfilter methods, despite the fact that the performance of both techniques is about the same. Transmission techniques perform poorly for multipath components with a wide angular spread, because it is difficult to estimate the channel parameters effectively from a small number of reverse link data snapshots. It is possible to use a form of transmission diversity to improve the signal distribution observed at the mobile; alternatively the forward link may be observed directly using time division duplex or transmission feedback techniques.

Finally, chapter 7 considered an algorithm for locating the position of a mobile in an urban environment. The technique was based on a modification of the two–ray model commonly used in HF channels and SONAR applications. Results suggest that the algorithm can work well, although it is very sensitive to the relative bearings of the two multipath signals. One potential problem is the accurate estimation of the time delays between the two multipath components; a modified version of the MUSIC algorithm operating in time and space has been proposed for this task. A second deficiency of the algorithm is that it requires estimates of the position of the major reflector which gave rise to the second multipath component. A technique for estimating the position of the reflector using a mobile array has been

presented, although it requires two widely spaced bearing estimates of the second multipath for locating the reflector. This requirement may mean that the source location algorithm operates poorly; it is also difficult to ensure that the same multipath component is being measured at both positions.

8.2 Suggestions for Further Work

The work of this thesis has been concerned with the development and analysis of a bearing estimation receiver for spread spectrum signals, with application to the location of a mobile in an urban environment. This has permitted only limited research into the operation of such receivers in realistic urban cellular environments. There are a number of points which have not been addressed here and which merit much more work:

- Channel modelling to determine multipath scattering widths.
- Characterisation of CDMA interference observed at antenna arrays operating in urban areas.
- Comparing the relative performance of antenna array receiver structures operating on the reverse link in the presence of multipath.
- Solving the forward link problem: determining the best method for using antenna arrays to re–transmit to mobiles over multipath channels.
- Implementation and operation issues.

Each of these points will now be briefly discussed, presenting suggestions for possible further research work.

8.2.1 Channel Modelling

One of the difficulties with modelling multipath channels for antenna arrays is that the scattering widths of each multipath component can only be guessed at. In practice, the multipath scattering width will vary widely with the mobile to base station distance and the type of surrounding environment. However, much more data on multipath scattering widths, which can be estimated from the average cross–correlation between the signals received at an antenna array, would be very useful. In particular, measurements using spread spectrum signals would help to determine the likely scattering widths of different multipath components.

8.2.2 Characterising CDMA Interference

The form of asynchronous CDMA interference observed on the reverse link is an important problem. The exact distribution will depend on the array configuration and on the location and number of transmitting mobiles. Techniques such as bearing estimation and eigenfilter methods usually perform well when the

background noise is spatially and temporally white Gaussian noise. If the distribution differs significantly from this ideal, other approaches may provide considerable performance improvements.

8.2.3 Antenna Arrays: The Reverse Link

The relative performance of algorithms operating on the reverse link is of tremendous practical importance. There are a number of techniques available, ranging from the very simple beamspace transformation techniques, to complex interference cancellation and adaptive beamforming approaches. Interference cancellation techniques for CDMA have been the subject of considerable research in the last few years [44, 46]. However, one of the arguments against these systems is that they are computationally complex and often provide only a marginal gain in system performance. However, incorporating such techniques in antenna array receivers may be of interest for a different purpose; to cope with scenarios where a number of mobiles arrive from similar directions. The receiver may only have to cancel interference from a small number of co–channel mobiles, which means that the system is more likely to work successfully; additionally, the computational burden is unlikely to be excessive.

Inevitably, the requirement of cellular systems operators is to obtain the best possible capacity improvements that antenna arrays have to offer, whilst minimising the cost and computational complexity of such systems. If it turns out that complex receiver structures do not provide large capacity increases, practical systems may deploy simple receivers such as the beamspace transformation technique.

8.2.4 Antenna Arrays: The Forward Link

In general, the forward link of a CDMA system provides better performance than the equivalent reverse link, because the interference observed at each mobile can controlled much more easily. However, if large capacity gains can be obtained on the reverse link, the forward link may need to be improved accordingly. Choosing transmission weights for an antenna array operating on the forward link of a frequency division duplex system is difficult without direct estimation of the channel, although diversity transmission techniques may be used to suppress the effects of fading. However, it may be that time division duplex techniques are more suited to antenna array systems.

8.2.5 Operational issues

There are a number of practical limitations to current antenna array technology. Two major hardware problems for antenna array operators are 1) to implement linear amplifiers in the receiver and 2) to compensate for phase drift across the array which occurs over time. In addition, analogue to digital converters (ADCs) can sample the received signal only to a finite precision. As technology progresses, sampling rates and the accompanying number of quantisation levels available from ADCs are ever increasing [191]. There is also a growing interest in so–called software radios [192], as the position of

the ADC may shifted ever closer the radio frequency (RF) front end. However, a practical system designer must find the best compromise in terms of dividing the receiver tasks between specialist hardware and general purpose software. Perhaps, the critical decision for antenna array design is the choice of the ADC sampling rate and number of quantisation levels to obtain the desired bit error ratios without an excessive computational burden.

References

[1] D.C. Cox. “Wireless personal communications: What is it?”. *IEEE Personal Communications Magazine*, Vol 2(2):pp20–35, April 1995.

[2] K. Pahlavan and A.H. Levesque. “Wireless data communications”. *Proceedings of the IEEE*, Vol 82(9):pp1398–1430, September 1994.

[3] W.H.W. Tuttlebee. “Cordless personal communications”. *IEEE Communications Magazine*, Vol 30(12):pp42–53, December 1992.

[4] D.T. Magill, F.D. Natali, and G.P. Edwards. “Spread spectrum technology for commerical applications”. *Proceedings of the IEEE*, Vol 82(4):pp572–84, April 1994.

[5] C.I. Cook. “Development of air interface standards for PCS”. *IEEE Personal Communications Magazine*, Vol 1(4):pp30–34, Fourth Quarter 1994.

[6] J. Rapeli. “UMTS: Targets, system concept and standardization in a global network”. *IEEE Personal Communications Magazine*, Vol 2(1):pp20–28, February 1995.

[7] R. Steele. “The evolution of personal communications”. *IEEE Personal Communications Magazine*, Vol 1(2):pp6–11, Second Quarter 1994.

[8] P.G. Andermo and L.M. Ewerbring. “A CDMA–based radio access design for UMTS”. *IEEE Personal Communications Magazine*, Vol 2(1):pp48–53, February 1995.

[9] J.E. Padgett, C.G. Gunther, and T. Hattori. “Overview of wireless personal communications”. *IEEE Communications Magazine*, Vol 33(1):pp28–42, January 1995.

[10] Y. Yeh and D.O Reudink. “Efficient spectrum utilisation for mobile radio systems using space diversity”. *IEEE Transactions on Communications*, Vol 30(3):pp447–55, March 1982.

[11] J.H. Winters. “Optimum combining in digital mobile radio with cochannel interference”. *IEEE Transactions on Vehicular Technology*, Vol 33(3):pp144–55, August 1984.

[12] S.C. Swales, M.A. Beech, D.J. Edwards, and J.P. McGeehan. “The performance enhancement of multibeam adaptive base station antennas for cellular land mobile radio systems”. *IEEE Transactions on Vehicular Technology*, Vol 39(1):pp56–67, February 1990.

[13] J.H. Winters. “Signal aquisition and tracking with adaptive arrays in the digital mobile radio system IS–54 with flat fading”. *IEEE Transactions on Vehicular Technology*, Vol 42(4):pp377–84, November 1993.

[14] A.F. Naguib, A. Paulraj, and T. Kailath. “Capacity improvement with base–station antenna arrays in cellular CDMA”. *IEEE Transactions on Vehicular Technology*, Vol 43(3):pp691–8, August 1994.

[15] J.C. Liberti and T.S. Rappaport. “Analytical results for capacity improvements in CDMA”. *IEEE Transactions on Vehicular Technology*, Vol 43(3):pp680–90, August 1994.

[16] A.F. Naguib and A. Paulraj. “A base-station antenna array receiver for cellular DS/CDMA with M–ary orthogonal modulation”. In *Proceedings of IEEE 28th ASIMOLAR Conference on Circuits, Signals and Computers, Pacific Grove (USA)*, pages 858–62, November 1994.

[17] R. Arnott, M. Barrett, A. Bull, and A.G. Carr. "Development of an adaptive antenna demonstrator for DECT". In *IEE Colloquium on Smart Antennas, Digest 1994/182*, December 1994.

[18] R.A. Scholtz. "The origins of spread spectrum communication". *IEEE Transactions on Communications*, Vol 30(5):pp822–854, May 1982.

[19] R.A. Scholtz. "The evolution of spread–spectrum multiple–access communications". In *Proceedings of the 3rd IEEE International Symposium on Spread Spectrum Techniques and Applications (ISSSTA), Oulu (Finland)*, pages 4–13, July 1994.

[20] R. Price and P.E. Green. "A communications technique for multipath channels". *Proceedings of the IRE*, Vol 2:pp555–70, March 1958.

[21] R.A. Scholtz. "Notes on spread spectrum history". *IEEE Transactions on Communications*, Vol 31(1):pp82–84, January 1983.

[22] R. Price. "Further notes and anecdotes on spread–spectrum origins". *IEEE Transactions on Communications*, Vol 31(1):pp85–97, January 1983.

[23] R.E. Ziemer and R.L. Peterson. *"Digital Communications and Spread Spectrum Systems"*. Macmillan Publishing (New York), 1985.

[24] W.K. Alem, G.K. Huth, J.K. Holmes, and S. Udalov. "Spread spectrum acquisition and tracking performance for shuttle communications links". *IEEE Transactions on Communications*, Vol 26(11):pp1689–1703, November 1978.

[25] R.C. Dixon. *"Spread Spectrum Systems with Commerical Applications"*. John Wiley, New York, 1994.

[26] J.A. Brendler. "Tactical military communications". *IEEE Communications Magazine*, Vol 30(1):pp62–72, January 1992.

[27] J.L. Massey. "Information theory aspects of spread spectrum communications". In *Proceedings of the 3rd IEEE International Symposium on Spread Spectrum Techniques and Applications (ISSSTA), Oulu (Finland)*, pages 16–21, July 1994.

[28] D.D. Falconer, F. Adachi, and B. Gudmundson. "Time division multiple access methods for wireless personal communications". *IEEE Communications Magazine*, Vol 33(1):pp50–7, January 1995.

[29] M.K. Simon, J.K. Omura, R.A. Scholtz, and B.K. Levitt. *"Spread Spectrum Communications Handbook (Revised Edition)"*. McGraw–Hill, 1994.

[30] W.C. Jakes Jr. *"Microwave Mobile Communications"*. Wiley, New York, 1974.

[31] N. Yee, J.P. Linnartz, and G. Fettweis. "Multi–carrier CDMA in indoor wireless radio networks". *IEICE Transactions on Communications"*, Vol E77-B(7):pp900–4, July 1994.

[32] R.A. Scholtz. "The spread spectrum concept". *IEEE Transactions on Communications*, Vol 25(8):pp748–55, August 1977.

[33] R.L. Pickholtz, D.L. Schilling, and L.B. Milstein. "Theory of spread spectrum communications - a tutorial". *IEEE Transactions on Communications*, Vol 30(5):pp855–84, May 1982.

[34] D.C. Cox. "910 MHz urban mobile radio propagation: Multipath characteristics in New York city". *IEEE Transactions on Communications*, Vol 21(11):pp1188–94, November 1973.

[35] A.S. Bajwa and J.D. Parsons. "Small–area characterisation of UHF urban and suburban mobile radio propagation". *IEE Proceedings Part F*, Vol 129(2):pp102–9, April 1982.

[36] E.S. Sousa, V.M. Jovanovic, and C. Daigneault. "Delay spread measurements for the digital cellular channel in Toronto". *IEEE Transactions on Vehicular Technology*, Vol 43(4):pp837–47, November 1994.

[37] W.C.Y. Lee. "Overview of cellular CDMA". *IEEE Transactions on Vehicular Technology*, Vol 40(2):pp291–302, May 1991.

[38] K.S. Gilhousen, I.M. Jacobs, R. Padovani, A.J. Viterbi, L.A. Weaver, and C.E. Wheatley. "On the capacity of a cellular CDMA system". *IEEE Transactions on Vehicular Technology*, Vol 40(2):pp303–12, May 1991.

[39] A.J. Viterbi. "The orthogonal–random waveform dichotomy for digital mobile communication". *IEEE Personal Communications Magazine*, Vol 1(1):pp18–24, First Quarter 1994.

[40] D.V. Sarwate and M.B. Pursley. "Crosscorrelation properties of pseudorandom and related sequences". *Proceedings of the IEEE*, Vol 68(No 5):pp 593–619, May 1980.

[41] F.J. MacWilliams and N.J.A. Sloane. "Pseudo–random sequences and arrays". *Proceedings of the IEEE*, Vol 64(12):pp1715–29, December 1976.

[42] R. Gold. "Optimal binary sequences for spread spectrum multiplexing". *IEEE Transactions on Information Theory*, Vol 13:pp619–621, October 1967.

[43] J.G. Proakis. *"Digital Communications"*. McGraw-Hill, 1989.

[44] S. Verdu. "Adaptive multiuser detection". In *Proceedings of the 3rd IEEE International Symposium on Spread Spectrum Techniques and Applications (ISSSTA), Oulu (Finland)*, pages 43–50, July 1994.

[45] R.S. Mowbray and P.M. Grant. "Wideband coding for uncoordinated multiple access communications". *IEE Electronics and Communications Engineering Journal*, Vol 4(6):pp351–361, December 1992.

[46] R. Kohno. "Spatial and temporal filtering for co–channel interference in CDMA". In *Proceedings of the 3rd IEEE International Symposium on Spread Spectrum Techniques and Applications (ISSSTA), Oulu (Finland)*, pages 51–60, July 1994.

[47] A.J. Viterbi. "Error–correcting coding for CDMA systems". In *Proceedings of the 3rd IEEE International Symposium on Spread Spectrum Techniques and Applications (ISSSTA), Oulu (Finland)*, pages 22–6, July 1994.

[48] G.K. Chan. "Effects of sectorisation on the spectrum efficiency of cellular radio systems". *IEEE Transactions on Vehicular Technology*, Vol 41(3):pp217–25, August 1992.

[49] R. Padovani. "Reverse link performance of IS–95 based cellular systems". *IEEE Personal Communications Magazine*, Vol 1(3):pp28–34, Third Quarter 1994.

[50] D.P. Whipple. "North American cellular CDMA". *Hewlett–Packard Journal*, pages 90–7, December 1993.

[51] S. Haykin, J.P. Reilly, V. Kezys, and E. Vertatschitsch. "Some aspects of array signal processing". *IEE Proceedings Part F*, Vol 139(1):pp1–26, February 1992.

[52] D.H. Brandwood. "A complex gradient operator and its application in adaptive array theory". *IEE Proceedings Part F*, Vol 130(1):pp11–16, Feb 1983.

[53] R.O. Schmidt. "Multiple emitter location and signal parameter estimation". *IEEE Transactions on Antennas and Propagation*, Vol 34(3):pp276–280, March 1986.

[54] B.D. Van Veen and K.M. Buckley. "Beamforming: A versatile approach to spatial filtering". *IEEE ASSP Magazine*, pages 4–24, April 1988.

[55] R. Monzingo and T. Miller. *"Introduction to Adaptive Arrays"*. Wiley and Sons (New York), 1980.

[56] J.E. Hudson. *"Adaptive Array Principles"*. Peter Peregrinus (Stevenage), 1981.

[57] O.L. Frost. "An algorithm for linearly constrained adaptive beamforming". *Proceedings of the IEEE*, Vol 60(8):pp926–35, August 1972.

[58] B. Widrow, K.M. Duvall, R.P. Gooch, and W.C. Newman. "Signal cancellation phenomena in adaptible antennas: Causes and cures". *IEEE Transactions on Antennas and Propagation*, Vol 30(5):pp469–78, May 1982.

[59] T. Shan, M. Wax, and T. Kailath. "On spatial smoothing for direction-of-arrival estimation of coherent signals". *IEEE Transactions on Acoustics, Speech and Signal Processing*, Vol 33(4):pp806–811, August 1985.

[60] S. Haykin. *"Adaptive Filter Theory"*. Prentice–Hall, Englewood Cliffs, 1991.

[61] S.C. Swales and M.A. Beach. "Direction finding in the cellular land mobile radio environment". In *Proceedings of the IEE 5th International Conference on Radio Receivers and Associated Systems (RRAS90) University of Cambridge (UK)*, pages 192–6, July 1990.

[62] W.C.Y. Lee. "Applying the intelligent cell concept to PCS". *IEEE Transactions on Vehicular Technology*, Vol 43(3):pp672–9, August 1994.

[63] S. Anderson, M. Millnert, M. Viberg, and B. Wahlberg. "An adaptive array for mobile communications systems". *IEEE Transactions on Vehicular Technology*, Vol 40(1):pp230–6, February 1991.

[64] M. Nagatsuka, N. Ishii, R. Kohno, and H. Imai. "Adaptive array antenna based on spatial spectrum estimation using maximum entropy method". *IEICE Transactions on Communications*, Vol E77-B(5):pp624–33, May 1994.

[65] S. Simanapalli. "Adaptive array methods for mobile communication". In *Proceedings of IEEE Vehicular Technology Conference (VTC), Stockholm (Sweden)*, pages 1503–6, June 1994.

[66] I. Chiba, T. Takahashi, and Y. Karasawa. "Transmitting null beamforming with beam space adaptive array antennas". In *Proceedings of IEEE Vehicular Technology Conference (VTC), Stockholm (Sweden)*, pages 1498–1502, June 1994.

[67] P. Zetterberg and B. Ottersten. "The spectral efficiency of a basestation antenna array system for spatially selective transmission". In *Proceedings of the IEEE Vehicular Technology Conference (VTC), Stockholm (Sweden)*, pages 1517–21, June 1994.

[68] R.T. Compton. "An adaptive array for a spread spectrum system". *Proceedings of the IEEE*, Vol 66(3):pp289–98, March 1978.

[69] J.H. Winters. "Spread spectrum in a four–phase communication system employing adaptive antennas". *IEEE Transactions on Communications*, Vol 30(5):pp929–36, May 1982.

[70] P.S. Henry and B.S. Glance. "A new approach to high–capacity digital mobile radio". *The Bell System Technical Journal*, Vol 60(8):pp1891–1904, October 1981.

[71] J.H. Winters, J. Salz, and R.D. Gitlin. "The impact of antenna diversity on the capacity of wireless communication systems". *IEEE Transactions on Communications*, Vol 42(2/3/4):pp1740–50, February/March/April 1994.

[72] R. Kohno, H. Imai, M. Hatori, and S. Pasupathy. "Combination of an adaptive array antenna and a canceller of interference for direct–sequence spread–spectrum multiple–access system". *IEEE Journal on Selected Areas in Communications*, Vol 8(4):pp675–81, May 1990.

[73] C.P. Tou. "A spread spectrum system with an adaptive array for combatting interference". In *Proceedings of the IEEE International Symposium on Electromagnetic Compatibility, Seattle (USA)*, pages 164–7, August 1988.

[74] T.C. Liu. "The modular covariance adjustment adaptive array for CDMA wireless communications". In *Proceedings of the IEEE International Conference on Acoustics, Speech and Signal Processing (ICASSP), Minneapolis (USA)*, pages IV 180–3, April 1993.

[75] M.A. Jones and M.A. Wickert. "Interference nulling in direct-sequence spread-spectrum systems using a main-beam reference in the delay space". In *Proceedings of IEEE MILCOM '92, San Diego (USA)*, pages 468–72, October 1992.

[76] M. Wells. "Adaptive antennas for frequency resue in every cell of a GSM network". In *IEE Colloquium on mobile communications towards the year 2000, Digest 1994/188*, 1994.

[77] J. Fernandez, I.R. Corden, and M. Barrett. "Adaptive array algorithms for optimal combining in digital mobile communications systems". In *IEE 8th International Conference on Antennas and Propagation (ICAP), Edinburgh (UK)*, pages 983–6, March 1993.

[78] S.A. Hanna, M.S. El-Tanany, S.A. Mahmoud, and S.R. Todd. "Applications of adaptive antenna combining to digital radio communications within buildings". In *Proceedings of IEEE Canadian International Conference on Selected Topics in Wireless Communications, Vancouver (Canada)*, pages 107–10, June 1992.

[79] S Nam, I.D. Robertson, and A.H. Aghvami. "RF system design with optimum combining diversity using sectored antennas for high bit rate indoor radio communications systems". In *IEE Colloquium on Smart Antennas, Digest 1994/182*, December 1994.

[80] M. Barrett and R. Arnott. "Adaptive antennas for mobile communications". *IEE Electronics and Communication Engineering Journal*, Vol 5(4):pp203–14, August 1994.

[81] M.A. Beach, P. Guemas, and A.R. Nix. "Capacity and service extension for wireless networks using adaptive antennas". *Electronics Letters*, Vol 20(22):pp1813–4, October 1994.

[82] R.G. Petroit and D.R. Ucci. "A LMS and RLS look-ahead adaptive array for spread spectrum signals". In *Proceedings of IEEE International Symposium Digest - Antennas and Propagation, Dallas (USA)*, pages 1442–5, May 1990.

[83] D. Gerlach. "Base station antenna receivers in cellular CDMA". In *Proceedings of IEEE 26th ASIMOLAR Conference on Circuits, Signals and Computers, Pacific Grove (USA)*, pages 646–50, October 1992.

[84] G.V. Tsoulos, M.A. Beach, and S.C. Swales. "Application of adaptive antenna technology to third generation mixed cell architectures". In *Proceedings of IEEE Vehicular Technology Conference (VTC), Stockholm (Sweden)*, pages 615–9, June 1994.

[85] G.V. Tsoulos, M.A. Beach, and S.C. Swales. "Adaptive antennas for third generation DS-CDMA cellular systems. In *IEE Colloquium on Smart Antennas, Digest 1994/182*, pages 1/1–1/5, December 1994.

[86] J.M. Khalab and M.K. Ibrahim. "Novel multirate adaptive beamforming technique". *Electronics Letters*, Vol 30(15):pp1194–5, July 1994.

[87] D. Godard. "Self–recovering equalisation and carrier–tracking in two–dimensional data communications systems". *IEEE Transactions on Communications*, Vol 28(11):pp1867–75, November 1980.

[88] T. Ohgane, T. Shimura, N. Matsuzawa, and H. Sasaoka. "An implementation of a CMA adaptive array for high speed GMSK transmission in mobile communications". *IEEE Transactions on Vehicular Technology*, Vol 42(3):pp282–8, August 1992.

[89] T. Ohgane, N. Matsuzawa, T. Shimura, M. Mizuno, and H. Sasaoka. "BER performance of CMA adaptive array for high–speed GMSK mobile communication – a description of measurements in Tokyo". *IEEE Transactions on Vehicular Technology*, Vol 42(4):pp484–90, November 1992.

[90] A.V. Keerthi, A. Mathur, and J.J. Shynk. "Direction finding performance of the multistage CM array". In *Proceedings of IEEE 28th ASIMOLAR Conference on Circuits, Signals and Computers, Pacific Grove (USA)*, pages 847–52, November 1994.

[91] L. Tong, G. Xu, and T. Kailath. "Fast blind equalisation via antenna arrays". In *Proceedings of the IEEE International Conference on Acoustics, Speech and Signal Processing (ICASSP), Minneapolis (USA)*, pages IV 272–5, April 1993.

[92] E. Moulines, P. Duchamel, J.F. Cardoso, and S. Mayrargue. "Subspace methods for the blind identification of multichannel FIR filters". *IEEE Transactions on Signal Processing*, Vol 43(2):pp516–25, February 1995.

[93] J.F. Cardoso. "Blind identification of independent components with higher order statistics". In *Proceedings of the IEEE Workshop on Higher Order Spectral Analysis, Vail*, pages 157–62, 1989.

[94] J.F. Cardoso. "Eigen–structure of the fourth order cumulant tensor with application to the blind source separation problem". In *Proceedings of the IEEE International Conference on Acoustics, Speech and Signal Processing (ICASSP), Albuquerque (USA)*, pages 2655–8, 1990.

[95] P. Comon. "Higher–order separation: Application to detection and localisation". In *Proceedings of EURASIP 5th European Signal Processing Conference (EUSIPCO)*, pages 277–80, 1990.

[96] W.A. Gardner, S.V. Schell, and P.A. Murphy. "Multiplication of cellular radio capacity by blind adaptive spatial filtering". In *Proceedings of IEEE Canadian International Conference on Selected Topics in Wireless Communications, Vancouver (Canada)*, pages 102–6, June 1992.

[97] S.V. Schell. "An overview of sensor array processing for cyclostationary signals". In W.A. Gardner, editor, *"Cyclostationarity in Communications and Signal Processing"*, chapter 3, pages 168–239. IEEE Press, 1994.

[98] S.V. Schell, W.A. Gardner, and J. Schenck. "Adaptive spatial filtering for co-channel interference rejection in narrowband digital cellular systems". In *Proceedings of IEEE 28th ASIMOLAR Conference on Circuits, Signals and Computers, Pacific Grove (USA)*, pages 1149–53, November 1994.

[99] B. Suard, A.F. Naguib, G. Xu, and A. Paulraj. "Performance of CDMA mobile communication systems using antenna arrays". In *Proceedings of the IEEE International Conference on Acoustics, Speech and Signal Processing (ICASSP) Minneapolis (USA)*, pages IV 153–6, April 1993.

[100] A.F. Naguib and A. Paulraj. "Performance of CDMA cellular networks with base-station antenna arrays". In *International Zurich Seminar on Digital Communications*, 1994.

[101] P. Stoica and K.C. Sharman. "Maximum likelihood methods of direction-of-arrival estimation". *IEEE Transactions on Acoustics,Speech and Signal Processing*, Vol 38(7):pp1132–1143, July 1990.

[102] M. Wax and T. Kailath. "Detection of signals by information theoretic criteria". *IEEE Transactions on Acoustics, Speech and Signal Processing*, Vol 33(2):pp387–92, April 1985.

[103] K.M. Wong, Q.T. Zhang, J.P. Reilly, and P.C.Yip. "On information theoretic criteria for determining the number of signals in high resolution array processing". *IEEE Transactions on Acoustics, Speech and Signal Processing*, Vol 38(11):pp1959–74, November 1990.

[104] Q. Wu and D.R. Fuhrmann. "A parametric method for determining the number of signals in narrow–band direction finding". *IEEE Transactions on Signal Processing*, Vol 39(8):pp1848–57, August 1991.

[105] Q.T. Zhang and K.M. Wong. "Information theoretic criteria for the determination of the number of signals in spatially correlated noise". *IEEE Transactions on Signal Processing*, Vol 41(4):pp1652–63, April 1993.

[106] M. Wax and I. Ziskind. "Detection of the number of coherent signals by the MDL principle". *IEEE Transactions on Acoustics, Speech and Signal Processing*, Vol 37(8):pp1190–6, August 1989.

[107] R.J. Muirhead. *"Aspects of Multivariate Statistical Theory"*. Wiley, New York, 1982.

[108] Q.T. Zhang, K.W. Wong, P.C.Yip, and J.P. Reilly. "Statistical analysis of the performance of information theoretic criteria in the detection of the number of signals in array processing". *IEEE Transactions on Acoustics, Speech and Signal Processing*, Vol 37(10):pp1557–1566, October 1989.

[109] S.U. Pillai and H.K. Byung. "Performance analysis of MUSIC-type high-resolution estimators for direction finding in correlated and coherent sources". *IEEE Transactions on Acoustics, Speech and Signal Processing*, Vol 37(8):pp1176–1189, August 1989.

[110] R.T. Williams, S. Prasad, A.K. Mahalanabis, and L.H. Sibul. "An improved spatial smoothing technique for bearing estimation in a multipath environment". *IEEE Transactions on Acoustics, Speech and Signal Processing*, Vol 36(4):pp425–431, April 1988.

[111] T. Shan, A. Paulraj, and T. Kailath. "On smoothed rank profile tests in eigenstructure methods for directions-of-arrival estimation". *IEEE Transactions on Acoustics, Speech and Signal Processing*, Vol 35(10):pp1377–1385, October 1987.

[112] A.J. Weiss and B.Friedlander. "Performance analysis of spatial smoothing with interpolated arrays". *IEEE Transactions on Signal Processing*, Vol 41(5):pp1881–92, May 1993.

[113] A. Polydoros and C.L. Weber. "A unified approach to serial search spread–spectrum code acquisition - Part I: General theory". *IEEE Transactions on Communications*, Vol 32(5):pp542–9, May 1984.

[114] S.S. Rappaport and D.M. Grieco. "Spread spectrum acquisition: Methods and technology". *IEEE Communications Magazine*, Vol 22(6):pp7–21, June 1984.

[115] A. Polydoros and S. Glisic. "Code synchronisation: A review of principles and techniques". *Proceedings of the 3rd IEEE International Symposium on Spread Spectrum Techniques and Applications (ISSSTA), Oulu (Finland)*, pages 115–37, July 1994.

[116] P.M. Hopkins. "A unified analysis of pseudonoise synchronisation by envelope correlation". *IEEE Transactions on Communications*, Vol 25(8):pp770–8, August 1977.

[117] L.E. Brennan and I.S. Reed. "An adaptive array signal processing algorithm for communications". *IEEE Transactions Aerospace and Electronic Systems*, Vol 18(1):pp124–30, January 1982.

[118] D.M. Dlugos and R.A. Scholtz. "Acquisition of spread spectrum signals by an adaptive array". *IEEE Transactions on Acoustics, Speech and Signal Processing*, Vol 37(8):pp1253–70, August 1989.

[119] D.H. Johnson. "The application of spectral estimation methods to bearing estimation problems". *Proceedings of the IEEE*, Vol 70(9):pp1018–1028, September 1982.

[120] J. Capon. "High–resolution frequency–wavenumber spectrum analysis". *Proceedings of the IEEE*, Vol 57(8):pp1408–18, August 1969.

[121] R. Kumaresan and D.W. Tufts. "Estimation of arrival of multiple plane waves". *IEEE Transactions Aerospace and Electronic Systems*, Vol 19(1):pp123–33, January 1983.

[122] R. Roy, A. Paulraj, and T. Kailath. "ESPRIT - A subspace rotation approach to estimation of parameters of cisoids in noise". *IEEE Transactions on Acoustics, Speech and Signal Processing*, Vol 34(5):pp1340–1342, October 1986.

[123] M. Viberg and B. Ottersten. "Sensor array processing based on subspace fitting". *IEEE Transactions on Signal Processing*, Vol 39(5):pp1110–20, May 1991.

[124] B. Porat and B. Friedlander. "Direction finding algorithms based on higher-order statistics". *IEEE Transactions on Signal Processing*, Vol 39(9):pp2016–2023, September 1991.

[125] P. Forster and C.L. Nikias. "Bearing estimation in the bispectrum domain". *IEEE Transactions on Signal Processing*, Vol 38(9):pp1994–2006, September 1991.

[126] P.M. Grant, C.F.N. Cowan, B. Mulgrew, and J. Dripps. *"Analogue and Digital Signal Processing and Coding"*. Chartwell–Bratt, 1989.

[127] I. Ziskind and M. Wax. "Maximum likelihood localisation of multiple sources by alternating projection". *IEEE Transactions on Acoustics,Speech and Signal Processing*, Vol 36(10):pp1553–60, October 1988.

[128] M. Kaveh and A.J. Barabell. "The statistical performance of the music and the minimum-norm algorithms in resolving plane waves in noise". *IEEE Transactions on Acoustics,Speech and Signal Processing*, Vol 34(2):pp331–340, April 1986.

[129] D.J. Jeffries and D.R. Farrier. "Asymptotic results for eigenvector methods". *IEE Proceedings Part F*, Vol 132(7):pp589–94, December 1986.

[130] B.D. Rao and K.V.S. Hari. "Performance analysis of root–MUSIC". *IEEE Transactions on Acoustics,Speech and Signal Processing*, Vol 37(12):pp1939–49, December 1989.

[131] B. Porat and B. Friedlander. "Analysis of the asymptotic relative efficiency of the MUSIC algorithm". *IEEE Transactions on Acoustics,Speech and Signal Processing*, Vol 36(4):pp532–543, April 1988.

[132] P. Stoica and A. Nehorai. "MUSIC,maximum likelihood, and Cramer-Rao bound". *IEEE Transactions on Acoustics,Speech and Signal Processing*, Vol 37(5):pp720–741, May 1989.

[133] M. Wax and J. Sheinvald. "Direction finding of coherent signals via spatial smoothing for uniform circular arrays". *IEEE Transactions on Antennas and Propagation*, Vol 42(5):pp613–20, May 1994.

[134] R. Eiges and H.D. Griffiths. "Mode–space spatial spectral estimation for circular arrays". *IEE Proceedings Part F*, Vol 141(6):pp300–6, December 1994.

[135] J.S. Thompson, P.M. Grant, and B. Mulgrew. "Correspondence: Generalised algorithm for DOA estimation in a passive sonar". *IEE Proceedings Part-F*, Vol 140(5):pp339–340, October 1993.

[136] S.U. Pillai and H.K. Byung. "Forward/backward spatial smoothing techniques for coherent signal identification". *IEEE Transactions on Acoustics, Speech and Signal Processing*, Vol 37(1):pp8–14, January 1989.

[137] L. Chang and C. Yeh. "Resolution threshold for coherent sources using smoothed eigenstructure methods". *IEE Proceedings Part F*, Vol 138(5):pp470–478, October 1991.

[138] B.D. Rao and K.V.S. Hari. "Effect of spatial smoothing on the performance of MUSIC and the minimum norm method". *IEE Proceedings Part F*, Vol 137(6):pp449–458, December 1990.

[139] V.U. Reddy, A. Paulraj, and T. Kailath. "Performance analysis of the optimum beamformer in the presence of correlated sources and its behaviour under spatial smoothing". *IEEE Transactions on Acoustics, Speech and Signal Processing*, Vol ASSP-35(7):pp927–936, July 1987.

[140] W. Du and R.L. Kirlin. "Improved spatial smoothing techniques for DOA estimation of coherent signals". *IEEE Transactions on Signal Processing*, Vol 39(5):pp1208–10, May 1991.

[141] J. Li. "Improved angular resolution for spatial smoothing techniques". *IEEE Transactions on Signal Processing*, Vol 40(12):pp3078–81, December 1992.

[142] A. Moghaddamjoo. "Application of spatial filters to DOA estimation of coherent sources". *IEEE Transactions on Signal Processing*, Vol 39(1):pp222–4, January 1991.

[143] Y. Zhou and P. Yip. "The steered pattern averaging technique (SPAT) for direction finding in a multiple coherent signal environment". *Proceedings of the IEEE International Conference on Acoustics, Speech and Signal Processing (ICASSP), San Fransisco (USA)*, pages 586–90, 1992.

[144] R. Rajagopal and P.R. Rao. "Generalised algorithm for DOA estimation in a passive sonar". *IEE Proceedings Part F*, Vol 140(1):pp12–20, February 1993.

[145] S. Haykin. "*Digital Communications*". John Wiley (New York), 1988.

[146] J.S. Thompson, P.M. Grant, and B. Mulgrew. "Diversity receiver improvements for spread spectrum". In *Proceedings of the 3rd IEEE International Symposium on Spread Spectrum Techniques and Applications (ISSSTA), Oulu (Finland)*, pages 455–9, July 1994.

[147] D. Rogers and B. Davis. "Code properties: Influences on the peformance of a quaternary CDMA system". In *Proceedings of the 3rd IEEE International Symposium on Spread Spectrum Techniques and Applications (ISSSTA), Oulu (Finland)*, pages 494–99, July 1994.

[148] C.K. Chan and W.L. Lam. "A simplified aperiodic cross–correlation model for direct–sequence spread–spectrum multiple–access communication systems". In *Proceedings of the IEEE International Conference on Communications (ICC), New Orleans (USA)*, pages 1516–20, May 1994.

[149] R.G. Vaughan. "On optimum combining at the mobile". *IEEE Transactions on Vehicular Technology*, Vol 37(4):pp181–8, November 1988.

[150] P. Newson. "An analysis of the effects of power control error on CDMA systems". In *Proceedings of the IEEE Globecom Conference, Houston (USA)*, pages 924–8, December 1993.

[151] J.B. Andersen, T.S. Rappaport, and S. Yoshida. "Propagation measurements and models for wireless communication channels". *IEEE Communications Magazine*, Vol 33(1):pp42–49, January 1995.

[152] J.D. Parsons. *"The Mobile Radio Propagation Channel"*. Pentech Press, 1992.

[153] W.C.Y. Lee. *"Mobile Communications Engineering"*, chapter 6. McGraw–Hill, 1982.

[154] R Steele (ed). *"Mobile Radio Communications"*. Pentech Press, London, 1992.

[155] R.C. French. "The effects of fading and shadowing on channel reuse in mobile radio". *IEEE Transactions on Vehicular Technology*, Vol 28(3):pp171–181, August 1979.

[156] G.R. Cooper and C.D. McGillem. *"Probabilistic Methods of Signal and System Analysis"*. CBS Publishing, Japan, 1986.

[157] P.A. Bello. "Characterisation of randomly time–variant linear channels". *IEEE Transactions on Circuits and Systems*, Vol 11(4):pp360–393, December 1963.

[158] G.L. Turin, F.D. Clapp, T.L. Johnston, S.B. Fine, and D. Lavry. "A statistical model of urban multipath propagation". *IEEE Transactions on Vehicular Technology*, Vol 21(1):pp1–9, February 1972.

[159] R.H. Clarke. "A statistical theory of mobile–radio reception". *Bell System Technical Journal*, Vol 47(6):pp957–1000, July-August 1968.

[160] T. Aulin. "A modified model for the fading signal at a mobile radio channel". *IEEE Transactions on Vehicular Technology*, Vol 28(3):pp182–203, 1979.

[161] G.J.R. Povey. *"Spread Spectrum Receiver Architectures for Mobile Channels subject to Multipath Fading"*. PhD thesis, Edinburgh University, 1992.

[162] D.I. Laurenson, D.G.M. Cruickshank, and G.J.R. Povey. "A computationally efficient channel simulator for the COST–207 channel models". In *IEE Colloquium on Computer Modelling of Communication Systems, Digest 1994/115*, May 1994.

[163] Commission of the European Communities. *"Digital Land Mobile Radio Communications: COST–207 Final Report"*, chapter 2. 1988.

[164] G. Xu, H. Liu, W.J. Vogel, H.P. Lin, S.S. Jeng, and G.W. Torrence. "Experimental studies of space-division multiple access schemes for spectral efficient wireless communications". In *Proceedings of the IEEE International Conference on Communications (ICC), New Orleans (USA)*, pages pp800–4, May 1994.

[165] G. Raleigh, S.N. Diggavi, A.F. Naguib, and A. Paulraj. "Characterisation of fast fading vector channels for multi–antenna communications systems". In *Proceedings of the 28th IEEE ASIMOLAR Conference, Pacific Grove (USA)*, pages 853–7, November 1994.

[166] J.H. Winters. "The diversity gain of transmit diversity in wireless systems with Rayleigh fading". In *Proceedings of the IEEE International Conference on Communications (ICC), New Orleans (USA)*, pages 1121–5, May 1994.

[167] H. Iwai and Y. Karasawa. "A CDMA mobile radio station antenna system robust for multipath fading". In *Proceedings of the IEEE 2nd International Symposium on Spread Spectrum Techniques and Applications (ISSSTA) Yokohama (Japan)*, pages 357–60, November-December 1992.

[168] A.J. Viterbi and R. Padovani. "Implications of mobile cellular CDMA". *IEEE Communications Magazine*, Vol 30(12):pp38–41, December 1992.

[169] V. Weerackody. "Diversity for the direct sequence spread spectrum system using multiple transmit antennas". In *Proceedings of the IEEE International Conference on Acoustics, Speech and Signal Processing (ICASSP), Minneapolis (USA)*, pages 1775–9, April 1993.

[170] W.C.Y. Lee. "Effects on correlation between two mobile radio base–station antennas". *IEEE Transactions on Communications*, Vol 21(11):pp1214–23, November 1973.

[171] F. Adachi, M.T. Sweeney, A.G. Williamson, and J.D. Parsons. "Correlation between the envelopes of 900 MHz signals received at a mobile radio base station site". *IEE Proceedings Part F*, Vol 133(6):pp506–12, October 1986.

[172] J. Salz and J.H. Winters. "Effect of fading correlation on adaptive arrays in digital wireless communications". In *Proceedings of IEEE International Conference on Communications (ICC), Geneva (Switzerland)*, pages 1768–74, May 1993.

[173] P. Zetterberg. "Mobile communication with base station antenna arrays: Propagation modelling and system capacity". Master's thesis, Royal Institute of Technology, Stockholm (Sweden), January 1995.

[174] M. Nakagami. "The m-distribution, a general formula of intensity of rapid fading". In W.G. Hoffman, editor, *Statistical Methods in Radio Wave Propagation: Proceedings of a Symposium held at the University of California*, pages 3–36. Pergamon Press, 1960.

[175] D.G. Brennan. "Linear diversity combining techniques". *Proceedings of the IRE*, pages 1075–1102, June 1959.

[176] C. Farsakh and J.A. Nossek. "Application of space division multiple access to mobile radio". In *Proceedings of the 5th IEEE International Symposium on Personal Indoor and Mobile Communications (PIMRC), The Hague (Holland)*, pages 1736–9, September 1994.

[177] D. Gerlach and A. Paulraj. "Adaptive transmitting antenna arrays with feedback". *IEEE Signal Processing Letters*, Vol 1(10):pp150–2, October 1994.

[178] G.J.R. Povey. "Capacity of a cellular time division duplex CDMA system". *IEE Proceedings Part I*, Vol 141(5):pp351–6, October 1994.

[179] R. Keen. "*Wireless Direction Finding*". Iliffe and Sons, London, third edition, 1941.

[180] P.J.D. Gething. "*Radio Direction Finding*". Peter Peregrinus, Stevenage, 1978.

[181] H. Staras and S.N. Honickman. "The accuracy of vehicle location by trilateration in a dense urban environment". *IEEE Transactions on Vehicular Technology*, Vol 21(1):pp38–43, February 1972.

[182] H. Song. "Automatic vehicle location in cellular communications systems". *IEEE Transactions on Vehicular Technology*, Vol 43(4):pp902–8, November 1994.

[183] K.A Struckman. "Radio location through high resolution eigenstructure processing techniques that yield accurate multipath AOA and differential time delay estimates". In *Proceedings of the IEEE National Telesystems Conference, Washington DC (USA)*, pages 3.9–3.12, May 1992.

[184] M. Hamilton and P.M. Schultheiss. "Passive ranging in multipath dominant environments, Part I: Known multipath parameters". *IEEE Transactions on Signal Processing*, Vol 40(1):pp1–12, January 1992.

[185] R.L. Johnson, Q.R. Black, and A.G. Sonsteby. "HF multipath passive single site radio location". *IEEE Transactions on Aerospace and Electronic Systems*, Vol 30(2):pp462–70, April 1994.

[186] Bajwa A.S. "UHF wideband statistical model and simulation of mobile radio multipath propagation effects". *IEE Proceedings Part F*, Vol 132(4):pp327–333, August 1985.

[187] J.B. Frayleigh. *"Calculus with Analytic Geometry"*. Addison-Wesley, New York, second edition, 1985.

[188] M. Wax, T. Shan, and T. Kailath. "Spatio-temporal spectral analysis by eigenstructure methods". *IEEE Transactions on Acoustics, Speech and Signal Processing*, Vol 32(4):pp817–27, August 1984.

[189] M. Pallas and G. Jourdain. "Active high resolution time delay estimation for large BT signals". *IEEE Transactions on Signal Processing*, Vol 39(4):pp781–7, April 1991.

[190] T. Manabe and H. Takai. "Superresolution of multipath delay profiles measured by PN–correlation method". *IEEE Transactions on Antennas and Propagation*, Vol 40(5):pp500–9, May 1992.

[191] J.A. Wepman. "Analog–to–digital converters and their application in radio receivers". *IEEE Communications Magazine*, Vol 33(5):pp39–45, May 1995.

[192] J. Mitola. "The software radio architecture". *IEEE Communications Magazine*, Vol 33(5):pp26–38, May 1995.

Appendix A

Original Publications

The author of this thesis has the following publications:

- J. S. Thompson, G. J. R. Povey, P. M. Grant; "*Real-Time Communications Multipath Compensation*", Electronics Letters, 28, No 23, pp2131-2133, 5 November 1992.
- G. J. R. Povey, J. S. Thompson, R. D. Pringle, P. M. Grant; "*Adaptive Spread Spectrum Receiver for Mobile Communications*", IEE DSP in Communications Colloquium, Digest 1993/064, pp5.1-5.5, March 1993.
- † J. S. Thompson, P. M. Grant, B. Mulgrew. "*Generalised Algorithm for DoA estimation in Passive Sonar*", IEE Proceedings, Part F (Correspondence), Vol 140, No 5, pp339-340, October 1993.
- † J. S. Thompson, P. M. Grant, B. Mulgrew. "*Receiver Diversity Spread Spectrum*", IEE Colloquium on Spread Spectrum Techniques for Radio Communication Systems, Digest No 1994/098, pp2/1-2/4, 15 April 1994.
- † J. S. Thompson, B. Mulgrew, P. M. Grant."*Analysis of Diversity Reception Improvements in Spread Spectrum Receivers*", Proceedings IEEE 3rd International Symposium on Spread Spectrum Techniques and Applications, pp455-459, July 1994.
- † J. S. Thompson, B. Mulgrew, P. M. Grant. "*Bearing Estimation Techniques for Improved Reception of Spread Spectrum Signals*", Proceedings IEEE 3rd International Symposium on Spread Spectrum Techniques and Applications, pp544-548, July 1994.
- † J.S. Thompson, P.M. Grant and B. Mulgrew. "*Analysis of Spatial Smoothing Algorithms*", IEE Colloquium on High Resolution Spectral Estimation and Direction Finding, Digest No 1995/068, pp 6/1-6/6.
- † J. S. Thompson, P. M. Grant, B. Mulgrew."*Performance of Spatial Smoothing Algorithms for Correlated Sources*", IEEE Transactions on Signal Processing, To be published April 1996.

In Preparation:

- J. S. Thompson, P. M. Grant, B. Mulgrew."*Analysis of Spatial Smoothing and the Minimum Description Length Criterion*", IEE Proceedings Part F.

- J. S. Thompson, P. M. Grant, B. Mulgrew."*Smart Antenna Arrays for Cellular CDMA Systems*", IEEE Communications Magazine.

† Reprinted in this appendix.

Comments on "Generalised algorithm for DOA estimation in a passive sonar" [1]

Section 3.4 of the paper stated that the differential covariance matrix technique could be used to resolve P coherent sources, provided that array contained at least (P+1) sensor elements. Further investigation shows that the method is only capable of resolving two coherent sources.

We believe the original premise in your paper was inaccurate and it invalidates your subsequent analysis. The mathematical reason for our new conclusion is as follows: A simple model for the $N * 1$ signal vector x(t) received at time t from an N sensor array, when there are P signals impinging on it, is given by:

$$x(t) = A * s(t) + n(t) \tag{1}$$

The $N * P$ matrix A=[a(θ_1),a(θ_2),...,a(θ_P)] contains the steering vectors a(θ) for the P incoming signals. The $P * 1$ signal vector $s(t)=[X_1 e^{jw_1 t}, X_2 e^{jw_2 t}, \ldots, X_P e^{jw_P t}]^T$ contains the carriers generating the P signals and X_l is the amplitude of the l^{th} carrier. The $N * 1$ noise vector n(t) contains the white Gaussian noise samples of variance σ^2 which are added to each sensor.

In order to perform the bearing estimation algorithm MUSIC [2], the $N * N$ covariance matrix R of the data is required. This is formed by taking M "snapshots" of the data vector x(t). The i^{th} column and j^{th} row entry of R is formed as follows:

$$R_{ij} = \frac{1}{M} \sum_{m=1}^{M} x_i(m) * x_j^*(m) \tag{2}$$

Where $x_i(m)$ is the m^{th} sample from the i^{th} array sensor. Now the matrix R may be written as follows:

$$R = ASA^* + \sigma^2 I \tag{3}$$

where the $P * P$ matrix $S = E[s(t).s^*(t)]$ and I[1] is the $N * N$ identity matrix. Normally, the P signals are uncorrelated, such that $E[e^{jw_k t}.e^{jw_l t}] = 0$ for $k \neq l$. In this case, the rank of the matrix ASA^* is P and the eigenvalue decomposition of R yields P "signal" eigenvectors whose corresponding eigenvalues are greater than σ^2. These vectors are implicitly required by the MUSIC algorithm to locate the bearings of the P sources.

In the case where all P signals are coherent, then throughout all the snapshots of the array, there is a constant phase relationship between each of the signals and $E[e^{jw_k t}.e^{jw_l t}] \neq 0$ for $k \neq l$. This normally means that all P signals originate from the same transmitter and are multipaths. Therefore, the vector s(t) reduces to a single row[2] and $s(t) = [e^{jwt}]$. The matrix A then reduces to a $N * 1$ vector given by:

$$A = [X_1.a(\theta_1) + \mu_2 X_2.a(\theta_2) + \ldots + \mu_P X_P.a(\theta_P)] \tag{4}$$

Where μ_a is a complex constant indicating the phase relationship between the first signal and the a^{th} signal at the reference sensor. Thus, the matrix ASA^* reduces to rank 1 in accordance with the following equation [4]:

$$\text{rank}(ASA^*) \leq \min[\text{rank}(A), \text{rank}(S)] \tag{5}$$

For a linear array, all possible steering vectors a(θ) are of a Vandermonde form:

$$a(\theta) = [1 \; t(\theta) \; t^2(\theta) \; \ldots t^{N-1}(\theta)] \tag{6}$$

Where t() is an complex function of θ. Now it is well known that adding two (Vandermonde) steering vectors a(θ_1) and a(θ_2), with $\theta_1 \neq \theta_2$, cannot give another legitimate Vandermonde steering vector, a(θ_3). Hence, MUSIC will fail to resolve any of the K signals correctly. The differential technique forms a modified covariance matrix R_1 according to the equation:

$$R_1 = R - ER^*E = ASA^* - E(ASA^*)^*E \tag{7}$$

Where E is given by:

$$E = \begin{bmatrix} 0 & 0 & \ldots & 0 & 1 \\ 0 & 0 & \ldots & 1 & 0 \\ \vdots & \vdots & \ddots & \vdots & \\ 1 & 0 & \ldots & 0 & 0 \end{bmatrix} \tag{8}$$

Now, the rank of both ASA^* and $-E(ASA^*)^*E$ is 1. So, by the well known inequality [4]:

$$\text{rank}(C + D) \leq \text{rank}(C) + \text{rank}(D) \tag{9}$$

[1] The following proof holds for any noise covariance matrix that is of Toeplitz form.

[2] The idea of the reduction in rank of the matrix S is consistent with the proof of the Spatial Smoothing technique presented by Shan et al in 1985 [3]

It is impossible for the rank of R_1 to be greater than 2. Hence when MUSIC operates on the matrix R_1, it will only operate successfully if two coherent signals are present. The algorithm appears to operate in a similar fashion to forward-backward spatial smoothing [5] for 2 coherent sources. However, the latter method adds the two matrices, rather than subtracting one from another.

In a similar way, one can show that spatial smoothing algorithms require to average over at least P different coherent signal covariance matrices (each containing only one "signal eigenvector") to separate P coherent sources. For spatial smoothing this means losing the effect of at least (P-1) sensors and for forward/backward spatial smoothing , the integer part of (P-1)/2 sensors.

In figure 1, some typical simulation results are shown, comparing the performance of MUSIC, differential MUSIC and forward/backward spatial smoothing. The graphs in figure 1 a) are for two sources at 50^o and 60^o. The graphs in part b) show what happens when a third source at 70^o is added and those in c) display the effect of a fourth source at 83^o. These clearly show the necessity of using forward/backward spatial smoothing for resolving multiple coherent sources.

John S. Thompson, Peter M. Grant, Bernard Mulgrew.

REFERENCES

[1] RAJAGOPAL R., RAO P.R., "Generalised Algorithm for DOA Estimation in a passive sonar", IEE Proceedings Part F, February 1993, Vol. 140, No. 1, pp12-20.

[2] SCHMIDT R.O., "Multiple Emitter Location and Signal Parameter Estimation", IEEE Transactions on Antennas and Propagation, March 1986, Vol. AP-34, No.3, pp 276-280.

[3] SHAN T., WAX M., KAILATH T., "On Spatial Smoothing for Direction-of-Arrival Estimation of Coherent Signals", IEEE Transactions on Acoustics, Speech and Signal Processing, August 1985, Vol. ASSP-33, No.4, pp806-811.

[4] HORN R.A., JOHNSON C.R., "Matrix Analysis", Cambridge University Press 1985, p13.

[5] PILLAI S.U., KWON B.Y., "Forward/Backward Spatial Smoothing Techniques for Coherent Signal Identification", IEEE Transactions on Acoustics, Speech and Signal Processing, January 1989, Vol. 37, No. 1, pp8-15.

Figure 1:Resolving Coherent Sources with the MUSIC Algorithm.

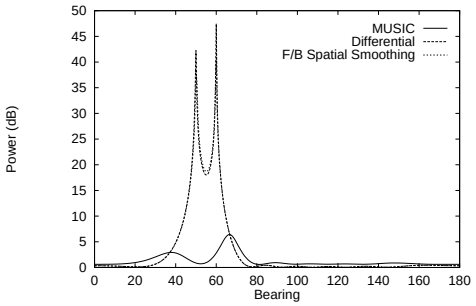

a) MUSIC,Differential MUSIC and F/B Spatial Smoothing for 2 sources.

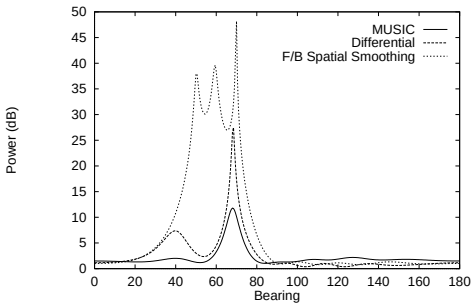

b) MUSIC,Differential MUSIC and F/B Spatial Smoothing for 3 sources.

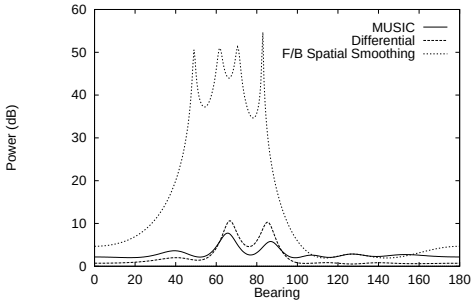

c) MUSIC,Differential MUSIC and F/B Spatial Smoothing for 4 sources.

Reply by Dr R. Rajagopal:

I agree with your observation with the following corrections:

1). The difference matrix is obtained as:

$$D = R - ER^*E = H - EH^*E \qquad (10)$$

Where H is the source cross-covariance matrix.

$$Rank(D) \leq Rank(H) + Rank(-EH^*E) = 2p \qquad (11)$$

It can be verified that rank(H) = rank(EH^*E) = p where p is the number of sources (subject to the condition that A consists of p linearly independent columns).

In my paper, I had given a proof in section 3.4 to show that Rank(D) = p by using the argument of contradiction. Unfortunately, I did not test that case by computer simulation. My simulations also confirm your above results and I regret the misleading claim in my original paper.

RECEIVER DIVERSITY FOR SPREAD SPECTRUM

John S. Thompson, Peter M. Grant, Bernard Mulgrew. [1]

Abstract One method to improve the capacity of a code division multiple access (CDMA) system is to use an array of receivers in the base station. In order for such a system to work, it must be able to locate the directions of arrival (DOA) of all the active users present within the cell. One of the most popular algorithms to perform this task is the MUSIC algorithm, which provides a compromise between good resolution and computational complexity. One problem present in the MUSIC algorithm is its inability to cope with correlated multipath signals: the spatial smoothing technique is shown to be a simple and effective method of overcoming this difficulty. The receiver can utilise the DOA information to exploit spatial diversity present within the cell and some simple BER results are given to illustrate the mean improvement in performance that is obtained.

Introduction In recent years, there has been great interest in the application of spread spectrum concepts to the field of mobile communications. Code division multiple access (CDMA) techniques have been established as a serious alternative to the time division multiple access systems that are being used in the current generation of mobile telephones [1]. However, one of the main limitations to the capacity of a conventional CDMA system is the cross-correlation interference that is generated by the different codes present on the same channel.

This paper proposes the use of array processing techniques in order to ameliorate the effect of this type of interference and increase the capacity of the system. If the number of receivers in the base station of a mobile telephone cell is increased, the base station is able to employ electronic steering to receive signals from a desired direction and to reduce interference from other users who transmit from different locations. A block diagram of the base station is shown in figure 1.

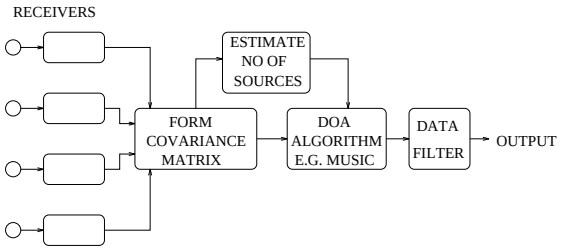

Figure 1: A cellular antenna-array base station.

There are two main components to this system: 1) to determine the directions of arrival (DOA) of all the desired users, 2) to employ a spatial filter to enhance the signal-to-noise ratio (SNR) of each user. This paper will look at each aspect of the system in turn.

DOA Estimation There are a large number of algorithms documented in the literature that are capable of determining the DOA of narrowband signals which are centred about a carrier frequency f [2]. It may seem counter-intuitive to consider a spread-spectrum system as a narrow-band signal, but in many proposed CDMA systems the data rates are low, which means that the ratio of the carrier frequency to the spread-spectrum baseband bandwidth is high.

The receivers sample the incoming signals simultaneously and pass them through the code-correlator for the desired code, so that for a code of length L, L time-samples are produced for each symbol that is received. If one considers a single CDMA signal impinging on the antenna array, the narrowband assumption means the output of each code-correlator will have the same amplitude, but a different phase according to the direction of arrival.

[1] Signals and Systems Group, Department of Electrical Engineering, The University of Edinburgh, Mayfield Road, Edinburgh, EH9 3JL.

In order to determine the direction of arrival successfully, the phase rotations across the whole array must be known for all possible bearings θ. Assume that the array contains N receivers spaced by half the carrier wavelength λ in a line - a uniform linear array (ULA). If the phase at sensor one is set to zero as a reference, the phase rotation along the ULA may be represented by a N row $\times$ 1 column vector $\underline{q}(\theta)$. For a ULA, $\underline{q}$ is given by:

$$\underline{q}(\theta) = [1, e^{j\pi \cos(\theta)}, \ldots, e^{j(N-1)\pi \cos(\theta)}]^T \tag{1}$$

In a realistic multipath environment the base station can resolve up to L different multipath signals in time, each of which are considered separately by the DOA algorithm. One set of samples $\{y(n,l,t)\}$ received from the code-correlators is termed a snapshot of the array, where n denotes the n^{th} receiver, l the l^{th} time sample and t the absolute time. It is assumed that the l^{th} time sample contains M multipaths. The snapshots of the array can be placed in a $N \times 1$ column vector $\underline{y}(l,t)$, which can be written as:

$$\underline{y}(l,t) = Q(l)\underline{s}(l,t) + \underline{n}(t) \tag{2}$$

Where $\underline{s}(l,t)$ is an $N \times 1$ column vector containing the M signals measured at the reference sensor and $Q(l)$ is an N row $\times$ M column matrix given by:

$$Q(l) = [\underline{q}(\theta_1), \underline{q}(\theta_1), \ldots, \underline{q}(\theta_M)] \tag{3}$$

Where θ_m is the bearing of the m^{th} signal. The $N \times 1$ vector $\underline{n}(t)$ contains the Gaussian white noise of variance σ^2 that corrupts the snapshot data. In order to perform bearing estimation, the data covariance matrix $R(l)$ must be formed from the snapshots. The matrix equation for $R(l)$ is given by:

$$R(l) = \frac{1}{K}\sum_{k=1}^{K} \underline{y}(l,t_k)\underline{y}^H(l,t_k) \tag{4}$$

where K denotes the number of snapshots used to form R, t_k denotes the time at which the k^{th} snapshot was taken and $\underline{x}^H$ denotes the complex conjugate transpose operation. Once the covariance matrix has been formed, it can be passed to a DOA algorithm. One of the most popular of these is the multiple signal classification (MUSIC) [3].

The MUSIC Algorithm If an eigenvalue decomposition (EVD) of the matrix $R(l)$ is performed, the eigenvalues and eigenvectors fall into two classes. The largest M eigenvalues and vectors correspond to the M signals and are collectively called the signal subspace. The eigenvectors span the columns of the matrix $Q(l)$. The other $N - M$ eigenvectors form the noise subspace and their eigenvalues are approximately equal to σ^2. Their only property of interest is that they are orthogonal to the signal eigenvectors and the steering vectors in $Q(l)$. MUSIC exploits this property to determine which bearings have the smallest projection on the noise subspace, indicating the presence of a desired signal. To generate the MUSIC power spectrum, the following equation is used:

$$P_{MUS}(l,\theta) = \frac{1}{q^H(\theta).W(l).W(l)^H.q(\theta)} \tag{5}$$

where $W(d)$ is an $N - M \times N$ matrix containing the $N - M$ noise eigenvectors. Before the MUSIC algorithm can be used, the number of signals present must be estimated. This is usually done with a model order algorithm [2]. A typical power spectrum generated by the MUSIC algorithm is shown in figure 2. There are two sources of power 20dB at bearings 85^o and 110^o - the desired bearings are shown as vertical dotted lines, a convention used throughout this paper.

Coherent Multipath Sources The MUSIC algorithm performs well when resolving signals that are uncorrelated or partially-correlated with each other. This usually implies that the signals originate from different transmitters. However, in the case where the signals arise due to multipath propagation from one transmitter, the MUSIC algorithm fails. This is because the multipaths are completely correlated and the EVD of the covariance matrix yields only one signal eigenvalue for all the multipaths.

The simplest method found to date to overcome this problem is spatial smoothing [4], but the original method only works in the case of the ULA. This technique forms covariance matrices from subsets of the ULA and averages these matrices to form

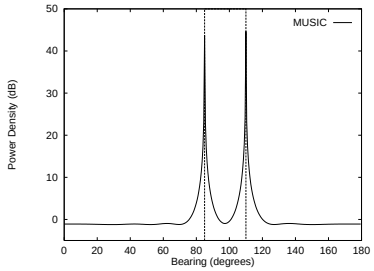

Figure 2: A typical power spectrum generated by the MUSIC algorithm.

a smaller matrix for the MUSIC algorithm. The algorithm forms submatrices by moving in one direction along the array to form sub-matrices - forward only spatial smoothing (FOSS). This technique clearly trades the size of the covariance matrix, and therefore the resolution of the MUSIC algorithm, for the ability to resolve coherent sources. In order to locate the bearings of M sources, a ULA containing $2M$ receivers is required.

The situation can be improved by forward-backward spatial smoothing (FBSS) [5], which forms matrices by working both forward and backward along the array.This technique means that only $(3M/2)$ sensors are required to resolve M coherent signals. However, there is a tradeoff: this improvement is obtained at a cost of reduced robustness in the MUSIC algorithm. The performance of the FBSS technique is known to be sensitive to the relative phases of the incoming signals - in some cases it destroys signal correlation completely, in others it can fail completely.

The performance of the two techniques is demonstrated in two graphs shown in figure 3. The ULA contains 8 receivers and for the left hand-graph, it is trying to resolve two coherent sources at bearings of 100^o and 115^o, both at an SNR of 20dB. The conventional MUSIC algorithm fails, but FOSS and FBSS both successfully resolve the two signals. For the right hand graph, another two sources at 90^o and 125^o have been added. In this case, FBSS is the only algorithm to find the four sources, while FOSS is only able clearly show two signals.

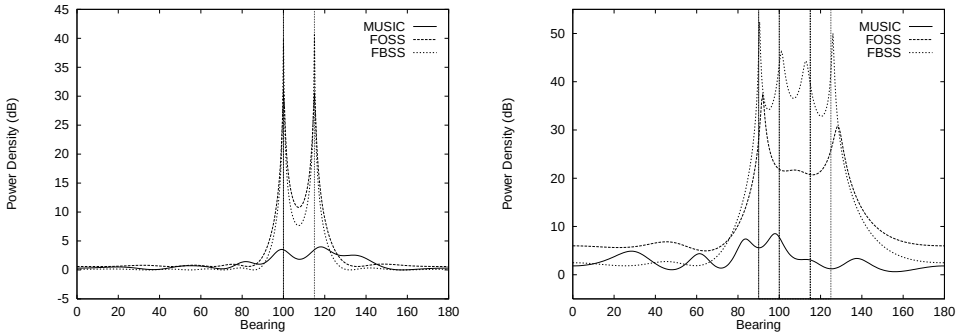

Figure 3: A comparison of smoothing techniques with coherent signals present

Spatial Filtering It is a well known result of filter theory that the optimum detector of any signal corrupted by Gaussian white noise is a matched-filter which correlates the input with the desired signal [6]. In the case of a single DS-SS signal which is detected in the l^{th} time sample and which has bearing θ, the optimum filter $\underline{w}(l)$ for the data $\underline{y}(l,t)$ is simply $\underline{w}(l) = \underline{q}(\theta)$. Once $\underline{w}(l)$ has been determined, it may be used to generate a complex-valued data sequence $\overline{d}(l,t)$ which is then utilised to make decisions on the data. The value $d(l,t)$ is generated by the equation:

$$d(l,t) = \underline{w}^H \underline{y}(l,t) \tag{6}$$

In a more general case, where several multipaths are present, the data $\{d(l,t)\}$ is passed to a RAKE filter, which combines them before making a decision.

In [7], there is a full description of some simulation work that was performed to determine the bit error rate (BER) of an antenna array with different numbers of receivers. The purpose of the simulations was to determine for a simple case the increase in capacity that was provided by an antenna array.

The simulation was performed for a CDMA system which employed a set of 33 length-31 Gold codes, so that the maximum capacity was 33 users. The simulation assumed that the bearing of the desired user was known and that each mobile had one line-of-sight path to the base station. Each other mobile was given a random bearing and the simulation was then performed for the reverse-path (i.e. from the mobiles to the base station). The results should also hold for the forward-path, from the base station to the mobiles, if the base station transmitter is an antenna array as well. The modulation scheme used was differential phase-shift keying (DPSK).

The table below displays the mean simulated BER for different sizes of the base station array at full capacity, i.e. 33 users.

Number of Array Receivers	BER
1	0.124
2	1.16×10^{-2}
4	6.55×10^{-4}
8	2.77×10^{-5}

It is generally assumed that a BER of 10^{-3} is acceptable for a vocoder speech encoding system and this is attained on average by a base station with four receivers. It should be pointed out, however, that that spatial filters are only useful when the desired signal has a different bearing to that of the interferers. In some circumstances this may not be true and the system performance will degrade, but the probability of this occurring may be reduced by increasing the array size.

Conclusion This paper has discussed the advantages of antenna arrays for use in the base stations of direct-sequence spread-spectrum CDMA systems. Bearing estimation techniques determine the angle of arrival of a source, which allows the receiver to reduce the effect of directional interference from other users. The BER results demonstrate the mean performance improvement due to these algorithms, which should increase the capacity of CDMA systems.

Acknowledgements The sponsorship of this work by a SERC studentship and MoD CASE support is gratefully acknowledged.

References

[1] Gilhousen K.S. et al, "On the capacity of a cellular CDMA system," *IEEE Transactions on Vehicular Technology*, Vol 40(2), pp303–311, May 1991.

[2] Haykin S., Reilly J.P., Kezys V., and Vertatschitsch E., "Some aspects of array processing," *IEE Proceedings Part F*, Vol 139(1), pp1–26, February 1992.

[3] Schmidt R.O., "Multiple emitter location and signal parameter estimation," *IEEE Transactions on Antennas and Propagation*, Vol AP-34(3), pp276–280, March 1986.

[4] Shan T., Wax M., and Kailath T., "On spatial smoothing for direction-of-arrival estimation of coherent signals," *IEEE Transactions on Acoustics, Speech and Signal Processing*, Vol ASSP-33(4), pp806–811, August 1985.

[5] Williams R.T., Prasad S., Mahalanabis A.K., and Sibul L.H., "An improved spatial smoothing technique for bearing estimation in a multipath environment," *IEEE Transactions on Acoustics, Speech and Signal Processing*, Vol 36(4), pp425–431, April 1988.

[6] Stremler F.G., "Introduction to Communications Systems," *Addison-Wesley*, 1990.

[7] Thompson J.S., Grant P.M., and Mulgrew B., "Analysis of Diversity Reception Improvements in Spread Spectrum Receivers," *Proceedings 3rd ISSSTA (Finland)*, July 1994.

Analysis of Diversity Reception Improvements in Spread Spectrum Receivers.

John S. Thompson, Bernard Mulgrew and
Peter M. Grant
Department of Electrical Engineering,
The University of Edinburgh,
Edinburgh,
Scotland. EH9 3JL

Abstract – This paper describes how bearing estimation techniques may be applied to a direct sequence spread spectrum (DS-SS) system in order to provide an effective spatial diversity receiver. This structure is proposed as a method of increasing the capacity of a cellular code division multiple access (CDMA) system.

Firstly, the subject of an optimum diversity system using bearing estimation is addressed. It is demonstrated that a N-element antenna diversity system improves the mean signal-to-noise ratio for a CDMA system in proportion to N, which can considerably improve bit error rate (BER) performance.

The operation of the receiver in a cellular telephone network is discussed and the improvement in user capacity provided by such a system with perfect power control is shown.

INTRODUCTION

The idea of a spread-spectrum sensor array was first proposed in the 1970s by Compton[1]. Recently, as researchers have strived to improve the performance of spread-spectrum CDMA systems, more work has been carried out in this area [2, 3, 4]. This companion paper to [2] uses the bearing estimation techniques discussed there to realise a novel spread-spectrum diversity receiver. The basic results of optimum diversity combination will be revised first.

In the 1950s, researchers such as Kahn and Brennan [5] addressed the problem of combining a set of N noise-corrupted signals $\{s_n(t)\}$ to maximise the signal-to-noise ratio (SNR). If the noise on each signal is white, Gaussian and of constant variance σ^2, then the optimum output signal $S_0(t)$ is given by:

$$S_0(t) = \frac{1}{N}\sum_{n=1}^{N} s_n(t)k_n^* \tag{1}$$

where k_n is a complex constant proportional to the complex signal $s_n(t)$ and k^* denotes the complex conjugate operation. This equation gives rise to the well known result that if N signals of equal amplitude are combined, the SNR of the resulting signal is 10 log N (dB) greater than that of each individual signal.

If we now apply this to the case of a single source at bearing θ impinging on an N - element uniform linear array (ULA), then from [2], the N row $\times$ 1 column output vector $\underline{x}(t)$ from the array is given by:

$$\underline{x}(t) = \underline{q}(\theta)s(t) + \underline{n}(t) \tag{2}$$

where $s(t)$ represents the signal seen at ULA sensor 1, $\underline{n}(t)$ is a $N \times 1$ vector containing samples of a complex valued white Gaussian noise process of variance σ^2 and $\underline{q}(\theta)$ is the steering vector [2], which is given by:

$$\underline{q}(\theta) = [1, e^{j\pi\cos(\theta)}, \ldots, e^{j(N-1)\pi\cos(\theta)}]^T \tag{3}$$

where T denotes the vector transpose operation. From the above, the optimum output signal $x_0(t)$ is given by:

$$x_0(t) = \underline{q}^H(\theta)\underline{x}(t) \tag{4}$$

Where H denotes the complex conjugate vector transpose operation. Equation (4) leads to the receiver structure that is shown in figure 1.

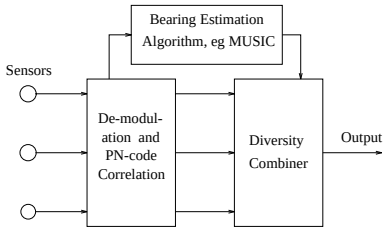

Figure 1: The Adaptive Receiver Structure.

This "data independent" combiner or beamformer [6] will be used throughout this paper. The data from the ULA sensors is used to perform bearing estimation on the incoming signals, so that the weights of the combiner can be set to enhance the desired signals at the output.

A spread spectrum receiver is capable of resolving L separate multipath returns or time samples for each symbol, where L is the pseudo-noise (PN) code length. Therefore, the adaptive structure proposed above must be repeated for each significant multipath component, as shown in figure 2. The outputs will be a set of signals of different SNRs that may be combined as shown using an adaptive RAKE filter [7]. The receiver is therefore operating in two dimensions, one in space and one in time.

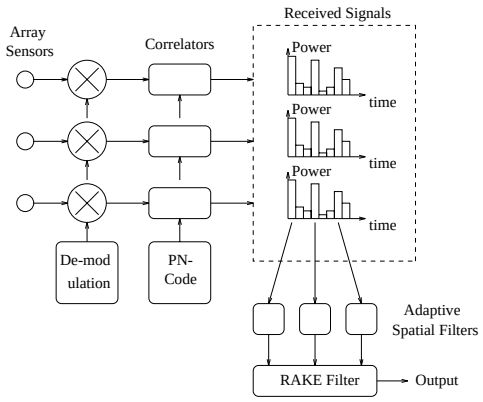

Figure 2: The Spatial Filter Structure.

DIVERSITY RECEIVER SIMULATION

In order to analyse the effect of using a diversity receiver in a code division multiple access (CDMA) system, simulation work was undertaken, based on the following assumptions:

a) Length 31 Gold codes were used to model multiple-access interference.

b) Each user had random bearing chosen from a uniform deviate. The receiver was a uniform linear array, which can only detect signals unambiguously from one side of the array. The range of bearings was therefore restricted to [0^o,180^o], with 90^o representing a signal arriving perpendicular to the linear array.

c) Perfect power control was in operation.

d) Rectangular pulse shaping was assumed, so that the receiver PN-code correlation operation is a linear process.

e) No assumption was made about the timing of codes: each code has a random time of arrival chosen from a uniform probability density function (PDF) and a random phase drawn from a uniform deviate in the range [0,2π].

In a CDMA system, both the forward path (from the main transmitter to each mobile) and the reverse path (from each mobile to the main receiver) are of interest. To start with, the latter will be analysed.

The Reverse Path.
The aim of this section is to derive an equation for the average signal-to-interference ratio (S/I) generated when a set number of users, M, are present. Gilhousen et al [8] state that the average interference generated for the reverse path is given by the equation:

$$S/I = \frac{L}{(M-1) + (\sigma^2/s)} \tag{5}$$

where s is the signal power of each CDMA user. Note that this equation defines S/I to include the in-phase and quadrature noise components, with respect to the desired signal, so that the correlator receiver suppresses the power of all other users by a factor of $(1/L)$. In the simulations, it was found that the average power suppression was slightly better than this.

To see why this is true, the PDF of the amplitude of Gold code cross-correlation interference must be considered. Gold codes are block codes [9], because $(L+2)$ codes in total are produced by the modulo-2 addition of two preferentially selected PN-codes of length L. Therefore, one may determine the possible cross-correlation levels by determining the weight or sum of each code.

The preferential polymonials octal 51 and 73 were used to generate 33 length 31 Gold codes. The distribution of weights for these codes, assuming random +1 or -1 data, is as follows:

Amplitude	No of Occurrences (out of 33)
± 1	17
± 7	10
± 9	6

The auto-correlation peak of each code is ± 31. The assumption of random times of arrival means that there is likely to be a non-integer shift of chips between two Gold codes. As a result, the interference between each user will lie on a linear transition between two of the states in the table above, anywhere in the range [-9,9]. The Gold code interference may be viewed as the output of a finite state machine and this representation is shown in figure 3.

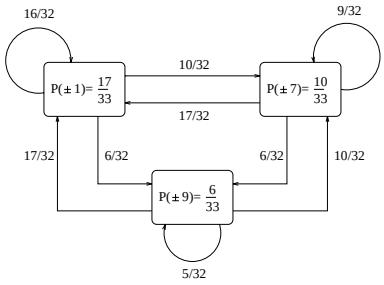

Figure 3: The Finite State Machine Interpretation of Gold Code Interference.

The boxes show the probabilities of the interference being at a given amplitude for a single interferer. The lines then show the conditional probabilities for the amplitude changing from one state to another. For example, the probability of the interference being in the transition from ± 9 to ± 7 is:

$$P(\pm 9 \rightarrow \pm 7) = \frac{6}{33} \times \frac{10}{32} = 0.05682 \text{(4 sig.fig.)} \tag{6}$$

This table may be used to determine the probability density function for the Gold code interference due to a single user, which is shown in figure 4.

To calculate the average interference power $\overline{P}_1$ due to one interfering source, the following integration is performed:

$$\overline{P}_1 = \int_{-9}^{9} x^2 p(x) dx = 19.75 (4s.f.) \tag{7}$$

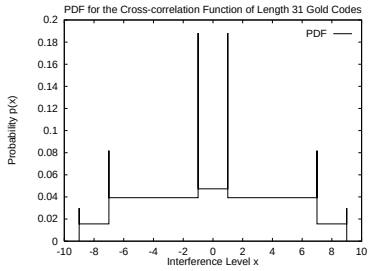

Figure 4: The PDF of Gold Code Cross-correlation Interference.

This clearly does not cover the situation where a data transition occurs on an interferer's signal during the correlation process. To include this eventuality, one must analyse the aperiodic correlation function of the Gold codes in a similar manner to the above. There are many more interference levels possible, because the three-level cross-correlation property no longer holds, and the resulting PDF has non-zero values in the range [-15,15]. It is shown in figure 5.

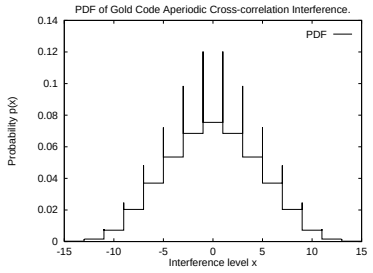

Figure 5: The PDF of Gold Code Aperiodic Cross-correlation Interference.

The mean power $\overline{P}_2$ in this case becomes 21.19 (4 s.f.). Assuming that data transitions occur with probability 0.5, the two power values may be averaged to give $\overline{P}$ = 20.47 (4 s.f.), which represents the mean interference power due to one user.

In the simulation, the desired user always used a code of weight ± 1, which meant that there were only 32 possible interfering codes, 16 of whom had weight ± 1. This changed the value of $\overline{P}$ slightly to 20.67 (4 s.f.).

Normalising $\overline{P}$ to the power output from the auto-correlation peak, which is L^2 = 961, gives the interference power P_0 = 0.02150 $\equiv$ -16.67dB. This can be incorporated into the equation for the simulated S/I, giving:

$$S/I = \frac{L}{k_1(M-1) + (\sigma^2/s)} \tag{8}$$

Where $k_1 = L P_0$.

The next issue to be discussed is the power suppression of other CDMA users by a linear array. It has already been pointed out that an N antenna diversity system suppresses white Gaussian noise by a factor N. Is the same true of other CDMA users?

The effect of one unwanted CDMA user on the desired signal may be specified by the vector $c\underline{q}(\phi)$, where ϕ is the user's bearing (in radians) and c is the complex cross-correlation output from the reference sensor. In order to check the mean power suppression, $P_s(N)$, the following integral must be performed:

$$P_s(N) = \frac{1}{\pi}\int_0^{\pi} |\underline{q}^H(\theta)\underline{q}(\phi)|^2 d\phi \tag{9}$$

Where θ is the desired signal bearing and $\underline{q}(\theta)$ is defined in equation (3). If θ is set to $\frac{\pi}{2}$(i.e.90^0) then $\underline{q}(\frac{\pi}{2}) = [11\ldots1]^T$. This makes the calculation simpler and $(\underline{q}^H(\frac{\pi}{2})\underline{q}(\phi))$ may be written as:

$$(\underline{q}^H(\frac{\pi}{2})\underline{q}(\phi)) = \sum_{n=1}^{N} e^{j(n-1)\pi\cos(\phi)} \tag{10}$$

Combining equations (9) and (10) gives the following equation:

$$\begin{aligned} P_s(N) &= \frac{1}{\pi}\int_0^{\pi} (\underline{q}^H(\theta)\underline{q}(\phi))(\underline{q}^H(\theta)\underline{q}(\phi))^H d\phi \\ &= \frac{1}{\pi}\int_0^{\pi} (N + \sum_{n=1}^{N-1}(N-n)e^{jn\pi\cos(\phi)})d\phi \\ &\quad + \frac{1}{\pi}\int_0^{\pi}\sum_{n=1}^{N-1}(N-n)e^{-jn\pi\cos(\phi)}d\phi \end{aligned} \tag{11}$$

Now, Bessel functions of the first kind $J_0(k)$ are defined as:

$$J_0(k) = \frac{1}{2\pi}\int_0^{2\pi} e^{\pm jk\cos(\phi)}d\phi \tag{12}$$

In addition $e^{jk\cos(\phi)} = e^{jk\cos(2\pi-\phi)}$, so this integral may be performed over the interval [0,π] rather than [0,2π]. Therefore equation (11) becomes:

$$P_s(N) = N + \sum_{n=1}^{N-1} 2(N-n)J_0(n\pi) \tag{13}$$

This result holds for any choice of θ because the magnitude of each component in $\underline{q}(\theta)$ is always 1. Now set $k_2 = P_s(N)$. If equation (8) is now applied to an N–antenna receiver, the expression for S/I becomes:

$$S/I = \frac{LN^2}{k_1k_2(M-1) + (N\sigma^2/s)} \tag{14}$$

For the simulation, the noise power σ^2 was set to be $\frac{1}{31}$ times that of the desired signal. The bearing of the desired signal was set to be 90°. Theoretical and simulation results are shown in figure 6. The former are plotted as lines, whereas the latter are shown as points. Clearly, equation (14) provides a good fit to the simulated data.

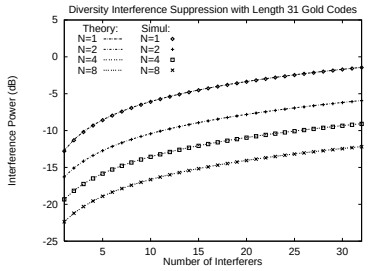

Figure 6: Theoretical and simulated results for Interferer Power Suppression in an N–sensor element receiver.

One may proceed from equation (14) in an attempt to predict bit error rates (BER) for the system. This simulation used differential phase shift keying (DPSK) modulation, a scheme which is often used to allow DS-SS receivers to cope with Doppler-shifted fading signals. The equation for the BER for a DPSK receiver, receiving a stationary signal corrupted by Gaussian white noise is given by[9]:

$$\mathrm{BER} = \frac{1}{2}\exp(-S/N) \tag{15}$$

Where the S/N is the signal-to-noise ratio of the incoming signal. For the purposes of calculating the BER, it has been assumed that the Gold code interference in each case has a Gaussian distribution, so that equation (15) holds.

The graph in figure 7 shows a comparison between predicted and simulated BERs. Again, the predicted results are plotted as lines, while the simulation results are shown as points.

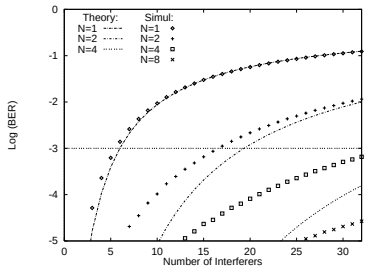

Figure 7: Theoretical and simulated results for Bit Error Rates in N–sensor element receivers.

ANALYSIS OF RESULTS

The simulated BER curves show a considerable improvement in performance as the the number of receivers in the base station increases. If the CDMA system uses a vocoder for human speech this normally entails a BER of 10^{-3} or better [8] - this is shown as a horizontal dotted line in figure 7. From the above results, this criterion is fulfilled on average, even at 100% loading, by the time the receiver has four sensor elements.

For $N = 1$, the Gold code interference is very close to being Gaussian, as the simulated and theoretical results match well. However, for $N > 1$, the assumption is no longer true and the curves no longer match. As the number of users M increases, the simulation results converge towards the predicted BER curve, as predicted by the central limit theorem progressively introducing Gaussian statistics. The non-Gaussian nature of the interference statistics for diversity systems of order 2 or greater may be explained by calculating the PDF of the Gold code interference produced by a 2 element array.

The equation for the magnitude response of a 2-element array to an interferer at bearing θ is given by:

$$G(\theta) = \sqrt{\frac{1}{2} + \frac{1}{2}\cos(\pi\cos(\theta))} \tag{16}$$

If one restricts the possible values of θ to $[0, \frac{\pi}{2}]$ then $G(\theta)$ is strictly increasing and is one-to-one and onto the range $[0, 1]$. Under these conditions the function G is invertible, with inverse G^{-1}.

The cumulative distribution function (CDF) of the variable x , defined as $\{x : x = G(\theta),\, 0 \le \theta \le \frac{\pi}{2}\}$, is given by:

$$CDF(x_0) = p(x < x_0) = \frac{2}{\pi}G^{-1}(x_0) \tag{17}$$

Differentiating the CDF function gives the probability density function $PDF(x_0)$, which is defined as $\lim_{\Delta x \to 0} p(x_0 \le x \le x_0 + \Delta x)$. For the function G, it is given by:

$$\begin{aligned} PDF(x_0) \quad = \quad & \frac{8x_0}{\pi^2}[1-(2x_0^2-1)^2]^{-\frac{1}{2}} \times \\ & [1-(\frac{1}{\pi}cos^{-1}(2x_0^2-1))^2]^{-\frac{1}{2}} \\ & (0 \le x_0 \le 1) \end{aligned} \tag{18}$$

The PDF function is shown in figure 8.

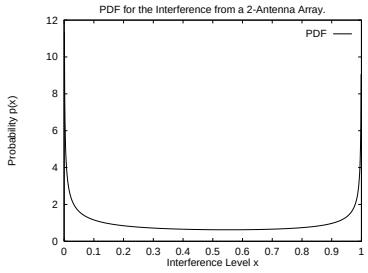

Figure 8: The PDF of interference from a 2–element antenna array.

This function evaluates to infinity at both x=0 and x=1. The area under the curve approaching x=1 is greater than for the corresponding Gaussian distribution of identical variance. This part of the curve is responsible for generating more errors than expected when $N > 1$.

When $N > 2$, the magnitude function G contains more than one sinusoidal function of θ and becomes difficult to invert analytically. Each time the gradient of $G(\theta)$ is zero, then there is an infinite spike in the PDF. As the value of N increases, the PDF will contain more infinite spikes. This will make the statistics of the Gold code interference less Gaussian. The magnitude response $G(\theta)$ for the array sizes N=2,4 and 8 are shown in figure 9. In each case the desired signal is at 90^{o}.

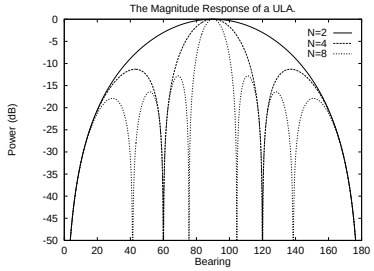

Figure 9: The Magnitude Response of ULAs with 2,4 and 8 sensor elements.

The Forward Path.
The forward path, from the main transmitter to each mobile receiver, may be subjected to a similar analysis. The same set of weights may be applied to the transmitter as to the receiver, so as to transmit most of the power in the line-of-sight path to the desired receiver.

It is also assumed that each CDMA signal is transmitted with equal power, so that forward path conditions are identical to those of the reverse path. The equation for the signal-to-interference ratio (S/I) is therefore identical to equation (15), except that the signal power, s, will vary with the distance, r, from the main transmitter.

Three important points should be stated concerning these results.

1) These results are mean results, which assume a uniform distribution of users. In practice, the system performance will depend on the geography of the mobile cell. The diversity antenna receiver can only exploit spatial diversity if the transmitters are spaced apart. If two transmitters impinge on the receiver from the same bearing, then increasing the number of sensor elements will not reduce the interference. However, if the number of receivers is increased, the width of the main lobe is reduced, which will reduce the outage probability of the system in turn.

2) It has been assumed that each transmitter had a single line-of-sight path to the receiver. In practice, there may be several multipaths received from each source. This increases the complexity of the signal processing and may reduce the system gain.

3) The combiner used in the above analysis is of a simple form, which allows general results to be obtained. It is not, however, statistically optimal in the sense of maximising the output S/I. Several beamformers exist to reduce the effect of directional (CDMA) interference and fulfil this criterion[6]. These techniques explicitly use the covariance matrix R (defined in [2]) to calculate the beamformer weights. The effectiveness of these techniques is dependent on the number of array sensors and on the amplitude of the interference.

CONCLUSION

This paper proposed a novel diversity receiver structure for use in direct-sequence spread-spectrum CDMA systems. Bearing estimation techniques determine the angle of arrival of a source, which allows the receiver to ameliorate interference.

It has shown that a diversity receiver can offer a considerable improvement in bit error rate performance on average. This permits a large increase in the capacity of the CDMA system.

ACKNOWLEDGEMENTS

The sponsorship of these studies by a SERC studentship and MoD CASE support is gratefully acknowledged.

REFERENCES

[1] R.T. Compton , "An Adaptive Array in a Spread Spectrum Communication System," *Proceedings of the IEEE*, Vol 66(3), March 1978, pp 289-298.

[2] J.S. Thompson, "Bearing Estimation Techniques for Improved Reception of Spread Spectrum Signals," in *Proceedings ISSSTA 94 (Finland)*.

[3] B. Suard, F.N.Naguib, G. Xu and A. Paulraj "Performance of CDMA Mobile Communication Systems Using Antenna Arrays," in *Proceedings ICASSP-93*, Vol IV, pp 153-156.

[4] T. Liu, "The Modular Covariance Adjustment Adaptive Array for CDMA Wireless Communications," in *Proceedings ICASSP-93*, Vol IV, pp180-183.

[5] D.G. Brennan, "On the Maximum Signal-to-Noise Ratio Realisable From Several Noisy Signals," *Proceedings of the IRE*, Vol 43, October 1955, p1530.

[6] B.D. Van Veen, K.M. Buckley, "Beamforming: A Versatile Approach to Spatial Filtering," *IEEE Acoustics Speech and Signal Processing Magazine*, April 1988, pp4-24.

[7] G.J.R. Povey, P.M. Grant and R.D. Pringle, "Performance of a Spread Spectrum Receiver Design," in *Proceedings ISSSTA 92 (Japan)*, pp71-74.

[8] K.S. Gilhousen et al, "On the Capacity of a Cellular CDMA System," *IEEE Transactions on Vehicular Technology*, Vol 40(2), May 1991, pp303-311.

[9] S. Haykin, "Digital Communications," *John Wiley and Sons* 1988, pp370-393.

Bearing Estimation Techniques for Improved Reception of Spread Spectrum Signals.

John S. Thompson, Bernard Mulgrew and
Peter M. Grant
Department of Electrical Engineering,
The University of Edinburgh,
The Kings Buildings,
Edinburgh,
Scotland, EH9 3JL.

Abstract – In this paper, the novel use of bearing estimation techniques to determine the direction of arrival of direct sequence spread spectrum signals is described. Firstly, the basic ideas behind bearing estimation are discussed and it is shown how these may be best applied to a spread spectrum receiver array. Then, some simple algorithms are compared and it is shown that the multiple signal classification algorithm (MUSIC) provides good angular resolution for a fixed computational overhead. One major shortcoming of the MUSIC algorithm is that it fails in the presence of coherent spread spectrum multipath returns. Spatial smoothing algorithms are shown to be a solution to this problem and the behaviour of such techniques is discussed.

INTRODUCTION

The problem that motivates the use of bearing estimation techniques is simply put. An array of omnidirectional sensors, set up in a known configuration, receives a set of N signals from unknown directions $(\theta_1, \theta_2, \ldots, \theta_N)$ relative to a fixed reference axis. How are the unknown parameters to be determined?

A very large number of algorithms to solve the problem have been documented in the literature [1]. Among the most popular are the minimum variance technique, the MUSIC algorithm [2] and maximum likelihood techniques [3]. The following set of assumptions are usually included in such algorithms:

a) All incoming signals are in the far field with respect to the receiver, so that they are all plane waves.

b) The data from each array element is assumed to be corrupted by Gaussian white noise of zero mean and variance σ^2.

c) The receiver for each sensor is non-coherent and demodulates the signal in both the I and Q channels. One clock provides the timing for all sensors, so that data from the whole array is sampled synchronously.

d)The received signals all have a carrier frequency centred about frequency f Hz and are narrowband in nature, so that the data bandwidth B Hz << f Hz. The number of impinging signals, M, is assumed to be less than the number of array elements, N.

A simple type of receiver array is the uniform linear array (ULA), shown in figure 1. Each sensor is spaced by a distance $\frac{\lambda}{2}$ m where λ m is the wavelength of the carrier. The diagram also defines the broadside and endfire regions of a ULA.

There are two main limitations to the ULA - this type of array cannot distinguish signals coming from opposite sides of the array. Secondly, the ULA suffers from "endfire effects" - large errors occur in measuring the bearings of signals arriving from these directions. Clearly, the ULA receiver must be designed with these points in mind.

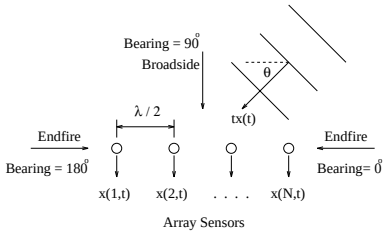

Figure 1: A Typical Uniform Linear Array.

Consider a narrowband signal at baseband, $s(t)$. It is modulated up to a carrier of angular frequency $\omega = 2\pi f$, so that the transmitted signal $tx(t)$ is:

$$tx(t) = s(t)e^{j\omega t} \tag{1}$$

This signal impinges on a ULA at bearing θ as shown in figure 1. Consider the two signals $r(1,t)$ and $r(2,t)$ received at sensors 1 and 2. These are given by the expressions:

$$r(1,t) = s(t)e^{\mathrm{j}\omega \mathrm{t}} \tag{2}$$

and:

$$r(2,t) = s(t-t_{\mathrm{d}})e^{\mathrm{j}\omega(\mathrm{t}-\mathrm{t_d})} \tag{3}$$

Where $t_d = (\lambda \cos\theta)/2c$ and c is the speed of light. $r(1,t)$ and $r(2,t)$ are demodulated and sampled to produce the signals $x(1,t)$ and $x(2,t)$, so that the $e^{j\omega t}$ term disappears. Assumption d) means that one may write that $s(t) \simeq s(t-t_{\mathrm{d}})$. Now the only difference between signals $x(1,t)$ and $x(2,t)$ is a phase rotation term, $e^{j\omega t_d}$.

In order to perform bearing estimation successfully, the phase rotations across the whole array must be known for all possible bearings θ. If the phase at sensor one is set to zero as a reference, the phase rotation can be represented by a N row $\times$ 1 column vector $\underline{q}(\theta)$. For a ULA, $\underline{q}$ is given by:

$$\underline{q}(\theta) = [1, e^{j\pi\cos(\theta)}, \ldots, e^{j(N-1)\pi\cos(\theta)}]^T \tag{4}$$

One set of samples $\{x(n,t)\}$ received from the array elements is termed a snapshot of the array. An equation can be written for the vector $\underline{x}(t)$ which contains the snapshot sampled at time t:

$$\underline{x}(t) = [x(1,t), x(2,t), \ldots, x(N,t)]^T \tag{5}$$

where T denotes the vector transpose operation. If a ULA receives signals from M sources $\{s_m(t)\}$ at bearings $\{\theta_m\}$, then the vector $\underline{x}(t)$ may be written as:

$$\underline{x}(t) = Q\underline{s}(t) + \underline{n}(t) \tag{6}$$

where Q is an N row $\times$ M column matrix given by:

$$Q = [\underline{q}(\theta_1), \underline{q}(\theta_2), \ldots, \underline{q}(\theta_M)] \tag{7}$$

and $\underline{s}(t)$ is given by:

$$\underline{s}(t) = [s_1(t), s_2(t), \ldots, s_M(t)]^T \tag{8}$$

The $N \times 1$ vector $\underline{n}(t)$ contains the Gaussian white noise of variance σ^2 that corrupts the snapshot data. In order to perform bearing estimation, the first requirement is to form the data covariance matrix R from the snapshots. The matrix equation for R is given by:

$$R = \frac{1}{K}\sum_{k=1}^{K} \underline{x}(t_k)\,\underline{x}^H(t_k) \tag{9}$$

where K denotes the number of snapshots used to form R, t_k denotes the time at which the k^{th} snapshot was taken and $\underline{x}^H$ denotes the complex conjugate transpose operation.

SPREAD SPECTRUM BEARING ESTIMATION

Direct-sequence spread spectrum systems modulate the narrowband data with a pseudo-noise (PN) code of length L, before upconversion to a carrier. If the data rate is f_d Hz then the spread-spectrum chip rate $f_c = f_d \times L$ Hz. Bearing estimation algorithms may be directly applied to the output of a spread-spectrum receiver, provided that assumptions a)-d) are complied with.

The most problematic assumption is d), as the spread-spectrum signal should not be changing very much across the array, when it is sampled. The correlation peaks at the output of the DS-SS code detectors should be aligned in time, with only the phase changing. Clearly, if the receiver signals at opposite ends of the array are mis-aligned by one chip, the algorithms will fail.

The worst case occurs when the signal approaches in the endfire region. In this case there is a time shift in the signal between array sensors of $\frac{\lambda}{2c} = \frac{1}{2f}$ seconds. Clearly, the time shift across the whole array t_{sh} should represent only a small fraction of one chip period t_c to keep the correlation peaks aligned, so:

$$\frac{t_{sh}}{t_c} = \frac{N-1}{2f} \times \frac{1}{1/f_c} = \frac{(N-1)f_c}{2f} << 1 \tag{10}$$

The point at which the bearing estimation algorithm is applied must also be selected. It is possible to apply the algorithms before the DS-SS code detector or after it. However, the latter option is much preferable for the following reasons.

1) The transmitted DS-SS codes are normally received with a low power, which may be equal to or less than the noise power. If bearing estimation is applied directly to the received signal, the results will be poor unless the array size is large and a lot of data is used.

2) Consider a code division multiple access (CDMA) system using power control. At the code detector input, there are a lot of different codes present at roughly the same power and there is no means of discriminating the desired user. Bearing estimation algorithms can usually only resolve as many signals as there are array elements, so a very large array would be needed.

3) In most realistic scenarios, multipath signal returns will be present. These increase the number of signals at the input of the code correlator that have to be resolved.

Performing bearing estimation after the code correlator allows the system to take advantage of the processing gain of the

system in order to reduce the variance of the bearing estimate, suppress undesired CDMA codes and to separate multipath returns in time.

Spread-spectrum diversity over a multipath channel provides the ability to resolve L separate returns for each symbol, where L is the PN code length. This means that narrowband bearing estimation may be performed for each separate multipath return or time sample. The receiver now uses a maximum of L covariance matrices, which are denoted $R(d)$ - where d indicates the time sample of interest.

BEARING ESTIMATION ALGORITHMS

This section introduces the ideas behind some of the better known bearing estimation algorithms. The search for signals coming from different bearings is analogous to finding the major frequency components in a given signal. Hence, it is not surprising to find that bearing estimation algorithms have a lot in common with spectral estimation techniques.

a)Conventional Beamforming (CBF)
This technique [4] operates in a similar manner to the discrete Fourier transform (DFT) with the output power spectrum for the d^{th} time sample at bearing θ, $P_{CBF}(d,\theta)$, produced by the equation:

$$P_{CBF}(d,\theta) = \underline{q}^H(\theta) R(d) \underline{q}(\theta) \qquad (11)$$

The same techniques can be applied to conventional beamforming as to the DFT, such as windowing the data, zero padding, etc. However, as with the DFT, the CBF algorithm provides a poor trade-off between the number of sensors and resolution, so that a number of better techniques have been devised.

b)Minimum Variance Technique (MV)
The problem with CBF techniques arises from beam pattern constraints: there is a trade-off between the sidelobe level and the width of the main beam. In this technique [1], the best possible beam pattern is chosen mathematically. It turns out that the minimum variance beam pattern involves the inverse of the covariance matrix. The resulting power spectrum, $P_{MV}(d,\theta)$ is given by the equation:

$$P_{MV}(d,\theta) = \frac{1}{\underline{q}^H(\theta) R(d)^{-1} \underline{q}(\theta)} \qquad (12)$$

where $R(d)^{-1}$ denotes the matrix inverse of $R(d)$.

Calculating the inverse of the covariance data matrix makes this technique more computationally intensive than the CBF technique. However the MV estimate of the spatial power spectrum has a smaller resolution than that of the CBF technique.

c)Multiple Signal Classification (MUSIC)
If one substitutes equation (6) into equation (9) and applies the expectation operator, the following expression is obtained:

$$E[R(d)] = R_{av}(d) = Q(d).S(d).Q(d)^H + \sigma^2.I \qquad (13)$$

The matrix $S(d)$ is an $M \times M$ diagonal matrix, whose m^{th} diagonal entry relates to the power in the m^{th} impinging signal in the d^{th} time sample. The matrix I is the $N \times N$ identity matrix.

Therefore, if the eigenvalue decomposition of the matrix $R(d)$ is performed, M signal eigenvectors will be obtained, which span the M columns of the matrix $Q(d)$. The corresponding eigenvalues will similarly be related to the non-zero entries in the matrix $S(d)$.

The other $N - M$ eigenvectors are noise eigenvectors whose eigenvalues are approximately equal to σ^2. Their only property of interest is that they are orthogonal to the signal eigenvectors and the steering vectors in $Q(d)$. MUSIC [2] exploits this property to determine which bearings have the smallest projection on the noise eigenvectors, indicating the presence of a signal.

To generate the MUSIC power spectrum, the following equation is used:

$$P_{MUS}(d,\theta) = \frac{1}{q^H(\theta).W(d).W(d)^H.q(\theta)} \qquad (14)$$

where $W(d)$ is an $N \times N - M$ matrix containing the $N - M$ noise eigenvectors. The eigenvalue decomposition of $R(d)$ is more computationally intensive than either the CBF or the minimum variance techniques, but the quality of the power spectrum is improved.

One problem with the MUSIC algorithm is that the number of signals present must be estimated before the power spectrum is calculated. This may be done by an examination of the eigenvalues, or by the use of a model order algorithm [1].

For uncorrelated signals, large array sizes and a large number of data snapshots, the MUSIC algorithm is known to approach theoretical lower bounds on parameter estimation performance[5].

d)Maximum Likelihood Techniques
Maximum likelihood statistical methods [1, 3] provide the optimum estimate of spatial power spectrum. This is achieved for N incoming signals, by performing an N-dimensional search over all the possible values of the bearing signals, to find the best fit to the given covariance matrix.
Not surprisingly this technique is much more computationally intensive than any of the previous algorithms and is not considered further in this paper.

e)Comparison of Algorithms

In figure 2, the CBF, minimum variance and MUSIC algorithm techniques are compared. All three are attempting to resolve two separate, statistically independent signals. Both signals have a signal-to-noise ratio (SNR) of 20dB, with one at a bearing of 35^o and the other at 45^o - the desired bearings are shown as vertical lines. All three are using 50 data snapshots from a 8 sensor linear array. As can be seen, only the MUSIC algorithm successfully resolves the signals under the given conditions.

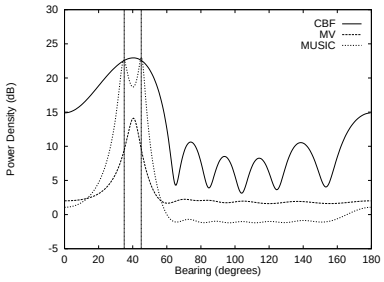

Figure 2: A comparison of bearing estimation algorithms with two signal sources present.

COHERENT DS-SS SOURCES

In order to obtain the best performance the MUSIC algorithm requires the correlation factor between signals C to fulfil the following constraint [5]:

$$C = \frac{E[s_i(t).s_j(t)]}{\sqrt{E[s_i(t)^2]E[s_j(t)^2]}} = 0 \quad \text{if} \quad i \neq j \qquad (15)$$

If the signals originate from different transmitters, this criterion will normally be approximately true. As the value of C increases from the ideal value of zero towards the worst case value of one, the variance of the bearing estimates will increase. In the situation where the two signals are multipath returns from the same transmitter, the value of C is one. In this case, the eigenvalue decomposition will fail to produce two distinct signal eigenvectors, so that the MUSIC algorithm will fail.

The simplest method found to date to overcome this problem is spatial smoothing [6], but the original method only works in the case of the ULA. This technique forms matrices from subsets of the ULA and averages them to form a smaller covariance matrix for the MUSIC algorithm. The original algorithm only uses one direction along the array to form matrices - forward only spatial smoothing (FOSS).

If there are J subarrays, the matrices are in fact $(N - J + 1) \times (N - J + 1)$ partitions of the original covariance matrix: the j^{th} matrix $R(d, j)$ begins at the (j, j) entry of $R(d)$. The averaged matrix $R_{ss}(d)$ is given by the equation:

$$R_{ss}(d) = \frac{1}{J} \sum_{j=1}^{J} R(d, j) \qquad (16)$$

In order to resolve M sources, at least M subarrays are required so that at least $2M$ ULA array sensors are needed. Thus, the FOSS algorithm places serious restrictions on the number of coherent signals that may be resolved by an array of a given size. The situation can be improved by forward-backward spatial smoothing (FBSS) [7], which forms matrices by working both forward and backward along the array as shown in figure 3.

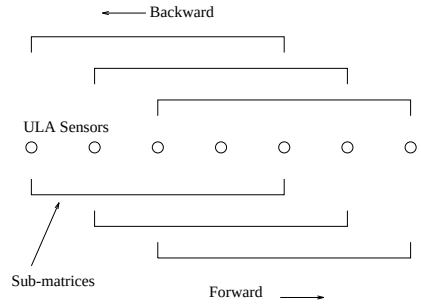

Figure 3: Forward-backward spatial smoothing.

This operation is equivalent to forward-backward smoothing the original covariance matrix and spatially smoothing the resulting matrix. The forward-backward covariance matrix $R_{fb}(d)$ is given by the equation:

$$R_{fb}(d) = R(d) + U R(d)^* U \qquad (17)$$

Where $R(d)^*$ denotes the complex conjugate of $R(d)$ and U is given by:

$$U = \begin{bmatrix} 0 & \dots & 0 & 1 \\ 0 & \dots & 1 & 0 \\ \vdots & \ddots & \vdots & \vdots \\ 1 & \dots & 0 & 0 \end{bmatrix} \qquad (18)$$

The partitions of the matrix $R_{fb}(d)$ from equation (17) are then substituted into equation (16) in place of those formed from the original matrix $R(d)$. This technique reduces the number of submatrices so that only $(3M/2)$ sensors are required to resolve M coherent signals. However, there is a tradeoff: this improvement is obtained at a cost of reduced robustness in the MUSIC algorithm. The FOSS algorithm performs consistently but the performance of FBSS varies as the phases of the incoming signals are changed [8].

Consider a practical situation, where the ULA contains 8 sensors. In a multipath environment, there may be several time samples containing significant signal power, each of which might be made up of two coherent multipaths. In this case, FOSS normally requires two subarrays (J=2) [6], each containing seven elements. FBSS needs only to apply forward-backward smoothing, so that the smoothed matrix is still of size eight(J=1) [7]. In figure 4, these algorithms are applied to a scenario where the two multipaths have bearings 130^o and 150^o and each SNR is 20dB. There were 50 data snapshots available and the resulting power spectrum of the MUSIC algorithm without smoothing and with FOSS or FBSS applied is shown. The MUSIC algorithm fails to work, but the smoothing techniques overcome the problem.

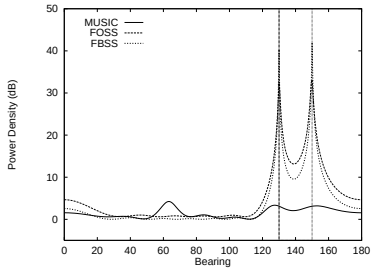

Figure 4: Typical power spectra for the coherent multipath case.

The smoothing algorithms work well in this case, but how do they perform more generally? An indication of this can be obtained by looking at the variance of the bearing estimates under different conditions. Equations have been derived for the variance of the MUSIC algorithm with smoothing [9] and these can be applied to the signal scenario above: see figure 5.

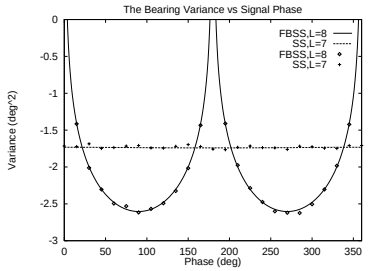

Figure 5: Variance of the MUSIC algorithm using smoothing techniques.

The relative phase of the two signals at the reference sensor (which is at the middle of the ULA in this case) was varied in the simulation work to observe the effect on the performance of MUSIC. The variance of the bearing estimate of the first source (bearing 130^o) is plotted in figure 5, though the estimate for the second source (bearing 150^o) behaves similarly. To back up the theoretical equation, simulation results using 1000 Monte Carlo runs are also shown and are plotted as points.

The FOSS algorithm with J=2 is seen to behave consistently, unlike the FBSS algorithm with J=1 which can perform very well or very badly. The instability in the FBSS algorithm may be avoided by increasing the number of subarrays J to the same number required by FOSS [8]. The fact that these algorithms reduce the size of the covariance matrix means that the performance of the MUSIC algorithm degrades compared to the equivalent uncorrelated signal scenario. To obtain the same performance, one can increase the number of snapshots K, the number of array elements N or the SNR.

CONCLUSION

This paper has introduced the notion of applying narrowband bearing estimation to the output from a spread-spectrum receiver array. The basic algorithms have been described and the MUSIC technique has been shown to provide good performance for a fixed computational overhead.

The problem of coherent multipath returns has also been discussed. Spatial smoothing techniques have been suggested as a method to overcome this for linear arrays. FOSS is a robust technique, but requires a subarray for each coherent signal. FBSS reduces the number of subarrays, but the performance varies with the incoming signal phases.

ACKNOWLEDGEMENTS

The sponsorship of these studies by a SERC studentship and MoD CASE support is gratefully acknowledged.

REFERENCES

[1] S. Haykin , J.P. Reilly, V. Kezys, and E. Vertatschitsch "Some aspects of array processing," *IEE Proceedings Part F*, Vol 139(1),pp1–26, February 1992.

[2] R.O. Schmidt "Mutiple emitter location and signal parameter estimation," *IEEE Trans AP*, Vol 34(3), pp276–280, March 1986.

[3] P. Stoica and K.C. Sharman "Maximum likelihood methods of direction-of-arrival estimation," *IEEE Trans ASSP*, Vol 38(7), pp1132–1143, July 1990.

[4] D.H. Johnson "The application of spectral estimation methods to bearing estimation problems," *Proceedings of the IEEE*, Vol 70(9), pp1018–1028, September 1982.

[5] P. Stoica and A. Nehorai "Music,maximum likelihood, and Cramer-Rao bound," *IEEE Trans ASSP*, Vol 37(5), pp720–741, May 1989.

[6] T. Shan , M. Wax, and T. Kailath "On spatial smoothing for direction-of-arrival estimation of coherent signals," *IEEE Trans ASSP*, Vol 33(4), pp806–811, August 1985.

[7] S.U. Pillai and H.K. Byung "Forward/backward spatial smoothing techniques for coherent signal identification," *IEEE Trans ASSP*, Vol 37(1), pp8–14, January 1990.

[8] J.S. Thompson, P.M. Grant, and B. Mulgrew "Performance of spatial smoothing algorithms for correlated sources," Submitted to *IEEE Trans SP*.

[9] B.D. Rao and K.V.S. Hari "Effect of spatial smoothing on the performance of music and the minimum norm method," *IEE Proc Part F*, Vol 137(6), pp449–458, December 1990.

ANALYSIS OF SPATIAL SMOOTHING ALGORITHMS

John S. Thompson, Peter M. Grant, Bernard Mulgrew. [1]

Abstract One of the most popular algorithms for performing bearing estimation is the MUSIC algorithm. However, the main limitation on its use is the fact that it performs very poorly in the presence of highly–correlated or coherent sources. A simple method to avoid this problem is to employ a spatial smoothing pre-processing technique. These algorithms trade the effective array size for the ability to correctly locate coherent sources.

In this paper, two techniques will be considered: 1) spatial smoothing (SS) and 2) forward–backward spatial smoothing (FBSS). The structure of the smoothed covariance matrix provides some insight into the likely performance of the two techniques. The analysis is backed up numerically through the use of equations for the variance of the bearing estimates produced by the MUSIC algorithm.

Introduction The problem that motivates the use of bearing estimation techniques is quite simple. There are P plane waves impinging on a M–element array of known configuration. The receiver has access to a $M \times 1$ noise-corrupted data vector $\underline{y}(t)$ seen at the array. In order to determine the bearings of the P incoming signals, the underlying model that generates the available data is assumed to be of the form:

$$\underline{y}(t) = A(\Theta)\underline{s}(t) + \underline{n}(t) \tag{1}$$

The vector $\underline{n}(t)$ contains the M zero-mean Gaussian white noise processes of variance σ^2 that corrupt the data and $\underline{s}(t)$ is the vector of the P signal amplitudes. The vector Θ contains the P bearings of interest and the $M \times P$ matrix $A(\Theta)$ is made up as shown:

$$A = [\underline{a}(\theta_1), \underline{a}(\theta_2), \ldots, \underline{a}(\theta_P)] \tag{2}$$

where the parameters $\{\theta_p\}$ are the bearings of the P signals, while the "steering" vector $\underline{a}(\theta)$ is the impulse response of the array to direction θ. For an M–element uniform linear array (ULA) with an antenna spacing of half the signals' carrier wavelength, the steering vector is given by:

$$\underline{a}(\theta) = [1, e^{j\pi\cos(\theta)}, \ldots, e^{j(M-1)\pi\cos(\theta)}] \tag{3}$$

The MUSIC Algorithm The MUSIC algorithm [1] makes some assumptions about the incoming data, so that it conforms to the model in equation (1) and the problem is tractable. There are P narrow–band plane wave signals impinging on an M element linear array, where $M > P$. The data from each array element is assumed to be corrupted by Gaussian white noise of zero mean and variance σ^2. The signals and noise are ergodic random processes with zero mean and are assumed to be mutually uncorrelated. For the purposes of the algorithm, all the impinging signals are assumed to be uncorrelated.

In practice, one has access to N snapshots of the noisy signal vector $y(t)$, from which an $M \times M$ covariance matrix $\hat{R}$ is calculated. It may be utilised to generate a power density spectrum for all bearings of interest, where the peaks of the spectrum identify the bearings of the signals present. The mean of $\hat{R}$ is given by:

[1] Signals and Systems Group, Department of Electrical Engineering, The University of Edinburgh, Mayfield Road, Edinburgh, EH9 3JL.

$$E[\hat{R}] = E[y(t)y(t)^H] = R = ASA^H + \sigma^2 I_M \tag{4}$$

where A^H denotes the Hermitian transpose of A, I_M is the $M \times M$ identity matrix and the signal matrix $S = E[\underline{s}(t)\underline{s}^H(t)]$. The expansion of R in equation (4) shows that the eigenvalues of R ordered by decreasing size, $\lambda_i(R)$, are given by the expression $\lambda_i(R) = \lambda_i(X) + \sigma^2$, where the signal matrix $X = ASA^H$. Provided all the signals are mutually uncorrelated, the matrix S is of rank P, so the P largest eigenvalues are the sum of the signal and noise power. These eigenvalues and their associated eigenvectors correspond to the incoming signals and they form the "signal subspace".

If $i > P$, $\lambda_i(X) = 0$ and so the smallest $M - P$ eigenvectors of R are "noise" eigenvectors whose eigenvalues are equal to σ^2. Their only property of interest is that they form a "noise subspace" which is orthogonal to the signal subspace. This means that each noise eigenvector is orthogonal to every steering vector in the matrix A. The MUSIC algorithm exploits this property to locate signals by determining which bearings have the smallest projection on the noise subspace. The following equation is used to generate the power density spectrum:

$$\text{MUS}(\theta) = \frac{1}{a^H(\theta) E_n E_n^H a(\theta)} \tag{5}$$

where E_n is the $M \times (M - P)$ matrix of column noise eigenvectors.

One problem with the MUSIC algorithm is that the number of signals present must be estimated in order to determine the rank of the noise subspace. This may be done by an examination of the eigenvalues, or by the use of a model order algorithm [2]. This paper will assume that the number of signals present has been determined correctly.

Coherent Sources and Spatial Smoothing One assumption made above states that the incoming signals are mutually uncorrelated over the time of observation. If all the signals present originate from different transmitters or are modulated with different data streams then this assumption is at least approximately true. However, if they result from multipath responses from the same transmitter, the signals are "coherent" and the assumption is invalid.

The signal subspace is always spanned by the the vectors present in the matrix A. However, if the signals are coherent, the matrix S becomes singular, so that some of its eigenvalues are zero. This means that part of the signal subspace is indistinguishable from the noise subspace. As a result, the observed noise subspace is no longer orthogonal to the steering vectors in the matrix A and the MUSIC algorithm fails.

To overcome these problems, a technique called spatial smoothing (SS) [3] has been developed to allow the MUSIC algorithm to be applied to the coherent signal case. The algorithm was originally designed only for uniform linear array (ULA) geometries. The basic idea is to form covariance matrices from subsets of the array - which is equivalent to partitioning the original covariance matrix. If there are K subarrays, each subarray is of size $L = M - K + 1$ and the partition for the k^{th} subarray is the matrix $F(k)RF(k)^T$. The $L \times M$ matrix $F(k)$ is defined by:

$$F(k)_{ij} = \begin{cases} 1 & \text{if } j = i + k - 1 \text{ and } 1 \leq i \leq L \\ 0 & \text{otherwise} \end{cases} \tag{6}$$

The notation F_{ij} denotes the i^{th} row and j^{th} column element of the matrix F. The partitioned matrices are used to form a smoothed matrix R_{SS} of size $L \times L$, which is calculated as follows:

$$R_{SS} = \frac{1}{K} \sum_{k=1}^{K} F(k) R F(k)^T \tag{7}$$

where $F(k)^T$ denotes the transpose of $F(k)$. Clearly, the size of the covariance matrix and thus the performance of the MUSIC algorithm is traded for the ability to resolve coherent sources. In order to resolve P coherent sources, an array containing at least $2P$ elements is required. In a similar way, it is very simple to show that to resolve P coherent sources, it is required to average over at least P independent submatrices.

Soon afterwards, it was reported [4] that an additional technique called forward-backward spatial smoothing (FBSS) can be used to improve performance. The FBSS technique applies forward–backward smoothing (FBS) to the forward and backward covariance matrices R_F and R_B to form a matrix R_{ave} as shown:

$$R_{ave} = \frac{1}{2}(R_F + R_B) = \frac{1}{2}(R + JR^*J) = \frac{1}{2}(R + \begin{bmatrix} 0 & \dots & 0 & 1 \\ 0 & \dots & 1 & 0 \\ \vdots & \ddots & \vdots & \vdots \\ 1 & \dots & 0 & 0 \end{bmatrix} R^* \begin{bmatrix} 0 & \dots & 0 & 1 \\ 0 & \dots & 1 & 0 \\ \vdots & \ddots & \vdots & \vdots \\ 1 & \dots & 0 & 0 \end{bmatrix}) \tag{8}$$

where R^* denotes the complex conjugate of R. The matrix R_{ave} is then spatially smoothed as required to form the FBSS matrix R_{FB}.It has been shown [4, 5] that to resolve P coherent sources, as little as $3P/2$ array elements may be required to restore the rank of S. However, there are some situations where FBSS behaves in the exactly the same manner as the SS technique: in these cases $2P$ array elements are still required.

Statistical Analysis of the MUSIC Algorithm There are a number of approaches to determine the performance of the MUSIC algorithm, but one useful technique is to determine the variance of bearing estimates produced by the MUSIC algorithm for a given set of conditions. An excellent introduction to this approach is given in [6]. This analysis has been extended to spatial smoothing algorithms in [7] and the required result for this paper is given in terms of the error in the estimate of the bearing of the x^{th} signal, $\delta\theta_x$. The asymptotic variance of the error is given by:

$$E[\delta\theta_x^2] = \frac{2}{d_\theta(\theta_x)^2 N K^2}[\sum_{p,q=1}^{K} \beta^H R(p,q)\beta\, \alpha^H N(q,p)\alpha + Re\{\sum_{p,q=1,p\neq q}^{K} \beta^H N(p,q)\alpha\, \beta^H N(q,p)\alpha\}] \tag{9}$$

The scalar value $d_\theta(\theta_x)$ is given by the matrix product $2\{\underline{d}_{SS}^H(\theta)E_{SS}E_{SS}^H\underline{d}_{SS}(\theta)\}$, where $\underline{d}_{SS}(\theta)$ is the Brandwood vector derivative of the length L steering vector $\underline{a}_{SS}(\theta)$ [8]. The matrix $E_{SS}E_{SS}^H$ is the noise subspace of the smoothed covariance matrix and the matrix $R(p,q)$ is given by $F(p)RF(q)^T$. The vectors α and β are defined as:

$$\alpha = E_{SS}E_{SS}^H\underline{d}_{SS}(\theta_x) \quad \text{and} \quad \beta = X_{SS}^+\underline{a}_{SS}(\theta_x) \tag{10}$$

The matrix X_{SS}^+ denotes the pseudo–inverse of the smoothed signal matrix X_{SS}. The matrix $N(p,q)$ is defined in a similar way to $R(p,q)$ with $N(p,q) = \sigma^2 F(p)F(q)^T$.

Analysis of the Covariance Matrix The performance of the MUSIC algorithm depends critically on the condition of the signal matrix S [6]. In the simple case of two sources, this matrix is given by:

$$S = \begin{bmatrix} s_1^2 & s_1 s_2 c e^{j\phi(1,2)} \\ s_1 s_2 c e^{-j\phi(1,2)} & s_2^2 \end{bmatrix} \tag{11}$$

Where s_1 and s_2 denote the amplitudes of the two sources, c the magnitude of their cross-correlation and $\phi(1,2)$ the relative phase between the sources at the reference sensor. If the value of c is unity, the matrix S is singular and the MUSIC algorithm fails. The underlying purpose of spatial smoothing algorithms is to reduce the value of c so that the smoothed signal matrix S_{SS} is well–conditioned numerically.

It is possible to show that for the SS technique with K subarrays, the correlation value c_{SS} becomes [9]:

$$c_{SS} = \frac{1}{K} \sum_{k=0}^{K-1} e^{-j(((K-1)/2)+k)\pi(cos(\theta_1)-cos(\theta_2))} \tag{12}$$

This means the numerical condition of the matrix S_{SS} depends on both the source bearings and their angular separation. The correlation value for FBSS with L subarrays is the same as for SS, but it is scaled by the term $\cos(\phi(1,2))$. This means the FBSS algorithm can offer an improvement over SS for the same array size, which depends on the relative signal phase.

Results In this section, the equations quoted for the MUSIC algorithm and for the spatial smoothing techniques will be applied to particular scenarios to illustrate the points made above. It should be pointed out, however, that equation (9) is very complex and the above analysis is only intended to explain the major effects observed in the behaviour of SS/FBSS. In all the simulations the number of elements M in the uniform linear array was eight and each signal's SNR was set to be 17dB. All signals were generated using complex exponentials of constant amplitude and one hundred snapshots were used to form covariance matrices in each case.

Figure 1 shows the effect of angular separation on SS, FBS, FBSS with two coherent sources and MUSIC with two uncorrelated sources. The first source is at a bearing of 90^o and the bearing of the second source is chosen to give the correct angular separation. The variance of the 90^o source is shown in the diagram, but the variance of the other source will follow a similar trend. The reference sensor was set at one end of the ULA, so that the relative phase of the two signals at the middle of the array changes. The phase dependence of the FBS technique causes the correlation factor c_{SS} to vary between 0 and 1 according to the value of $\cos(\phi(1,2))$: the variance curve is seen to oscillate accordingly.

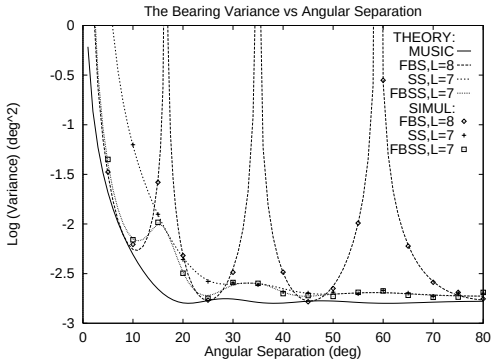

Figure 1: Comparison of variance of MUSIC, SS, FBS and FBSS techniques vs angular separation.

The SS algorithm with $L = 7$ improves more slowly than the MUSIC algorithm with no correlation, as the signal separation is increased. This is because the condition of both the matrix S and the matrix A depend on signal separation. The FBSS technique with $L = 7$ generally performs better than SS and for closely spaced sources the variance can be improved a lot according to the relative phase between the two sources $\phi(1,2)$.

Figure 2 shows the effect of signal phase on the performance of SS, FBS, FBSS algorithms and MUSIC (with zero correlation). The two sources are at 96^o and 78^o and their relative phase at the centre of the ULA varies from $0 - 360^o$. The variance is plotted for the source at 96^o and the performance of the SS algorithm with $L = 7$ is approximately constant with the signal phase. The FBS technique is again shown to provide good performance for some signal

phases, but no improvement at all when $\phi(1,2) = 0^o$ or 180^o [10]. In a similar manner, the FBSS algorithm with $L = 7$ is seen to perform as well as or better than SS , with the variance also sinusoidally changing with signal phase.

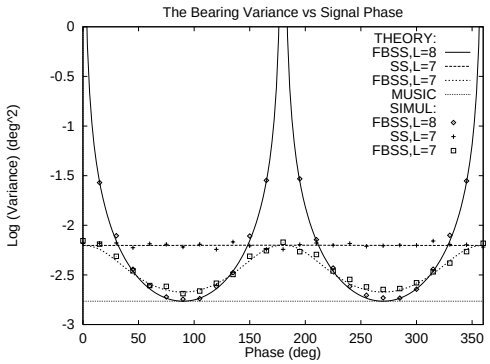

Figure 2: Comparison of variance of MUSIC, SS, FBS and FBSS techniques vs signal phase.

It seems likely that the variations in phase will affect the performance of the FBSS technique for larger numbers of signals. In figure 3, the FBSS algorithm with $L = 7$ is attempting to resolve three sources at 60^o, 120^o and 90^o. The phases of the first two sources at the centre of the ULA are varied with respect to that of the third source, which is fixed at 0^o.The theoretical variance is shown for the source at 120^o. When the relative phases of the three signals are 0^o or 180^o, the algorithm cannot restore the full rank of the signal matrix and the variance is seen to become very large. Of course, the variance of the SS algorithm with $L = 7$ is theoretically infinite for all signal phases.

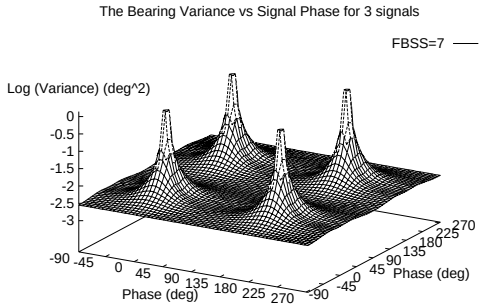

Figure 3: The Variance of FBSS with $L = 7$ for a source at bearing 120^o vs signal phase for 3 sources.

From the above discussion, it is clear that to resolve P sources with P subarrays, the FBSS algorithm is usually preferable to the SS technique. In addition, FBSS may resolve P sources using less than P subarrays, unlike the SS technique.

Conclusion The MUSIC algorithm performs robustly in the presence of uncorrelated signals and signals with small correlation factors. When the correlation factor tends towards one, the signal scenario resembles that of coherent multipath returns, or smart signal jamming. In the case of coherent signals, the MUSIC algorithm is unable to resolve the different bearings, even at high SNRs. In this case, an alternative approach, such as spatial smoothing, must be

used. The performance of two techniques, SS and FBSS, have been compared - the former depends on the source bearings and angular separations. The FBSS technique can considerably improve the performance of MUSIC for closely spaced sources, according to the relative signal phases.

Acknowledgements The sponsorship of this work by a SERC studentship and MoD CASE support is gratefully acknowledged.

References

[1] Schmidt R.O. "Multiple emitter location and signal parameter estimation." *IEEE Transactions on Antennas and Propagation*, Vol 34(3), pp276–280, March 1986.

[2] Haykin S., Reilly J.P., Kezys V., and Vertatschitsch E. "Some aspects of array processing." *IEE Proceedings Part F*, Vol 139(1), pp1–26, February 1992.

[3] Shan T., Wax M., and Kailath T. "On spatial smoothing for direction-of-arrival estimation of coherent signals." *IEEE Transactions on Acoustics, Speech and Signal Processing*, Vol 33(4), pp806–811, August 1985.

[4] Williams R.T., Prasad S., Mahalanabis A.K., and Sibul L.H. "An improved spatial smoothing technique for bearing estimation in a multipath environment." *IEEE Transactions on Acoustics, Speech and Signal Processing*, Vol 36(4), pp425–431, April 1988.

[5] Pillai S.U. and Byung H.K. "Forward/backward spatial smoothing techniques for coherent signal identification." *IEEE Transactions on Acoustics, Speech and Signal Processing*, Vol 37(1), pp8–14, January 1990.

[6] Stoica P. and Nehorai A. "Music,maximum likelihood, and Cramer-Rao bound." *IEEE Transactions on Acoustics,Speech and Signal Processing*, Vol 37(5), pp720–741, May 1989.

[7] Rao B.D. and Hari K.V.S. "Effect of spatial smoothing on the performance of music and the minimum norm method." *IEE Proceedings Part F*, Vol 137(6), pp449–458, December 1990.

[8] Brandwood D.H. "A complex gradient operator and its application in adaptive array theory." *IEE Proceedings Part F*, Vol 130(1), pp11–16, Feb 1983.

[9] Reddy V.U., Paulraj A., and Kailath T. "Performance analysis of the optimum beamformer in the presence of correlated sources and its behaviour under spatial smoothing." *IEEE Transactions on Acoustics, Speech and Signal Processing*, Vol 35(7), pp927–936, July 1987.

[10] Chang L .and Yeh C-C. "Resolution threshold for coherent sources using smoothed eigenstructure methods." *IEE Proceedings-F*, Vol 138(5), pp470–478, October 1991.

Performance of Spatial Smoothing Algorithms for Correlated Sources

John S. Thompson, Peter M. Grant and Bernard Mulgrew

Abstract— **The problem of identifying the angles of arrival of a set of plane waves impingeing on a narrow-band array of sensors, and related spectral analysis problems, have been addressed with a large number of algorithms. One of the most popular techniques is the multiple signal classification (MUSIC). The major shortcoming of the MUSIC algorithm is that it performs poorly when the sources are highly correlated. Fortunately, two algorithms exist to overcome this problem - spatial smoothing (SS) and forward-backward spatial smoothing (FBSS). The performance of the SS technique depends on signal bearings and spatial separation. For the same smoothing, FBSS can offer improved performance, but this depends on the signal phases. Numerical results for the variance of the algorithms are given to illustrate the points made.**

I. Introduction

One of the most popular algorithms for performing bearing estimation is the MUSIC algorithm[1]. Its attractiveness is due to the fact that it provides good resolution, whilst limiting the search for incoming signals to a single dimension. This is in contrast to maximum likelihood (ML) algorithms which generally involve an P–dimensional search to resolve P sources[2].

The main limitation of the MUSIC algorithm is that it performs poorly in the presence of highly correlated and coherent sources. In order to overcome this problem, it is possible to use techniques like ML, which still work in such situations. This negates all the advantages of using the MUSIC algorithm in the first place. Fortunately, two techniques exist to resolve correlated and coherent sources for uniform linear array geometries – the spatial smoothing (SS) algorithm[3] and the forward-backward spatial smoothing algorithm (FBSS)[4]. These methods modify the covariance matrix of data, so that the MUSIC algorithm can still be applied.

One method of analysing the effect of spatial smoothing techniques is to look at the variance of the bearing estimates produced by the MUSIC algorithm. Equations for this purpose have been derived in [5][6]. The variance equations are complex and hard to interpret in a simple fashion, so in this correspondence the condition number or eigenvalue ratio (EVR) of the resulting signal matrices will be analysed to obtain some insight into how smoothing techniques work. Numerical results are provided to compare the signal matrix EVR with the variance of the MUSIC algorithm.

The structure of this correspondence is as follows. Section II provides an introduction to the MUSIC algorithm and the equations that describe its performance. It will also look briefly at the effect of spatial smoothing techniques on the covariance matrix; section III will present some numerical results to illustrate the points made. Finally, section IV presents the conclusions for this correspondence.

Manuscript received ——; revised ——. The associate editor coordinating the review of this paper and approving it for publication was Prof Fu Li. This research was supported by a UK SHFRC CASE award and an MOD studentship.

The authors are with the Signals and Systems Group, Dept of Electrical Engineering, University of Edinburgh, Edinburgh, UK, EH9 3JL.

IEEE Log Number ——.

II. Principles of Direction of Arrival Estimation

A. Background

The problem that motivates the use of bearing estimation techniques is quite simple. There are P plane waves impingeing on a M–element array of known configuration. The receiver has access to a noise-corrupted data vector $\underline{y}(t) \in C^{M\times 1}$ seen at the array. In order to determine the bearings of the P incoming signals, the underlying model that generates the available data is assumed to be of the form:

$$\underline{y}(t) = A(\underline{\Theta})\underline{s}(t) + \underline{n}(t) \tag{1}$$

The vector $\underline{n}(t) \in C^{M\times 1}$ contains the M zero-mean Gaussian white noise processes of variance σ^2 that corrupt the data and $\underline{s}(t) \in C^{P\times 1}$ is the vector of the P signal amplitudes. The vector $\underline{\Theta} \in R^{P\times 1}$ contains the P bearings of interest and the matrix $A(\underline{\Theta}) \in C^{M\times P}$ is made up as shown:

$$A = [\underline{a}(\theta_1), \underline{a}(\theta_2), \ldots, \underline{a}(\theta_P)] \tag{2}$$

where the parameters $\{\theta_p\}$ are the bearings of the P signals, while the "steering" vector $\underline{a}(\theta) \in C^{M\times 1}$ is the impulse response of the array to direction θ.

B. The MUSIC Algorithm

Algorithms that perform bearing estimation are required to make some assumptions about the incoming data, so that it conforms to the model in equation (1) and the problem is tractable. There are P narrow–band plane wave signals impingeing on an M element linear array, where $M > P$. The data from each array element is assumed to be corrupted by Gaussian white noise of zero mean and variance σ^2. The signals and noise are ergodic random processes with zero mean and are assumed to be mutually uncorrelated. For the purposes of the MUSIC algorithm, all the arriving signals are assumed to be uncorrelated. These assumptions are the same as those made in [3], for example.

In practice, one has access to N snapshots of the noisy signal vector $\underline{y}(t)$, from which a covariance matrix $\hat{R} \in C^{M\times M}$ is calculated. The mean of $\hat{R}$ is given by:

$$E[\hat{R}] = E[\underline{y}(t)\underline{y}(t)^H] = R = ASA^H + \sigma^2 I_M \tag{3}$$

where A^H denotes the Hermitian transpose of A, I_M is the $M \times M$ identity matrix and the signal matrix $S = E[\underline{s}(t)\underline{s}^H(t)]$. The covariance matrix $\hat{R}$ may be utilised to generate a power density spectrum for all bearings of interest and the peaks of the spectrum identify the bearings of the signals present. The expansion of R in equation (3) shows that the eigenvalues of R ordered by decreasing size, $\lambda_i(R)$, are given by the expression $\lambda_i(R) = \lambda_i(X) + \sigma^2$, where the matrix $X = ASA^H$. Provided all the signals are mutually uncorrelated, the matrix S is of rank P, so the P largest eigenvalues are the sum of the signal and noise power. These eigenvalues and their associated eigenvectors correspond to the incoming signals and they form the "signal subspace".

If $i > P$, $\lambda_i(X) = 0$ and so the smallest $M - P$ eigenvectors of R are "noise" eigenvectors whose eigenvalues are equal to σ^2. Their only property of interest is that they form a "noise subspace" which is orthogonal to the signal subspace. This means that each noise eigenvector is orthogonal to every steering vector in the matrix A. The MUSIC algorithm exploits this property to locate signals by determining which bearings have the smallest projection on the noise subspace. The following equation is used to generate the power density spectrum:

$$\mathrm{MUS}(\theta) = \frac{1}{\underline{a}^H(\theta) E_n E_n^H \underline{a}(\theta)} \tag{4}$$

where $E_n \in C^{M \times M-P}$ is the matrix of column noise eigenvectors.

One problem with the MUSIC algorithm is that the number of signals present must be estimated in order to determine the rank of the noise subspace. This may be done by an examination of the eigenvalues, or by the use of a model order algorithm[2][7]. This paper will assume that the number of signals present has been determined correctly.

C. Spatial Smoothing Algorithms

One assumption made above states that the incoming signals are mutually uncorrelated over the time of observation. If all the signals present originate from different transmitters or are modulated with different data streams they will only be partially correlated. However, if they result from multipath responses from the same transmitter, the signals are "coherent" and the assumption is invalid.

The signal subspace is always spanned by the the vectors present in the matrix A. However, if the signals are coherent, the matrix S becomes singular, so that some of its eigenvalues are zero. This means that part of the signal subspace is indistinguishable from the noise subspace. As a result, the observed noise subspace is no longer orthogonal to the steering vectors in the matrix A and the MUSIC algorithm fails.

To overcome these problems, a technique called spatial smoothing(SS)[3] has been developed to allow the MUSIC algorithm to be applied to the coherent signal case. The algorithm was originally designed only for uniform linear array (ULA) geometries. The basic idea is to form covariance matrices from subsets of the array - which is equivalent to partitioning the original covariance matrix. If there are K subarrays, each subarray is of size $L = M - K + 1$ and the partition or submatrix for the k^{th} subarray is the matrix $F(k)RF(k)^T$. The matrix $F(k) \in C^{L \times M}$ is defined by:

$$F(k)_{ij} = \begin{cases} 1 & \text{if } j = i + k - 1 \text{ and } 1 \le i \le L \\ 0 & \text{otherwise} \end{cases} \tag{5}$$

The notation F_{ij} denotes the i^{th} row and j^{th} column element of the matrix F. The partitioned matrices are used to form a smoothed matrix $R_S \in C^{L \times L}$, which is calculated as follows:

$$R_S = \frac{1}{K} \sum_{k=1}^{K} F(k) R F(k)^T \tag{6}$$

where $F(k)^T$ denotes the transpose of $F(k)$. Clearly, the size of the covariance matrix and thus the performance of the MUSIC algorithm is traded for the ability to resolve coherent sources. In order to resolve P coherent sources, an array containing at least $2P$ elements is required. In a similar way, it is very simple to show[8] that to resolve P coherent sources, it is required to average over at least P independent submatrices.

Soon afterwards, it was reported[4] that an additional technique called forward-backward spatial smoothing (FBSS) can be used to improve performance. The FBSS technique applies forward–backward smoothing (FBS) to the forward and backward covariance matrices R_F and R_B to form a matrix R_{ave} as shown:

$$R_{ave} = \frac{1}{2}(R_F + R_B) = \frac{1}{2}(R + JR^*J)$$

$$= \frac{1}{2}(R + \begin{bmatrix} 0 & \dots & 0 & 1 \\ 0 & \dots & 1 & 0 \\ \vdots & \ddots & \vdots & \vdots \\ 1 & \dots & 0 & 0 \end{bmatrix} R^* \begin{bmatrix} 0 & \dots & 0 & 1 \\ 0 & \dots & 1 & 0 \\ \vdots & \ddots & \vdots & \vdots \\ 1 & \dots & 0 & 0 \end{bmatrix}) \tag{7}$$

where R^* denotes the complex conjugate of R. The matrix R_{ave} is then spatially smoothed as required to form the FBSS matrix $R_{F/B}$.It has been shown[4][9] that to resolve P coherent sources, as little as $3P/2$ array elements may be required to restore the rank of S. However, there are some situations where FBSS behaves in the exactly the same manner as the SS technique: in these cases $2P$ array elements are still required. A geometrical interpretation of the two techniques is shown in figure 1. The SS algorithm forms sub–matrices by working in the forward direction only, while FBSS uses sub–matrices from both directions.

D. Statistical Analysis of the MUSIC Algorithm

Determining the performance of the MUSIC algorithm, with or without spatial smoothing techniques applied, has been the subject of several papers in the last few years. There are two main approaches to this subject.

The first method is to determine a resolvability criterion for the MUSIC algorithm[10–12] – that is to find the conditions under which two closely spaced sources will be resolved as two separate peaks, rather than combining to form one peak. However, this type of analysis is usually restricted to the case of two sources and will not be considered in this paper.

A more general technique for analysing the MUSIC algorithm is to derive an equation for the variance of the signal peaks of the MUSIC spectrum[5][13][14]. One useful form of the variance equation for the unsmoothed MUSIC algorithm is given in [5]. Denoting the error in the estimate of the bearing of the x^{th} signal as $\delta\theta_x$, the asymptotic variance of that error is given by the equation:

$$E[\delta\theta_x^2] = \frac{\sigma^2}{N d_\theta(\theta_x)} \{ [S^{-1}]_{xx} + \sigma^2 [S^{-1}(A^H A)^{-1} S^{-1}]_{xx} \} \tag{8}$$

The scalar value $d_\theta(\theta)$ is given by the matrix product $2\{\underline{d}^H(\theta) E_n E_n^H \underline{d}(\theta)\}$, where $\underline{d}(\theta)$ is the Brandwood vector derivative of $\underline{a}(\theta)$[15]. S^{-1} denotes the matrix inverse of S. For large values of the signal-to-noise-ratio (SNR) with mutually uncorrelated sources, the variance is inversely proportional to the SNR of the desired source. However, as the correlation between the sources increases the matrix S^{-1} becomes ill-conditioned and the variance can become very large.

The equivalent equation for the MUSIC algorithm combined with spatial smoothing techniques is more complex. The results have been obtained by Rao and Hari[6] and for spatial smoothing the equation is:

$$E[\delta\theta_x^2] = \frac{2}{d_\theta(\theta_x)^2 N K^2} [\sum_{p,q=1}^{K} \underline{\beta}^H R(p,q) \underline{\beta} \; \underline{\alpha}^H N(q,p) \underline{\alpha}$$

$$+ Re\{\sum_{p,q=1,p\neq q}^{K} \underline{\beta}^H N(p,q)\underline{\alpha}\ \underline{\beta}^H N(q,p)\underline{\alpha}\}] \quad (9)$$

where Re denotes the real part of a complex value. The matrix $R(p,q)$ is given by $F(p)RF(q)^T$, $\underline{\alpha}$ and $\underline{\beta}$ are defined as:

$$\underline{\alpha} = E_n E_n^H \underline{d}_S(\theta_x) \quad \text{and} \quad \underline{\beta} = U_S \Lambda_S^{-1} U_S^H \underline{a}_S(\theta_x) \quad (10)$$

The matrix $U_S \in C^{L\times P}$ contains the P signal eigenvectors of the smoothed covariance matrix R_S, $\Lambda_S \in R^{P\times P}$ is a diagonal matrix containing the P smoothed signal eigenvalues. The matrix $N(p,q)$ is defined in a similar way to $R(p,q)$ with $N(p,q) = \sigma^2 F(p)F(q)^T$. The vector $\underline{a}_S$ is the steering vector for the smoothed array and $\underline{d}_S$ is its derivative. It has been noted[6], that the second part of equation (9) becomes very small compared to the first part at high SNRs. The vector $\underline{\beta}$ may be expressed as:

$$\underline{\beta} = (A_S^+)^H S_S^{-1} \underline{i}_x \quad (11)$$

where S_S is the smoothed signal matrix and A_S is the matrix of smoothed steering vectors. The vector $\underline{i}_x \in C^{1\times P}$ is the x^{th} column of the identity matrix I_P, and the notation A^+ denotes the pseudo-inverse of A. Expanding the matrix $R(p,q)$ as $F(p)ASA^HF^T(q) + N(p,q)$, equation (9) may be written as:

$$E[\delta\theta_x^2] = \frac{\sigma^2}{NKd_\theta(\theta_x)}\{[S_S^{-1}]_{xx} + \sigma^2[S_S^{-1}(A_S^HA_S)^{-1}S_S^{-1}]_{xx}\}$$

$$+\frac{2}{d_\theta(\theta_x)^2NK^2}(\sum_{p,q=1,p\neq q}^{K}[\{S_S^{-1}B(p,\underline{\Theta})^HSB(q,\underline{\Theta})S_S^{-1}\}_{xx}$$

$$\times\underline{\alpha}^HN(q,p)\underline{\alpha}] + \underline{\beta}^HN(p,q)\underline{\beta}\ \underline{\alpha}^HN(q,p)\underline{\alpha}$$

$$+ Re\{\underline{\beta}^HN(p,q)\underline{\alpha}\ \underline{\beta}^HN(q,p)\underline{\alpha}\}) \quad (12)$$

where $B(q,\Theta) \in C^{P\times P}$ is a diagonal matrix, given by:

$$B(q,\Theta) = A^HF(q)^T(A_S^+)^H = \begin{bmatrix} b_1 & 0 & \dots & 0 \\ 0 & b_2 & \dots & 0 \\ \vdots & \vdots & \ddots & \vdots \\ 0 & \dots & 0 & b_P \end{bmatrix} \quad (13)$$

The p^{th} diagonal entry of B, b_p, depends on the phase shift between the steering vectors $\underline{a}^H(\theta_P)F(q)^T$ and $\underline{a}_S^H(\theta_P)$. For the FBSS case, the matrix S_S would be replaced by the equivalent signal matrix $S_{F/B}$ in the equations above. The first term of equation (12) is equivalent to equation (8) and the other terms are cross terms to compensate for the formation of R_S from partitions of R.

E. Analysis of the Covariance Matrix

Equations (8) and (12) explicitly show that the performance of the MUSIC algorithm with or without smoothing techniques is proportional to entries of the inverse matrices of S, S_S or $S_{F/B}$. Therefore, if one looks at what the smoothing techniques do to the eigenvalues of these matrices, it should be possible to explain the major effects observed in the behaviour of the MUSIC algorithm. In the analysis of the matrix eigenvalues, a useful criterion is the condition or eigenvalue ratio (EVR), which is defined to be:

$$\text{EVR} = \frac{\lambda_{max}}{\lambda_{min}} \quad (14)$$

where λ_{min} and λ_{max} represent the smallest and the largest eigenvalues, respectively, of the given matrix. To make legitimate comparisons, the received signal powers should be kept constant: other parameters such as signal bearings and phase may then be varied to see the effect on the EVR. If the EVR is small, the columns of S and hence the underlying signals are approximately uncorrelated, which suggests MUSIC will perform well. If the EVR is large, the matrix is close to being singular and MUSIC will perform poorly. In terms of the variance equations, the scalar value $(1/\lambda_{min})$ is the largest eigenvalue of S^{-1}: the more ill-conditioned the S matrix is, the larger the variance of the MUSIC bearing estimates.

Similarly, the variance equations involve the inverse of the matrix A^HA (or $A_S^HA_S$), which is altered as the source bearings change. When the sources are sufficiently spaced, the off-diagonal terms of this matrix are small, so that the eigenvalues are all approximately unity. However, when the sources are closely spaced, the off-diagonal terms become large and the EVR of A^HA becomes very large.

In the general case of P coherent sources, the matrix S is of the form:

$$S = \begin{bmatrix} s_1^2 & s_1s_2e^{j\phi(1,2)} & \dots & s_1s_Pe^{j\phi(1,P)} \\ s_1s_2e^{-j\phi(1,2)} & s_2^2 & \dots & s_2s_Pe^{j\phi(2,P)} \\ \vdots & \vdots & \ddots & \vdots \\ s_1s_Pe^{-j\phi(1,P)} & s_2s_Pe^{-j\phi(2,P)} & \dots & s_P^2 \end{bmatrix} \quad (15)$$

The amplitude of the p^{th} source is denoted as s_p and the scalar $\phi(i,j)$ indicates the phase at the reference sensor between sources i and j. For the rest of this correspondence, the reference for the phases $\phi(i,j)$ will be placed at the centre of the ULA.

E.1 Spatial Smoothing

For spatial smoothing, K sub-matrices R_k are formed from L element subarrays and are averaged to form a smoothed covariance matrix R_S. The reference for the smoothed steering vector $\underline{a}_S(\theta)$ will be defined to be at the centre of the array, so that:

$$\underline{a}_S(\theta) = [e^{-j(\frac{L-1}{2})\pi\cos(\theta)}, e^{-j(\frac{L-3}{2})\pi\cos(\theta)}, \dots, e^{j(\frac{L-1}{2})\pi\cos(\theta)}]^T \quad (16)$$

This definition may be used in combination with results from[16]to show that the i^{th} row and j^{th} column entry of the smoothed signal matrix S_S is given by:

$$(S_S)_{ij} = s_is_je^{j\phi(i,j)}\frac{1}{K}\sum_{k=0}^{K-1} e^{-j(((K-1)/2)+k)\pi(cos(\theta_i)-cos(\theta_j))} \quad (17)$$

The summation term is real for both even and odd L: it will be denoted as c below. The behaviour of this cross-correlation value has been analysed extensively in [16]. The magnitude of $(S_S)_{ij}$ generally decreases as K increases, so that the EVR of S_S will also improve. The rate of the decrease in c with K depends on the source bearings and their separation. For the simple case of two sources, the matrix S_S is given by:

$$S_S = \begin{bmatrix} s_1^2 & s_1s_2ce^{j\phi(1,2)} \\ s_1s_2ce^{-j\phi(1,2)} & s_2^2 \end{bmatrix} \quad (18)$$

The eigenvalues of the smoothed signal matrix S_S are given by:

$$\det(S_S - \lambda I_2) = 0 \tag{19}$$

This equation leads to a quadratic equation in λ: applying the formula for the roots of a quadratic equation gives:

$$\lambda = \frac{(s_1^2 + s_2^2)}{2} \pm \frac{1}{2}\sqrt{(s_1^4 + s_2^4 + 2s_1^2 s_2^2(2c^2 - 1)} \tag{20}$$

The eigenvalues of S_S depend on the value c. If If c is close to one, λ has roots near 0 and $(s_1^2 + s_2^2)$: if c is small, the eigenvalues are close to s_1^2 and s_2^2. It is useful to note that the eigenvalues do not depend on the phase term $\phi(1,2)$, which suggests that varying the signal phases will not significantly affect the variance of the SS algorithm.

E.2 Forward–backward Spatial Smoothing

To simplify the analysis of forward-backward spatial smoothing, spatial smoothing is applied as before. The forward-backward smoothing may be applied to the resulting forward and backward matrices to form the final covariance matrix, $R_{F/B}$. Thus:

$$\begin{aligned} R_{F/B} &= \frac{1}{2}(R_S + JR_S^* J) \\ &= \frac{1}{2}(A_S S_S A_S^H + JA_S^* S_S^* A_S^T J) + \sigma^2 I \\ &= \frac{1}{2}(A_S[S_S + S_S^*]A_S^H) + \sigma^2 I \\ &= A_S S_{F/B} A_S^H + \sigma^2 I \end{aligned} \tag{21}$$

The third line of the above formula follows because $JQ^* = Q$, etc. Therefore, the value of $(S_{F/B})_{ij}$ is given by:

$$(S_{F/B})_{ij} = (S_S)_{ij} + (S_S^*)_{ij} = s_i s_j c \cos\phi(i,j) \tag{22}$$

The magnitude of the cross-correlation term can lie between $s_i s_j c$ and zero, depending on the relative signal phase $\phi(i,j)$. In the case of two sources, $S_{F/B}$ is given by:

$$S_{F/B} = \begin{bmatrix} s_1^2 & s_1 s_2 c\cos\phi(1,2) \\ s_1 s_2 c\cos\phi(1,2) & s_2^2 \end{bmatrix} \tag{23}$$

Solving the eigenvalue equation as before gives the values of λ:

$$\lambda = \frac{(s_1^2 + s_2^2)}{2} \pm \frac{1}{2}\sqrt{(s_1^4 + s_2^4 + 2s_1^2 s_2^2[2c^2\cos^2(\phi(1,2)) - 1])} \tag{24}$$

For two coherent signals, the variance of the FBSS method clearly depends on the relative signal phase $\phi(1,2)$. If $\phi(1,2) = 0^\circ, 180^\circ$, the matrix $S = S^*$, so the off-diagonal terms of $S_{F/B}$ are not cancelled, leaving the EVR identical to the spatial smoothing case. This means the error variance will be the same as for spatial smoothing. Alternatively, if $\phi(1,2) = 90^\circ, 270^\circ$ radians, the off-diagonal terms of $S_{F/B}$ cancel completely, so that the EVR reaches a minimum. The improvement that may be offered by FBSS depends on how well SS alone has reduced the magnitude of the correlation c. Similarly, for the FBS algorithm alone, the performance of the MUSIC algorithm can be improved, except in the case where $\phi(1,2) = 0^\circ, 180^\circ$[12].

In general, the EVR of a forward–backward smoothed covariance matrix is less than or equal to that of the original smoothed or unsmoothed covariance matrix[6]. Depending on the signal phases, the FBSS algorithm can offer significant improvements in scenarios where spatial smoothing has failed to reduce signal correlation, particularly when signals are closely spaced.

The phase dependence of the FBSS algorithm means that in some cases, FBSS with $(P/2)$ subarrays is insufficient to restore the full rank of the signal matrix $S_{F/B}$[4]. Indeed, if all the relative phase terms $\phi(i,j)$ are 0° or 180°, the algorithm performs in the same manner as SS with the same subarray size L. However, this is an extreme case: applying FBS to a spatially smoothed covariance matrix usually improves the performance of the MUSIC algorithm and in some cases, FBSS may be able to resolve the same number of sources using a larger subarray size than SS. Where the number of sources is larger than half the number of antenna elements, it provides the only opportunity to resolve all the sources.

III. Results and Discussion

In this section, the equations quoted for the MUSIC algorithm and for the spatial smoothing techniques will be applied to particular scenarios to illustrate the points made in the analysis of spatially smoothed covariance matrices. It should be pointed out, however, that equation (9) is very complex and the above analysis is only intended to explain the major effects observed in the behaviour of SS/FBSS. In all the simulations the number of elements M in the uniform linear array was eight and each signal's SNR was set to be 17dB. All signals were generated using complex exponentials of constant amplitude and one hundred snapshots were used to form covariance matrices in each case.

Figures 2 and 3 show the effect of signal correlation on the variance and the S matrix EVR for various algorithms. There are two sources, the first at a bearing of 90° (which is defined to be perpendicular to the array) and the second at 60°. The correlation between the two sources is varied from zero to one and the variance plots are all for the first source, though the variance of the other source behaves in a similar manner. It is noticeable that behaviour of the EVR curves in figure 3 is similar to that of the variance curves in figure 2. However, it should be pointed out that it is only meaningful to compare EVR graphs whose subarray size, L, is the same.

The spatial smoothing algorithm, formed from two submatrices ($K = 2$) so that the subarray size $L = 7$, is reasonably robust to signal correlation, although in this case the FBS algorithm with $L = 8$ out-performs it at low signal correlation. The performance of the FBS algorithm is less clear-cut for high correlations. The best possible outcome occurs when the relative signal phase is 90° as shown on the graph. The variance for a relative signal phase of 30° is also shown: it is inferior to the previous curve, but better than that for a phase shift of 0°, where FBS cannot reduce the signal correlation so it gives the same performance as for MUSIC without FBS. The fact that the variance depends considerably on the relative signal phases means that the variance curve for a given phase can lie anywhere in the region spanned by the three curves.

The next two figures, 4 and 5, shows the effect of angular separation on SS, FBS, FBSS with two coherent sources and MUSIC with two uncorrelated sources. The first source is at a bearing of 90° and the bearing of the second source is chosen to give the correct angular separation. The variance of the 90° source is plotted only for angular separations up to 80°: as the bearing of the second source approaches 0° or 180°, "endfire" effects mean that the variance of the bearing estimate increases without bound. The EVR of the matrix $A^H A$ has been plotted for L=8 in figure 5 (denoted AhA) to show its effect on the MUSIC algorithm. The EVR of $A^H A$ and thus the variance

of the MUSIC algorithm is large for closely spaced sources, as one would expect, but reduces to an approximately constant level for an angular separation of greater than 10^o or so. The reference sensor was set at one end of the ULA, so that the relative phase of the two signals at the middle of the array changes. This emphasises the relative phase dependence of the FBS algorithm. As expected from the analysis, the performance of FBS is oscillating between that of MUSIC with no signal correlation and MUSIC with a correlation factor of 1 - ie infinite EVR and variance.

The SS algorithm with $L = 7$ improves more slowly than the MUSIC algorithm with no correlation, as the signal separation is increased. This is because the EVR of both the matrix S and the matrix A depend on signal separation. The FBSS technique with $L = 7$ generally performs better than SS and for closely spaced sources the variance can be improved a lot according to the relative signal phase.

Figures 6 and 7 show the effect of signal phase on the performance of SS, FBS, FBSS algorithms and MUSIC (with zero correlation). The two sources are at 96^o and 78^o and their relative phase at the centre of the ULA varies from $0 - 360^o$. The variance is plotted for the source at 96^o and the performance of the SS algorithm with $L = 7$ is approximately constant with the signal phase. The FBS technique is again shown to provide improved performance for some signal phases – the sinusoidal variation in the eigenvalues show up in the EVR of the S matrix and in the variance curve. This type of behaviour is also shown in the results of Chang and Yeh[12]. In a similar manner, the FBSS algorithm with $L = 7$ is seen to perform as well as or better than SS, with the variance also sinusoidally changing with signal phase.

The analysis of FBSS in the previous section showed that its performance will normally be as good as or better than SS with the same amount of spatial smoothing and this is demonstrated in these results. Similarly, FBSS with less than P subarrays for P coherent sources (in the case of figures 6 and 7, simply the FBS technique with $L = 8$) still has some chance of resolving the sources, unlike the SS algorithm.

It seems likely that the variations in phase will affect the performance of the FBSS technique for larger numbers of signals, and this effect is shown in figures 8 and 9. In the figure 8, the FBSS algorithm with $L = 7$ is attempting to resolve three sources at 60^o, 120^o and 90^o. The phases of the first two sources at the centre of the ULA are varied with respect to that of the third source, which is fixed at 0^o.The theoretical variance is shown for the source at 120^o. When the relative phases of the three signals are 0^o or 180^o, the algorithm cannot restore the full rank of the signal matrix and the variance is seen to rise towards infinity. A similar effect is shown in the figure 9. In this case, four signals are impinging on the array from bearings 60^o, 120^o, 80^o and 100^o. The phases of the first two sources are varied with respect to those of the second two sources, which are both fixed at 0. The theoretical variance shown is for the source at 80^o. Here the situation is more complex: if the relative phases of three of more sources coincide at 0 or 180^o, the variance of those sources will again rise to infinity. In both cases, there is a reasonable statistical chance of resolving all sources, but where FBSS with $L = 7$ fails, the amount of smoothing required for FBSS must be increased towards that required by SS.

The number of subarrays required in SS/FBSS algorithms to minimise the variance of the MUSIC algorithm is an interesting problem. Figure 10 shows the variance of spatial smoothing for different numbers of subarrays vs signal separation. As in figure 4, the first source is at 90^o and the bearing of the other source is varied to obtain the correct angular separation. In this case, there is little difference in performance for the different subarray sizes in general. For closely spaced sources, it seems that the improvement in the condition of S obtained by increasing K is cancelled out by the smaller effective array size. No single array size performs significantly better than all the others under all conditions, so it seems simplest to pick one subarray size that performs reasonably well, such as $L = 7$.

From the above analysis, it is clear that to resolve P sources with P subarrays, the FBSS algorithm is usually preferable to the SS technique. In addition, FBSS may resolve P sources using less than P subarrays, unlike the SS technique.

IV. Conclusion

The MUSIC algorithm performs robustly in the presence of uncorrelated signals and signals with small correlation factors. When the correlation factor tends towards one, the signal scenario resembles that of coherent multipath returns, or smart signal jamming. In the case of coherent signals, the MUSIC algorithm is unable to resolve the different bearings, even at high SNRs. In this case, an alternative approach, such as spatial smoothing, must be used.

The performance of spatial smoothing techniques has been qualitatively linked to the eigenvalue ratio of the signal matrix S. The performance of spatial smoothing depends on the bearings and separation of the sources. The FBSS algorithm with the same smoothing as SS has the potential to provide better estimates of the source bearings, depending on the relative signal phases. In some cases, the FBSS can resolve P sources with less than P subarrays, unlike the SS technique. Theoretical and simulation results have been presented to confirm these points.

References

[1] R.O. Schmidt, "Multiple emitter location and signal parameter estimation." *IEEE Transactions on Antennas and Propagation*, Vol 34(3), pp276–280, March 1986.

[2] S. Haykin, J.P. Reilly, V. Kezys, and E. Vertatschitsch, "Some aspects of array processing." *IEE Proceedings Part F*, Vol 139(1), pp1–26, February 1992.

[3] T. Shan, M. Wax, and T. Kailath, "On spatial smoothing for direction-of-arrival estimation of coherent signals." *IEEE Transactions on Acoustics, Speech and Signal Processing*, Vol 33(4), pp806–811, August 1985.

[4] R.T. Williams, S. Prasad, A.K. Mahalanabis, and L.H. Sibul, "An improved spatial smoothing technique for bearing estimation in a multipath environment." *IEEE Transactions on Acoustics, Speech and Signal Processing*, Vol 36(4), pp425–431, April 1988.

[5] P. Stoica and A. Nehorai, "Music,maximum likelihood, and Cramer-Rao bound." *IEEE Transactions on Acoustics,Speech and Signal Processing*, Vol 37(5), pp720–741, May 1989.

[6] B.D. Rao and K.V.S. Hari, "Effect of spatial smoothing on the performance of music and the minimum norm method." *IEE Proceedings Part F*, Vol 137(6), pp449–458, December 1990.

[7] T. Shan, A. Paulraj, and T. Kailath, "On smoothed rank profile tests in eigenstructure methods for directions-of-arrival estimation." *IEEE Transactions on Acoustics, Speech and Signal Processing*, Vol 35(10), pp1377–1385, October 1987.

[8] J.S. Thompson, P.M. Grant, and B. Mulgrew, "Correspondence:generalised algorithm for DOA estimation in a passive sonar." *IEE Proceedings Part F*, Vol 140(5), pp339–340, October 1993.

[9] S.U. Pillai and H.K. Byung, "Forward/backward spatial smoothing techniques for coherent signal identification." *IEEE*

Transactions on Acoustics, Speech and Signal Processing, Vol 37(1), pp8–14, January 1989.

[10] M. Kaveh and A.J. Barabell, "The statistical performance of the music and the minimum-norm algorithms in resolving plane waves in noise." *IEEE Transactions on Acoustics,Speech and Signal Processing*, Vol 34(2), pp331–340, April 1986.

[11] S.U. Pillai and H.K. Byung, "Performance analysis of music-type high-resolution estimators for direction finding in correlated and coherent sources." *IEEE Transactions on Acoustics, Speech and Signal Processing*, Vol 37(8), pp1176–1189, August 1989.

[12] L. Chang and C. Yeh, "Resolution threshold for coherent sources using smoothed eigenstructure methods." *IEE Proceedings Part F*, Vol 138(5), pp470–478, October 1991.

[13] B. Porat and B. Friedlander, "Analysis of the asymptotic relative efficiency of the music algorithm." *IEEE Transactions on Acoustics,Speech and Signal Processing*, Vol 36(4), pp532–543, April 1988.

[14] A.J. Weiss and B. Friedlander, "Performance analysis of spatial smoothing with interpolated arrays." *IEEE Transactions on Signal Processing*, Vol 41(5), pp1881–92, May 1993.

[15] D.H. Brandwood, "A complex gradient operator and its application in adaptive array theory." *IEE Proceedings Part F*, Vol 130(1), pp11–16, Feb 1983.

[16] V.U. Reddy, A. Paulraj, and T. Kailath, "Performance analysis of the optimum beamformer in the presence of correlated sources and its behaviour under spatial smoothing." *IEEE Transactions on Acoustics, Speech and Signal Processing*, Vol 35(7), pp927–936, July 1987.

Figure Titles

Figure 1: Forward-backward spatial smoothing.
Figure 2: Comparison of variance of MUSIC, SS and FBS techniques vs signal correlation.
Figure 3: Comparison of the signal matrix EVR of MUSIC, SS and FBS techniques vs signal correlation.
Figure 4: Comparison of variance of MUSIC, SS, FBS and FBSS techniques vs angular separation.
Figure 5: Comparison of the signal matrix EVR of MUSIC, SS, FBS and FBSS techniques and the EVR of the matrix $A^H A$ with $L = 8$ vs angular separation.
Figure 6: Comparison of variance of MUSIC, SS, FBS and FBSS techniques vs signal phase.
Figure 7: Comparison of the signal matrix EVR of MUSIC, SS, FBS and FBSS techniques vs signal phase.
Figure 8: The Variance of FBSS with $L = 7$ for a source at bearing 120^o vs signal phase for 3 sources.
Figure 9: The Variance of FBSS with $L = 7$ for a source at bearing 80^o vs signal phase for 4 sources.
Figure 10: Comparison of variance of Spatial Smoothing vs angular separation.

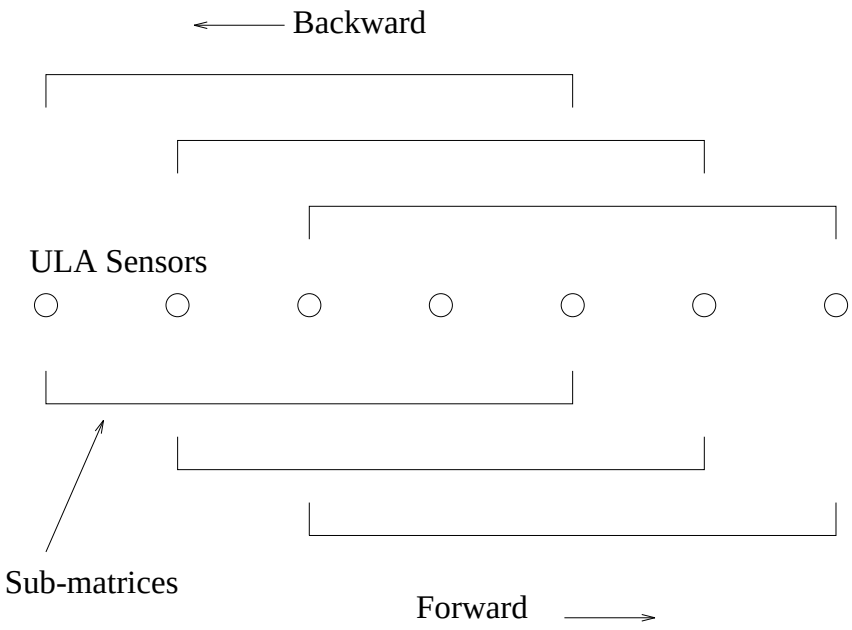
Backward
ULA Sensors
Sub-matrices
Forward

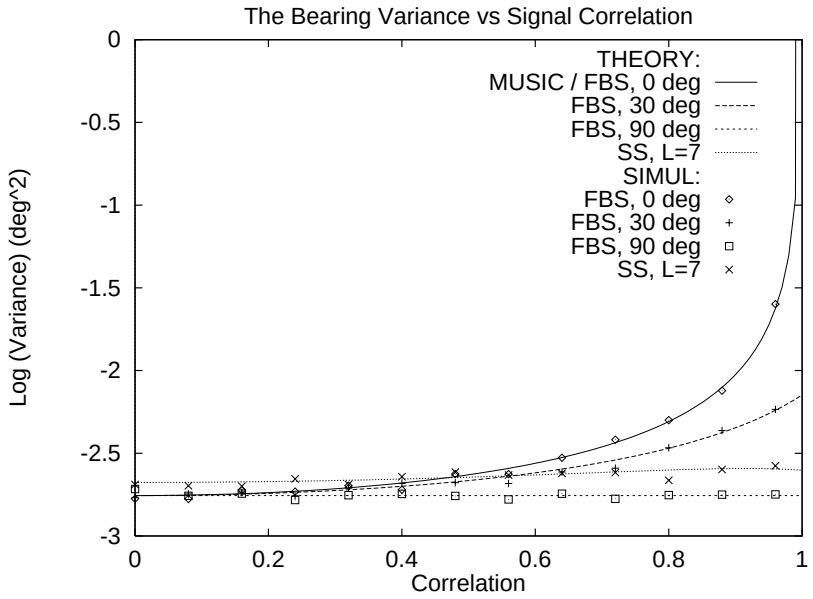
The Bearing Variance vs Signal Correlation
Log (Variance) (deg^2)
Correlation
0
-0.5
-1
-1.5
-2
-2.5
-3
0
0.2
0.4
0.6
0.8
1
THEORY:
MUSIC / FBS, 0 deg
FBS, 30 deg
FBS, 90 deg
SS, L=7
SIMUL:
FBS, 0 deg
FBS, 30 deg
FBS, 90 deg
SS, L=7

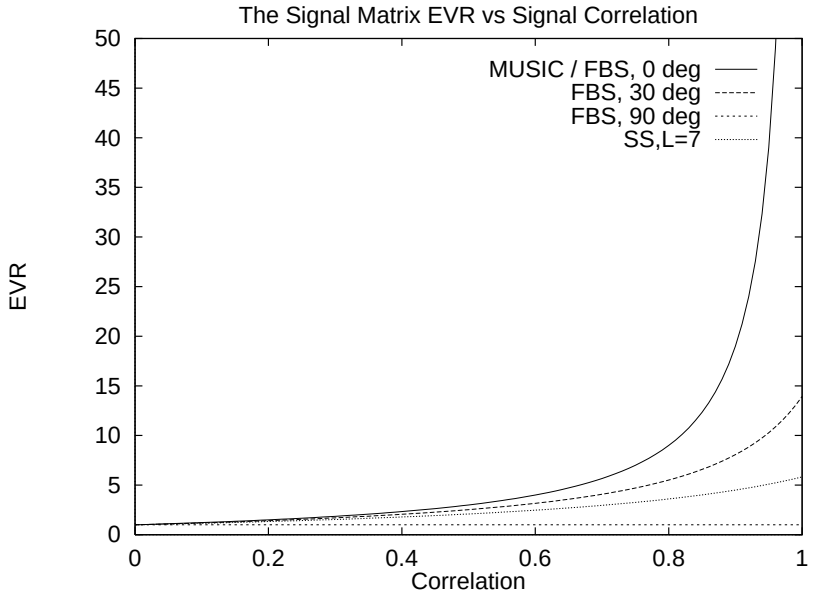
The Signal Matrix EVR vs Signal Correlation
MUSIC / FBS, 0 deg
FBS, 30 deg
FBS, 90 deg
SS,L=7
EVR
Correlation
0
5
10
15
20
25
30
35
40
45
50
0
0.2
0.4
0.6
0.8
1

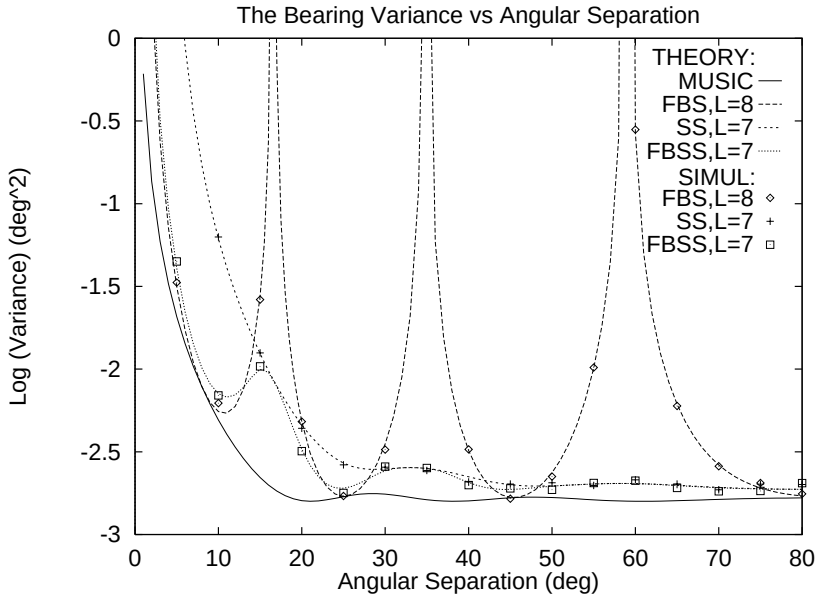
The Bearing Variance vs Angular Separation
THEORY:
MUSIC
FBS,L=8
SS,L=7
FBSS,L=7
SIMUL:
FBS,L=8
SS,L=7
FBSS,L=7
Log (Variance) (deg^2)
Angular Separation (deg)
0
-0.5
-1
-1.5
-2
-2.5
-3
0
10
20
30
40
50
60
70
80

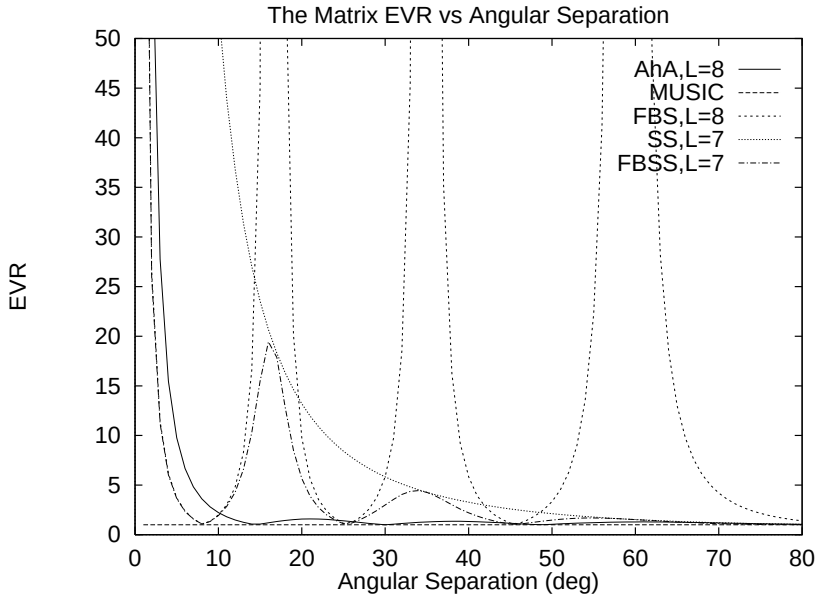
The Matrix EVR vs Angular Separation
EVR
Angular Separation (deg)
AhA,L=8
MUSIC
FBS,L=8
SS,L=7
FBSS,L=7
0
5
10
15
20
25
30
35
40
45
50
0
10
20
30
40
50
60
70
80

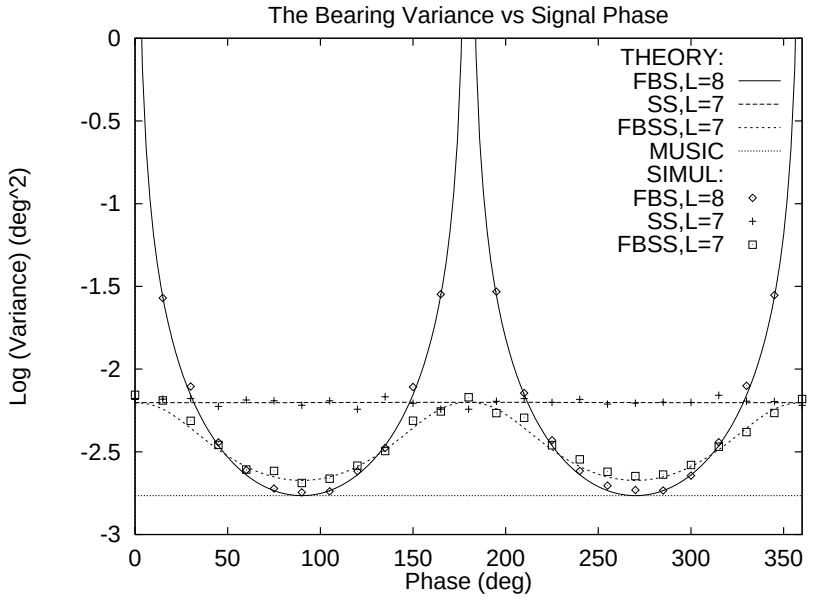
The Bearing Variance vs Signal Phase
Log (Variance) (deg^2)
Phase (deg)
THEORY:
FBS,L=8
SS,L=7
FBSS,L=7
MUSIC
SIMUL:
FBS,L=8
SS,L=7
FBSS,L=7
0
-0.5
-1
-1.5
-2
-2.5
-3
0
50
100
150
200
250
300
350

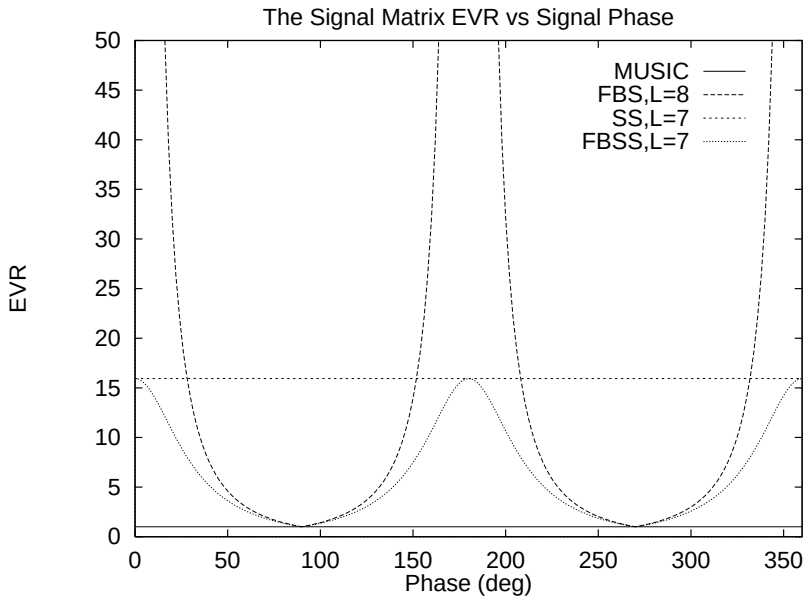
The Signal Matrix EVR vs Signal Phase
MUSIC
FBS,L=8
SS,L=7
FBSS,L=7
EVR
Phase (deg)
0
5
10
15
20
25
30
35
40
45
50
0
50
100
150
200
250
300
350

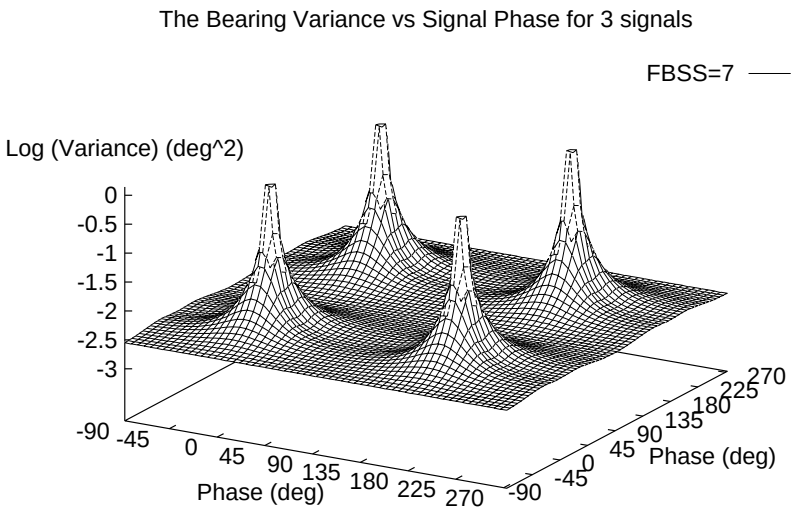
The Bearing Variance vs Signal Phase for 3 signals
FBSS=7
Log (Variance) (deg^2)
0
-0.5
-1
-1.5
-2
-2.5
-3
-90
-45
0
45
90
135
180
225
270
Phase (deg)
Phase (deg)

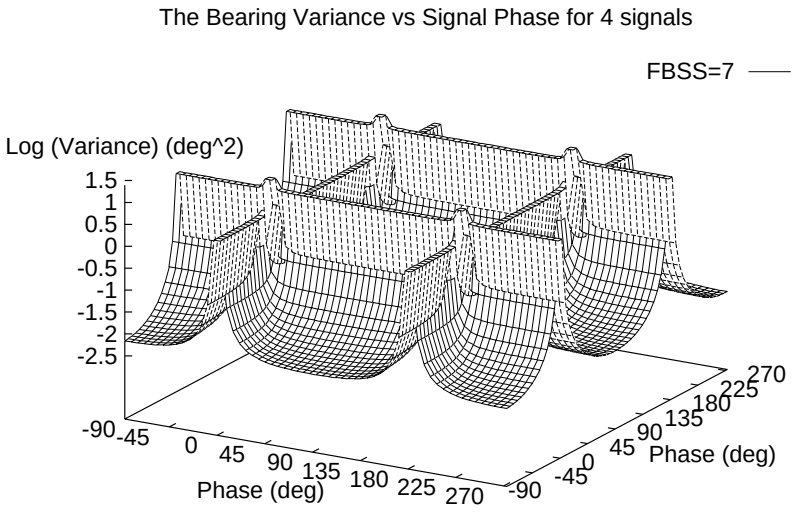
The Bearing Variance vs Signal Phase for 4 signals
FBSS=7
Log (Variance) (deg^2)
1.5
1
0.5
0
-0.5
-1
-1.5
-2
-2.5
-90
-45
0
45
90
135
180
225
270
Phase (deg)
Phase (deg)

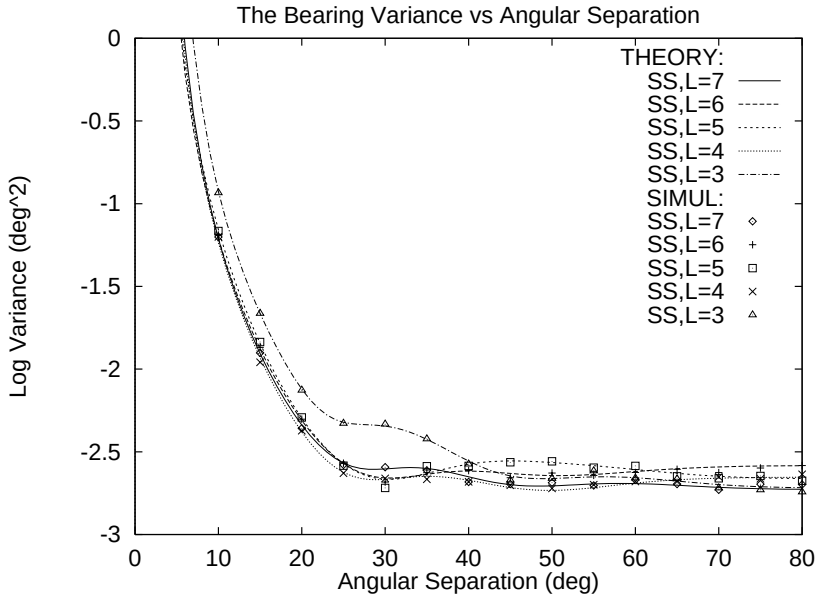
The Bearing Variance vs Angular Separation
THEORY:
SS,L=7
SS,L=6
SS,L=5
SS,L=4
SS,L=3
SIMUL:
SS,L=7
SS,L=6
SS,L=5
SS,L=4
SS,L=3
Log Variance (deg^2)
0
-0.5
-1
-1.5
-2
-2.5
-3
0
10
20
30
40
50
60
70
80
Angular Separation (deg)

Appendix B

Evaluating The Probability $p(A_1)$

In order to evaluate the probability $p(A_1)$, the mean and variance of the K^{th} eigenvalue l_K and the noise eigenvalue $\hat{\sigma}_n^2$ are required. The probability value is then simply given by equation 3.7, where γ is defined as:

$$\gamma = \frac{\alpha(N)(2M - 2K + 1)/N - \Delta\Lambda_K}{\sigma_{\Delta\Lambda_K}} \tag{B.1}$$

The parameter $\alpha(N)$ is defined in equation (3.6) and the following text. The parameter N denotes the number of snapshots used to form the estimated covariance matrix and $\Delta\Lambda_K$ is equal to:

$$\Delta\Lambda_K = \ln\{\frac{\sigma_n^2}{\lambda_K}[1 + \frac{1}{M - K + 1}(\frac{\lambda_K}{\sigma_n^2} - 1)]^{M-K+1}\} \tag{B.2}$$

The standard deviation term $\sigma_{\Delta\Lambda_K}$ is the square root of the following variance equation:

$$\sigma^2_{\Delta\Lambda_K} = (\frac{\partial(\Delta\Lambda_K)}{\partial\sigma_n^2})^2(\Delta\sigma_n^2)^2 + (\frac{\partial(\Delta\Lambda_K)}{\partial\lambda_K})^2(\Delta\lambda_K)^2 \tag{B.3}$$

where the terms $(\Delta\sigma_n^2)^2$ and $(\Delta\lambda_K)^2$ denote the variance of $\hat{\sigma_n}^2$ and λ_K respectively. The derivative terms are given as follows:

$$\frac{\partial(\Delta\Lambda_K)}{\partial\sigma_n^2} = \frac{(M-K)(\sigma_n^2 - \lambda_K)}{(\lambda_K + (M-K)\sigma_n^2)\sigma_n^2} \qquad \text{and} \qquad \frac{\partial(\Delta\Lambda_K)}{\partial\lambda_K} = \frac{(M-K)(\lambda_K - \sigma_n^2)}{(\lambda_K + (M-K)\sigma_n^2)\lambda_K} \tag{B.4}$$

If the estimated covariance matrix follows a Wishart distribution with N data snapshots, the variance term $\sigma^2_{\Delta\Lambda_K}$ reduces to $(a^2/N)(1+[1/(M-K)])$ The constant a is given by $(M-K)(\lambda_K - \sigma_n^2)/(\lambda_K + (M-K)\sigma_n^2)$.

Appendix C
Derivation of Results for Chapter 6

C.1 Finite Fading Effects on The Bit Error Ratio

The equation for DPSK de–modulation of a single tap fading signal is given by:

$$D(n) = \Re\{z(1,n)z^*(1,n-1)\} \tag{C.1}$$

where $D(n)$ denotes the decision variable and $z(1,n)$ denotes the noise–corrupted tap output for the n^{th} symbol. As a result, the effective SNR of the signal measured at the decision variable $D(n)$ depends on the real part only of the auto–correlation of the underlying signal, with the time delay set to one symbol period t_s. Denote the required signal auto–correlation value as $R(\tau_0, t_s)$, where $R()$ is given by equation (6.8) or (6.11) with a set to 1. The time delay τ_0 denotes the excess time delay of the given tap relative to the first incoming multipath. The term $[1 - |R(\tau_0, t_s)|]$ denotes the irreducible equivalent noise power due to the finite fading effects. The signal SNR for the variable $D(n)$ is therefore given by:

$$\text{SNR} = \frac{\Re\{R(\tau_0, t_s)\}}{[1 - |R(\tau_0, t_s)|] + (\sigma^2/S)} \tag{C.2}$$

where S denotes the mean signal power measured on one symbol interval only and σ^2 denotes the white noise power present. Clearly, the higher the value of ν_m, the lower the real part of $R(\tau_0, t_s)$ which leads to a high irreducible BER because of tracking errors. Figure C.1 shows the performance of a base station receiver with one antenna using a single tap RAKE filter for three different fading frequencies. The signals were generated using the classical Doppler fading model. Simulation results are shown as points and theoretical results using equation (C.2) as lines.

C.2 Derivation of the Nakagami Fading Equation

The Nakagami m–parameter for a fading signal is defined as the inverse normalised variance of that signal. For the x^{th} row and y^{th} column entry of the covariance matrix $\hat{\boldsymbol{R}}(1)$ formed from N snapshots of the channel vector $\boldsymbol{h}(1,t)$, the m–parameter is given by:

$$m = \frac{E[\hat{\boldsymbol{R}}(1)_{xy}]^2}{E[\hat{\boldsymbol{R}}(1)_{xy}\hat{\boldsymbol{R}}(1)_{xy}] - E[\hat{\boldsymbol{R}}(1)_{xy}]^2} \tag{C.3}$$

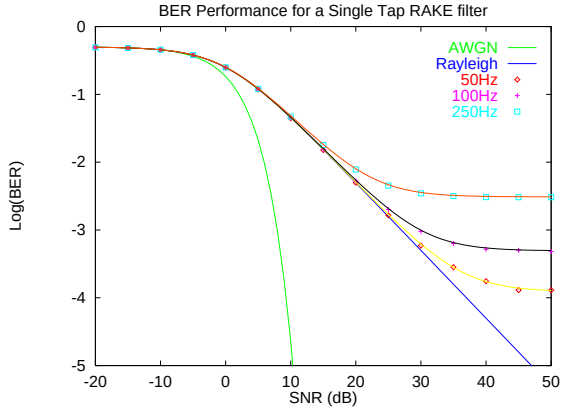

Figure C.1: *The BER Performance of a Single Tap RAKE Filter*

where $\hat{\boldsymbol{R}}(1)_{xy}$ is the x^{th} row and y^{th} column entry of $\hat{\boldsymbol{R}}(1)$. Now the denominator of equation (C.3) is given by:

$$\begin{aligned}
E[\hat{\boldsymbol{R}}(1)_{xy}\hat{\boldsymbol{R}}(1)_{xy}] &= \frac{1}{N^2}\sum_{i,j=1}^{N} E[h_x(1,t_i)h_y^*(1,t_i)h_x(1,t_j)h_y^*(1,t_j)] \\
&= \frac{1}{N^2}\sum_{i=1}^{N} E[h_x(1,t_i)h_y^*(1,t_i)h_x(1,t_i)h_y^*(1,t_i)] \\
&\quad + \frac{1}{N^2}\sum_{i=1}^{N}\sum_{j=1,j\neq i}^{N} E[h_x(1,t_i)h_y^*(1,t_j)h_x(1,t_j)h_y^*(1,t_i)] \\
&= \frac{2}{N^2}\sum_{i=1}^{N} E[h_x(1,t_i)h_y^*(1,t_i)]E[h_x(1,t_i)h_y^*(1,t_i)] \\
&\quad + \frac{1}{N^2}\sum_{i=1}^{N}\sum_{j=1,j\neq i}^{N} E[h_x(1,t_i)h_y^*(1,t_i)]E[h_x(1,t_j)h_y^*(1,t_j)] \\
&\quad + \frac{1}{N^2}\sum_{i=1}^{N}\sum_{j=1,j\neq i}^{N} E[h_x(1,t_i)h_y^*(1,t_j)]E[h_x(1,t_j)h_y^*(1,t_i)] \\
&= \frac{\boldsymbol{R}(1)_{xy}\boldsymbol{R}(1)_{xy}}{N^2}[N^2 + N + \sum_{i=1}^{N}\sum_{j=1,j\neq i}^{N} R(0,(i-j)t_s)R(0,(j-i)t_s)]
\end{aligned} \tag{C.4}$$

where $R(0,(i-j)t_s)$ is defined in section C.1. Substituting equation (C.4) into (C.3) and cancelling the $(\boldsymbol{R}(1)_{xy})^2$ term gives equation (6.22).

$$m = [(1/N) + (1/N^2)\sum_{i,j,i\neq j}^{N} R(0,(i-j)t_s)R(0,(j-i)t_s)]^{-1} \tag{C.5}$$

C.3 Derivation of the Spatial Smoothing SNR Equation

In this case the receiver has identified J multipath bearings $\{\theta_j\}$. There are J signals to be combined by ideal maximal ratio combining (MRC), and their amplitudes are given by $\{\boldsymbol{a}^H(\theta_j)\boldsymbol{h}(1,t)\}$. The mean noise power of the j^{th} signal is simply $\boldsymbol{a}^H(\theta_j)\boldsymbol{a}(\theta_j)$, assuming that the noise power at each antenna is scaled to unity. Before combining, each signal amplitude is scaled by the complex conjugate of itself (namely $\boldsymbol{h}^H(1,t)\boldsymbol{a}(\theta_j)$ for the j^{th} signal), so that the j^{th} scaled amplitude is $\boldsymbol{a}^H(\theta_j)\hat{\boldsymbol{R}}(1)\boldsymbol{a}(\theta_j)$. Similarly, the noise power for the j^{th} signal becomes $\boldsymbol{a}^H(\theta_j)\hat{\boldsymbol{R}}(1)\boldsymbol{a}(\theta_j)\boldsymbol{a}^H(\theta_j)\boldsymbol{a}(\theta_j)$. The scaled signals are simply added, so that the signal amplitude at the output of the MRC is $\sum_{j=1}^{J}\boldsymbol{a}^H(\theta_j)\hat{\boldsymbol{R}}(1)\boldsymbol{a}(\theta_j)$.

The mean noise power at the output of the MRC must take account of the fact that the J inputs to the MRC are generally correlated in some way, according to the bearings $\{\theta_j\}$. The cross–correlation of the noise at the j^{th} input with that at the k^{th} input is simply $\boldsymbol{a}^H(\theta_j)\boldsymbol{a}(\theta_k)$: after the signals are scaled, this term becomes $\boldsymbol{a}^H(\theta_j)\boldsymbol{a}(\theta_k)\boldsymbol{a}^H(\theta_k)\hat{\boldsymbol{R}}(1)\boldsymbol{a}(\theta_j)$. Hence the SNR at the output of the MRC is:

$$SNR = \frac{[\sum_{j=1}^{J}\boldsymbol{a}^H(\theta_j)\hat{\boldsymbol{R}}(1)\boldsymbol{a}(\theta_j)]^2}{\sum_{j=1}^{J}\sum_{k=1}^{J}\boldsymbol{a}^H(\theta_j)\boldsymbol{a}(\theta_k)\boldsymbol{a}^H(\theta_k)\hat{\boldsymbol{R}}(1)\boldsymbol{a}(\theta_j)} \tag{C.6}$$

Equation (C.6) may be simplified easily to obtain equation (6.26).

Appendix D

Derivatives for The Taylor Series Expansion

In order to evaluate the expressions given in equation (7.9), the derivatives of X and Y in terms of the independent variables υ, θ_1, θ_2 and ξ are required. In order to calculate them, it is possible to use direct expressions for X and Y; alternatively, the calculations may be simplified through the use of the chain rule [187].

To begin with, X and Y may be expressed in terms of R and θ_1 as:

$$X = R\cos\theta_1 \quad Y = R\sin\theta_1 \tag{D.1}$$

This means that the derivatives become:

$$\begin{aligned}
\frac{\partial X}{\partial \upsilon} &= \frac{\partial R}{\partial \upsilon}\cos\theta_1 & \frac{\partial Y}{\partial \upsilon} &= \frac{\partial R}{\partial \upsilon}\sin\theta_1 \\
\frac{\partial X}{\partial \theta_1} &= \frac{\partial R}{\partial \theta_1}\cos\theta_1 - R\sin\theta_1 & \frac{\partial Y}{\partial \theta_2} &= \frac{\partial R}{\partial \theta_1}\sin\theta_1 + R\cos\theta_1 \\
\frac{\partial X}{\partial \theta_2} &= \frac{\partial R}{\partial \theta_2}\cos\theta_1 & \frac{\partial Y}{\partial \theta_2} &= \frac{\partial R}{\partial \theta_2}\sin\theta_1 \\
\frac{\partial X}{\partial \xi} &= \frac{\partial R}{\partial \xi}\cos\theta_1 & \frac{\partial Y}{\partial \xi} &= \frac{\partial R}{\partial \xi}\sin\theta_1
\end{aligned} \tag{D.2}$$

In order to avoid un-necessary complication the next task will be to take derivatives of R, as expressed in equation (7.8), in terms of the independent variables A, B and C. If the $\pm$ sign is substituted by a positive sign, the derivatives become:

$$\begin{aligned}
\frac{\partial R}{\partial A} &= \frac{B}{2A^2} - \frac{B^2 - 2AC}{2A^2\sqrt{B^2 - 4AC}} \\
\frac{\partial R}{\partial B} &= \frac{1}{2A}\left(\frac{B}{\sqrt{B^2 - 4AC}} - 1\right) \\
\frac{\partial R}{\partial C} &= \frac{-1}{\sqrt{B^2 - 4AC}}
\end{aligned} \tag{D.3}$$

Alternatively is the $\pm$ sign is changed to be negative, the derivatives are altered to:

$$\begin{aligned}
\frac{\partial R}{\partial A} &= \frac{B}{2A^2} + \frac{B^2 - 2AC}{2A^2\sqrt{B^2 - 4AC}} \\
\frac{\partial R}{\partial B} &= \frac{-1}{2A}\left(\frac{B}{\sqrt{B^2 - 4AC}} + 1\right) \\
\frac{\partial R}{\partial C} &= \frac{1}{\sqrt{B^2 - 4AC}}
\end{aligned} \tag{D.4}$$

Next, the derivatives of the expressions in equation (7.7) for A,B and C with respect to x, y and ξ may be calculated. The results are:

$$\begin{aligned}
\frac{\partial A}{\partial x} &= -8\xi & \frac{\partial A}{\partial y} &= 8y & \frac{\partial A}{\partial \xi} &= -8x - 8\xi \\
\frac{\partial B}{\partial x} &= 16x\xi - 4\xi^2 & \frac{\partial B}{\partial y} &= 16\xi y & \frac{\partial B}{\partial \xi} &= 8x^2 + 8y^2 - 8\xi x - 12\xi^2 \\
\frac{\partial C}{\partial x} &= 8x\xi^2 & \frac{\partial C}{\partial y} &= 8y\xi^2 & \frac{\partial C}{\partial \xi} &= 8\xi x^2 + 8\xi y^2 - 4\xi^3
\end{aligned} \tag{D.5}$$

In the derivation of the algorithm, the co-ordinates (x, y) are expressed relative to the LOS path as x–axis. So, the derivatives of x and y in terms of the remaining variables υ, θ_1 and θ_2 are:

$$\begin{aligned}
\frac{\partial x}{\partial \upsilon} &= \cos(\theta_2 - \theta_1) & \frac{\partial x}{\partial \theta_1} &= \upsilon \sin(\theta_2 - \theta_1) & \frac{\partial x}{\partial \theta_2} &= -\upsilon \sin(\theta_2 - \theta_1) \\
\frac{\partial y}{\partial \upsilon} &= \sin(\theta_2 - \theta_1) & \frac{\partial y}{\partial \theta_1} &= -\upsilon \cos(\theta_2 - \theta_1) & \frac{\partial y}{\partial \theta_2} &= \upsilon \cos(\theta_2 - \theta_1)
\end{aligned} \tag{D.6}$$

All the results necessary for determining the derivative values have been presented in equations (D.2), (D.3), (D.5) and (D.6). To obtain the correct result, the chain rule must be applied to all possible derivatives at each stage. As an example, the derivative $\partial X/\partial \upsilon$ may be calculated as follows:

$$\begin{aligned}
\frac{\partial X}{\partial \upsilon} &= \frac{\partial R}{\partial \upsilon}\sin\theta_1 \\
&= \left(\frac{\partial R}{\partial A}\frac{\partial A}{\partial \upsilon} + \frac{\partial R}{\partial B}\frac{\partial B}{\partial \upsilon} + \frac{\partial R}{\partial C}\frac{\partial C}{\partial \upsilon}\right)\sin\theta_1 \\
&= \left(\frac{\partial R}{\partial A}\left[\frac{\partial A}{\partial x}\frac{\partial x}{\partial \upsilon} + \frac{\partial A}{\partial y}\frac{\partial y}{\partial \upsilon}\right] + \frac{\partial R}{\partial B}\left[\frac{\partial B}{\partial x}\frac{\partial x}{\partial \upsilon} + \frac{\partial B}{\partial y}\frac{\partial y}{\partial \upsilon}\right] + \frac{\partial R}{\partial C}\left[\frac{\partial C}{\partial x}\frac{\partial x}{\partial \upsilon} + \frac{\partial C}{\partial y}\frac{\partial y}{\partial \upsilon}\right]\right)\sin\theta_1
\end{aligned} \tag{D.7}$$